

FORCE SPECTROSCOPY WITH DNA ORIGAMI

PHILIPP NICKELS



München 2017

FORCE SPECTROSCOPY WITH DNA ORIGAMI

PHILIPP NICKELS

Dissertation
durchgeführt an der Fakultät für Physik
der Ludwig-Maximilians-Universität
München

vorgelegt von
Philipp Nickels
aus München

München, 2017

Erstgutachter: Prof. Dr. Tim Liedl
Zweitgutachter: Prof. Dr. Philip Tinnefeld

Tag der Abgabe: 14.02.2017

Tag der mündlichen Prüfung: 08.05.2017

ZUSAMMENFASSUNG

Die Stabilität, Biokompatibilität und molekulare Erkennung von DNA hat dazu geführt dass sich DNA zu einem vielversprechendem Baumaterial in der Nanotechnologie entwickelt hat. Besonders DNA Origami nutzt die molekulare Erkennung von DNA um supramolekulare Strukturen beliebiger Form mit Genauigkeit im Nanometerbereich herzustellen. Diese Positionsgenauigkeit bietet die Möglichkeit, biomolekulare Systeme mit bisher unerreichter Kontrolle zu untersuchen. In dieser kumulativen Dissertation fasse ich die folgenden drei DNA Origami basierten Forschungsprojekte zusammen:

Im ersten Teil präsentiere ich die Nutzung von intakten Bakteriophagen M13 und λ as Quelle für einzelsträngige und doppelsträngige Gerüststränge ohne vorherige Aufreinigung der genomischen DNA und zeige desweiteren die erfolgreiche Herstellung von verschiedenen DNA Origami Strukturen aus dieser Gerüststrangquelle.

Im zweiten Teil zeige ich eine DNA Origami basierte differentielle molekulare Kraftwaage. Die wippenartige DNA Origami Struktur vergleicht Bindungspartner auf einer Seite mit Referenzbindungspartnern auf der anderen Seite. Das Bindungspaar mit der höheren Bindungsenergie lässt die Struktur in einer geometrisch eindeutigen Form einrasten.

Im dritten Teil demonstriere ich wie man mit Hilfe von DNA Origami eine nanometergroße Kraftklammer bauen kann welche autonom in Lösung agiert und keinerlei Verbindung zur makroskopischen Welt hat. Nach erfolgreicher Charakterisierung der Kraftklammer analysiere ich die Schaltungskinetik der Holliday Struktur als Funktion der angelegten Kraft. Daraufhin untersuche ich die Biegung von Promotor DNA durch das TATA-Box Bindeprotein.

ABSTRACT

The physical stability, biocompatibility, and molecular recognition have made DNA a promising building material in nanotechnology. In particular, DNA origami uses the molecular recognition properties of DNA to create supramolecular structures of virtually any geometry with nanometer precision. This positional control offers the possibility to investigate biomolecular systems at unequaled levels of control. In this cumulative dissertation, I present the following three DNA origami centered research projects:

In the first part, I present the direct use of intact bacteriophages M13 and λ without further purification of the genomic DNA as a source of single- and double-stranded scaffolds and show the successful one-pot assembly of various DNA origami structures.

In the second part, I show a DNA origami structure as a differential molecular force balance. The structure is a seesaw-like DNA origami that compares a pair of binding partners on one side of the balance to a reference pair on the other side. The binding pair with the stronger interaction locks the structure in a distinct, geometrically distinguishable conformation.

In the third part, I demonstrate the use of DNA origami to build a nanoscopic force clamp that operates autonomously in solution and has no connection to the macroscopic world. After characterization of the device, I show how it can be used to study the Holliday junction switching kinetics as a function of applied force. In a next step, I use the force clamp to investigate the TATA-box binding protein mediated bending of promoter DNA.

PUBLICATIONS

PEER-REVIEWED PUBLICATIONS THAT ARE PART OF THIS CUMULATIVE THESIS

- [1] P. C. Nickels, B. Wunsch, P. Holzmeister, W. Bae, L. M. Kneer, D. Grohmann, P. Tinnefeld, and T. Liedl. "Molecular force spectroscopy with a DNA origami-based nanoscopic force clamp." In: *Science* 354.6310 (2016), pp. 305–307. DOI: [10.1126/science.aah5974](https://doi.org/10.1126/science.aah5974).
- [2] P. C. Nickels, H. C. Høiberg, S. S. Simmel, P. Holzmeister, P. Tinnefeld, and T. Liedl. "DNA Origami Seesaws as Comparative Binding Assay." In: *ChemBioChem* 17.12 (2016), pp. 1093–1096. DOI: [10.1002/cbic.201600059](https://doi.org/10.1002/cbic.201600059).
- [3] P. C. Nickels, Y. Ke, R. Jungmann, D. M. Smith, M. Leichsenring, W. M. Shih, T. Liedl, and B. Högberg. "DNA origami structures directly assembled from intact bacteriophages." In: *Small* 10.9 (2014), pp. 1765–1769. DOI: [10.1002/smll.201303442](https://doi.org/10.1002/smll.201303442).

OTHER PEER-REVIEWED PUBLICATIONS

- [1] V. Cassinelli, B. Oberleitner, J. Sobotta, P. Nickels, G. Grossi, S. Kemper, T. Frischmuth, T. Liedl, and A. Manetto. "One-Step Formation of "Chain-Armor"-Stabilized DNA Nanostructures." In: *Angewandte Chemie (International ed in English)* 54.27 (2015), pp. 7795–7798. DOI: [10.1002/anie.201500561](https://doi.org/10.1002/anie.201500561).
- [2] S. S. Simmel, P. C. Nickels, and T. Liedl. "Wireframe and tensegrity DNA nanostructures." In: *Accounts of Chemical Research* 47.6 (2014), pp. 1691–1699. DOI: [10.1021/ar400319n](https://doi.org/10.1021/ar400319n).
- [3] R. Schreiber, J. Do, E.-M. Roller, T. Zhang, V. J. Schüller, P. C. Nickels, J. Feldmann, and T. Liedl. "Hierarchical assembly of metal nanoparticles, quantum dots and organic dyes using DNA origami scaffolds." In: *Nature Nanotechnology* 9.1 (2013), pp. 1–5. DOI: [10.1038/nnano.2013.253](https://doi.org/10.1038/nnano.2013.253).
- [4] R. Schreiber, N. Luong, Z. Fan, A. Kuzyk, P. C. Nickels, T. Zhang, D. M. Smith, B. Yurke, W. Kuang, A. O. Govorov, et al. "Chiral plasmonic DNA nanostructures with switchable circular dichroism." In: *Nature Communications* 4 (2013), pp. 2948–6. DOI: [10.1038/ncomms3948](https://doi.org/10.1038/ncomms3948).
- [5] J. J. Schmied, C. Forthmann, E. Pibiri, B. Lalkens, P. Nickels, T. Liedl, and P. Tinnefeld. "DNA origami nanopillars as standards for three-dimensional superresolution microscopy." In: *Nano Letters* 13.2 (2013), pp. 781–785. DOI: [10.1021/nl304492y](https://doi.org/10.1021/nl304492y).

- [6] V. J. Schueller, S. Heidegger, N. Sandholzer, P. C. Nickels, N. A. Suhartha, S. Endres, C. Bourquin, and T. Liedl. “Cellular immunostimulation by CpG-sequence-coated DNA origami structures.” In: *ACS nano* 5.12 (2011), pp. 9696–9702. DOI: [10.1021/nn203161y](https://doi.org/10.1021/nn203161y).
- [7] R. Schreiber, S. Kempter, S. Holler, V. Schüller, D. Schiffels, S. S. Simmel, P. C. Nickels, and T. Liedl. “DNA origami-templated growth of arbitrarily shaped metal nanoparticles.” In: *Small* 7.13 (2011), pp. 1795–1799. DOI: [10.1002/sml1.201100465](https://doi.org/10.1002/sml1.201100465).

ACKNOWLEDGEMENTS

I would like to thank my family and Mara for their unconditional support.

Thank you Tim for being a great supervisor and friend and for all the freedom you gave me during the last couple of years. I really enjoyed working in your group!

Special thanks to my co-supervisor Philip Tinnefeld and to Joachim Rädler for creating such a friendly atmosphere at the chair.

Last but not least, I want to thank all my collaborators, the current and former members of the group, and all the other people that supported me, namely:

Alex Maier	Georg Urtel	Philip Böhm
Amelie H.-Jungemann	Gerlinde Schwake	Philipp Altpeter
Andrea Cooke	Guillermo Acuna	Philipp Paulitschke
Andreas Gietl	Hans Høiberg	Ralf Jungmann
Angelika Kardinal	Iain MacPherson	Robert Schreiber
Bert Nickel	Ingo Stein	Samet Kocabey
Bettina Wunsch	Jan Lipfert	Sara Schulz
Björn Högberg	Johanna Schappert	Stefan Fischer
Carolin Vietz	Jürgen Schmied	Stephanie Simmel
Caroline Hartl	Kevin Martens	Susanne Hennig
Carsten Forthmann	Kilian Frank	Susanne Kempfer
Christof Mast	Luisa Kneer	Susanne Rappl
Daniel Schiffels	Magnus Bauer	Tao Zhang
David Smith	Mandy Häusler	Thomas Nikolaus
Deborah Fygenon	Marc Ablay	Tim Schröder
Diana Pippig	Marc Leichsenring	Timon Funck
Dina Grohmann	Margarete Meixner	Travis Del B.-O'Donell
Dinesh Khara	Marina Polo	Verena Schüller
Dustin McIntosh	Mario Raab	Willem Vanderlinden
Enrico Pibiri	Mauricio Pilo-Pais	William Shih
Eva-Maria Roller	Max Scheible	Wooli Bae
Eyal Nir	Megan Engel	Yonggang Ke
Francesca Nicoli	Omar Saleh	Yongzheng Xing
Franziska Kriegel	Phil Holzmeister	and all the others from the Rädler chair

Thank you!

CONTENTS

1	INTRODUCTION	1
1.1	A Brief History of Nanotechnology	1
1.2	Top-down vs Bottom-up	3
1.3	Self-Assembly	4
1.4	Structural Nucleic Acid Nanotechnology	5
1.4.1	State of the Art of DNA Origami	8
1.4.2	Challenges and Future Perspectives	9
1.5	Content of this Work	9
2	THEORETICAL BASICS	11
2.1	The DNA Molecule	11
2.1.1	The Structure of DNA	11
2.1.2	Chemical and Physical Properties of DNA	13
2.1.2.1	Optical Properties	13
2.1.2.2	DNA as Polyelectrolyte	13
2.1.2.3	Mechanical Properties of ssDNA	13
2.1.2.4	Mechanical Properties of dsDNA	14
2.1.2.5	Melting Behavior	15
2.2	DNA Origami	15
2.3	Exerimental Methods	19
2.3.1	UV/Vis Spectroscopy	20
2.3.2	Electrophoresis	20
2.3.3	Atomic Force Mircoscopy	22
2.3.4	Transmission Electron Microscopy	23
2.3.5	Single-Molecule FRET and ALEX	24
3	DNA ORIGAMI STRUCTURES DIRECTLY FOLDED FROM INTACT BACTERIOPHAGES	27
3.1	Intact Bacteriophages as a Source of Scaffold	27
3.2	Scaling the Size of DNA Origami	29
3.3	Associated Publication P1	31
4	DNA ORIGAMI SEESAWS AS COMPARATIVE BINDING ASSAY	39
4.1	DNA Hybridization Assay	39
4.2	DNA-DNA Binding Assay	40
4.3	Outlook	40
4.4	Associated Publication P2	41
5	MOLECULAR FORCE SPECTROSCOPY WITH A DNA ORIGAMI BASED NANOSCOPIC FORCE CLAMP	47
5.1	Limitations of Conventional Force Spectroscopy	47
5.2	DNA Origami Force Clamp	48
5.3	Associated Publication P3	51
6	OUTLOOK TO FUTURE WORK	71
6.1	DNA Origami Components from a Single Bacterial Culture	71

6.2	Improved Modeling of Entropic Force in the DNA Origami Force Clamp	71
6.3	Bulk Force Spectroscopy Measurements	72
A	APPENDIX	73
A.1	Supporting information for associated Publication P1 . .	73
A.2	Supporting information for associated Publication P2 . .	103
A.3	Supporting information for associated Publication P3 . .	113
	BIBLIOGRAPHY	175

LIST OF FIGURES

Figure 1	Pre-modern Examples of Nanotechnology	2
Figure 2	First Scanning Tunneling Microscope and IBM Logo	2
Figure 3	Ribosomal Subunits	4
Figure 4	3D DNA Lattice and Holliday Junction	6
Figure 5	DNA Cube and 3D DNA crystal	7
Figure 6	DNA and RNA origami	8
Figure 7	Plaque in Memory of the Discovery of “Nuclein”	11
Figure 8	Structure of DNA	12
Figure 9	DNA Origami Concept	16
Figure 10	2D DNA Origami	16
Figure 11	3D DNA Origami	17
Figure 12	TEM Image of Many DNA Origami Structures	18
Figure 13	DNA Origami as Nano-Breadboard	19
Figure 14	Atomic Force Microscope	22
Figure 15	First Transmission Electron Microscope	23
Figure 16	Single-Molecule FRET and ALEX	25
Figure 17	Crude Bacteriophage Suspension as a Source of Scaffold for DNA Origami	28
Figure 18	DNA Origami based Comparative Binding Assay	39
Figure 19	Future Binding Assays	40
Figure 20	Illustration of the ssDNA Entropic Spring in the DNA Origami Force Clamp	48
Figure 21	DNA origami Force Clamp and TBP-induced Bending of DNA under Force	49

ACRONYMS

2D two-dimensional

3D three-dimensional

6HB six helix bundle

ALEX alternating laser excitation

AFM atomic force microscope

bp base pair

DNA deoxyribonucleic acid

dsDNA double-stranded DNA

E.coli Escherichia coli

FRET Förster resonance energy transfer

FJC freely jointed chain

mRNA messenger RNA

PCR polymerase chain reaction

RNA ribonucleic acid

ssDNA single-stranded DNA

ssRNA single-stranded RNA

STM scanning tunneling microscope

TBP TATA-box binding protein

TEM transmission electron microscope

WLC worm like chain

INTRODUCTION

Nanotechnology is a tremendously interdisciplinary field that combines concepts from various engineering and scientific disciplines, ranging from surface chemistry to molecular self-assembly and semiconductor physics. Nanotechnology aims to study and, more importantly, manipulate matter on the nanometer length scale. Although experts from all sciences have conducted research on the nanometer scale to gain fundamental knowledge, the ambition of nanotechnologists is to use that knowledge to directly control matter on the atomic, molecular, and supra-molecular scale to develop new materials, functional systems, and drugs.

Today, several applications of nanotechnology have found their way into commercial products. Examples are silver nanoparticles as disinfection agents in food packaging, clothing, and various household appliances or titanium and zinc oxide nanoparticles in sunscreen, food products, and cosmetics. Nevertheless, all of these commercial products that are sold as “nanotechnology” are based on the bulk use of passive nanomaterials, more a product of conventional material science than of nanotechnology. Real world applications that require controlled manipulation of matter on the nanoscale as envisioned by many of the pioneers of nanotechnology have yet to be developed.

1.1 A BRIEF (AND INCOMPLETE) HISTORY OF NANOTECHNOLOGY

Although nanotechnology is a relatively young discipline, pre-modern examples of nanostructured materials date back to at least as early as the 4th century. Often, craftsmen used their empirical understanding to manipulate processes to produce materials with novel properties. Striking examples are the 4th-century roman Lycurgus cup (figure 1a), which contains colloidal gold and silver nanoparticles, and the Damascus sabre blades, which already made use of carbon nanotubes more than 400 years ago (figure 1b) [1].

More than a century ago, advances in colloidal and interface science made the characterization of dispersions of nanometer sized particles possible. Richard Zsigmondy was the first to study nanomaterials, especially colloidal gold, of sizes down to 10 nm using an ultramicroscope he developed in the early 1900's [5]. Langmuir introduced the concept of monolayers, materials with the thickness of only one layer of molecules, in the 1920's [6]. Most of nanoscience' development in the 1960's and 1970's was driven by the efforts of the electronic industry to increase

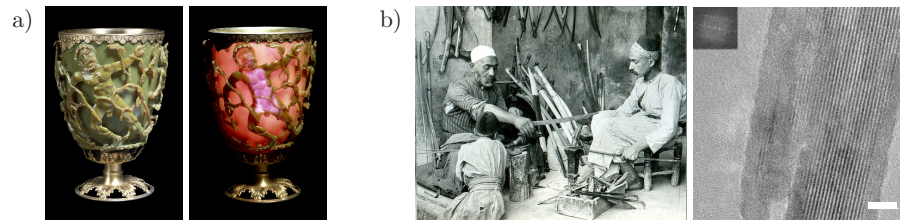


Figure 1: a) The Lycurgus cup is made of dichroic glass. Colloidal gold and silver nanoparticles in the glass make it appear green when illuminated from outside (left) and red when illuminated through the inside (right). Reproduced with permission from The British Museum [2] (CC BY-NC-SA 4.0). b) Sword maker in Damascus, Syria (ca. 1900) and TEM image of remnants of cementite nanowires encapsulated by carbon nanotubes in a 400 year old sabre (scale bar is 5 nm). Reprinted by permission from Macmillan Publishers Ltd: Nature [1], copyright (2006).

the number of transistors on integrated chips, as described by Intel's co-founder Gordon Moore [7]. The term nanotechnology was used for the first time by Norio Taniguchi in an article to describe the machining of materials with atomic-scale dimensional tolerances [8]. But it was Eric Drexler's 1986 book *Engines of Creation: The Coming Era of Nanotechnology* [9] that made the term nanotechnology widely known. Together with Drexler's popularized conceptual framework for nanotechnology, major scientific breakthroughs in the 1980's lead to the emergence of nanotechnology as its own field. The invention of the scanning tunneling microscope (STM) by Binnig and Rohrer at IBM [10, 11] made the visualization and later the manipulation of individual atoms by Eigler [4] possible (a photograph of the first STM is shown in figure 2a and the IBM logo made from individual atoms using the STM in figure 2b). Shortly after the invention of the STM, Binnig developed another scanning probe technique together with Quate and Gerber, the atomic force microscope (AFM) [12]. Other influential advances include the dis-

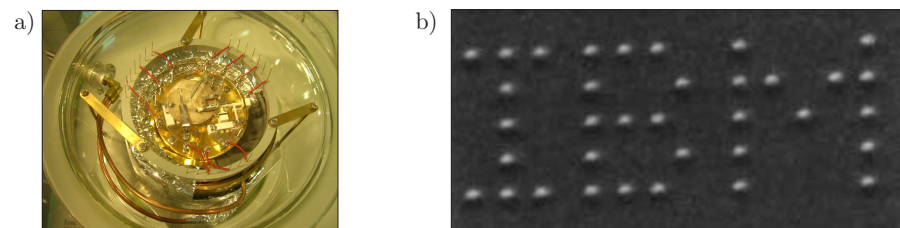


Figure 2: a) Photograph of the first STM, now on display at the Deutsches Museum in Munich, Germany. Image source: [3] (CC BY-NC-SA 2.0). b) IBM logo made from 35 Xenon atoms. Each letter is 50 Å in height. Reprinted by permission from Macmillan Publishers Ltd: Nature [4], copyright (1990).

covery of Fullerenes in 1985 [13] and the description of nanocrystals of a semiconducting material, the so-called quantum dots [14].

It nowadays seems to be widely accepted (and is often written) that the origin of nanotechnology is Richard Feynman's talk *There's plenty of room at the bottom* [15], which he gave at the American Physical Society meeting at the California Institute of Technology in 1959. The cultural anthropologist Christopher Toumey, however, asks the following question in his work entitled *Reading Feynman Into Nanotechnology: A Text for a New Science*: "Can we separate the early history of nanotechnology from Feynman's talk, and ask instead whether *Plenty of Room* is retroactively read into the history of nanotechnology?" [16]. He points to alternative, more instrumentation centered narratives that "could salute the STM as one of its founding ancestors". Toumey analyzes the publication and republication history of *Plenty of Room*, its scientific citation record, and comments from pioneers of nanotechnology. When asked by Toumey about Feynman's role in nanotechnology, George Whitesides writes:

His enthusiasm for small science has certainly boosted its [nanotechnology's] general attractiveness, and made it intellectually legitimate, especially in physics... I don't think that he was specifically important in the sense that Binnig / Rohrer / Quate were. My sense is that most people in nano became excited about it for their own reasons, and then... have leaned on Feynman as part of their justification for their interest.

Toumey concludes his article with the following:

Alternatively, one could accept that the history of nanotechnology will not fit neatly into the standards of the *naturwissenschaften*. Nanotech need not be one thing with one beginning and one neat line of historical causation. It could be a deep, rich, nuanced and sometimes contradictory body of scientific thought and practice that we understand partly by seeing it through different historical documents, and through different readings of the same document, namely, Richard P. Feynman's *There's Plenty of Room at the Bottom*.

1.2 TOP-DOWN VS BOTTOM-UP

Within the field of nanotechnology, two fundamentally different strategies exist: top-down and bottom-up. In top-down nanotechnology, externally controlled manipulation tools are used to remove and shape material from larger substrates. This principle is heavily applied in the

semiconductor industry and has reached a sophisticated level of precision. As structures decrease in size, however, the limitations of top-down nanotechnology start to become apparent: all top-down methods are inherently serial and parallelization comes with a great cost. Bottom-up nanotechnology, in contrast, is inspired by nature: all biological systems rely on self-assembly to produce ordered systems as a function of molecular recognition without any external guidance. The work presented in this thesis relies solely on the bottom-up approach and self-assembly in particular. A short introduction to self-assembly is given in the next section (1.3), followed by a brief overview of structural nucleic acid nanotechnology in section 1.4.

1.3 SELF-ASSEMBLY

In self-assembly, order forms from a disordered system of pre-existing building blocks. The resulting complexity is completely internal to the system and emerges from the characteristics of the components. Self-assembly can only happen in open systems: the interaction with the outside world has to compensate for the decrease in entropy due to the creation of order. Each organism in the living world is self-assembled. In each cell of each organism, a multitude of molecular machines floats around and each of these machines performs tasks on an atomic scale. All these machines are examples of sophisticated (bio-)nanotechnology. They were, however, not intentionally designed, but rather emerged by billions of years of evolution. One key feature of all of these molecular machines is the atomically precise positioning of its constituent components. This positional control typically accounts for their function.

One striking example of a self-assembled biological nano-machine is the ribosome (a visualization of the structure of the ribosomal subunits is shown in figure 3). The ribosome is responsible for the synthesis

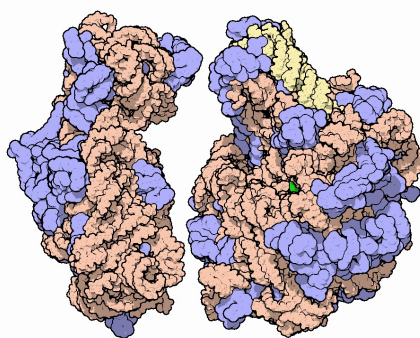


Figure 3: Small (left) and large (right) ribosomal subunits with RNA in orange and yellow and proteins in blue. The active center where the polypeptide synthesis takes place is colored green. Image by David Goodsell [17, 18]

of proteins in cells: it translates the genetic information coded on a messenger RNA (mRNA) into a chain of amino-acids. The ribosome itself is a molecular complex of proteins and ribonucleic acid (RNA) and its size ranges from 20 nm to 30 nm (it varies from prokaryotic to eukaryotic cells). It consists of a small and a large subunit. The ribosome can be produced by self-assembly in its simplest form: when mixing the building blocks together in a test tube under the right pH, temperature, and salt conditions, it assembles itself [19]. The RNA folds into a secondary structure and afterwards the proteins attach to the RNA “scaffold” and stabilize it.

Nanotechnology can learn a great deal from nature and the way virtually everything in the living world is self-assembled from nanoscale components. Over the last decades, deoxyribonucleic acid (DNA) and other biomolecules have been established as promising and powerful materials for bottom-up nanotechnology. Nadrian Seeman, the pioneer of DNA nanotechnology, stated the following in an interview after being awarded the Feynman Prize in Nanotechnology in 1995:

Nanotechnology is a very fancy buzzword for the chemistry of the next century. To a certain extent, we’re going to emulate the way things are done in cells. [20]

1.4 STRUCTURAL NUCLEIC ACID NANOTECHNOLOGY

Nucleic acids have unique molecular recognition properties that can be used to make self-assembled branched DNA or RNA complexes [21, 22]. Construction materials in the macroscopic world require, amongst others, the following properties: (I) robustness, (II) stability over a long period of time, (III) ease of operation, (IV) affordability, (V) modularity, and (VI) formability into custom shapes. It turns out that DNA as a construction material for the nanoscale fulfills these requirements. DNA is robust and stable under a wide range of conditions and can be stored easily for a long period of time (I & II). It is easy to handle in water and a variety of buffers (III) and is commercially available for a low price and short sequences up to 100 bases in length can be easily synthesized on a large scale (IV). It is biocompatible, modular, and the most important feature: it has a programmable sequence and offers molecular recognition (V). These features are employed to generate self-assembled structures of a designed shape from artificially designed DNA molecules (VI). A short overview of the field of structural nucleic acid nanotechnology with a focus on DNA is given in the next passage. A detailed description of the molecular structure of DNA is given in the section 2.1.

Nadrian Seeman, a crystallographer by training, wrote in 1982 in a theoretical work:

It appears to be possible to generate covalently joined three-dimensional networks of nucleic acids which are periodic in connectivity and perhaps in space. [23]

Although genetic engineers have made linear DNA constructs out of two or DNA molecules using sticky-end ligation techniques since the 1970's [24], more than just one-dimensional constructs are possible. In nature, branched DNA molecules are intermediates in the process of genetic recombination. Seeman realized that these DNA branches "...allow us to make something that is not just a long piece of spaghetti" [20]. Driven by the frustration that came with the crystallization of interesting biological macromolecules for X-ray crystallography experiments, his vision was, and still is, to design periodic three-dimensional (3D) lattices from DNA to host and orientate proteins (a cartoon illustrating this concept is shown in figure 4a), which would otherwise not be soluble on their own in aqueous solutions. To create a basic motif for the construction of orderly, crystal-like structures, Seeman examined a motif found in biological recombination systems, the Holliday junction. Holliday junctions are covalent phosphate linkages between two DNA duplexes. In organisms, these junctions are important for the recombination of homologous sequences during cell division. During recombination, the junction can freely slide along the two connected DNA double helices. Sequence asymmetry immobilizes the junction and can be used to create a spatially fixed connection between two DNA duplexes. Several immobilized junctions can be stitched together via sticky-end hybridization (figure 4b illustrates this concept). Sticky-ends are short, single-stranded DNA (ssDNA) overhangs with sequences complementary to each other.

Seemans group presented the first DNA based supramolecular assembly with connectivity greater than two in 1991: a 3D cube made of six

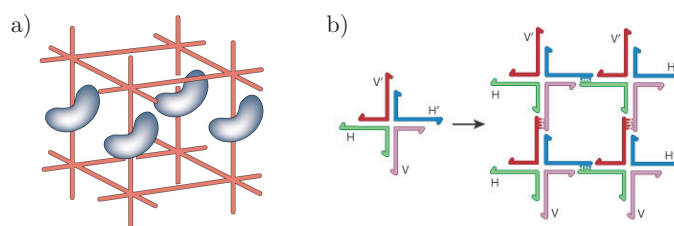


Figure 4: a) Vision of a DNA lattice as scaffolding for biological macromolecules. The macromolecules are arranged parallel to each other within the DNA lattice, rendering them amenable to structure determination by X-ray crystallography. b) Immobilized Holliday junction made from four ssDNA strands with sticky-end overhangs. Four of these branched junctions cohere based on the orientation of their complementary sticky ends and form a square unit with unpaired sticky-ends on the outside. More units can be added to the four sides to make a periodic, 2D crystal. Reprinted by permission from Macmillan Publishers Ltd: Nature [21], copyright (2003).

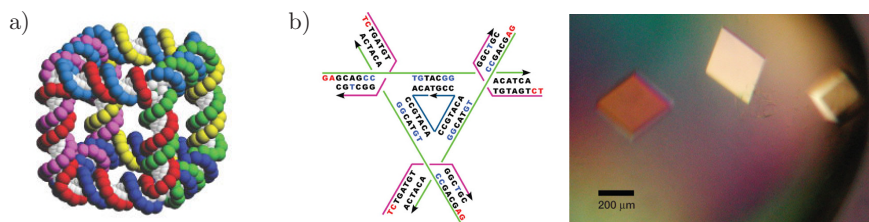


Figure 5: a) Seemans DNA Cube. Each of the six cyclic interlocked ssDNA strands is linked twice to each of its four neighbors. Reprinted by permission from Macmillan Publishers Ltd: Nature [21], copyright (2003). b) Left: 2D schematics of the tensegrity triangle motif. The over-under configuration of the three connected duplexes makes each of the three arms point to a different plane in space, resulting in a periodic 3D arrangement. Right: Optical image of the rhombohedral tensegrity triangle crystals. Reprinted by permission from Macmillan Publishers Ltd: Nature [29], copyright (2009)

ssDNA loops (figure 5a) [25]. The first periodic two-dimensional (2D) lattices were built from DNA double-crossover (DX) tiles by Erik Winfree in 1998 [26]. Other milestones of structural DNA nanotechnology include a tetrahedron by the Turberfield group [27] and an octahedron made from a 1.7 kilobase ssDNA from William Shih [28].

Almost 30 years after the initial proposal, Seeman presented the first rationally designed and self-assembled 3D DNA crystal (figure 5b) [29]. In 2006, Paul Rothemund revolutionized the field of DNA nanotechnology with the publication of the DNA origami technique: he used hundreds of synthetic short oligonucleotides to fold a viral 7-kilobase (7kb) ssDNA into arbitrary shapes (figure 6a) [30]. The extension of DNA origami to 3D by Douglas et al. [31] in 2009 and the introduction of curvature by Dietz et al. [32] expanded the design possibilities further. Additional structural design advances to create pre-stressed tensegrity structures [33], hollow shapes with complex curvature [34], and triangulated polyhedral objects [35–38] make it now possible to create objects of almost any geometry. These objects are comparable in size to viruses or ribosomes, while being fully addressable with nanometer precision. This positional precision has created the potential to investigate biomolecular systems at unequalled levels of control.

In recent years, RNA has gained attention in nucleic acid nanotechnology. Compared to DNA, RNA possesses a higher functional capacity such as releasing small interfering RNAs in response to stimuli [40] or scaffolding proteins [41, 42] as described for the ribosome in section 1.3. The large diversity of tertiary RNA motifs, which are not present in the DNA world, expands the design space tremendously. On top of that, RNA can be expressed genetically in large quantities and thus could lead to *in vivo* synthetic biology applications of nucleic acid nanotechnology. Early attempts to design and assemble structures comparable in size to DNA origami structures focussed on DNA-RNA hybrid systems [43, 44].

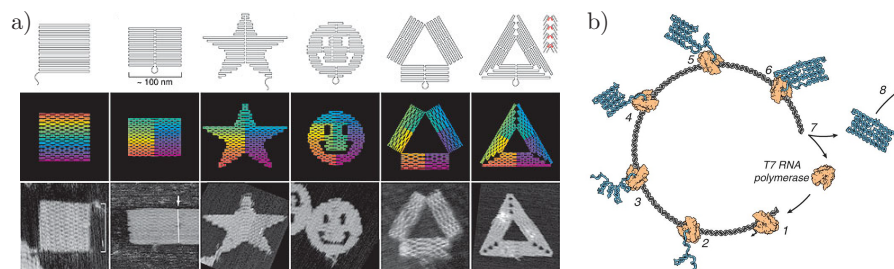


Figure 6: a) Different 2D DNA origami shapes from Rothemund's original publication. The top row shows the folding paths of the scaffold. The middle row shows how individual helices bend apart away from crossovers. The color indicates the base pair index along the folding path. The bottom row shows AFM images of the structures. Each image is 165 nm by 165 nm in size. Reprinted by permission from Macmillan Publishers Ltd: Nature [30], copyright (2006). b) Cotranscriptional folding pathway of a ssRNA origami motif. The T7 RNA polymerase transcribes the template DNA. The RNA folds back on itself as it is being synthesized. Reprinted by permission from AAAS: Science [39], copyright (2014).

In 2014, Geary et al. developed an architecture for the design of single-stranded RNA (ssRNA) origami structures that fold cotranscriptionally under isothermal conditions (figure 6b) [39].

1.4.1 State of the Art of DNA Origami

DNA origami has been established as a mature self-assembly technology in basic science. It has been used numerous times to investigate fundamental questions about the kinetics and thermodynamics of self-assembly itself [45–48]. At the core of most studies involving DNA origami structures lies the enormous positional precision that is unprecedented so far [49–55]. Areas of application include nanopores for sequencing [56–58] or the mimicry of natural pores [59, 60], the study of interactions with lipid membranes and their deformation [61–65], and the construction of 2D and 3D lattices [66–71]. DNA origami has been employed to study localized DNA- and enzymatic-reaction cascades [72–77] and for biophysical studies of collective behaviour of motor proteins [78–80] and biomolecular interactions [81–86]. In other great examples of the power of DNA origami to structure material on the nanoscale, the spatial arrangement of metallic nanoparticles, quantum dots, and fluorescent nanodiamonds was used to rationally design light-matter interactions [87–101]. Another promising route researchers pursued from the beginning is the use of DNA origami structures as drug delivery containers. Initial steps have already been taken towards the goal of a fully autonomous, site-directed delivery of drugs to target sites in organisms [102–106].

1.4.2 *Challenges and Future Perspectives*

So far, all the technical problems associated with nucleic acid nanotechnology and especially DNA origami did not significantly limit its application in basic research. Some of the problems associated are for example the impurity of the materials involved, imperfect stoichiometries, low assembly yields due to, for example, kinetic traps during thermal annealing, or increasingly lower efficiency of attachment of modified components as the complexity of the assemblies increases. Most of these inherent characteristics have been approached with the application of already available, small scale purification techniques, which work sufficiently well with the small volumes and low throughput needed for most proof-of-principle experiments. In order to establish DNA nanotechnology outside its niche in basic research, the following requirements have to be met: DNA nanostructures need to be produced at much higher quantity, with highly increased quality and purity of the materials involved, at much lower cost [107]. Additionally, the stability of the DNA nanostructures has to be improved for all applications that require other environmental conditions than the once used in the controlled laboratory scenario. Most of these limitations are already being addressed by the community [102, 103, 108–119], but there is still *plenty of room* for improvement.

1.5 CONTENT OF THIS WORK

This thesis is structured in the following way: In chapter two (2), I will give an overview over the structure of the DNA molecule (section 2.1), introduce DNA origami in more detail (2.2), and briefly explain the experimental techniques used to acquire all data presented in the associated publications reprinted in this thesis (section 2.3). The work presented in chapter three (3) is a humble contribution towards the goal of a high yield and low-cost production of DNA origami structures. It explores alternative sources of scaffold material than the typically used, purified genomic DNA of bacteriophage M13. Chapter four (4) proposes a DNA origami prototype for comparative binding assays. The prototype features an *in situ* readout through locked, geometrically distinguishable conformations and has no physical connection to the macroscopic world. Chapter four paves the way for the nanoscopic, DNA origami force clamp presented in chapter five (5). The force clamp is self-assembled, operates autonomously and has the potential for massive parallelization. We use this DNA origami force clamp to study the TATA-binding protein–induced bending of a DNA duplex under tension, a system previously inaccessible to conventional force spectroscopy techniques. Finally, in chapter six (6), I will give a short outlook to future work.

THEORETICAL BASICS

2.1 THE DNA MOLECULE

In all living organisms, DNA stores and transmits genetic information from one generation to another and is hence essential for the development and function of life. This makes DNA the central biomolecule of life and its discovery one of the remarkable tales of the history of molecular biology. The swiss physician Friedrich Miescher was the first to isolate nucleic acids from the nuclei of leukocytes in 1869 in Tübingen (figure 7) [120]. He named the substances “nuclein” and in subsequent work speculated that it plays a role in the transmission of hereditary traits. Decades later, in 1944, Avery, MacLeod, and McCarty corroborated this theory when they identified DNA as the molecule responsible for bacterial transformation [121]. In 1952, Hershey and Chase used radioactively labeled T2 Phage DNA to irrevocably confirm that DNA and not proteins carry the genetic information [122]. Based on the x-ray diffraction data of Franklin and Gosling, Watson and Crick published the first correct double-helix model of the structure of DNA in 1953 [123].



Figure 7: Commemorative plaque in memory of the discovery of the “nuclein” by Friedrich Miescher in 1869 in the laboratory of Felix Hoppe-Seyler at the University of Tübingen, located in the *Schloss Hohentübingen*.

2.1.1 *The Structure of DNA*

DNA is a polymeric macromolecule. It is made from repeating units called nucleotides (sthe chemical structure of DNA is shown in figure 8). Each nucleotide is composed of 3 entities: one of the four nucleobases adenine (A), cytosine (C), guanine (G), and thymine (T). the monosaccharide deoxyribose, and a mono-, di,- or triphosphate. The nucleobase is linked to the 1' carbon atom of the deoxyribose - this is called a nucleoside. The mono-, di,- or triphosphate attached to the

The information presented in this section and the following (2.1.2) is, if not stated otherwise, based on reference [124].

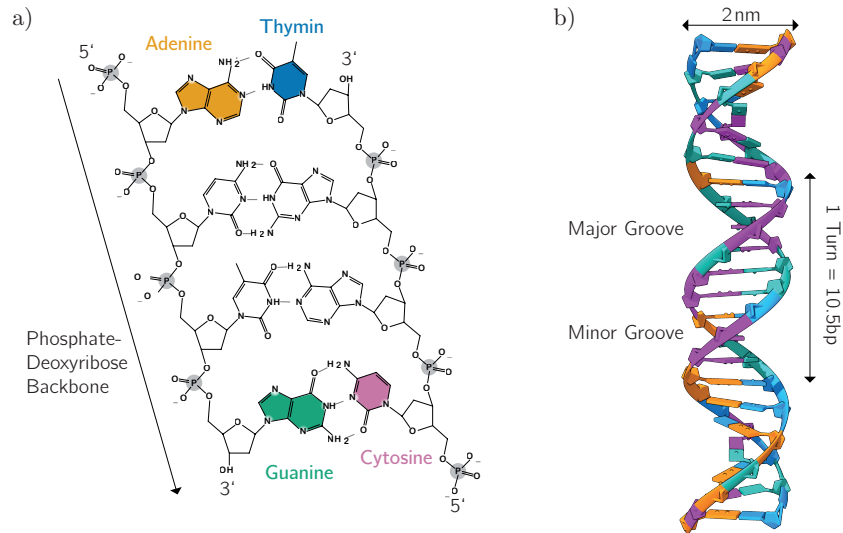


Figure 8: a) Chemical Structure of the four nucleobases and the DNA double helix. b) 3D structure of the right-handed DNA double helix in B-form geometry.

5' carbon atom of the deoxyribose ring in the nucleoside completes the nucleotide. Nucleotides play a central role in the metabolism of each organism: they serve as energy storage entities (e.g., adenosine triphosphate), participate in signaling pathways (e.g., cyclic adenosine monophosphate), and are parts of important cofactors of enzymatic reactions (e.g., flavin mononucleotide). Long polymers of an arbitrary composition of monophosphate nucleotides are made by linking phosphate to the 3' carbon of another nucleotide's deoxyribose ring. These polymers are then called polynucleotides or ssDNA. A direction can be assigned to a ssDNA molecule due to the asymmetric phosphodiester bond between two adjacent deoxyribose rings. One end of the ssDNA molecule terminates with a phosphate group at the 5' carbon (the 5'-end) while the opposite end terminates with a hydroxyl group at the 3' carbon (the 3'-end). Enzymes are sensitive to this directionality and usually process DNA from the 5'-end to the 3'-end.

Under physiological conditions, the four nucleobases undergo hydrogen bond mediated base pairing. A and T with two hydrogen bonds and G and C with three hydrogen bonds form the two canonical base pairs. G and C form the slightly more stable base pair (bp). In aqueous solutions, the four bases form hydrogen bonds with water as well. The aromatic rings of the nucleotides are positioned almost perpendicular to the length of the DNA strand, therefore the π -orbitals of the aromatic ring of one base overlap with π -orbitals of the aromatic ring of the adjacent base. The aromatic rings align and water is expelled from the space between the nucleobases. This effect is called stacking and the sum of all these stacking interactions greatly stabilizes the double helix. Two ssDNA molecules with a reverse complementary sequence can

bind together and the antiparallel strands form together a double helix. Under physiological conditions, the DNA double helix usually adopts the right-handed B-form. One full turn (10.5 base pairs) stretches over 3.5 nm with a diameter of 2 nm and a vertical distance between two adjacent bp of 3.32 Å. The B-form double helix exhibits a major and a minor groove (figure 8b). Under special buffer conditions, other conformations of the double helix such as the A-form (right-handed, 11 bp per turn, 2.3 nm diameter) or the Z-form (left-handed, 12 bp per turn, 1.8 nm diameter) occur.

2.1.2 *Chemical and Physical Properties of DNA*

2.1.2.1 *Optical Properties*

The four nucleobases, A, T, G, and C, have an absorption maxima at a wavelength of 260 nm. The total absorbance of a ssDNA strand depends on the sum of the absorbance of the single nucleotides plus the effect of the interactions between the nucleotides. This means that a single strand absorbs less than the sum of its nucleotides and a double strand less than the sum of its two component single strands. This effect is called hypochromicity: the absorption of double-stranded DNA (dsDNA) decreases up to 25% relative to the absorption of ssDNA and up to 40% relative to the absorption of the single nucleotides. This effect can be used to monitor hybridization events spectroscopically (see section 2.3.1 for more details).

2.1.2.2 *DNA as Polyelectrolyte*

DNA in aqueous solution is a highly charged polymer. At neutral pH, every phosphate in the backbone is deprotonated and thus negatively charged. The distribution of associated ions, the so called ion atmosphere, can be approximated by the Debye-Hückel theory. The discretely charged polymer is idealized as a chain with linear charge density and two layers of ions around the DNA strand are described. The first layer comprises of condensed counterions on the DNA strand. These counterions are free to translate along the elongation axis of the DNA strand, but are confined to the phosphate backbone and remain within a short distance called the Bjerrum length l_b . l_b describes the distance at which the Coulomb energy between two unit charges equals the thermal energy $k_B T$. In water at room temperature, $l_b = 7 \text{ \AA}$, roughly the typical interphosphate distance between two nearest-neighbor nucleotides. The second layer is a diffusive layer of anions and cations loosely associated to the first layer.

A very detailed and thorough description of nucleic acid-ion interactions can be found in reference [125]

2.1.2.3 *Mechanical Properties of ssDNA*

ssDNA in a fully screened state is a very flexible polymer. It can be approximated to a certain degree with the freely jointed chain (FJC)

model. The FJC model treats the polymer as a random walk and does not take any kind of interactions between the individual monomers that make the polymer into account. The polymer is described as a chain of rigid rods of a fixed length l_K (Kuhn length) whose orientation is completely independent of neighboring monomers. With N monomers forming the polymer the mean square end-to-end distance can be described as:

$$\langle L^2 \rangle = l_K^2 * N$$

The Kuhn length for semiflexible polymers such as ssDNA equals twice the persistence length l_P [126]. Next, we have to take thermal fluctuations and entropic effects into account. A random coil usually will resist elongation since it is accompanied by a significant decrease in entropy (ΔS). Assuming a chain with an end-to-end distance x , if x is only a fraction of its full contour length L_C , many more conformations for this compacted state than for its almost fully stretched state exist. The result of this effect is called entropic elasticity. The force exerted on each end of a long polymer can be expressed as:

$$\langle F \rangle = \frac{-3k_B T * L_C}{l_K^2 * N}$$

The relation between the force F and the end-to-end distance x for ssDNA can be described with a modified FJC model:

$$x(F) = L_C \left[\coth \left(\frac{F * L_K}{k_B T} - \frac{k_B T}{F * L_K} \right) \right] \left(1 + \frac{F}{S} \right)$$

where S is the stretch modulus of ssDNA. Experimentally determined values for the Kuhn length and the stretch modulus are: $L_K = 1.5$ nm and $S = 800$ pN [127].

2.1.2.4 Mechanical Properties of dsDNA

dsDNA can be well described with the worm like chain (WLC) model. In contrast to the FJC model, the WLC model treats the polymer as an isotropic rod that is continuously flexible. The persistence length L_P is a measure of its rigidity and equals the distance at which the correlation of two tangent vectors has decreased to $1/e$:

$$\langle \vec{t}_{(s)} * \vec{t}_{(0)} \rangle = e^{-s/L_P}$$

where s is the contour distance between two points along the polymer. Under physiological conditions, the persistence length L_P of dsDNA is approximately 50 nm [127].

2.1.2.5 Melting Behavior

For many applications involving DNA, the melting temperature T_m is significant. T_m is defined as the temperature at which half of the dsDNA has been denatured into ssDNA. This makes the melting temperature a measure for the stability of a dsDNA sequence. The T_m of a given duplex depends on the length and the sequence of the duplex, as well as the pH value and the salt concentration of the buffer. A variety of numerical methods for the calculation of the melting temperature exist [128]. Empirical approximations give a good result in calculating the melting temperature. The simple Wallace rule [129] is applicable for perfect duplexes 15 to 20 bases in length [130]:

$$T_m = 2^\circ\text{C} * N(AT) + 4^\circ\text{C} * N(GC)$$

Here, $N(AT)$ and $N(GC)$ stand for the number of AT and GC base pairs, respectively. For oligonucleotides longer than 50 bases, the following expression [131] is valid :

$$T_m = (81.5 + 16.6 \log[M+] + 0.41(\%GC) - \frac{500}{n} - 0.62(\%F) - 1.2 * D)^\circ\text{C}$$

Here, $[M+]$ is the concentration of monovalent ions, $(\%GC)$ is the ratio between GC and AT base pairs, $(\%F)$ the formamide content and D the number of mismatches. These two methods are adequate for most purposes, however, they do not take the effect of base sequence (as opposed to base composition) into account. A more accurate estimation of T_m includes the thermodynamic interactions of all nearest-neighbor parameters [132]. In this method, changes of entropy and enthalpy (ΔS and ΔH) of the melting process are calculated for each dimer in the duplex and then T_m is estimated as following:

$$T_m = \frac{\Delta H}{\Delta S + R \ln c/4} - 273.15^\circ\text{C}$$

where R is the gas constant and c the molar strand concentration. A detailed explanation of melting and secondary structure formation can be found in reference [133].

2.2 DNA ORIGAMI

In DNA origami [30], a long DNA single strand of viral origin (the scaffold) is folded into a desired shape by hundreds of short, chemically synthesized oligonucleotides (the staples) (figure 9). Typically, M13mp18 bacteriophage derived genomic DNA of lengths of around 7 to 8 kbp is used as scaffold material. For the assembly, the scaffold is mixed with

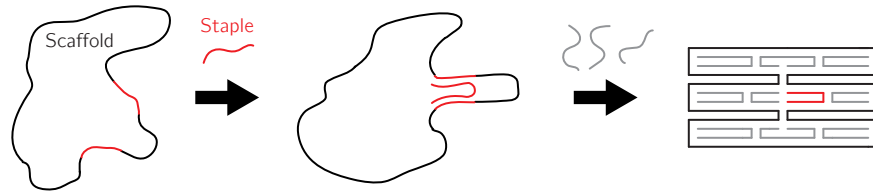


Figure 9: The long circular single stranded scaffold is “stapled” by a short oligonucleotide (red), the staple, which has at least two complementary sections on the scaffold molecule. When all staple oligonucleotides are added, the scaffold is folded into the predefined shape. The adjacent antiparallel helices are held in place by double crossovers in the form of holliday junctions.

the staples in a molar excess (typically five or ten times molar excess of each individual staple over the scaffold) together with salt (usually divalent magnesium ions) in a buffer solution. The mixture is heated to at least 65°C in order to render all the DNA in solution single-stranded. This mixture is then slowly cooled down to room temperature over the course of one hour to up to several days, depending on the complexity of the designed geometry. During this cooling process, the staples attach to their complementary parts on the scaffold and an array of antiparallel double helices is formed (an exemplary structure is shown in figure 10).

Theoretical and experimental results confirmed Paul Rothemunds’s original assumption [30] that this process is highly cooperative: scaffold-staple duplexes with a high melting temperature (indicated by a high G-C content) form at higher temperatures. These duplexes then act as nuclei that promote the hybridization of neighboring staples with a lower T_m [45, 47, 116]. This also explains the experimentally observed hysteresis between the critical annealing temperature of origami struc-

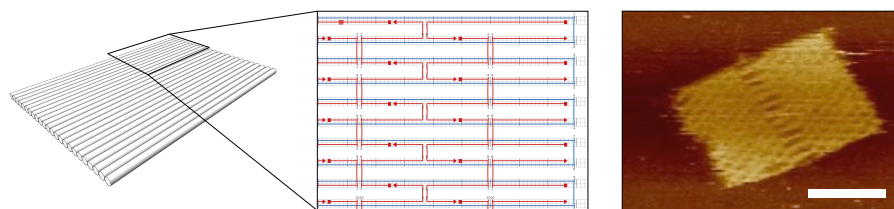


Figure 10: A 2D DNA origami rectangular structure. It measures $70\text{ nm} \times 100\text{ nm}$ and is 2 nm high (the diameter of a double helix). Left: Computer animated representation of the design: it consists of 24 neighboring antiparallel double helices represented as cylinders. Middle: Section of the design blueprint. It shows the scaffold path through the structure (in blue) folded into shape by the staple oligonucleotides (in red) via double crossovers between two adjacent helices. The 5'-end of the staples is represented by squares, the 3'-end by arrow heads. Right: AFM image of the folded object. The scale bar is 50 nm

tures during cooling and the critical melting temperature of structures during heating [45, 116]. Branch migration functions as an error correction during the assembly: incorrectly bound staples and intra-molecular secondary structures of the scaffold will be displaced eventually by the perfectly complementary staples. This error correction, combined with the fact that the relative stoichiometry between the staples (they are not designed to bind to each other as they would be in non-scaffolded DNA nanostructures) is not important, makes the self-assembly of DNA origami structures not only work, but extremely efficient.

The groups of Kurt Gothelf and William Shih extended the DNA origami method to three dimensions [31, 134]. The two approaches are fundamentally different. Andersen and co-workers from Gothelf's group designed a 3D box out of 2D rectangular origami sheets with a controllable lid. Shawn Douglas and co-workers from William Shih's group showed that a flat array of parallel helices can be folded into 3D objects (figure 11 illustrates this concept with the six helix bundle (6HB) origami as an example). In their work, individual helices are arranged on a hexagonal honeycomb lattice with staple crossovers to adjacent helices. The inherent geometry of dsDNA allows the construction of crossovers at angles of exactly 120° while maintaining the B-form DNA configuration with 10.5 bp per full helical turn.

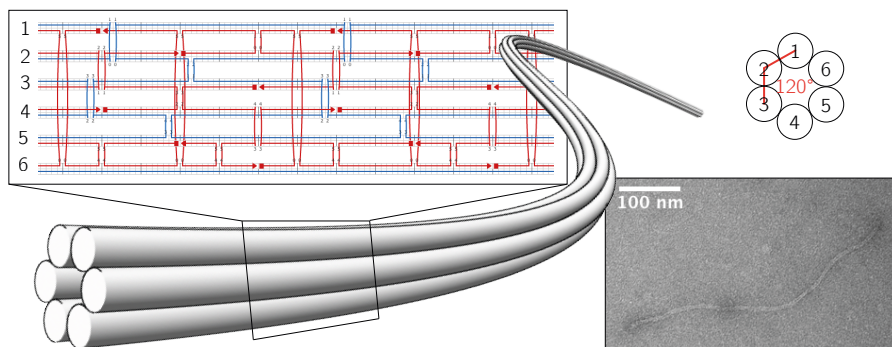


Figure 11: 3D DNA origami structure: a 6HB. The 6HB can be conceptualized as six neighboring antiparallel helices folded into a hexagon, which is the unit cell of a honeycomb lattice. In this arrangement, each helix has a maximum of three direct neighbors and double crossovers to adjacent helices are possible in 120° angles. 2D schematic of the scaffold (blue) and staple (red) paths. Scaffold and staple crossovers are only possible between helices that are adjacent in the honeycomb lattice. The TEM image shows a 420 nm long 6HB.

The method was further extended when, in the same year, Dietz et al. showed that by a controlled pattern of base deletions and insertions, twisted and curved origami objects of nearly all possible geometries can be realized [32]. Since then, the DNA origami design space has been more and more extended. Densely packed arrangement of helices in a square lattice were realized by Ke et al. [135]. Hao Yan's group published hollow 3D origami structures with complex curvature [34] and

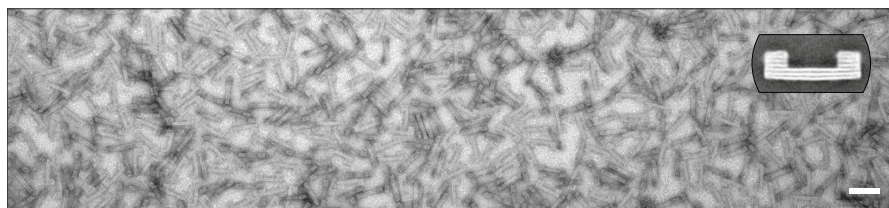


Figure 12: Section of a zoomed out TEM image of assembled origami structures. The inset shows an average image of the same structure. The scale bar is 100 nm. A detailed description of this structure is given in chapter 5.

DNA gridiron nanostructures [136]. 3D pre-stressed tensegrity origami structures were presented by Tim Liedl et al. [33] and most recently, several groups accomplished the automated design of virtually any polyhedral geometrie with triangulated DNA origami structures [35–38].

The great promise of the DNA origami technique results from the following two main characteristics. First, DNA origami folding is a highly parallel self assembly process. In a typical assembly reaction (for example in a 100 μ L volume with a concentration of scaffold material of 10 nM/L), the simple one-pot thermal annealing yields 10^9 individual structures, assembled at the same time without any outside manipulation. To illustrate the high degree of parallelization, a zoomed out TEM image of origami structures adsorbed on a surface after a typical annealing reaction is shown in figure 12. Second, every base of every staple in a DNA origami structure can theoretically be individually adressed. Modern chemical synthesis makes it possible to modify each base in an oligonucleotide with a variety of chemical moieties such as organic fluorophores, reactive groups for click chemistry, conjugation molecules for peptides and proteins, and many others. Combined with the knowledge of the position in space of every base in an origami structure, we can think of such an origami structure as a nano-breadboard with sub-nanometer addressability. Some examples of this addressability are shown in figure 13.

The design of DNA origami structures is typically done using the computer aided design software package caDNAno [135, 138]. The design routine contains three steps: (I) a geometrical model that approximately matches the desired shape is defined; (II) the structure is filled with antiparallel double helices and a scaffold path passing through the whole structure is selected; (III) complementary staple strands (typically around 200 individual staples) are assigned to the scaffold. Finite element [139] and coarse-grained [140–143] simulation tools help to refine the design *in silico* before any physical experiment has to be run. So far, however, definite design rules (regarding for example the crossover density, sequence composition at crossovers, staple-scaffold segment lengths, etc.) are not yet formulated and are still being investigated [117, 144]. Experimental techniques for the assessment of the

The open source software package caDNAno can be downloaded from <http://cadnano.org/>

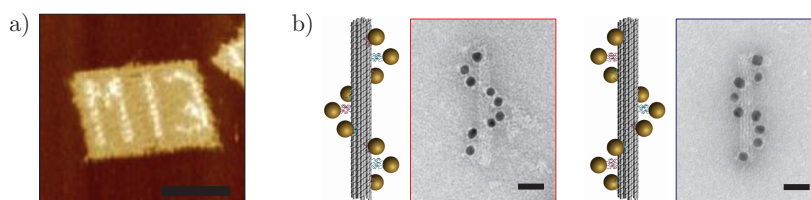


Figure 13: a) AFM image of a 2D origami structure with “M13” written on top of it [137] using dumbbell shaped hairpins [30]. The scale bar is 50 nm. A detailed description of this structure is given in chapter 3. Reprinted by permission from WILEY-VCH: SMALL [137], copyright (2014). b) Left- and right-handed origami and gold nanoparticle nano-helix and their corresponding TEM image next to it. The scale bar is 20 nm. Reprinted by permission from Macmillan Publishers Ltd: Nature [101], copyright (2012)

quality of folding and structural integrity include Cryo-EM [145], fluorescent probes [112], and Small Angle X-ray Scattering [146, 147].

2.3 EXPERIMENTAL METHODS

DNA origami structures are usually smaller than 100 nm, at least on two of the three spatial axes. It is not possible to fully visualize these structures with conventional optical microscopy due to the diffraction limit of visible light. However, biochemistry and biophysics offer other experimental techniques to study these objects. The quantification of the DNA-specific absorption of light is carried out with UV/Vis spectroscopy. UV/Vis spectroscopy and another spectroscopic technique, fluorescence spectroscopy, can be used to monitor DNA hybridization and even the folding of full origami structures in real-time [45, 46, 116]. A commonly used technique to study conformational changes and enzymatic modifications of DNA and DNA based structures is gel electrophoresis. Imaging of DNA and DNA assemblies is routinely carried out using TEM and AFM [30, 31, 83, 145]. The latter, together with other manipulation tools such as optical- and magnetic tweezers is also used for force measurements on single DNA strands [127, 148, 149], DNA devices [150], and DNA nanostructures [151–155]. An optical method to obtain insight into conformational changes of DNA based machines and structures is fluorescence and Förster resonance energy transfer (FRET) in particular [134, 156–158]. Recent advances in far-field fluorescence microscopy below the diffraction limit (super-resolution microscopy) have made it possible to analyze DNA origami structures in the sub-100 nm regime optically [49, 52, 159, 160].

2.3.1 UV/Vis Spectroscopy

UV/Vis spectroscopy can be used to determine the molar concentration of nucleic acids present in solution (see 2.1.2.1 for the optical properties of DNA). The concentration of nucleic acids in solution can be derived after measuring the optical density A at 260 nm of a sample by the law of Lambert-Beer:

$$A = \log \frac{I_0}{I} = \epsilon * l * c$$

I_0 is the intensity of incident light and I the intensities of transmitted light, ϵ is the wavelength-dependent molar extinction coefficient of the molecule of interest, l the length of the light path through the sample, and c the molar concentration. For long sequences of DNA, approximate conversion factors exist: the average mass for a measured optical density (OD) of 1 is 50 μg of dsDNA and 33 μg of ssDNA in 1 mL solution. The absorbance of the four individual bases are different, thus these conversion factors are not accurate enough to be applied to short oligonucleotides where the influence of the particular sequence matters. Greater accuracy is achieved when the exact value of ϵ is calculated [161, 162] for each particular sequence by the following equation:

$$\epsilon_{260\text{nm}} = 2 * \left(\sum_1^{N-1} \epsilon_{\text{nearest-neighbor}} \right) - \sum_2^{N-1} \epsilon_{\text{individual}} + \sum_1^N \epsilon_{\text{modification}}$$

Here, N is the total number of bases, $\epsilon_{\text{nearest-neighbor}}$ the nearest neighbor coefficient for a base pair, $\epsilon_{\text{individual}}$ the coefficient for an individual base, and $\epsilon_{\text{modification}}$ the coefficient for a base modification. Typical modifications are fluorescent dyes or chemical residues such as biotin.

2.3.2 Electrophoresis

The information presented in this sub-section is primarily based on reference [130].

Probably the most common technique for the analysis of DNA is gel electrophoresis. It is also routinely used for the purification of nucleic acids. It enables the sorting of charged molecules (it is not only used for nucleic acids but also routinely applied to proteins) based on a combination of molecular characteristics such as size, hydrodynamic radius, net charge, and surface charge density. An electric field is applied to a gel matrix to move charged molecules through a matrix. Typical matrices are agarose and polyacrylamide gels. Agarose and polyacrylamide are polymers that can be crosslinked and the porosity of the resulting gel can be controlled via the concentration of agarose or polyacrylamide's crosslinker in aqueous solution. The decision for a certain gel material depends on the sizes of the macromolecules that need to be separated.

Polyacrylamide gels are typically chosen for separating small fragments of DNA (up to 500 bp), and size differences as little as 1 bp in length can be separated from one another. Agarose gels, in contrast, yield a lower resolution, but have the advantage of a greater range of separation. Fragments from 50 bp to several megabases in length can be separated.

Agarose is a linear polysaccharide composed of alternating residues of D-galactose and 3,6-anhydro-L-galactose. Agarose chains form helical fibres and gelation of these agarose fibers results in a 3D net with channels of diameters ranging from 50 nm to more than 200 nm. Polyacrylamide gels are made via the polymerization of acrylamide monomers into long, crosslinked chains. This reaction requires the presence of the crosslinker bisacrylamide and is initiated by free radicals, which are typically provided by the reduction of ammonium persulfate by TEMED. The pore size in polyacrylamide gels is much smaller than in agarose gels.

To separate the samples, the gel is placed in a buffer-filled electrophoresis chamber, the samples are filled in wells in the gel, and an electric field is applied. The molecules migrate at different speeds through the gel: to the anode, if they are negatively charged (such as DNA), or towards the cathode if they are positively charged. The speed of migration of DNA through gels is determined by different factors. One factor is the molecular size of the DNA fragment. Larger molecules of dsDNA migrate more slowly because of higher frictional drag. They worm their way through the gel pores less efficiently than smaller molecules. Furthermore, the conformation of the DNA plays an important role. Linear, nicked circular, and supercoiled circular DNA's have different migration speeds. Although the relative mobilities of these forms primarily depend on the gel concentration, they are also influenced by the following aspects: the density of superhelical twists in the supercoiled form, the applied voltage, and the ionic strength of the buffer used. All of these aspects make the exact prediction of the migration speed of a given DNA sample difficult. Additionally, single-stranded DNA often folds into complex secondary structures, which influences its speed of migration in a largely unpredictable manner. This can be overcome by the use of chemical agents which destabilize hydrogen bonds (such as urea or formamide) to denature nucleic acids and therefore cause them to behave in a more predictable way.

After sufficient separation, the DNA molecules are usually stained with intercalating fluorescent dyes (such as ethidium bromide). These dyes render the DNA visible under ultraviolet light. For purification, the band of interest can be physically extracted and purified from the surrounding gel matrix.

2.3.3 Atomic Force Microscopy

The AFM, developed in 1986 [12], is a scanning probe microscopy technique with demonstrated sub-nanometer resolution. A sharp tip with a radius of curvature on the order of a few nanometers is mounted on the end of a flexible cantilever arm. This tip is used to scan the specimen surface. When the tip comes into proximity of the sample surface, forces between the tip and the surface lead to a deflection of the cantilever. Various interactions contribute to this deflection: (I) van der Waals interactions, (II) electrostatic interactions, and (III) dipole-dipole interactions. The deflection of the cantilever is measured via a laser spot that is reflected from the top surface of the cantilever into an array of photodiodes. This deflection information is used as a feedback parameter to adjust the distance between the tip and the sample.

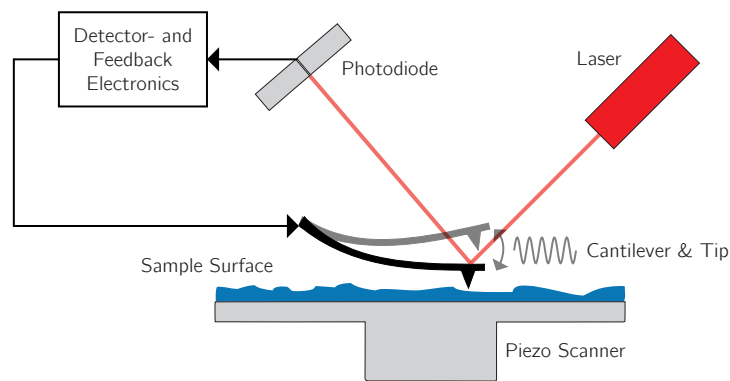


Figure 14: Schematic drawing of an AFM in intermittent contact mode.

Different imaging modes exist, however, the force exerted by the tip onto the sample is ideally maintained constant in all of them. For biological samples, the most gentle imaging mode is the intermittent contact mode and this mode was used for all AFM images presented in this thesis. A schematic drawing of an AFM operated in intermittent contact mode is shown in figure 14. In the intermittent contact mode, the cantilever is driven to oscillate near its resonance frequency. The tip-to-surface interactions damp the amplitude of the oscillation of the cantilever. The amplitude is used as a feedback parameter to keep the height of the cantilever over the surface on a constant level. This “tapping” method significantly reduces the damage done to the sample and the tip compared to imaging in full contact with the sample.

DNA can be easily immobilized to the surface via electrostatic interactions: Typically, a freshly cleaved mica surface (negatively charged) is saturated with divalent, positively charged ions such as magnesium. The negatively charged DNA structures can adsorb from the solution to the modified surface. Imaging in intermittent contact mode is then carried out in fluid usually using a buffer containing magnesium ions. [163]

2.3.4 *Transmission Electron Microscopy*

The TEM is capable of a significantly higher resolution than conventional optical light microscopes. Instead of visible light, it uses a beam of electrons that is transmitted through a thin specimen. Electrons that are not scattered or absorbed in the specimen are detected on either a fluorescent screen, photographic film, or a CCD camera. The maximum resolution can be defined as the minimal distance d between two points at which they can still be resolved as separate points. The minimum d of conventional optical light microscopy is limited by the wavelength of light being used to probe the sample of interest:

$$d = \frac{\lambda}{2 * NA}$$

with λ being the wavelength and NA the numerical aperture. For conventional optical light microscopy, d_{min} is around 250 nm. The wavelength of electrons, however, is related to their kinetic energy and is given by the de Broglie equation:

$$\lambda = \frac{h}{p}$$

with the Planck constant h and the momentum of the electron p . The de Broglie wavelength of electrons is several orders of magnitude smaller than the wavelength of visible light, thus theoretically allowing for imaging with atomic resolution. This was realized early on after the publication of the De Broglie hypothesis and the first commercial TEM from *Siemens* was installed already in 1939 (figure 15 shows a photograph of the machine). Ernst Ruska, one of the pioneers of the development of the TEM, shared the nobel prize for physics in 1986 with Binnig and Rohrer.



Figure 15: Photograph of the first commercial TEM. Originally installed at IG Farben Werke in 1939, it is now on display at the Deutsches Museum in Munich, Germany. Image source: [164] (CC BY-NC-SA 2.0)

In a TEM, the electrons are generated via thermionic emission from a filament and then accelerated in an electric field. The higher the acceleration voltage, the smaller the wavelength λ of the generated electrons and thus the theoretically achievable resolution. After acceleration, the beam of electrons is focused onto the specimen by electromagnetic lenses.

Most biological samples (including DNA) give a poor contrast in electron microscopy. Thus, these samples typically require a treatment with a staining solution containing heavy atoms prior to the imaging. All TEM images of DNA origami structures shown in this thesis were taken from samples stained with either uranyl acetate or uranyl formate.

2.3.5 *Single-Molecule FRET and ALEX*

The transfer of energy from one chromophore to another is called FRET. A donor fluorophore, which is initially in its excited state, transfers energy to an acceptor fluorophore, which is initially in its ground state, via nonradiative dipole-dipole coupling [165, 166]. Upon excitation, the donor fluorophore absorbs a photon and is excited from the ground state S_0 to a higher vibrational level of S_1 . The donor molecule relaxes into the lowest vibrational level of S_1 and subsequently to the ground state. If the acceptor molecule is in close proximity and its absorption spectrum overlaps with the emission spectrum of the donor, the energy difference between the two states is transferred radiationless to the acceptor. This means that the donor relaxes without the emission of a photon and is instead exciting the acceptor. After internal relaxation, the acceptor emits a redshifted photon (if it is a fluorophore) or dissipates the transferred energy without radiation (if it is a dark quencher). Figure 16a shows this effect schematically.

The efficiency of the energy transfer from donor to acceptor depends strongly on the distance r between the two (figure 16b). The Förster radius R_0 is the distance at which the energy transfer efficiency E is 50% and is described by the following equation:

$$E(r) = \frac{R_0^6}{R_0^6 + r^6}$$

Commonly used FRET pairs such as Cy3-Cy5 have a Förster radius R_0 of approximately 5 – 6 nm. R_0 is a function of the fluorescence quantum yield of the donor Q_D , the dipole orientation factor κ^2 , the refractive index of the medium n and the overlap integral $J(\lambda)$ of the donor emission spectrum with the acceptor absorption spectrum. It can be calculated for a given donor-acceptor pair from spectroscopic data. The overlap integral $J(\lambda)$ is defined by the following equation:

$$J(\lambda) = \int_0^{\infty} F_D(\lambda) \epsilon_A(\lambda) \lambda^4 d\lambda$$

where $F_D(\lambda)$ is the normalized fluorescence intensity of the donor fluorophore and $\epsilon_A(\lambda)$ is the extinction coefficient of the acceptor at the wavelength λ . For fluorophores that are able to rotate freely and are isotropically oriented during the lifetime of their excited state, the dipole orientation factor is typically approximated with $\kappa^2 = 2/3$ [167]. The fact that E scales with $1/r^6$ makes FRET spectroscopy a highly sensitive technique to measure distances in the range of 1 nm to 10 nm.

The analysis of ensemble FRET measurements is often complicated by a pronounced heterogeneity inherent to most samples. This heterogeneity can be attributed to several reasons: free fluorescent dye in the background, unlabeled molecules of interest that remain undetected, inactive fluorophores at the time of excitation, and unsynchronised species. Measuring FRET on the single-molecule level is a common way of addressing these problems, at least partially. Typical single-molecule FRET spectroscopy experiments use only a single excitation wavelength. A continuous multiwavelength excitation approach renders the extraction of accurate FRET efficiencies complicated due to the uncertainty over the source of the acceptor emission photons. Emission in the acceptor channel could result from FRET but also from direct acceptor excitation. Alternating laser excitation (ALEX) spectroscopy obtains donor excitation and acceptor excitation based observables for each single molecule by rapid alternation between the donor and acceptor excitation. The technique was developed in the group of Shimon Weiss in the early 2000's as a general FRET based method for the study of struc-

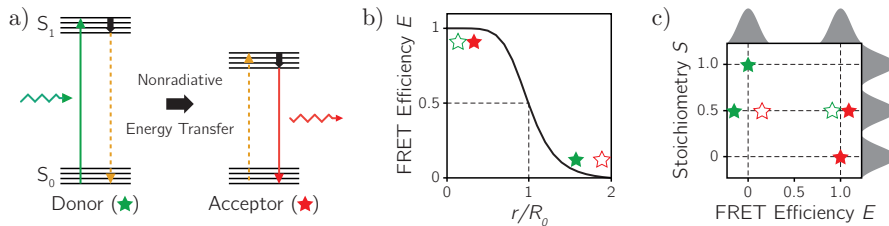


Figure 16: a) Jablonski diagram of nonradiative energy transfer between two fluorophores with overlapping emission and absorption spectra. b) The FRET efficiency E plotted as a function of the ratio between the donor-acceptor distance r and the Förster radius R_0 . At $r/R_0 = 1$, half of the energy is transferred from the donor to the acceptor molecule resulting in a FRET efficiency of $E = 0.5$. c) Idealized $E - S$ histogram showing four different populations: donor (green) only ($E = 0, S = 1$), acceptor (red) only ($E = 1, S = 0$), donor-acceptor pair separated by a long distance resulting in low FRET ($E = 0, S = 0.5$), and donor-acceptor pair separated by a short distance resulting in high FRET ($E = 1, S = 0.5$).

ture *and* interaction at the same time [168–170]. In ALEX, two distinct emission signatures are collected by calculating the following two fluorescence ratios: the FRET efficiency E and the stoichiometry S . E as a measure for the donor-acceptor distance is calculated from the recorded data as follows:

$$E = \frac{F_{D_{exc}}^{Aem}}{F_{D_{exc}}^{Aem} + \mu F_{D_{exc}}^{Dem}}$$

with the donor emission upon donor excitation $F_{D_{exc}}^{Dem}$, the acceptor emission upon donor excitation $F_{D_{exc}}^{Aem}$ and a detection correction factor μ . S is a distance-independent measure for the relative donor and acceptor stoichiometry and is calculated as follows:

$$S = \frac{F_{D_{exc}}}{F_{D_{exc}} + F_{A_{exc}}}$$

with the sum of donor excitation based emissions $F_{D_{exc}}$ and the sum of acceptor excitation based emissions $F_{A_{exc}}$. For donor-only species, $F_{A_{exc}} = 0$ and thus $S = 1$. For acceptor-only species, $F_{D_{exc}} = 0$ and thus $S = 0$. Species with exactly one donor and one acceptor ideally result in a S value of 0.5. Typically, a gaussian distribution around this value is observed due to photophysical properties of the dyes and slight variations in their efficiency of detection. Since S is independent of the distance between donor and acceptor, it is useful for the thermodynamic and kinetic analysis of interactions. S also reacts very sensitive to changes in brightness of the donor or acceptor dyes and thus can indicate changes in the local environment of the species. The values for E and S are typically plotted in a 2D histogram (an idealized $E - S$ histogram is shown in figure 16c) that allows virtual sorting of molecules. Another advantage of ALEX is its compatibility with time scales of sample dynamics ranging from nanoseconds to milliseconds.

DNA ORIGAMI STRUCTURES DIRECTLY FOLDED FROM INTACT BACTERIOPHAGES

For most applications of DNA origami beyond the proof-of-principle laboratory scale, whether this is in drug delivery, biosensing, or materials science, large quantities of DNA structures on at least the gram-scale are required [107, 109]. The two components of DNA origami structures are the single-stranded scaffold and the roughly 200 individual short staple oligonucleotides. The staples are chemically synthesized and purchased from commercial suppliers. Via chemical synthesis, single-stranded DNA of lengths up to 100 nucleotides can be produced routinely and economically with quality and purity sufficient for proof-of-principle laboratory scenarios. The coupling efficiency in chemical synthesis of roughly 99%, however, means that already an oligonucleotide of 20 base length will have a failure rate of 20%. Consequentially, the scaffold strand has to be derived from a different source than chemical synthesis.

3.1 INTACT BACTERIOPHAGES AS A SOURCE OF SCAFFOLD

Several enzymatic methods can be applied to make long ssDNA in vitro. Examples are asymmetric polymerase chain reaction (PCR) [171], rolling circle amplification [114, 172–175], or the separation of biotinylated strands with magnetic beads after denaturation [176]. Nevertheless, these methods rely on the use of purified enzymes and/or deoxynucleotides and the amount of ssDNA is practically limited to the milligram scale [109]. The most scalable method of production of ssDNA is the use of bacteriophages in *Escherichia coli* (*E.coli*) hosts. Bacteriophages are viruses that infect and replicate within bacteria. The scaffolds typically used for DNA origami are variants of bacteriophage M13mp18 genomic DNA. Most researchers purchase from commercial suppliers at great costs. The price of these scaffolds often dominates the cost (depending on the supplier, up to 80% of the cost can be attributed to the scaffold [30]). These costs can be reduced by using self-produced scaffold material. The method of choice for in-house production of bacteriophage scaffold DNA is a standard shake flask scale with reported yields on the order of 10 mg of purified ssDNA per liter of culture [130, 177]. Additionally, the purification from the bacteriophage particles involves several steps, which reduces the potential for scaling and automation. The challenge of scaling the scaffold production was recently addressed with the development of efficient production methods using high-cell-density fermentation in stirred-tank bioreactors [109].

In the first part of the associated publication P1, we presented a method that uses intact bacteriophage particles instead of purified genomic bacteriophage ssDNA directly in the thermal annealing of DNA origami structures. We tested this method with different DNA origami geometries and concluded that the assembly yield and quality is indistinguishable of the control structures prepared conventionally. As a next step, we used a crude bacteriophage suspension as a scaffold source. First, the *E. coli* cells are infected with bacteriophages in a liquid culture. After sufficient incubation, the *E. coli* cells are removed via simple centrifugation and the staples and some detergent is added to the crude suspension of intact phages. This suspension includes all the remaining components from the growth medium and excreted metabolic products from the bacteria. After an initial heating step to 65 °C, thermal annealing is then carried out at a constant temperature experimentally identified for each origami design according to reference [116]. As a prove of principle, we tested this approach with a 6HB origami structure on the milliliter scale with thermal annealing in a simple water bath (schematically shown in figure 17). Again, the yield and quality of assembled structures were indistinguishable from the control sample.

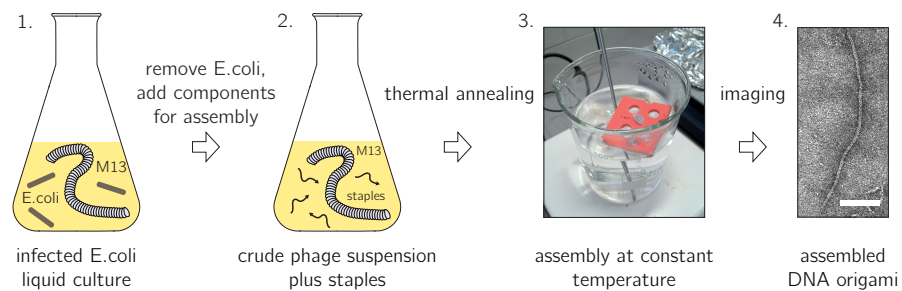


Figure 17: Illustration of the crude phage suspension as scaffold source. (1.) *E. coli* cells infected with M13 bacteriophage are grown in a liquid culture. The cells amplify the phage and secret progeny phage particles into the surrounding medium. (2.) The bulky *E. coli* cells are removed via centrifugation. The staples needed for DNA origami folding are added to the suspension. The scaffold is inside the intact phage particle. Detergent is added in small amounts to help the release of the scaffold from the phage. (3.) After an initial heating step to release the scaffold from the phage, the suspension is incubated at a constant temperature to anneal the origami. Shown is a photograph of a proof-of-principle experiment with 6HB structures, folded using a simple heating plate with temperature control instead of a thermocycler. (4.) TEM micrograph of a 6HB structure after annealing in the water bath. The scale bar is 100 nm.

Our results imply that DNA origami nanostructures can be successfully folded in a complex mixture of biological compounds. We envision that this approach can be easily combined with advances in enzymatic *in vitro* staple production developed in the Högberg group [114] and high-cell-density fermentation co-developed in the Dietz group [109].

Together with purification techniques such as rate-zonal centrifugation [115] or PEG-precipitation [111], all components for a fully automated, cheap, and easily scalable production of DNA origami structures from fully biotechnologically produced materials should now be available.

3.2 SCALING THE SIZE OF DNA ORIGAMI

The length of the scaffold molecule used for DNA origami limits the size of the assembled structure. The typically used bacteriophage M13 derived genomic ssDNA is the longest readily accessible scaffold up to now. Hierarchical assembly strategies were developed to increase the size of DNA origami structures, but these approaches typically suffer from low overall yields [178–180]. Increasing the length of the scaffold could enable the assembly of larger single structures while avoiding the low assembly yields in hierarchical assembly. Earlier efforts to produce longer ssDNA scaffolds achieved lengths of up to 26 kilobases [181–183]. In a second part of the associated publication P1, we presented a method where bacteriophage λ particles, which have 50 kilobasepair dsDNA genomes, were directly used as a scaffold source for an attempt to assemble a 2D DNA origami structure of a molecular weight of 64 MDa. The method used a double-stranded scaffold, earlier introduced by Högberg et al. [184]: a combination of heat and chemical denaturing agents is used to fully melt a double-stranded DNA. Followed by a sudden temperature drop and stepwise dialysis, two distinct DNA origami structures are folded in the presence of two separate sets of staple strands. In our approach, we designed two geometrically identical, but chemically different monomers that would together form a 2D homodimer origami structure, 200 nm by 400 nm in size. Unfortunately, we never succeeded to produce fully intact origami structures with satisfactory yield due to several experimental and technical limitations discussed in detail in the publication. In the meantime, the group of Thomas LaBean were able to produce a more than 50 kilobases long ssDNA scaffold from a λ /M13 hybrid phage [185].

3.3 ASSOCIATED PUBLICATION P1

**DNA Origami Structures Directly Assembled
from Intact Bacteriophages**

By

Philipp C. Nickels, Yonggang Ke, Ralf Jungmann, David M. Smith,
Marc Leichsenring, William M. Shih, Tim Liedl, and Björn Högberg

published in

Small (2014), 10, 1765 - 1769

Reprinted with permission from ref. [137]. Copyright 2014 WILEY-VCH.

DNA Origami Structures Directly Assembled from Intact Bacteriophages

Philipp C. Nickels, Yonggang Ke, Ralf Jungmann, David M. Smith, Marc Leichsenring, William M. Shih, Tim Liedl,* and Björn Högberg*

The scaffolded DNA origami technique^[1,2] has been successfully applied in a growing number of fields due to its simple and computer-aided design process,^[3–6] its versatility and its high production yields. It has enabled the self-assembly of a large variety of different two-dimensional (2D)^[1] and three-dimensional (3D)^[7–11] nanoscale geometries of high complexity as well as the super-assembly of individual constructs into large arrays of micrometer dimensions.^[12,13] Origami assemblies are usually composed of one long scaffold strand and hundreds of short oligonucleotides of programmed sequences that fold the long strand into a desired shape. Each construct can thus be designed *de novo* and is potentially addressable with nanometer precision. The most commonly used scaffold material is purified M13mp18 single-stranded DNA (ssDNA) derived from bacteriophage M13. The price of the scaffold molecule dominates the cost of M13 based DNA origami (about 80% of the overall cost when buying from the cheapest manufacturer and using a 10-fold excess of staple strands).^[1] These costs can be reduced by using self-produced and purified scaffold material, but the purification from the bacteriophage particles nevertheless involves several steps which reduces the potential for scaling and automation.

Different approaches to exploit various other scaffold sources have been reported: Hogberg *et al.* separated double-stranded DNA (dsDNA) – a 7560 kilobasepair (kbp) M13 derivative, the 4.7 kbp pEGFP plasmid and a 1.3 kbp polymerase chain reaction (PCR) product – to fold two distinct

DNA origami constructs from the two individual ssDNA molecules in a one-pot reaction.^[14] More recently Yang *et al.* used fragments of double-stranded λ -DNA as a unified scaffold for the assembly of single DNA origami structures and Pound and co-workers used PCR followed by strand separation to produce single-stranded scaffold molecules.^[15,16] Furthermore, as shown by Zhang and co-workers, where long-range PCR was used for the production of single-stranded scaffolds of up to 26 kb,^[17] alternative scaffold sources enable the assembly of larger single structures while avoiding often low-yield hierarchical assembly procedures.^[18–20] All these methods extend the DNA origami technique considerably but also rely on various time consuming and tedious modification steps of either naturally occurring or synthetic template DNA such as several purification steps, PCR, strand separation, enzymatic digestion and/or modification. In addition, for many promising applications of the DNA origami technique – such as nanomedicine or drug delivery – a large quantity of the material is needed. Scaling up the assembly process and maximizing the assembly yield while reducing both labor and cost remains a major challenge for the future development of the field.^[21]

Here we present a fast and versatile method for the direct employment of genomic nucleic acids from naturally occurring bacteriophages. Two bacteriophages (M13 and λ) were used as scaffold sources for the assembly of DNA origami constructs without further purification of the genomic DNA: intact bacteriophage M13 particles, which have ~7 kilobases long ssDNA genomes, were used as scaffold material to successfully fold four different 2D and 3D DNA origami structures; bacteriophage λ particles, which have ~50 kilobasepair (kbp) dsDNA genomes, were directly used as a scaffold source for an attempt to assemble a 2D DNA origami structure of a molecular weight of 64 MDa. Together with our recently published method for enzymatic generation of short oligonucleotides,^[22] the presented method opens a potential for scalable DNA origami production, deriving all necessary material directly from bacterial cultures without the need for downstream purification procedures.

Scheme 1 illustrates the basic principles behind our approach: the bacteriophage particles are mixed with the synthetic staple strands, chemical agents and enzymes to denature the phage particles as well as the dsDNA (in the case of bacteriophage λ), and buffer containing MgCl₂ needed for the assembly. The mixture is heated to assist

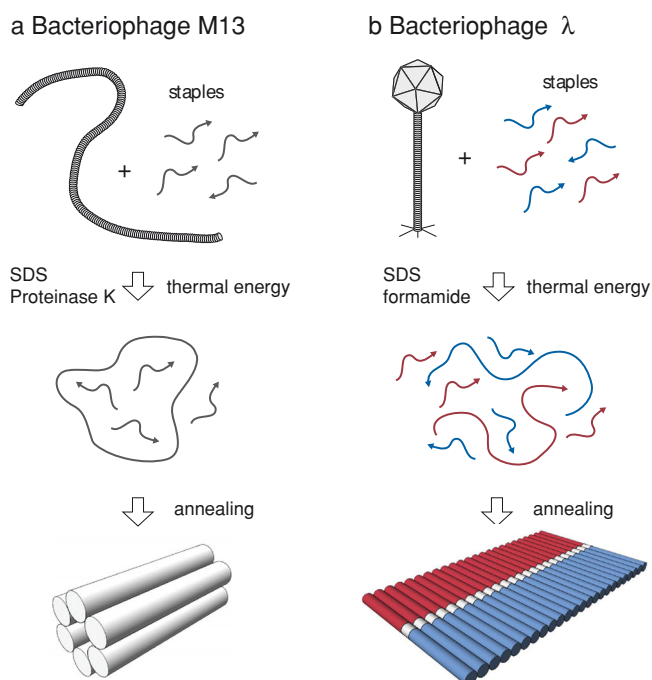
P. C. Nickels, D. M. Smith, M. Leichsenring, T. Liedl
Department of Physics & Center for Nanoscience (CeNS)
Ludwigs-Maximilians-Universität
Geschwister-Scholl-Platz 1, 80539, Munich, Germany
E-mail: tim.liedl@physik.lmu.de



B. Högberg
Department of Neuroscience
Swedish Medical Nanoscience Center
Karolinska Institute
Retzius väg 8, S-17177, Stockholm, Sweden
E-mail: bjorn.hogberg@ki.se

Y. Ke, R. Jungmann, W. M. Shih
Dana-Farber Cancer Institute
Harvard Medical School
44 Binney Street, Boston, MA 02115, USA

DOI: 10.1002/sml.201303442



Scheme 1. The phage particles are mixed with the staples and all components needed to denature the phage, release the scaffold DNA and assemble the DNA origami structure. The phages are denatured and the DNA origami structures are assembled via thermal annealing in a one-pot reaction. **(a)** Once the M13 phage is denatured, annealing is analog to conventional DNA origami: the staples fold the single-stranded scaffold into the designed shape. **(b)** After denaturing the λ phage, the double-stranded λ -DNA is denatured and the two single-strands (blue and red) are folded into shape by two sets of staples. Connector staples stitch the two parts together to create the final object.

the denaturing process of the phage particles and thus the genomic ssDNA or dsDNA is released. The DNA origami constructs are assembled in subsequent thermal annealing procedures as described later in the text.

First we used purified M13 suspensions to fold four previously described DNA origami assemblies directly from bacteriophage particles (**Figure 1a-d**, left): a 70×100 nm 2D rectangle^[1] from a 7249 base long M13 derivative, a 420 nm long six helix bundle^[23] (6HB) and a 70 nm long 24 helix bundle^[24] (24HB) from a 7560 base long M13 derivative, and a 30×50 nm three layer block^[25] from a 8064 base long M13 derivative. The M13 phages were prepared as previously described (supplementary note S1.1 & figure S1).^[23] For all four structures 5 nM of corresponding phage particles were mixed with 100 nM of each staple, 1x Tris-EDTA buffer, 5 mM NaCl, various MgCl_2 concentrations (12 mM for the 2D rectangle, 16 mM for the 6HB, 18 mM for the 24HB and 3 layer block), 0.1% SDS, and 1mg/mL Proteinase K. The samples were heated to 65 °C for 5 min and then cooled down to 25 °C via a nonlinear annealing ramp over the course of 2 to 40 hours (2 hours for the 2D rectangle, 16 hours for the 6HB and 3 layer block, 40 hours for the 24HB) (supplementary note S1.2 & figure S2).

After folding, the samples were analyzed and compared to control samples folded conventionally from purified scaffold via agarose gel electrophoresis. Comparing the intensity of the bands containing well formed structures to

the overall intensity of the lane shows that the constructs form with high yields comparable to those from the control sample folded from purified scaffold (**Figure 1a-d**). The 2D rectangle was dialyzed to remove the SDS for subsequent atomic force microscope (AFM) imaging. The 6HB, 24HB and three layer block were excised from the agarose gels for transmission electron microscope (TEM) imaging. AFM (**Figure 1a**) as well as TEM data (**Figure 1b-d**) confirm that indeed the designed geometries were formed, the structures are intact and after gel purification are free enough from contaminating protein to be used subsequently in applications requiring imaging of DNA origami (additional AFM/TEM data in figure S4). In all our experiments we could not observe a significant difference in assembly yield compared to conventional DNA origami assembly using purified scaffolding DNA. In addition, damage of the scaffold DNA due to protein degradation prior to the assembly could not be detected.

To test the potential of the presented method for the large-scale assembly of DNA origami structures, we folded structures directly from an M13 infected *E. coli* liquid culture without further purification of the phage particles. The only purification step was the removal of the *E. coli* bacteria via centrifugation at the point of harvest. First we tested whether a crowded environment full of biological compounds might inhibit the self-assembly process via the addition of increasing amounts of fetal bovine serum (FBS). The gel data (figure S3a) nicely shows that no significant decrease in assembly yield could be observed. Next we directly used a crude M13 phage suspension in liquid growth medium as a scaffold source to assemble the M13 based 6HB (figure S3b). A typical M13 liquid culture prep yielded a phage concentration of about 1 to 2nM. To the crude phage suspension (3/4 of the final sample volume) we added 12.5nM of each staple, 1xTris-EDTA buffer, MgCl_2 to a final concentration of 16nM, 0.1% SDS and 1 mg/mL Proteinase K. The mixture was then subjected to the same thermal annealing ramp as described before for the 6HB (detailed description in supplementary note S1.3 and figure S3b). The agarose gel analysis data as well as the TEM image of a gel purified sample (**Figure 1e**) show that the 6HB assembles directly from the crude phage suspension with a yield comparable to the control sample folded from the purified phage particles. The only difference is the small decrease in migration speed in the gel due to the high sodium concentration in the crude phage suspension (the *E. coli* growth medium used here contains 5g NaCl per 1L resulting in a final concentration of about 62nM NaCl when using 3/4 of the final sample volume).

Finally, we employed our method with the goal to increase the achievable size of single DNA origami structures to a larger bacteriophage, the bacteriophage λ . We designed two geometrically identical but chemically distinct monomers (rectangles, 100×400 nm in size) for each of the two λ -DNA single strands. Those monomers are connected via an extra set of staples to form the complete rectangular object of 200×400 nm in size (**Scheme 1**, detailed description in supplementary note S3.2 and figures S14-16). For initial control experiments we used commercially available λ -DNA.

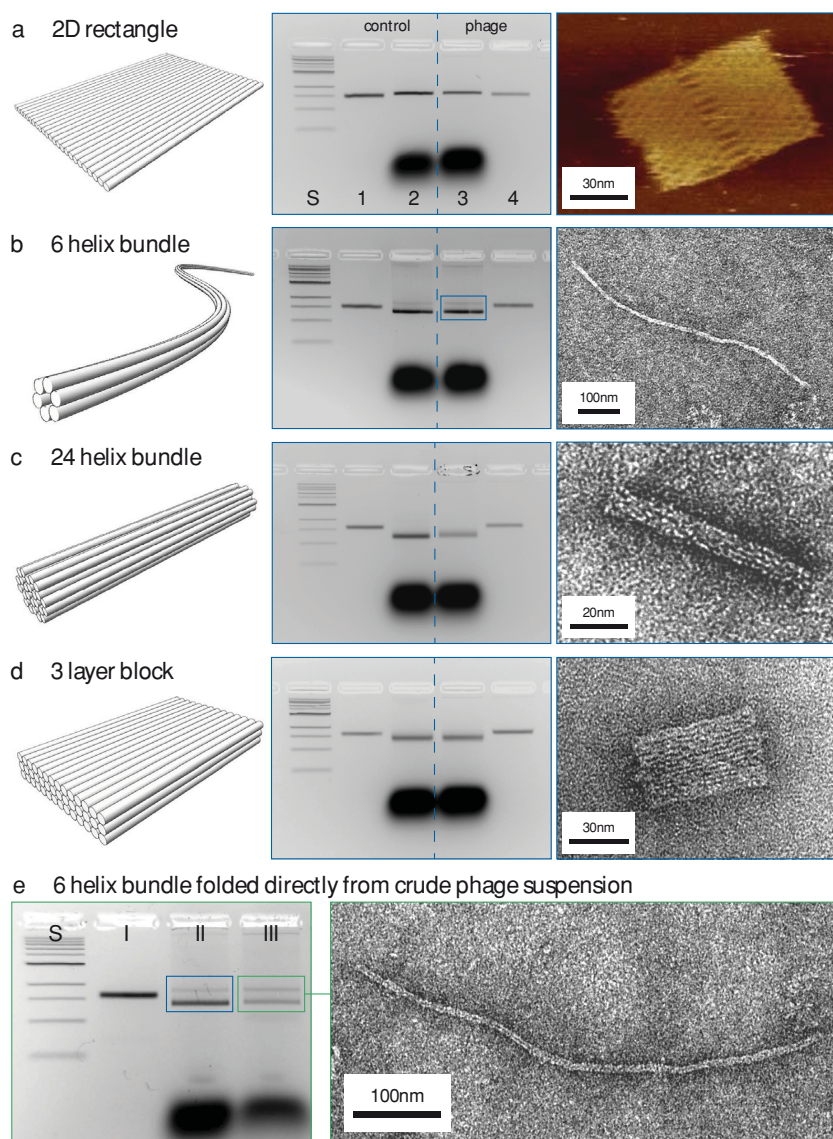


Figure 1. Folding directly from M13 phage. **(a-d) Left:** reduced complexity representations of the four different constructs. **(a)** 2D rectangle, **(b)** 6HB, **(c)** 24HB, **(d)** three layer block. **Middle:** 2% agarose gels of the four assemblies. **Lane S:** 1 kb DNA ladder. **Lane 1:** purified scaffold. **Lane 2:** folded from purified scaffold. **Lane 3:** folded from phage. **Lane 4:** denatured phage. **Right:** AFM **(a)** and TEM **(b-d)** images of structures folded from phage. **(e) Left:** agarose gel of the 6HB folded directly from the crude phage suspension. **Lane S:** 1 kb DNA ladder. **Lane I:** purified scaffold. **Lane II:** control 6HB, folded from purified phage (as in lane 3 from panel c). **Lane III:** 6HB folded directly from crude phage suspension. **Right:** TEM image of the 6HB folded directly from crude phage suspension, purified from lane III.

However, the purified λ -DNA exhibited nicks of the phosphate backbone, most likely resulting from mechanical stress during conventional DNA extraction and purification. Such nicked λ -DNA double strands dissociate into many random single-stranded fragments instead of just two single strands. This prevented the full assembly of the structure in our initial experiments (AFM images in **Figure 2d** and S9a). Next we prepared our own λ -phages (supplementary note S2.1 & figure S5) and compared the quality of the genomic DNA to the commercially available λ -DNA. Denaturing agarose gels showed that our ‘homemade’ λ -DNA directly released from

phage particles is intact (supplementary note S2.2 & figure S6).^[26,27]

We then proceeded to assemble the designed structure directly from our prepared λ phages. We mixed 0.2 nM λ -phage with 10 nM staples, 1x Tris-EDTA buffer containing 12 mM MgCl₂, 0.1% SDS, and 40% formamide. Formamide lowers the melting temperature of dsDNA by ~ 0.64 °C/%^[28] (melting curves of λ -DNA are shown in figure S7). The mixture was incubated at 80 °C for 15 min followed by a fast temperature drop to 25 °C in the presence of the excess of staple strands to prevent re-annealing of the two long λ -DNA single strands. The sample was subsequently cooled to 4 °C via a non-linear annealing and afterwards dialyzed overnight at 4 °C to remove the formamide and SDS (supplementary note S2.4 & figure S8).

Figure 2a shows an agarose gel of the assembled structure. Two separate bands – both migrating faster than the native dsDNA – are visible. High flexibility (and thus low stability) of our structure as well as the size and low concentration made the physical extraction from the gel with available purification methods impossible. Thus we were not able to directly identify these two species. In almost all instances AFM imaging of the sample after dialysis revealed only fragmented structures. This could be a result of mechanical stress during pipetting. Also the high amount of debris from the denatured λ -phage capsid proteins and remaining cell lysate covering the mica surface made finding as well as imaging the structures very difficult. AFM images also showed fully assembled monomers (Figure 2b) as well as almost completely folded rectangles (Figure 2c). Therefore we assume that the bands visible in the gel are indeed folded origami assemblies and represent assembled monomers (faster migrating band) and complete structures (slower migrating band). However, the results

shown in Figure 2 were the best results that could be imaged. All applied variations of the assembly procedure (elongated annealing times of up to 48 hours, changes in salt concentrations, higher scaffold to staple ratios, use of Proteinase K etc.) did not improve the results. Despite the unsatisfactory imaging results, we argue (the denaturing agarose gel data in figure S6 supports this) that our approach of using the intact λ -phage instead of the already purified λ -DNA has the advantage of preventing damage to the λ -DNA due to handling and storage that could otherwise greatly lower the quality of the scaffold material.

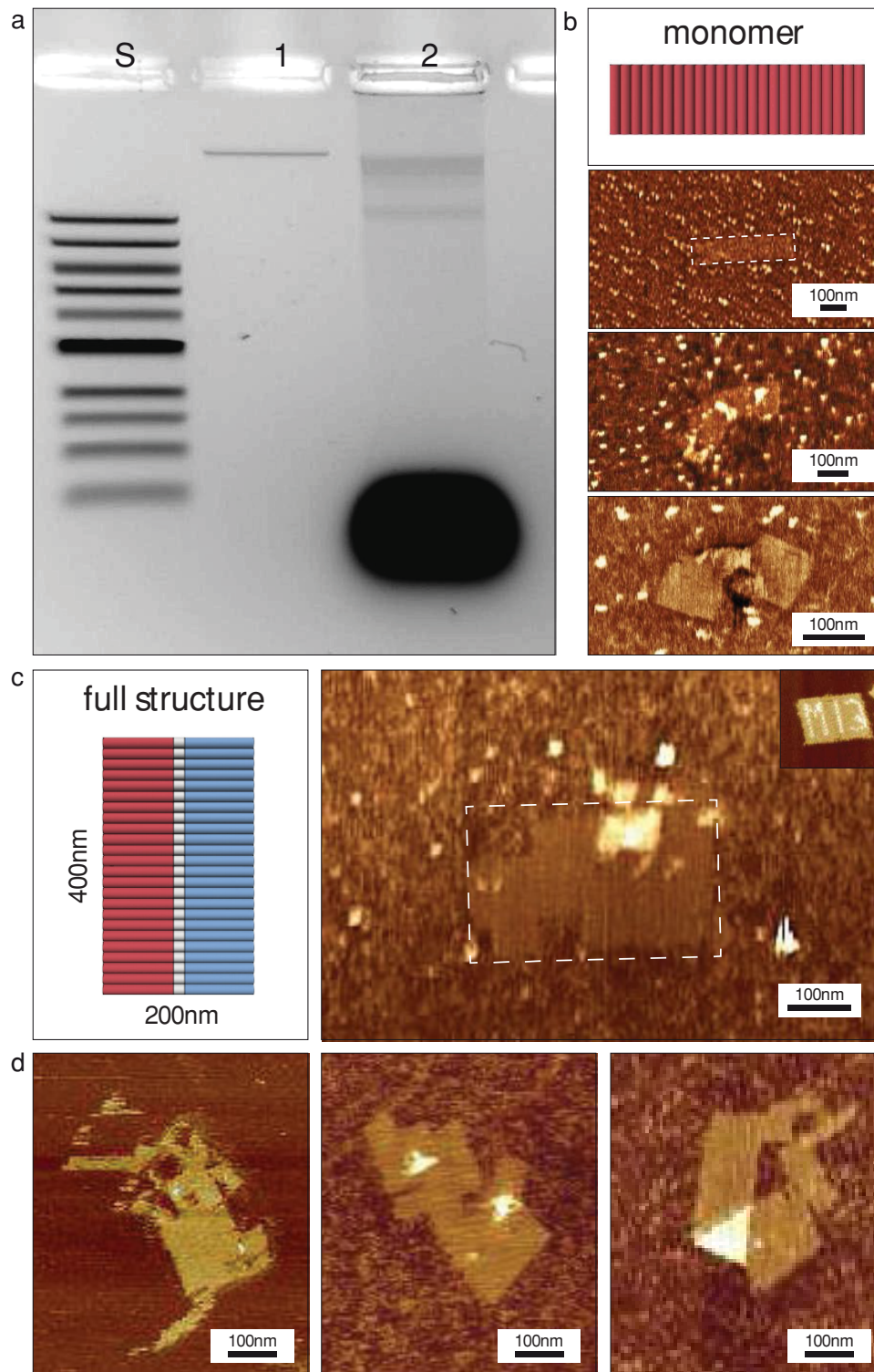


Figure 2. (a) 0.7% agarose gel: **Lane S:** 1kb DNA ladder. **Lane 1:** purified λ -DNA. **Lane 2:** folded structure after overnight dialysis. (b) AFM data of folded monomer structures w/o the connecting staples. The dashed line in the first image indicates the designed shape. The structure in the bottom image flipped over while being immobilized. (c) AFM data of full rectangular structure w/ connecting staples. The dashed line indicates the designed shape. The background of denatured phage proteins is clearly visible. The inset shows a M13 derived 2D rectangle (supplementary note S3.1 and figure S10) imaged with the same magnification for size comparison. We used dumbbell shaped hairpins for the 'M13' writing on the structure surface.^[1] (d) AFM data of full rectangular structure folded from commercially available λ -DNA.

To conclude, we demonstrated the successful high-yield folding of DNA origami structures directly from intact M13 bacteriophages and the direct assembly from a M13 infected

E. coli liquid culture. Furthermore we showed an approach to assemble a single DNA origami structure directly from the entire bacteriophage λ genome, although with low yields. Our

findings with the M13 bacteriophage imply that, combined with recent advances in enzymatic staple production,^[22] rapid folding at constant temperatures shown by Sobczak *et al.*^[29] and high-throughput purification methods such as rate-zonal centrifugation^[30] our approach might be one possible route towards a reliable large-scale, high yield and low-cost production of DNA origami structures.

Experimental Section

Detailed experimental procedures are presented in the Supporting Information.

Supporting Information

Supporting Information is available from the Wiley Online Library or from the author.

Acknowledgements

We thank J. Wohrstein for help with pipetting, S. Kempter for experimental support and S. Douglas, H. Høiberg and R. Schreiber for helpful discussions. This work was funded by a NIH New Investigator grant (1DP2OD004641-01) to W.M.S., the Swedish Research Council (Vetenskapsrådet) through a repatriation grant and a project grant to B.H. (grants 2010-6296 and 2010-5060) and the Deutsche Forschungsgemeinschaft DFG (TI 329/5-1). B.H. is a recipient of an assistant professorship with startup funding by Carl Bennet AB, Karolinska Institutet and Vinnova.

- [1] P. W. K. Rothmund, *Nature* **2006**, *440*, 297–302.
 [2] N. C. Seeman, *Annu. Rev. Biochem.* **2010**, *79*, 65–87.
 [3] S. M. Douglas, A. H. Marblestone, S. Teerapittayanon, A. Vazquez, G. M. Church, W. M. Shih, *Nucleic Acids Res.* **2009**, *37*, 5001–5006.
 [4] Y. Ke, S. Douglas, M. Liu, J. Sharma, A. Cheng, A. Leung, Y. Liu, W. Shih, H. Yan, *J. Am. Chem. Soc.* **2009**, *131*, 15903–15908.
 [5] D. N. Kim, F. Kilchherr, H. Dietz, M. Bathe, *Nucleic Acids Res.* **2011**, DOI 10.1093/nar/gkr1173.
 [6] E. S. Andersen, M. Dong, M. M. Nielsen, K. Jahn, A. Lind-Thomsen, W. Mamdouh, K. V. Gothelf, F. Besenbacher, J. Kjems, *ACS Nano* **2008**, *2*, 1213–1218.
 [7] E. S. Andersen, M. Dong, M. M. Nielsen, K. Jahn, R. Subramani, W. Mamdouh, M. M. Golas, B. Sander, H. Stark, C. L. P. Oliveira, et al., *Nature* **2009**, *459*, 73–76.
 [8] S. M. Douglas, H. Dietz, T. Liedl, B. Högberg, F. Graf, W. M. Shih, *Nature* **2009**, *459*, 414–418.
 [9] H. Dietz, S. M. Douglas, W. M. Shih, *Science* **2009**, *325*, 725–730.
 [10] T. Liedl, B. Högberg, J. Tytell, D. E. Ingber, W. M. Shih, *Nat. Nanotechnol.* **2010**, *5*, 520–524.
 [11] D. Han, S. Pal, J. Nangreave, Z. Deng, Y. Liu, H. Yan, *Science* **2011**, *332*, 342–346.
 [12] S. Woo, P. W. K. Rothmund, *Nat. Chem.* **2011**, *3*, 620–627.
 [13] W. Liu, H. Zhong, R. Wang, N. C. Seeman, *Angew. Chem.* **2010**, *123*, 278–281.
 [14] B. Högberg, T. Liedl, W. M. Shih, *J. Am. Chem. Soc.* **2009**, *131*, 9154–9155.
 [15] Y. Yang, D. Han, J. Nangreave, Y. Liu, H. Yan, *ACS Nano* **2012**, 120727170029009.
 [16] E. Pound, J. R. Ashton, H. A. Becerril, A. T. Woolley, *Nano Lett.* **2009**, *9*, 4302–4305.
 [17] H. Zhang, J. Chao, D. Pan, H. Liu, Q. Huang, C. Fan, *Chem. Commun.* **2012**, *48*, 6405.
 [18] Z. Zhao, H. Yan, Y. Liu, *Angew. Chem. Int. Ed.* **2010**, *49*, 1414–1417.
 [19] Z. Zhao, Y. Liu, H. Yan, *Nano Lett.* **2011**, *11*, 2997–3002.
 [20] A. Rajendran, M. Endo, Y. Katsuda, K. Hidaka, H. Sugiyama, *ACS Nano* **2011**, *5*, 665–671.
 [21] D. Smith, V. Schüller, C. Engst, J. Rädler, T. Liedl, *Nanomedicine* **2013**, *8*, 105–121.
 [22] C. Ducani, C. Kaul, M. Moche, W. M. Shih, B. Högberg, *Nat. Methods* **2013**, *10*, 647–652.
 [23] S. M. Douglas, J. J. Chou, W. M. Shih, *Proc. Natl. Acad. Sci. USA* **2007**, *104*, 6644–6648.
 [24] A. Kuzyk, R. Schreiber, Z. Fan, G. Pardatscher, E.-M. Roller, A. Högele, F. C. Simmel, A. O. Govorov, T. Liedl, *Nature* **2012**, *483*, 311–314.
 [25] I. H. Stein, V. Schüller, P. Böhm, P. Tinnefeld, T. Liedl, *Chem. Eur. J. of Chem. Phys.* **2011**, *12*, 689–695.
 [26] J. Sambrook, *Molecular Cloning: a Laboratory Manual*, Third Edition, Cold Spring Harbor Laboratory Press, **2001**.
 [27] E. Hegedus, E. Kokai, A. Kotlyar, V. Dombradi, G. Szabo, *Nucleic Acids Res.* **2009**, *37*, e112–e112.
 [28] R. D. Blake, S. G. Delcourt, *Nucleic Acids Res.* **1996**, *24*, 2095–2103.
 [29] J. P. J. Sobczak, T. G. Martin, T. Gerling, H. Dietz, *Science* **2012**, *338*, 1458–1461.
 [30] C. Lin, S. D. Perrault, M. Kwak, F. Graf, W. M. Shih, *Nucleic Acids Res.* **2013**, *41*, e40–e40.

Received: November 5, 2013
 Revised: December 29, 2013
 Published online:

DNA ORIGAMI SEESAWS AS COMPARATIVE BINDING ASSAY

The interaction of biomolecules often leads to conformational changes. DNA nanotechnology offers us the possibility to construct nanoscopic tools to study biomolecular interactions in a highly parallel fashion without any connection to the macroscopic world [186]. Several DNA nanostructures that undergo conformational changes upon interaction with biomolecules have been demonstrated, for example upon endonuclease activity [33], aptamer-ligand interactions [105], toehold-mediated branch migration [95], or hydrophobic interactions [62]. In the associated publication P2, we presented a DNA origami prototype for differential molecular binding assays. The structure is a seesaw-like DNA origami, shown in figure 18. Conceptually, a pair of binding partners on one side of the balance is compared to a reference pair on the other side. The binding pair with the stronger interaction locks the structure in a distinct, geometrically distinguishable conformation.

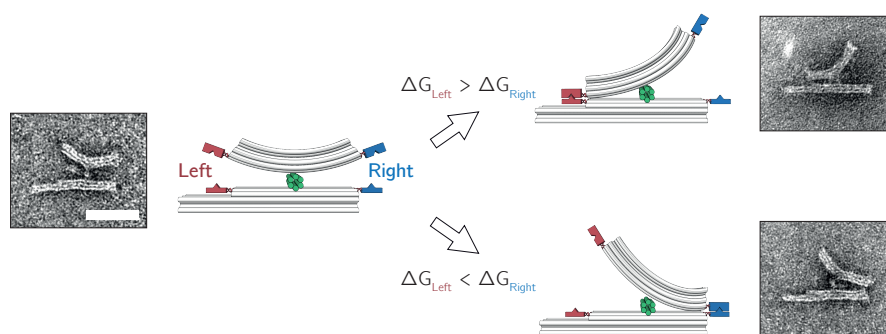


Figure 18: Concept of a DNA origami based comparative binding assay: A pair of binding partners is conjugated to each side of the seesaw-like balance structure. The stronger binding pair locks the structure in a geometrically distinguishable conformation. The TEM micrographs show the open state (on the left) and the two distinct conformations (on the right) of the structure. The scale bar is 50 nm.

4.1 DNA HYBRIDIZATION ASSAY

To test this concept, we developed a DNA hybridization assay with competing complementary ssDNA extensions on each side. This was inspired by the use of DNA as a programmable reference bond to quantitatively measure biomolecular interactions [187]. The probability of closing on one side depended on the number of hybridising extensions on each side and the binding energies of the formed duplexes. In these model

experiments, we observed a drastic shift (up to 90%) in concentrations towards the conformation with a higher binding energy.

4.2 DNA-DNA BINDING ASSAY

In a next step, we detected DNA-DNA binding events with a pre-formed, already locked structure. Hybridization closed the structure on the side with the higher binding energy. The DNA duplex on the side with the higher binding energy featured an additional toehold sequence. The addition of an input strand complementary to the toehold strand in the duplex forced the structure to open on this side. The structure subsequently closed on the other side. Via this conformational change, the presence of the input strand was detected.

4.3 OUTLOOK

The presented prototype can be used in future work as a platform to investigate biomolecular interactions in a comparative fashion with DNA as a highly tuneable reference interaction (figure 19 illustrates the concept schematically). This could be applied to study for example molecule–aptamer interactions and DNA–protein interactions.

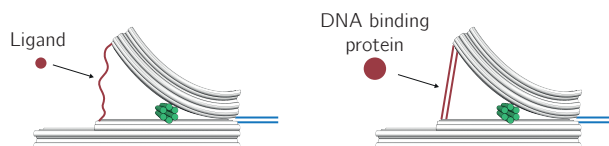


Figure 19: Future binding assays to investigate molecule–aptamer interactions (left) and DNA binding proteins in comparison to a reference DNA duplex of tuneable length (right).

4.4 ASSOCIATED PUBLICATION P2

DNA Origami Seesaws as Comparative Binding Assay

By

Philipp C. Nickels, Hans C. Høiberg, Stephanie S. Simmel, Phil
Holzmeister, Philip Tinnefeld, and Tim Liedl

published in

ChemBioChem (2016), 17, 1093 - 1096 [188]

Creative Commons (CC BY-NC-SA 4.0)

SPECIAL
ISSUE

DNA Origami Seesaws as Comparative Binding Assay

Philipp C. Nickels,^[a] Hans C. Høiberg,^[a] Stephanie S. Simmel,^[a] Phil Holzmeister,^[b]
Philipp Tinnefeld,^[b] and Tim Liedl^{*[a]}

The application of commonly used force spectroscopy in biological systems is often limited by the need for an invasive tether connecting the molecules of interest to a bead or cantilever tip. Here we present a DNA origami-based prototype in a comparative binding assay. It has the advantage of in situ readout without any physical connection to the macroscopic world. The seesaw-like structure has a lever that is able to move freely relative to its base. Binding partners on each side force the structure into discrete and distinguishable conformations. Model experiments with competing DNA hybridisation reactions yielded a drastic shift towards the conformation with the stronger binding interaction. With reference DNA duplexes of tuneable length on one side, this device can be used to measure ligand interactions in comparative assays.

In biological systems, the interaction of molecules often leads to conformational changes. The nature of these changes has been investigated with various single-molecule force spectroscopy tools, most prominently magnetic and optical tweezers and atomic force microscopy.^[1] Although these techniques feature single-nanometer resolution and piconewton force sensitivity, they suffer from two limitations: poor potential for parallelisation, and the need for an invasive connector between the biomolecule and the macroscopic device. In addressing the first of these, DNA has been used as a programmable reference bond to quantitatively measure biomolecular interactions in a highly parallel fashion.^[2] The second limitation could potentially be overcome by molecular tools such as DNA force sensors, as used to study DNA looping.^[3] Structural DNA nanotechnology, particularly DNA origami, opens up a promising route to construct such nanoscopic molecular tools.^[4] In DNA origami,

a long scaffold strand is folded into a designed shape by hundreds of short oligonucleotides with programmed sequences. The simple, computer-aided design process^[7–10] has enabled the self-assembly of a variety of complex 2D^[5,10] and 3D^[11–15] geometries with nanometer addressability. DNA origami structures have been frequently employed to arrange molecules, binding moieties and proteins in designed patterns.^[16–18] Furthermore, conformational changes of these structures have been demonstrated, for example by endonuclease activity,^[14] aptamer-ligand interactions,^[19] toehold-mediated branch migration^[20,21] and with hydrophobic moieties such as cholesterol.^[21]

In this work, we present a seesaw-like DNA origami structure that can potentially serve in a differential molecular binding assay (Figure 1). A pair of binding partners on one side of the balance-like structure is compared to a reference pair of binding partners on the other side. The binding pair with the stronger interaction locks the structure in a distinct conformation. This conformation can be easily identified by transmission electron microscopy (TEM). Moreover, there is no need for a physical tether to a macroscopic device, and thus, in principle, this approach allows efficient parallelisation.

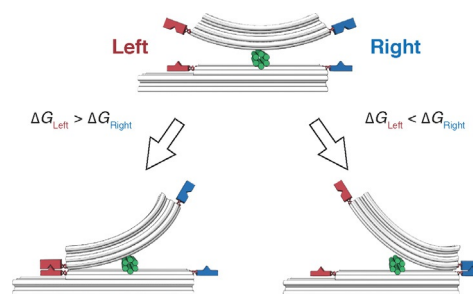


Figure 1. Seesaw-like force balance. A pair of binding partners is conjugated to each side of the device. The stronger binding pair locks the structure in a geometrically distinguishable conformation.

The prototype DNA origami structure (Figure 2A) consists of two 18-helix bundles connected by a short six-helix bundle hinge. The upper beam (lever) is 60 nm long and has a 60° bend along its length. The lower beam (base) is 60 nm long and straight, with a 25 nm extension of 12 helices on the left side to introduce asymmetry. This permits the detection of the orientation of the structure in TEM images. The 25 nm hinge (perpendicular between the base and the lever) serves to connect both beams by four scaffold double crossovers (two from base to hinge and two from hinge to lever). The scaffold crossovers are placed such that the lever and the base are free to

[a] P. C. Nickels, H. C. Høiberg, S. S. Simmel, Prof. T. Liedl
Faculty of Physics and Center for NanoScience
Ludwig-Maximilians-Universität (LMU)
Geschwister-Scholl-Platz 1, 80539 Munich (Germany)
E-mail: tim.liedl@physik.lmu.de

[b] P. Holzmeister, Prof. P. Tinnefeld
Institut für physikalische und theoretische Chemie
Technische Universität Braunschweig
Hans-Sommer-Strasse 10, 38106 Braunschweig (Germany)

Supporting information and the ORCID identification number(s) for the author(s) of this article can be found under <http://dx.doi.org/10.1002/cbic.201600059>.

© 2016 The Authors. Published by Wiley-VCH Verlag GmbH & Co. KGaA. This is an open access article under the terms of the Creative Commons Attribution-NonCommercial License, which permits use, distribution and reproduction in any medium, provided the original work is properly cited and is not used for commercial purposes.

This manuscript is part of a Special Issue on DNA Nanotechnology.

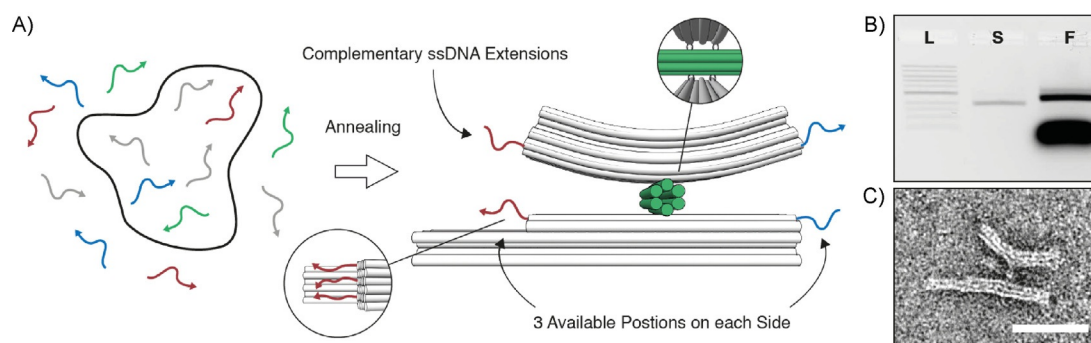


Figure 2. A) The circular scaffold molecule (black) and staple subsets for the hinge (green), base and lever (grey) with the three addressable positions on each side (red and blue) are thermally annealed to form the seesaw-like balance. At the addressable positions, the corresponding staples are extended at either the 5' or 3'-end (3'-ends depicted as arrow heads). B) Agarose gel electrophoresis confirms assembly after thermal annealing (L: 1 kb DNA ladder; S: scaffold-only control; F: folded structure). C) Representative TEM image of a gel-purified structure shows correct assembly. Scale bar: 50 nm.

pivot in one plane. Each crossover features a single-stranded scaffold spacer of three nucleotides. Each side of the structure is equipped with three individually addressable positions on both base and lever. At these positions, the corresponding staple strands can be extended with single-stranded DNA (ssDNA) either on the 5'-end (right side of the base, left side of the lever) or on the 3'-end (left side of the base, right side of the lever).

In order to verify the correct assembly of the structures, we analysed the folding by agarose gel electrophoresis directly after thermal annealing of the DNA origami structure. The gel demonstrated the successful, high-yield folding of our prototype (Figure 2B). Negative-stain TEM imaging of gel-purified structures (Figure 2C) confirmed that the intended geometry had formed.

As a proof of principle, we developed a DNA hybridisation assay with competing complementary ssDNA extensions on each side. During annealing, the complementary extensions form a duplex in a zipper conformation and lock the structure in a geometrically distinct conformation. The probability of closing on one side depends on two variables: the number of hybridising extensions on each side (maximum of three per side) and the binding energies of all formed duplexes. We choose 20 nucleotides for each extension, and the same complementary sequences on both sides. The number of DNA extensions was varied and is denoted "vs" to represent the number of extensions per side.

Samples with different numbers of competing hybridisation partners on each side were prepared and thermally annealed. After folding, the structures were subjected to agarose gel electrophoresis (Figure S4 in the Supporting Information) and purification. TEM images were taken from several randomly selected areas on the grid (example zoom-out images in Figure S5). The TEM images were analysed. Firstly, three distinct conformations of the structure were defined: left, open and right (Figure 3). Secondly, single seesaws immobilised on the TEM grid lying on the side were identified in the micrographs, and one of the three defined conformations was assigned to each particle (left or right when the lever was in contact with the base at the end; open otherwise). Finally, the number of

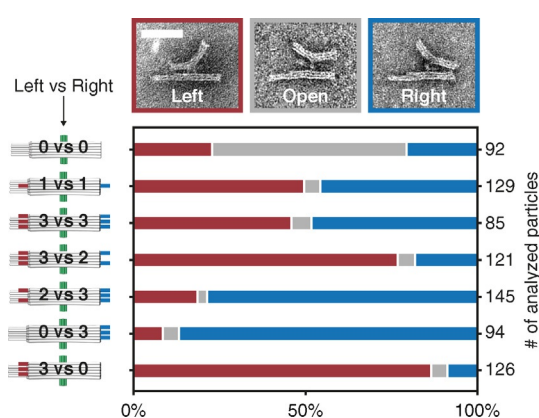


Figure 3. Analysis of TEM images of DNA origami structures with different numbers of competing DNA hybridisation partners. The TEM images show the three distinct conformations: left, open, and right. Scale bar: 50 nm.

particles in each of the three groups was counted. Figure 3 shows the results for different combinations of competing extensions. When none of the positions was addressed (0vs0), more than 60% of the particles were in the open conformation. For equal numbers of extensions on each side (1vs1 and 3vs3), we observed an almost 50:50 distribution, with only a small fraction in the open conformation. Unequal numbers of extensions resulted in a dramatic shift of concentration of closed structures towards the side with the higher number of extensions (3vs2 and 2vs3). A greater difference in the number of extensions on each side resulted in a more pronounced concentration shift: 90% correct closing was achieved by addressing all three positions on one side and none on the opposing side (0vs3 and 3vs0).

In order to compare our results with a theoretical prediction, we calculated the probability of our structure being either in the left or right conformation. For this, we assigned a Boltzmann factor to each side based on the computed ΔG of the formed duplexes (calculated at www.nupack.org^[22] for $T = T_w$) and assumed that the probability of one conformation is proportional to the ratio of the Boltzmann factors. A 20% increase in ΔG on one side should lead to virtually 100% of the struc-

tures being closed on that side (see Figure S3 for details). For the 3vs2 and 2vs3 samples (i.e. 50% increase in ΔG on one side), we observed only 80% closed objects. Even 3vs0 and 0vs3 were not able to achieve the expected 100% closing. We believe that two reasons explain the majority of incorrectly closed or open structures: firstly, the incorporation probability of each staple strand is not 100% (previously reported values are 96–99%, depending on the geometry of the origami design);^[23] and secondly, excess free extension oligomers in the solution (not incorporated as staples) can bind to complementary counterparts attached to the structure and thus saturate that position. Optimising the annealing process and implementing a hairpin-based reaction hierarchy in the closing reaction^[24] could further improve the yields of structures in the correct conformation in the future.

In order to test our prototype in a comparative binding assay after folding instead of in a one-pot reaction, we used a pre-formed, locked structure to detect DNA–DNA binding events (Figure 4A). We folded the structure with a 15-nucleotide extension on the left and a 30-nucleotide extension on

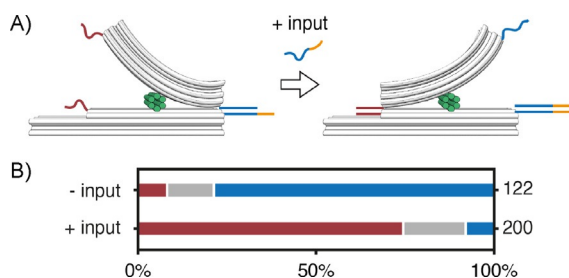


Figure 4. DNA–DNA binding detection on a pre-formed, closed, seesaw structure. A) The structure is annealed with an extension that is twice as long on the right (30 bases) as on the left (15 bases). The extension on the right also carries a toehold. Upon the addition of an input strand that is complementary to the toehold strand on the right, the structure opens and subsequently closes on the left. B) Analysis of TEM images before and after the addition of the input strand (red: left; grey: open; blue: right).

the right (15vs30). This is equivalent to the 1vs1 sample (Figure 3), except that we expected a dramatic shift towards the conformation with the stronger binding (the 30-nt extension on the right), similarly to the 2vs3 sample. Additionally, the long extension at the base on the right featured an eight-nucleotide toehold. After folding, the sample was subjected to agarose gel purification as for the samples in Figure 3. TEM imaging revealed that about 80% of the structures were closed on the right (Figure 4B). This is close to the results for 2vs3, which has a similar relative binding mismatch. Next, we added an input strand complementary to the 30-base toehold extension at 20× molar excess. TEM images were taken after 2 h incubation at RT. A dramatic shift in the concentration of closed structures towards the left was observed: about 75% were now closed on the left (Figure 4B).

In conclusion, we successfully assembled a DNA-origami-based prototype for a comparative binding assay. Discrete and geometrically distinguishable conformations were observed for DNA hybridisation reactions on both sides during one-pot an-

nealing, as a model system. DNA–DNA binding events were detected after the one-pot annealing on a pre-formed and locked structure, and this resulted in a switch of conformation. This device can potentially be used to study bio-molecular interactions in a comparative fashion with DNA as a tuneable reference, for example to investigate molecule–aptamer interactions and DNA–protein interactions, such as DNA bending (possible implementations illustrated in Figure 5). The lack of coupling to a cantilever or micrometre bead together with the possibility of in situ FRET readout will allow applications in biological systems with a high degree of parallelism. In future experiments, similar DNA origami tools containing ssDNA sections acting as entropic spring elements^[9,14] could greatly simplify the study of force dependence in dynamic DNA systems and for DNA–protein interactions.

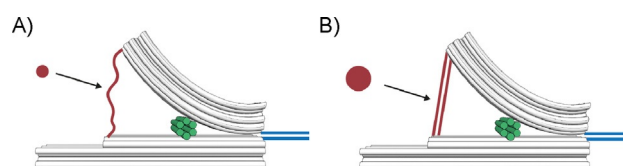


Figure 5. Potential binding assays to study A) molecule–aptamer interactions and B) DNA bending proteins in comparison to a reference DNA duplex of tuneable length.

Experimental Section

Sample preparation: The DNA origami structure was designed by using caDNAno software (version 0.2.3; <http://cadnano.org/legacy>;^[7] design schematics in Figure S1). Curvature along the length of the lever was introduced by a pattern of base deletions and insertions as described previously (deletion pattern in Figure S2).^[13] The 8634-nucleotide single-stranded scaffold DNA, derived from M13mp18, was prepared as previously described.^[12,25] Scaffold DNA (10 nM) was mixed with each staple strand (100 nM; high purity salt free, MWG Eurofins Operon) in TE buffer (Tris (10 mM, pH 7.6), EDTA (1 mM)) containing MgCl₂ (18 mM) and NaCl (5 mM). The mixture was subjected to a nonlinear thermal annealing ramp from 65 to 25 °C over 24 h (see the Supporting Information). Folded structures were electrophoresed on 0.7% agarose gels containing 0.5×TBE buffer (Tris (45 mM), boric acid (45 mM), EDTA (1 mM)) with MgCl₂ (11 mM) and ethidium bromide (0.5 μg mL⁻¹) at 5.5 V cm⁻¹ for 2 h in an ice-water bath. Bands were visualised with UV light and physically extracted. DNA was recovered by manually squeezing the excised gel slice and collecting the liquid.

TEM imaging: Gel-purified origami solution (3 μL) was adsorbed onto glow-discharged TEM grids (formvar/carbon, 300 mesh Cu; Ted Pella, Redding, CA) at 20 °C, and then stained with aqueous uranyl formate (2%) containing sodium hydroxide (25 mM). Imaging was performed at 30 000× magnification (zoom-out images in Figure S5 at 12 000× magnification) with a JEM1011 transmission electron microscope (JEOL) operated at 80 kV, equipped with a FastScan-F114 camera (TVIPS, Gauting, Germany). Particles in TEM images were picked by the interactive boxing routine (e2boxer.py) of Eman2 software (<http://blake.bcm.edu/emanwiki/EMAN>; example set of particles in Figure S6).^[26]

Acknowledgements

We thank Ingo Stein, Robert Schreiber, and Tao Zhang for discussions and Susanne Kempfer for technical assistance. We acknowledge funding from the Deutsche Forschungsgemeinschaft (DFG; LI 1743/2-1, TI 329/6-1, and SFB 1032 (TPA6)) the Nanosystems Initiative Munich (NIM), and the Center for NanoScience (CeNS) Munich.

Keywords: DNA hybridisation · DNA origami · DNA structures · self-assembly · sensors

- [1] K. C. Neuman, A. Nagy, *Nat. Methods* **2008**, *5*, 491–505.
- [2] C. Albrecht, K. Blank, M. Lalic-Mülthaler, S. Hirler, T. Mai, I. Gilbert, S. Schiffmann, T. Bayer, H. Clausen-Schaumann, H. E. Gaub, *Science* **2003**, *301*, 367–370.
- [3] H. Shroff, B. M. Reinhard, M. Siu, H. Agarwal, A. Spakowitz, J. Liphardt, *Nano Lett.* **2005**, *5*, 1509–1514.
- [4] H. Gu, W. Yang, N. C. Seeman, *J. Am. Chem. Soc.* **2010**, *132*, 4352–4357.
- [5] P. W. K. Rothemund, *Nature* **2006**, *440*, 297–302.
- [6] N. C. Seeman, *Annu. Rev. Biochem.* **2010**, *79*, 65–87.
- [7] S. M. Douglas, A. H. Marblestone, S. Teerapittayanon, A. Vazquez, G. M. Church, W. M. Shih, *Nucleic Acids Res.* **2009**, *37*, 5001–5006.
- [8] Y. Ke, S. M. Douglas, M. Liu, J. Sharma, A. Cheng, A. Leung, Y. Liu, W. M. Shih, H. Yan, *J. Am. Chem. Soc.* **2009**, *131*, 15903–15908.
- [9] D.-N. Kim, F. Kilchherr, H. Dietz, M. Bathe, *Nucleic Acids Res.* **2012**, *40*, 2862–2868.
- [10] E. S. Andersen, M. Dong, M. M. Nielsen, K. Jahn, A. Lind-Thomsen, W. Mamdouh, K. V. Gothelf, F. Besenbacher, J. Kjems, *ACS Nano* **2008**, *2*, 1213–1218.
- [11] E. S. Andersen, M. Dong, M. M. Nielsen, K. Jahn, R. Subramani, W. Mamdouh, M. M. Golas, B. Sander, H. Stark, C. L. P. Oliveira, J. S. Pedersen, V. Birkedal, F. Besenbacher, K. V. Gothelf, J. Kjems, *Nature* **2009**, *459*, 73–76.
- [12] S. M. Douglas, H. Dietz, T. Liedl, B. Högberg, F. Graf, W. M. Shih, *Nature* **2009**, *459*, 414–418.
- [13] H. Dietz, S. M. Douglas, W. M. Shih, *Science* **2009**, *325*, 725–730.
- [14] T. Liedl, B. Högberg, J. Tytell, D. E. Ingber, W. M. Shih, *Nat. Nanotechnol.* **2010**, *5*, 520–524.
- [15] D. Han, S. Pal, J. Nangreave, Z. Deng, Y. Liu, H. Yan, *Science* **2011**, *332*, 342–346.
- [16] N. V. Voigt, T. Tørring, A. Rotaru, M. F. Jacobsen, J. B. Ravnsbæk, R. Subramani, W. Mamdouh, J. Kjems, A. Mokhir, F. Besenbacher, K. V. Gothelf, *Nat. Nanotechnol.* **2010**, *5*, 200–203.
- [17] K. Jahn, T. Tørring, N. V. Voigt, R. S. Sørensen, A. L. B. Kodal, E. S. Andersen, K. V. Gothelf, J. Kjems, *Bioconjugate Chem.* **2011**, *22*, 819–823.
- [18] A. Shaw, V. Lundin, E. Petrova, F. Fördös, E. Benson, A. Al-Amin, A. Herland, A. Blokzijl, B. Högberg, A. I. Teixeira, *Nat. Methods* **2014**, *11*, 841–846.
- [19] S. M. Douglas, I. Bachelet, G. M. Church, *Science* **2012**, *335*, 831–834.
- [20] A. Kuzyk, R. Schreiber, H. Zhang, A. O. Govorov, T. Liedl, N. Liu, *Nat. Mater.* **2014**, *13*, 862–866.
- [21] J. List, M. Weber, F. C. Simmel, *Angew. Chem. Int. Ed.* **2014**, *53*, 4236–4239; *Angew. Chem.* **2014**, *126*, 4321–4325.
- [22] J. N. Zadeh, C. D. Steenberg, J. S. Bois, B. R. Wolfe, M. B. Pierce, A. R. Khan, R. M. Dirks, N. A. Pierce, *J. Comput. Chem.* **2011**, *32*, 170–173.
- [23] K. F. Wagenbauer, C. H. Wachauf, H. Dietz, *Nat. Commun.* **2014**, *5*, 1–7.
- [24] T. E. Tomov, R. Tsukanov, M. Liber, R. Masoud, N. Plavner, E. Nir, *J. Am. Chem. Soc.* **2013**, *135*, 11935–11941.
- [25] S. M. Douglas, J. J. Chou, W. M. Shih, *Proc. Natl. Acad. Sci. USA* **2007**, *104*, 6644–6648.
- [26] G. Tang, L. Peng, P. R. Baldwin, D. S. Mann, W. Jiang, I. Rees, S. J. Ludtke, *J. Struct. Biol.* **2007**, *157*, 38–46.

Manuscript received: February 2, 2016

Accepted article published: April 1, 2016

Final article published: May 6, 2016

MOLECULAR FORCE SPECTROSCOPY WITH A DNA ORIGAMI BASED NANOSCOPIC FORCE CLAMP

Forces play an important role in all biological systems, especially during the interaction of biomolecules. Additionally, the mechanical properties of the involved (macro)molecules determine some aspects of the interactions. Over the last decades, several experimental techniques were developed to study these interactions and mechanical properties on the single-molecule level. The three most established techniques are the AFM and optical- and magnetic-tweezers. These techniques were successfully used to investigate for example the unfolding of proteins [189, 190], the elasticity [127, 148, 149] and stacking interactions of DNA [155], or the folding trajectory of proteins under constant force in a force clamp configuration [191]. An overview over these three techniques together with more examples of their application can be found in reference [192].

5.1 LIMITATIONS OF CONVENTIONAL FORCE SPECTROSCOPY

Despite the great success, all three techniques suffer from two major limitations. The first limitation is the serial nature of conventional force spectroscopy. This serial nature leads to a low throughput of data acquisition. One attempt to increase the data throughput is the development of increased parallel data acquisition, for example in magnetic tweezer experiments [193]. Other examples are centrifuge force microscopes [194] and acoustic force spectroscopy [195]. The second limitation is the requirement of a physical connection to the macroscopic world. All techniques require a connector from the nanometer sized system of interest to a micrometer sized macroscopic object such as a cantilever or magnetic bead. These connectors are typically long and flexible (often, the whole 16 μm long genomic DNA of bacteriophage λ or fragments of it are used) and make the techniques susceptible to drift and noise. The connectors also prevent the investigation of DNA-interacting systems that induce only minor conformational changes. Examples for such systems are many gene-regulatory proteins such as transcription factors. The Dietz group introduced rigid DNA origami bundles as spacers in dual optical traps to reduce the noise [152]. Nevertheless, these rigid spacers are still connectors to a macroscopic object and prohibit the access to biologically relevant complex environments.

One promising way to overcome these two limitations is the construction of self-assembled and autonomous nanoscopic manipulation tools.

Recent efforts to sense forces in such a way include simple nanomechanical DNA devices [186, 196, 197] and intracellular protein force sensors [198].

5.2 DNA ORIGAMI FORCE CLAMP

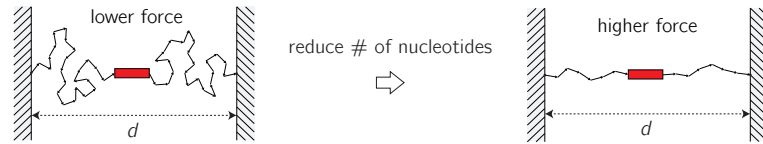


Figure 20: The ssDNA connects the system of interest (red) with two immobile anchor points. Reducing the number of nucleotides that span the distance d leads to a higher entropic force.

In the associated publication P3 we presented a nanoscopic DNA origami force clamp that overcomes the two limitations. We exerted defined and tunable forces on molecular systems of interest via the entropic spring behavior of ssDNA. Figure 20 illustrates the concept: ssDNA connects two immobile anchor points with the system of interest. To change the contour length and thus the entropic force acting on the system of interest, we simply adjusted the number of bases between the fixed anchor points. Reducing the number of nucleotides that span the distance between the anchor points lead to a smaller number of adoptable conformations of the ssDNA chain and thus resulted in a higher entropic force. The two anchor points were imparted by a rigid, square bracket shaped DNA origami structure (figure 21a).

As a benchmark system to test the function of the origami force clamp, we studied the Holliday junction transition between two isomers as a function of the applied force. Our results agreed well with reported values from work published by Taekjip Ha's group in which they investigate the same behaviour with a combined optical-tweezer and TIRF setup [199]. In a next step, we used our force clamp to study the interaction between the TATA-box binding protein (TBP) and promoter DNA (figure 21b illustrates the detection via FRET and shows two exemplary FRET histograms). TBP is a highly abundant transcription factor in the archaeal and eukaryotic domains of life. It is responsible for the site-specific recruitment and orientation of RNA polymerases at the transcription start site. So far, the role of mechanosensitivity in gene regulation involving TBP could not be quantified. Our results showed that TBP from the hyperthermophilic archaeal organism *Methanocaldococcus jannaschii* could not bend the promoter DNA significantly at forces above 10 pN. The bending step is crucial for all subsequent steps involved in the transcription initiation. Our collaborator Jan Lipfert and his student Franziska Kriegel from LMU kindly carried out control experiments with conventional magnetic tweezers on the same system.

However, the TBP-DNA interaction could not be detected, mainly due to the limitations explained before.

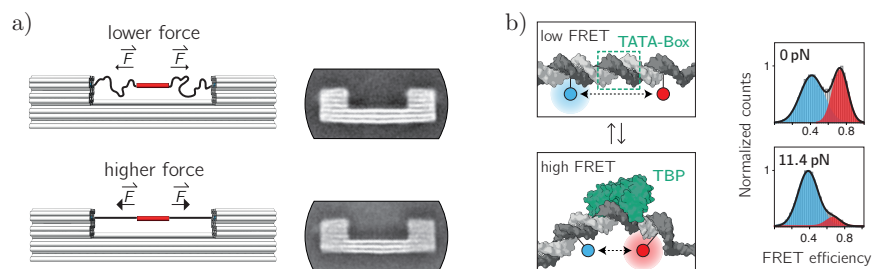


Figure 21: a) In order to change the entropic force acting on the system of interest (red), we prepared different force clamp structures with varying lengths of the ssDNA connecting the system to the anchor points on the force clamp structure. The average TEM micrographs show that the overall geometry of the force clamp structure remained unchanged, independent of the length of the ssDNA. b) The TBP induced bending was monitored by a donor-acceptor pair flanking the so-called TATA-box, the TBP recognition sequence. Upon binding and bending, the energy transfer between donor and acceptor changed from a low to a high FRET efficiency. The histograms over the FRET efficiency at 0 pN and 11.4 pN showed clearly that the population with a high FRET efficiency almost completely disappeared at 11.4 pN.

5.3 ASSOCIATED PUBLICATION P3

**Molecular force spectroscopy with a DNA
origami based nanoscopic force clamp**

By

Philipp C. Nickels, Bettina Wunsch, Phil Holzmeister, Wooli Bae,
Luisa M. Kneer, Dina Grohmann, Philip Tinnefeld, and Tim Liedl

published in

Science (2016), 354, 305 - 307

The accepted version of the manuscript is reprinted with permission from ref.
[200]. Copyright 2016 AAAS.

Title: Molecular force spectroscopy with a DNA-origami–based nanoscopic force clamp**Authors:** Philipp C. Nickels¹, Bettina Wünsch², Phil Holzmeister^{2, †}, Wooli Bae¹, Luisa M. Kneer¹, Dina Grohmann^{2, ‡}, Philip Tinnefeld^{2,*}, Tim Liedl^{1,*}**Affiliations:**

¹Faculty of Physics & Center for Nanoscience (CeNS), Ludwig-Maximilians-Universität (LMU), Geschwister-Scholl-Platz 1, 80539 München, Germany

²Institut für Physikalische und Theoretische Chemie, and Braunschweig Integrated Centre of Systems Biology (BRICS), and Laboratory for Emerging Nanometrology (LENA), Technische Universität Braunschweig, Rebenring 56, 38106 Braunschweig, Germany

*Correspondence to: p.tinnefeld@tu-braunschweig.de, tim.liedl@physik.lmu.de

[†]Current address: Bayer AG, Engineering & Technology, Enabling Technologies, Chempark E41, 51368 Leverkusen, Germany

[‡]Current address: Department of Biochemistry, Genetics and Microbiology, Institute of Microbiology, University of Regensburg, 93053 Regensburg, Germany

Abstract:

Forces in biological systems are typically investigated at the single-molecule level with atomic force microscopy or optical and magnetic tweezers, but these techniques suffer from limited data throughput and their requirement for a physical connection to the macroscopic world. We introduce a self-assembled nanoscopic force clamp built from DNA that operates autonomously and allows massive parallelization. Single-stranded DNA sections of a DNA origami structure

acted as entropic spring and exerted controlled tension in the low piconewton range to a molecular system, whose conformational transitions were monitored via single-molecule Förster resonance energy transfer. We used the conformer switching of a Holliday junction as a benchmark and studied the TATA-binding protein-induced bending of a DNA duplex under tension. The observed suppression of bending above 10 pN provides further evidence of mechano-sensitivity in gene regulation.

One Sentence Summary:

A self-assembled molecular force clamp built from DNA allows highly parallelized force spectroscopy measurements without interference from the macroscopic world.

Main Text:

The most widely used single-molecule force spectroscopy techniques to study minute forces and mechanical properties of biomolecules are atomic force microscopy and optical or magnetic tweezers. These methods helped to explore the unfolding and folding of proteins (1, 2), the elasticity of DNA (3), and the folding trajectory of proteins in force clamp configurations (4). Despite this great success, two limitations persist. One is the low data throughput arising from the serial nature of conventional force spectroscopy. Recent attempts to overcome this problem include the development of increased parallel data acquisition in magnetic tweezer experiments (6) and centrifuge force microscopes (7). The second limitation is the requirement of a physical connector to a micrometer-sized object that enables interaction with the macroscopic world (5). These typically long and flexible connector molecules are an intrinsic feature of all established techniques and make them susceptible to drift and noise. Further, they prevent the investigation of DNA interacting systems that induce only minor conformational changes, such as many gene regulatory proteins, e.g. transcription factors. One previous attempt to reduce noise is the

construction of DNA origami bundles as rigid spacers in optical traps (8). Regardless, any tether prohibits access to biologically relevant complex environments such as the inside of living cells.

A promising approach toward the complete removal of the invasive connection is the construction of autonomous, nanoscopic manipulation tools. Earlier efforts on the molecular scale to sense forces autonomously, although not in an adjustable fashion, include simple nanomechanical DNA devices (9-11) and intracellular protein force sensors (12). Here, we use programmable DNA self-assembly (13-18) to construct a nanoscopic device that overcomes both limitations. Extending prestressed DNA origami tensegrity (19), we use the entropic spring behavior of single-stranded DNA (ssDNA) to exert defined and tunable forces on molecular systems. Conceptually, the ssDNA connects the system of interest with two immobile anchor points (Fig. 1A). By adjusting the number of bases between the fixed anchor points, the contour length of the ssDNA is changed, directly affecting the entropic force acting on the system under study. The fixed distance imparted by the rigid DNA structure and the given contour length of the ssDNA provide an approximately constant force over time (also see supplementary text S1) (20). In analogy to the nomenclature of established constant force experiments, we call our device a nanoscopic force clamp.

In the experimental realization, the ssDNA spring spans the gap of a rigid, bracket-shaped DNA origami clamp and is part of the long scaffold strand that forms the backbone of the DNA origami structure (Fig. 1B). For our design, we located the multiple cloning site (MCS) of the M13mp18 scaffold in the middle of the spring, which allowed us to insert and probe any DNA sequence of interest via standard cloning procedures. Additional ssDNA scaffold was stored in reservoir loops on both ends of the clamp. This enabled us to cost-efficiently build multiple objects with ssDNA springs of different lengths, providing a flexible design with adjustable force (19). Individual structures were assembled for each chosen length of the ssDNA spring with a unique subset of

only ten oligonucleotides (staple strands) (Fig. 1C and figs. S1 to S3). For a zero force control, we enzymatically cut the single-stranded spring to release any tension from the region of interest (Fig. 1C).

To calculate the resulting force for a given contour length, we approximated the ssDNA as a purely entropic spring using a modified freely-jointed-chain model (3) with the contour length $L_C = N * L_B$ with N being the number of nucleotides and L_B the length per single base (supplementary text S1). For L_B we used $6.3 \text{ \AA} \pm 0.8 \text{ \AA}$ from a length comparison of five different crystal structures of ssDNA segments (21).

We thermally annealed the force clamp structure, providing $\sim 10^{12}$ force clamps in a single one-pot reaction. The chosen annealing ramp avoided temperatures above 65°C to minimize thermal degradation of the scaffold (fig. S4 and supplementary text S2) (20). We confirmed successful assembly via agarose gel electrophoresis (Fig. 1D and fig. S5), bulk FRET experiments (fig. S6) and transmission electron microscopy (TEM) (Fig. 1E and figs. S7 to S13).

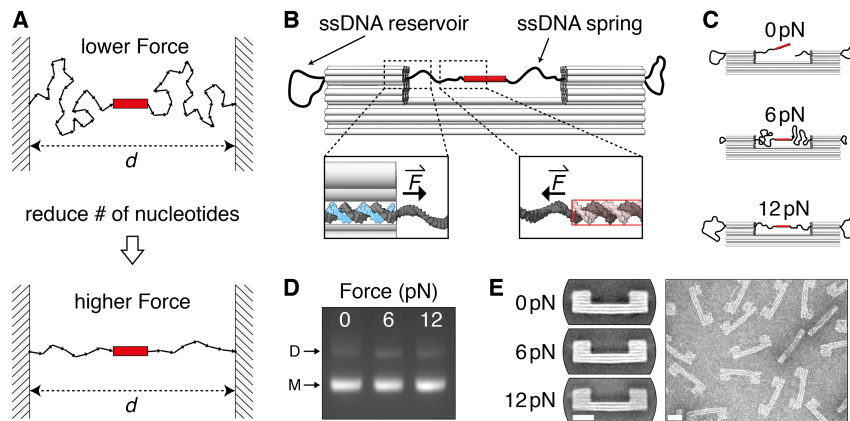


Fig. 1. DNA origami force clamp. (A) ssDNA connects the molecular system of interest (red rectangle) with two immobile anchor points. Reducing the number of nucleotides spanning the distance d leads to a smaller number of adoptable conformations of the ssDNA chain and thus results in a higher entropic force. (B) Scheme of the DNA origami force clamp structure. ssDNA exits the clamp duplexes in a shear conformation (left inset: scaffold in black, staple in blue) and spans the 43 nm wide gap. ssDNA reservoirs are located on each side of the clamp. The system of interest (here a DNA duplex) is probed in shear conformation (right inset). (C) For each constant force variant (three variants are shown here), individual origami samples were assembled. (D) Agarose gel of the three variants after annealing with the monomer (M) and dimer band (D) of the origami structure highlighted. (E) Average TEM micrographs of the three variants (left) and single negative-stain TEM image of the 6 pN variant (right). Scale bars: 20 nm.

To demonstrate the functionality and sensitivity of our force clamp, we cloned a sequence into the scaffold that, together with three other oligonucleotides, forms the well-studied four-way Holliday junction (HJ) (22). In the presence of magnesium, the HJ forms an X-like structure by pairwise coaxial stacking of its helical arms. The chosen sequence is known to constantly switch between the two stacking conformers *iso* I and *iso* II (Fig. 2A) (22), a process that can be efficiently monitored with the help of a donor-acceptor FRET pair positioned on two of the arms (Fig. 2B and fig. S14). We chose four force variants ranging from 0 pN to 4.0 pN and confirmed their successful assembly (figs. S15 to S23). We immobilized these structures on a coverslip surface and monitored donor- and acceptor-pair intensities from individual force clamps over time in a confocal single-molecule setup with alternating laser excitation (ALEX) (20, 23).

Figure 2C and 2D show exemplary FRET traces and FRET histograms from thousands of transitions for each constant force experiment (more traces in figs. S24 and S25). A low FRET population was centered at the FRET efficiency $E = 0.42$ (corresponding to *iso* I) and a high FRET population at $E = 0.85$ (corresponding to *iso* II). With increasing force, the equilibrium shifted toward the *iso* II conformation with almost zero low-FRET population left at 4.0 pN. We used two-state hidden Markov modeling (24) to calculate the transition rates between the low- and high-FRET conformations for each of the forces. The transition rate from low- to high-FRET (k_{high}) increased from $4.7 \text{ s}^{-1} \pm 0.4 \text{ s}^{-1}$ at 0 pN to $18.3 \text{ s}^{-1} \pm 1.4 \text{ s}^{-1}$ at 4.0 pN. Meanwhile, the rate from high- to low-FRET (k_{low}) decreased from $3.2 \text{ s}^{-1} \pm 0.6 \text{ s}^{-1}$ at 0 pN to $1.7 \text{ s}^{-1} \pm 0.4 \text{ s}^{-1}$ at 4.0 pN (Fig. 2E). These rate changes are in good agreement with reported values from combined FRET and optical- and magnetic-tweezer measurements (22, 25). Importantly, the heterogeneity of the HJ (26) was preserved in our measurements (fig. S26), indicating that the force clamp itself did not influence the dynamics of the HJ.

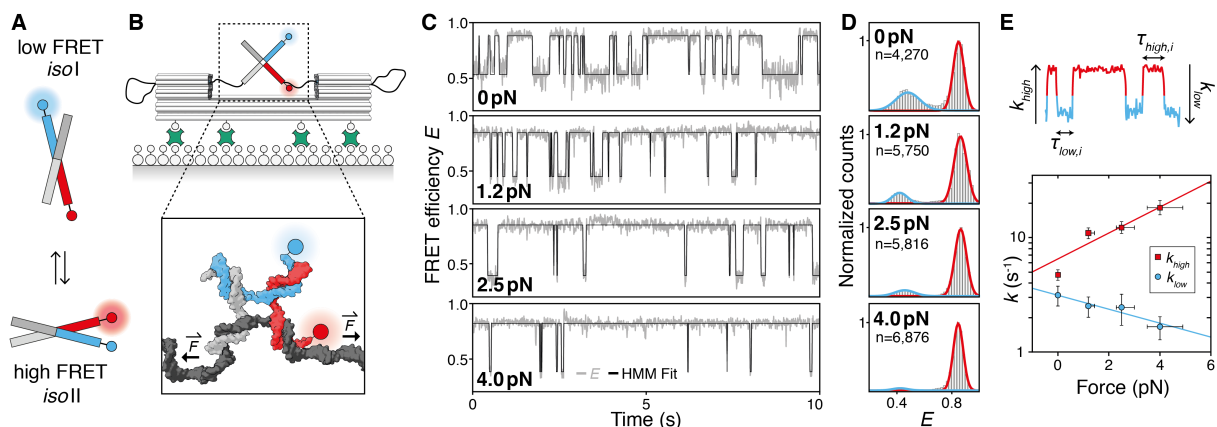


Fig. 2. Holliday junction conformer transitions under force. (A) Schematics of the HJ switching between two stacked isomers; Cy3 donor (blue) and Cy5 acceptor (red). (B) Force clamps were immobilized on a BSA-covered glass surface via biotin-streptavidin coupling. The HJ system is mounted in the force clamp with one of the four HJ-strands being the scaffold (black strand in inset). (C) FRET traces with the FRET efficiency E (gray line) and two-state hidden Markov fit (black line). (D) Histograms over all recorded FRET traces with Gaussian fits for the two FRET populations in blue (low-FRET) and red (high-FRET). Only traces with > 20 transitions were included in the analysis; n is the total number of transitions. (E) Dwell times for both states ($\tau_{low,i}$, $\tau_{high,i}$) were extracted for each trace. Transition rates (k_{low} , k_{high}) were first extracted from a mono-exponential decay fit for each dwell time histogram, then averaged and plotted (semi-log plot) as a function of force. Red squares: low- to high-FRET (k_{high}); blue circles: high- to low-FRET (k_{low}). Solid lines are exponential fits where the exponent relates the rates to the applied force. Y-axis error is the standard error of each average rate; x-axis error is the uncertainty of the calculated force (fig. S15)

Next, we studied the force dependency of the TATA-binding protein (TBP) induced bending of a DNA duplex. Such DNA distortions are an integral function of many transcription factors and DNA binding proteins. Although the correlation between transcriptional regulation and chromosome organization is well known, it has been challenging to quantify the impact of the DNA condensation state and the chromosome organization (e.g. the extent of strain in the DNA) on transcription factors such as TBP.

The general transcription factor TBP is found in the archaeal and eukaryotic domain of life. It recognizes the minor groove of the adenine- and thymidine-rich TATA-box in the core promoter sequence and introduces a severe bend of $\sim 90^\circ$ in the DNA. Together with transcription factor B (TFB/TF(II)B), TBP is responsible for the site-specific recruitment and orientation of RNA polymerases at the transcription start site. To date, force measurements of this system have been futile, at least partly because the TBP-induced changes in the DNA topology are not easily detectable through the long tethers that are unavoidable in standard force spectroscopy experiments.

We used TBP from the hyperthermophilic archaeal organism *Methanocaldococcus jannaschii* (MjTBP) (Fig. 3A), which bends the promoter DNA in a one-step bending mechanism without the need for TFB/TF(II) (27), and inserted a promoter sequence (derived from the Sulfolobus spindle-shaped virus 1 (SSV) T6 gene promoter), which contains a TATA-box motif and is recognized by MjTBP, into the scaffold (Fig. 3B and fig. S27). We chose six force clamp variants ranging from 0 pN to 11.4 pN and confirmed their successful assembly (figs. S28 to S40). The complementary strand of the 51 base pair long SSV T6 promoter was hybridized to the scaffold during folding. Bending was monitored by single-molecule FRET via a donor-acceptor pair flanking the TATA-box (Fig. 3C and fig. S27). Here, we chose in-solution over surface measurements to drastically

increase the data acquisition throughput (28). Fluorescence bursts of donor and acceptor were recorded before and after the addition of MjTBP at its saturation concentration.

Figure 3D shows the FRET efficiency histograms with MjTBP for the six different forces. Each histogram includes at least 10,000 measured force clamps, although the average recording time per sample was only ~ 30 min. All histograms showed a bimodal distribution with a low-FRET population centered at $E = 0.42$ (corresponding to the undistorted state) and a high-FRET population centered at $E = 0.74$ (corresponding to the bent state). The high FRET population disappeared gradually with increasing force and the TBP-induced bending was almost completely suppressed at 11.4 pN (full $E - S$ histograms in fig. S41). We calculated the probability of the bent state P_{bent} via its relative occurrence within the bimodal FRET distribution and plotted P_{bent} as a function of force (Fig. 3E). P_{bent} is well described by the free energy difference of the unbent and bent state expressed through a Boltzmann distribution (Fig. 3E and supplementary text S3) (20). An estimate of the change in binding affinity and Gibbs free energy is given in fig. S42.

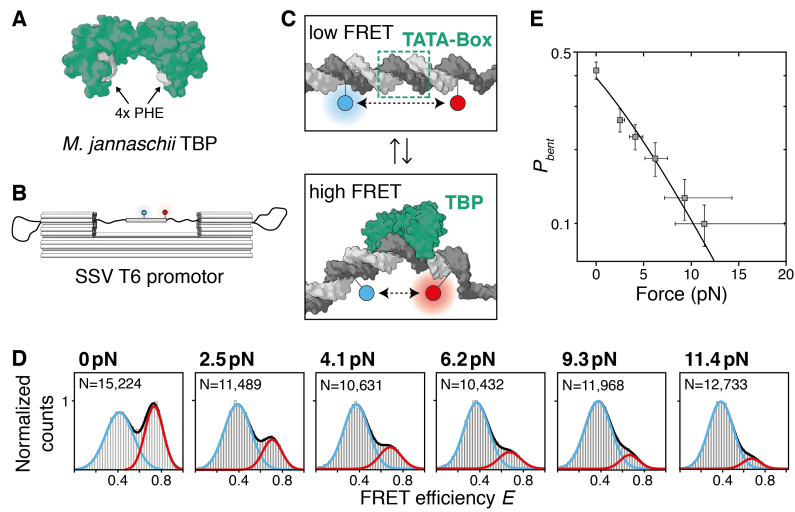


Fig. 3. TBP-induced DNA bending under force. (A) TBP from *M.jannaschii* (PDB: 2Z8U) (29). Two pairs of phenylalanines located in the DNA binding domain promote DNA bending. (B) The SSV T6 promoter including the TATA-box mounted on the force clamp; Atto532 donor (blue) and Atto647n acceptor (red). (C) TBP binds the minor groove of the TATA-box and bends the duplex by almost 90°, thus changing the distance between donor and acceptor. (D) FRET histograms and Gaussian fits for the low-FRET (blue) and high-FRET (red) population. N is the number of molecules measured for each force. (E) Semi-log plot of the probability of the bent state P_{bent} as a function of force. The solid line is a Boltzmann distribution fit. Y-axis error is the standard error of P_{bent} ; x-axis error is the uncertainty of the calculated force (fig. S28).

The presented DNA origami force clamp provides a new tool to quantify the sensitivity of transcription factor-induced distortion to DNA tension and thus to chromosome organization. This adds new information to the growing picture of transcriptional regulation and protein-DNA interactions in general. Our nanoscopic force clamp expands the range of available single-molecule force spectroscopy techniques and makes new molecular systems accessible to sensitive force spectroscopy analysis. The self-assembling clamps are easy to prepare and can be used to study any DNA-interacting and DNA-modifiable system, e.g. proteins conjugated with short DNA tethers. Simple operation and highly increased throughput compared to standard techniques facilitate the generation of force spectroscopy data with a dynamic range of 0 to 12 pN, which easily can be extended to ~ 50 pN (supplementary text S4) (20). As our method provides the flexibility to perform both on-surface and in-solution experiments, we further envision moving from elaborate and costly single-molecule tools toward simple and readily adaptable ensemble assays.

References and Notes:

1. M. S. Kellermayer, S. B. Smith, H. L. Granzier, C. Bustamante, Folding-unfolding transitions in single titin molecules characterized with laser tweezers. *Science*. **276**, 1112–1116 (1997).
2. M. Rief, M. Gautel, F. Oesterhelt, J. M. Fernandez, H. E. Gaub, Reversible unfolding of individual titin immunoglobulin domains by AFM. *Science*. **276**, 1109–1112 (1997).
3. S. B. Smith, Y. Cui, C. Bustamante, Overstretching B-DNA: the elastic response of individual double-stranded and single-stranded DNA molecules. *Science*. **271**, 795–799 (1996).
4. J. M. Fernandez, H. Li, Force-clamp spectroscopy monitors the folding trajectory of a single protein. *Science*. **303**, 1674–1678 (2004).
5. K. C. Neuman, A. Nagy, Single-molecule force spectroscopy: optical tweezers, magnetic tweezers and atomic force microscopy. *Nat Meth*. **5**, 491–505 (2008).
6. N. Ribeck, O. A. Saleh, Multiplexed single-molecule measurements with magnetic tweezers. *Rev. Sci. Instrum.* **79**, 094301 (2008).
7. K. Halvorsen, W. P. Wong, Massively parallel single-molecule manipulation using centrifugal force. *Biophys. J.* **98**, L53–5 (2010).
8. E. Pfitzner *et al.*, Rigid DNA Beams for High-Resolution Single-Molecule Mechanics. *Angew. Chem. Int. Ed.* **52**, 7766–7771 (2013).
9. H. Shroff *et al.*, Biocompatible Force Sensor with Optical Readout and Dimensions of 6 nm

- ³. *Nano Lett.* **5**, 1509–1514 (2005).
10. W. Shen, M. F. Bruist, S. D. Goodman, N. C. Seeman, A Protein-Driven DNA Device That Measures the Excess Binding Energy of Proteins That Distort DNA. *Angew. Chem. Int. Ed.* **43**, 4750–4752 (2004).
 11. H. Gu, W. Yang, N. C. Seeman, DNA scissors device used to measure MutS binding to DNA mis-pairs. *J. Am. Chem. Soc.* **132**, 4352–4357 (2010).
 12. C. Grashoff *et al.*, Measuring mechanical tension across vinculin reveals regulation of focal adhesion dynamics. *Nature.* **466**, 263–266 (2010).
 13. N. Seeman, DNA in a material world. *Nature.* **421**, 427–431 (2003).
 14. P. W. K. Rothmund, Folding DNA to create nanoscale shapes and patterns. *Nature.* **440**, 297–302 (2006).
 15. S. M. Douglas *et al.*, Rapid prototyping of 3D DNA-origami shapes with caDNAno. *Nucleic Acids Res.* **37**, 5001–5006 (2009).
 16. Y. Ke *et al.*, Multilayer DNA origami packed on a square lattice. *J. Am. Chem. Soc.* **131**, 15903–15908 (2009).
 17. E. S. Andersen *et al.*, Self-assembly of a nanoscale DNA box with a controllable lid. *Nature.* **459**, 73–76 (2009).
 18. S. M. Douglas *et al.*, Self-assembly of DNA into nanoscale three-dimensional shapes. *Nature.* **459**, 414–418 (2009).

19. T. Liedl, B. Högberg, J. Tytell, D. E. Ingber, W. M. Shih, Self-assembly of three-dimensional prestressed tensegrity structures from DNA. *Nat. Nanotechnol.* **5**, 520–524 (2010).
20. Materials and methods are available as supplementary materials on *Science* Online.
21. M. C. Murphy, I. Rasnik, W. Cheng, T. M. Lohman, T. Ha, Probing single-stranded DNA conformational flexibility using fluorescence spectroscopy. *Biophys. J.* **86**, 2530–2537 (2004).
22. S. Hohng *et al.*, Fluorescence-force spectroscopy maps two-dimensional reaction landscape of the holliday junction. *Science*. **318**, 279–283 (2007).
23. J. Ross *et al.*, Multicolor Single-Molecule Spectroscopy with Alternating Laser Excitation for the Investigation of Interactions and Dynamics. *J. Phys. Chem. B.* **111**, 321–326 (2007).
24. S. A. McKinney, C. Joo, T. Ha, Analysis of Single-Molecule FRET Trajectories Using Hidden Markov Modeling. *Biophys. J.* **91**, 1941–1951 (2006).
25. F. E. Kemmerich *et al.*, Simultaneous Single-Molecule Force and Fluorescence Sampling of DNA Nanostructure Conformations Using Magnetic Tweezers. *Nano Lett.* **16**, 381–386 (2016).
26. C. Hyeon, J. Lee, J. Yoon, S. Hohng, D. Thirumalai, Hidden complexity in the isomerization dynamics of Holliday junctions. *Nat. Chem.* **4**, 907–914 (2012).
27. A. Gietl *et al.*, Eukaryotic and archaeal TBP and TFB/TF(II)B follow different promoter DNA bending pathways. *Nucleic Acids Res.* **42**, 6219–6231 (2014).

28. A. N. Kapanidis *et al.*, Alternating-laser excitation of single molecules. *Acc. Chem. Res.* **38**, 523–533 (2005).
29. N. Adachi, M. Senda, R. Natsume, T. Senda, M. Horikoshi, Crystal structure of *Methanococcus jannaschii* TATA box-binding protein. *Genes to Cells.* **13**, 1127–1140 (2008).
30. J. Sambrook, D. W. Russell, *Molecular cloning: a laboratory manual* (CSHL Press, Cold Spring Harbour, NY, ed. 3, 2001).
31. S. M. Douglas, J. J. Chou, W. M. Shih, DNA-nanotube-induced alignment of membrane proteins for NMR structure determination. *Proc. Natl. Acad. Sci. U. S. A.* **104**, 6644–6648 (2007).
32. E. Stahl, T. G. Martin, F. Praetorius, H. Dietz, Facile and Scalable Preparation of Pure and Dense DNA Origami Solutions. *Angew. Chem. Int. Ed.* **53**, 12735–12740 (2014).
33. J. M. de la Rosa-Trevín *et al.*, Xmipp 3.0: an improved software suite for image processing in electron microscopy. *J. Struct. Biol.* **184**, 321–328 (2013).
34. T. Ha, P. Tinnefeld, Photophysics of fluorescent probes for single-molecule biophysics and super-resolution imaging. *Annu Rev Phys Chem.* **63**, 595–617 (2012).
35. E. Nir *et al.*, Shot-noise limited single-molecule FRET histograms: comparison between theory and experiments. *J. Phys. Chem. B.* **110**, 22103–22124 (2006).
36. T. E. Tomov *et al.*, Disentangling Subpopulations in Single-Molecule FRET and ALEX Experiments with Photon Distribution Analysis. *Biophys. J.* **102**, 1163–1173 (2012).

37. G. R. Strobl, *The Physics of Polymers* (Springer Science & Business Media, Berlin Heidelberg, Germany, ed. 3, 2007)
38. D. B. McIntosh, O. A. Saleh, Salt Species-Dependent Electrostatic Effects on ssDNA Elasticity. *Macromolecules* **44**, 2328–2333 (2011).
39. B. H. Zimm, Dynamics of Polymer Molecules in Dilute Solution: Viscoelasticity, Flow Birefringence and Dielectric Loss. *J. Chem. Phys.* **24**, 269–11 (1956).
40. T. Strunz, K. Oroszlan, R. Schafer, H. J. Guntherodt, Dynamic force spectroscopy of single DNA molecules. *Proc. Natl. Acad. Sci. U. S. A.* **96**, 11277–11282 (1999).

Acknowledgments:

We thank Hermann Gaub, Andreas Gietl, Alexander Maier, Iain MacPherson, Jan Lipfert, Mauricio Pilo-Pais, Omar Saleh, and Tao Zhang for discussions and Susanne Kempter and Gerlinde Schwake for technical assistance. Sarah Schulz kindly prepared the MjTBP.

Funding:

This work was supported by the Deutsche Forschungsgemeinschaft (LI 1743/2-1, TI 329/6-1, GrK1952/1 ‘Metrology for Complex Nanosystems’, Nanosystems Initiative Munich, SFB 1032 (TPA6) and SFB 960 (TPA7)), the Braunschweig International Graduate School of Metrology B-IGSM, the European Commission (FP7 - EScoDNA GA no. 317110 and ERC grant agreement n° 336440, ORCA), and the Boehringer Ingelheim Foundation.

Author contributions:

P.N., B.W. and P.H. performed the experiments. P.N., D.G., P.T. and T.L. designed the research. P.N., B.W., P.H., L.K., W.B., P.T. and T.L. analyzed the data. P.N. and W.B. prepared the figures. P.N., P.T., D.G. and T.L. wrote the manuscript. All authors edited the manuscript.

Competing interests:

The authors declare that they have no competing interests.

Data and materials availability:

Additional data described in this work can be found in the online supplementary materials.

Supplementary Materials:

Materials and Methods

Supplementary Text S1-S4

Figures S1-S42

References (30-40)

Custom M13mp18-based scaffold sequences

OUTLOOK TO FUTURE WORK

6.1 DNA ORIGAMI COMPONENTS FROM A SINGLE BACTERIAL CULTURE

Using intact bacteriophage particles as a material source could be one key component for future large-scale production of DNA origami structures. So far, the scaffold material is purified genomic virus DNA and the staples are chemically synthesized with purity and quality insufficient for most of the envisioned applications of DNA origami. One possible approach for such a large-scale production could be the following: all components could be part of a synthetic phagemid. A long un-interrupted region can serve as the scaffold strand. This region is followed by the individual staple sequences. The individual staple sequences are separated from the scaffold sequence and from the other staple sequences by short, self-cleaving DNA motifs [201, 202]. Once such a phagemid construct is synthesized for a given origami structure, it only needs to be transformed to *E.coli* bacteria. The production of M13 phage particles can then be triggered by either the addition of a M13 helper phage as used in conventional phage display or via an engineered helper plasmid [203]. This helper plasmid has the advantage of eliminating any helper phage DNA contamination. With such a construct, a perfect 1:1 stoichiometry of scaffold and staples would be programmed into the construct and a molar excess of staple strands over the scaffold might not be needed. Another advantage would be that expensive enzymatic treatment of the biologically produced staples as required in the paper by Ducani et al. [114] is not needed anymore. The bacteriophage particles carrying the ssDNA construct with both scaffold and staples can be produced on a large-scale via high-cell density fermentation [109]. This production of all required DNA material in just a single bacterial culture followed by direct folding of the origami structures from the intact bacteriophages has the potential to reduce the involved cost tremendously while improving the quality of the material at the same time.

6.2 IMPROVED MODELING OF ENTROPIC FORCE IN THE DNA ORIGAMI FORCE CLAMP

Although we already showed successful force spectroscopy experiments with the DNA origami force clamp in chapter 5, a better understanding as well as modeling of the applied force by the ssDNA segments is required. Our collaborator from Oxford University (Megan Engel in

the groups of Jonathan Doye and Ard Louis) is currently using the coarse-grained oxDNA model [140–143] to predict the forces applied to the systems we studied in the associated publication P3 (5.3). Preliminary results showed that the forces seem to be higher than what we predicted using the modified FJC model. Two effects make the ssDNA behave different than approximated with the simple FJC model: base stacking of neighboring bases and secondary structure formation. The first oxDNA simulations showed a high degree of secondary structure formation in the ssDNA segments applying the force, thus leading to higher forces than predicted. This result is consistent with estimates of secondary structure stabilities from the NUPACK web application [204]. In future work, we plan to address this problem as follows: first, we started to genetically engineer and delete all guanine bases in the scaffold segments that remain single-stranded and exert the force. This should result in a significantly lower probability of secondary structures and thus make the prediction of the force more reliable. Measurements of the Holliday junction kinetics under the same conditions will allow us to quantify the effect of the secondary structures in addition to the simulations. Second, we started to re-design the force clamp structure so that we can use synthetic ssDNA segments with poly-Thymidine sequences for the force generation. Theoretically, this should result in ssDNA segments that behave closest to the idealized entropic spring characteristics.

6.3 BULK FORCE SPECTROSCOPY MEASUREMENTS

One advantage of the DNA origami force clamp presented in chapter 5 is that it works autonomously in solution and does not have to be connected to any kind of surface. Theoretically, this should allow ensemble force spectroscopy measurements with simple bulk fluorescence or gel shift analysis. We are currently working on two assays that study enzymatic activity as a function of force in bulk and not on a single-molecule level. To test this concept, we started to look at the activity of the restriction enzyme *EcoRV* as a function of force and compare it to results obtained with optical tweezers [205]. The advantage here is that we can screen several forces in a single agarose gel. Together with the Gaub lab at LMU, we also started to mount force activated enzymes in our force clamp to study their enzymatic activity as a function of force in an ensemble fashion.



APPENDIX

A.1 SUPPORTING INFORMATION FOR ASSOCIATED PUBLICATION P1

Supporting Information

DNA Origami Structures Directly Assembled from Intact Bacteriophages

By

Philipp C. Nickels, Yonggang Ke, Ralf Jungmann, David M. Smith,
Marc Leichenring, William M. Shih, Tim Liedl, and Björn Högberg

published in

Small (2014), 10, 1765 - 1769

Reprinted with permission from ref. [137]. Copyright 2014 WILEY-VCH.

NANO MICRO
small

Supporting Information

for *Small*, DOI: 10.1002/smll.201303442

DNA Origami Structures Directly Assembled from Intact
Bacteriophages

*Philipp C. Nickels, Yonggang Ke, Ralf Jungmann, David M.
Smith, Marc Leichsenring, William M. Shih, Tim Liedl,* and
Björn Högberg**

Supplementary Information

DNA Origami Structures Assembled Directly from Intact Bacteriophages

Philipp C. Nickels¹, Yonggang Ke², Ralf Jungmann², David M. Smith¹, Marc Leichsenring¹, William M. Shih², Tim Liedl^{1,*}, Björn Högberg^{3,*}

¹ Center for Nanoscience and Department of Physics, LMU Munich (Germany)

² Dana-Farber Cancer Institute, Harvard Medical School, Boston (USA)

³ Department of Neuroscience, Swedish Medical Nanoscience Center, Karolinska Institute, Stockholm (Sweden)

* To whom correspondence should be addressed: tim.liedl@physik.lmu.de, bjorn.hogberg@ki.se

Supplementary Note S1: Folding from Bacteriophage M13	2
Note S1.1: Preparation of M13 Phage	2
Note S1.2: Assembling Structures from M13 Phage Particles	3
Note S1.3: Assembling Structures from M13 infected liquid <i>E.coli</i> Culture	4
Note S1.4: Agarose Gel Electrophoresis and Gel Purification of M13 DNA Origami Structures	5
Note S1.5: Transmission Electron Microscopy of M13 DNA Origami Structures	5
Note S1.6: Atomic Force Microscopy of M13 DNA Origami Structures	6
Supplementary Note S2: Folding from Bacteriophage λ	8
Note S2.1: Preparation of λ Phages	8
Note S2.2: Denaturing Agarose Gel Electrophoresis of λ -DNA and Phages	9
Note S2.3: λ -DNA Melting Curves	11
Note S2.4: Assembling Structures from λ Phage Particles	12
Note S2.5: Agarose Gel Electrophoresis of λ DNA Origami Structures	13
Note S2.6: Atomic Force Microscopy of λ DNA Origami Structures	13
Note S2.7: Transmission Electron Microscopy of λ DNA Origami Structures	13
Supplementary Note S3: DNA Origami Designs and DNA Sequences	15
Note S3.1: Design of M13 DNA Origami Structures	15
Note S3.2: Design of the λ DNA Origami Structure	15

Supplementary Note S1: Folding from Bacteriophage M13

Note S1.1: Preparation of M13 Phage

The 3 different M13 bacteriophages (p7249 phage, p7560 phage, and p8064 phage) were prepared as previously described.^[1] Instead of purifying the single-stranded M13 DNA we stored the PEG precipitated phage particles (re-suspended in 10mM Tris, pH=8.5) at -20°C until further use as scaffold material. Figure S1a shows a transmission electron micrograph of a purified M13 phage particle. Since phages consist of a protein shell and the genomic DNA inside, a quantitative measurement of the concentration of the phage particles via absorption spectroscopy is difficult. Titering the purified phage would give us the amount of infectious phage particles instead of the overall concentration. Thus we estimated the phage concentration via comparison to a standard DNA marker. We compared the fluorescence intensity of the target phage band on agarose gels to the intensity of a standard DNA marker with known mass value (shown in figure S1b, the double stranded 1.5kbp DNA from a 1kb DNA ladder (New England Biolabs)). The M13 phage samples were denatured prior to loading on the gel using 0.1% SDS, 10mM EDTA and incubation at 65°C for 5min.

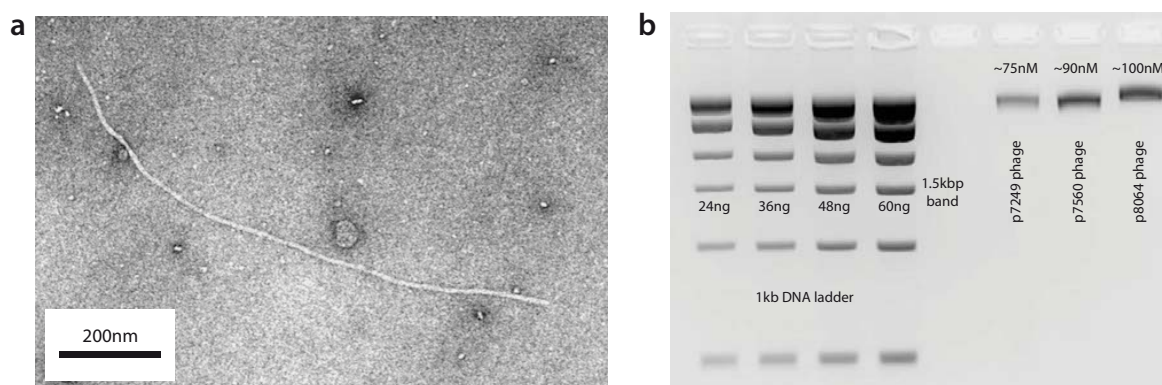


Figure S1: (a) Transmission electron micrograph of a ~1µm long filamentous M13 phage particle. (b) 2% agarose gel containing 0.5xTBE and 0.5µg/mL ethidium bromide run for 3.5 hours at 70V. We used 4 different concentrations of the 1kb DNA ladder. For each concentration we measured the intensity of the 1.5kbp band and together with the known mass value we derived an intensity-mass plot. Based on this intensity-mass plot we estimated the concentration of the phage particles using the intensity of the target phage bands.

Note S1.2: Assembling Structures from M13 Phage Particles

Assembly of M13 DNA origami structures was accomplished in a one-pot reaction. 5nM bacteriophage M13 particles were mixed with 100nM of every oligonucleotide staple strand (high purity salt free, Eurofins MWG Operon) in 1xTE buffer (10mM Tris-HCl pH=7.6, 1mM EDTA) containing 5mM NaCl, 0.1% SDS, 1mg/mL Proteinase K (New England Biolabs), and varying concentrations of MgCl₂ (12mM for the 2D rectangle, 16mM for the 6HB and the 24HB, 18mM for the three layer block). For the control samples 5nM of purified scaffold was used instead of the phage particles. The mixture was subjected to a thermal annealing ramp (using a PTC-225 DNA Engine Tetrad, MJ Research) as shown in figure S2a. It was heated to 65°C for 5 min and subsequently cooled to 25°C via a non-linear temperature ramp over the course of 2 hours for the 2D rectangle, 16 hours for the 6HB and the three layer block, and 40 hours for the 24HB.

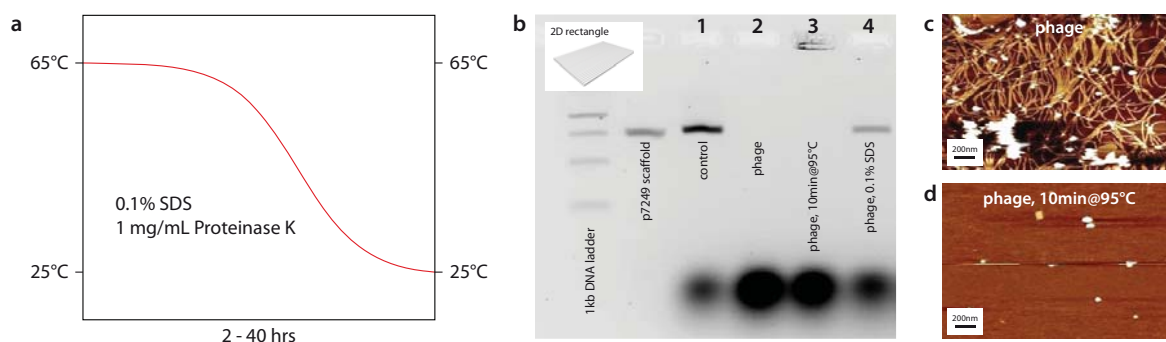


Figure S2: (a) Thermal annealing ramp used to assemble the M13 DNA origami structures (directly from phage as well as the control samples). (b) Comparison of different annealing procedures to fold directly from phage: only the addition of SDS results in a band of correctly assembled origami structures. (c) AFM image of the sample used for lane 2. (d) AFM image of the sample used for lane 3.

To make sure that the phage particles are denatured and origami structures are assembled from the released genomic DNA we tested different annealing schemes. The samples were compared to a control sample conventionally folded from purified scaffold (figure S2b, lane 1). Substituting the purified scaffold with phage particles without any denaturing agent or treatment followed by the depicted annealing ramp (figure S2a) did not yield a band of folded structures (lane 2). The AFM image of such a sample in figure S2c shows that the phages are still intact. A 10 min heat denaturing step followed by the described annealing

did not result in a detectable band of folded products as well (lane 3). The AFM image of such a sample in figure S2d shows that the phage particles are denatured but only a few origami structures are formed. The addition of SDS as denaturing agent without any extra heat denaturing steps yields a band of correctly folded structures migrating at the same speed as the control band (lane 4). Proteinase K is not needed for the folding process itself. However, it digests the M13 capsid protein debris and thus results in a cleaner background in AFM/TEM imaging.

Note S1.3: Assembling Structures from M13 infected liquid *E.coli* Culture

M13 bacteriophage was amplified in an *E.coli* liquid culture as previously described.^[1] At the point of harvest the *E.coli* cells were pelleted via centrifugation at 3,000rcf, 4°C for 30min. The cell pellet was discarded and the supernatant containing the unpurified bacteriophage was kept at 4°C until further usage as scaffold material. The concentration of bacteriophage particles in the crude suspension was estimated via gel electrophoresis as described in note S1.1 and figure S1. A typical liquid culture M13 prep yielded a bacteriophage concentration of about 1 to 2nM in the crude suspension after *E.coli* cell removal.

We tested whether a crowded environment full of biological compounds might inhibit the self-assembly process via the addition of fetal bovine serum (FBS). Figure S3a shows the agarose gel analysis data of the assembly of the M13 based 2D rectangle. We added four different concentrations between 10 and 40 volume-% FBS to the assembly reaction. The FBS was heat-inactivated at 65°C for 30 minutes prior to mixing the components to prevent DNA degradation while preparing the sample. A decrease in assembly yield with increasing FBS could not be observed.

The assembly of the M13 DNA origami structures from the crude bacteriophage suspension was accomplished in a one-pot reaction. About 1 to 1.5nM M13 bacteriophage ($\frac{3}{4}$ of the final sample volume was crude M13 suspension) was mixed with 12.5nM of every oligonucleotide staple strand for the six helix bundle structure (high purity salt free, Eurofins MWG Operon) in 1xTE buffer (10mM Tris-HCl pH=7.6, 1mM EDTA) containing a final concentration of 16mM MgCl₂, 62mM NaCl, 0.1% SDS and 1mg/mL Proteinase K (New England Biolabs). Note: the growth medium used for the M13 prep contains 83mM NaCl,

thus the high NaCl concentration in the final sample. Since it also contains 5mM MgCl₂, we adjusted the amount of added MgCl₂ to 12.25mM resulting in the final concentration of 16mM. The sample was subjected to the thermal annealing procedure described in note S1.2 (16 hour total annealing time for the 6 helix bundle).

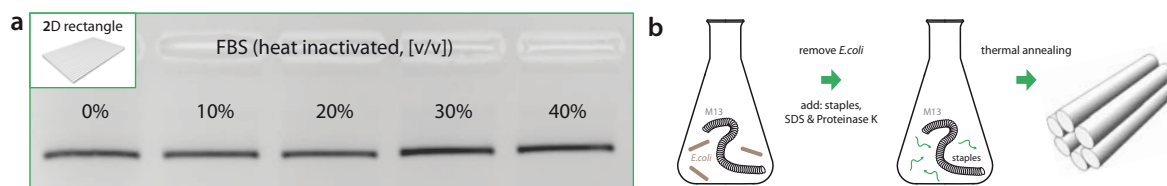


Figure S3: (a) Assembly of the 2D rectangle from purified M13 phage with different amounts of FBS. The crowded environment does not affect the assembly yield. The only detectable difference is the decrease in migration speed with increasing FBS concentrations due to the increasing amounts of sodium ions added with the FBS. (b) Illustration of the assembly process directly from an M13 infected *E.coli* liquid culture: first we removed the bacterial cells via centrifugation. Next, all components needed for the assembly are added and the structure is folded via thermal annealing without any purification of the phage particles.

Note S1.4: Agarose Gel Electrophoresis and Gel Purification of M13 DNA Origami Structures

Folded M13 origami constructs were electrophoresed on 2% agarose gels containing 0.5xTBE buffer (45mM Tris, 45mM boric acid, 1mM EDTA), 11mM MgCl₂, and 0.5 µg/mL ethidium bromide for 3 hours at 5.5 V/cm cooled in an ice water bath. Bands were visualized with ultraviolet light and physically extracted. DNA was recovered by pestle-crushing excised bands, freezing for 5min followed by centrifugation for 10min at 5000rcf in a microfuge at 4°C using Freeze'N'Squeeze DNA Gel Extraction spin columns (Bio-Rad). Recovered material in the flow-through was stored at -20°C for further usage. The 1kb DNA ladder was purchased from New England Biolabs.

Note S1.5: Transmission Electron Microscopy of M13 DNA Origami Structures

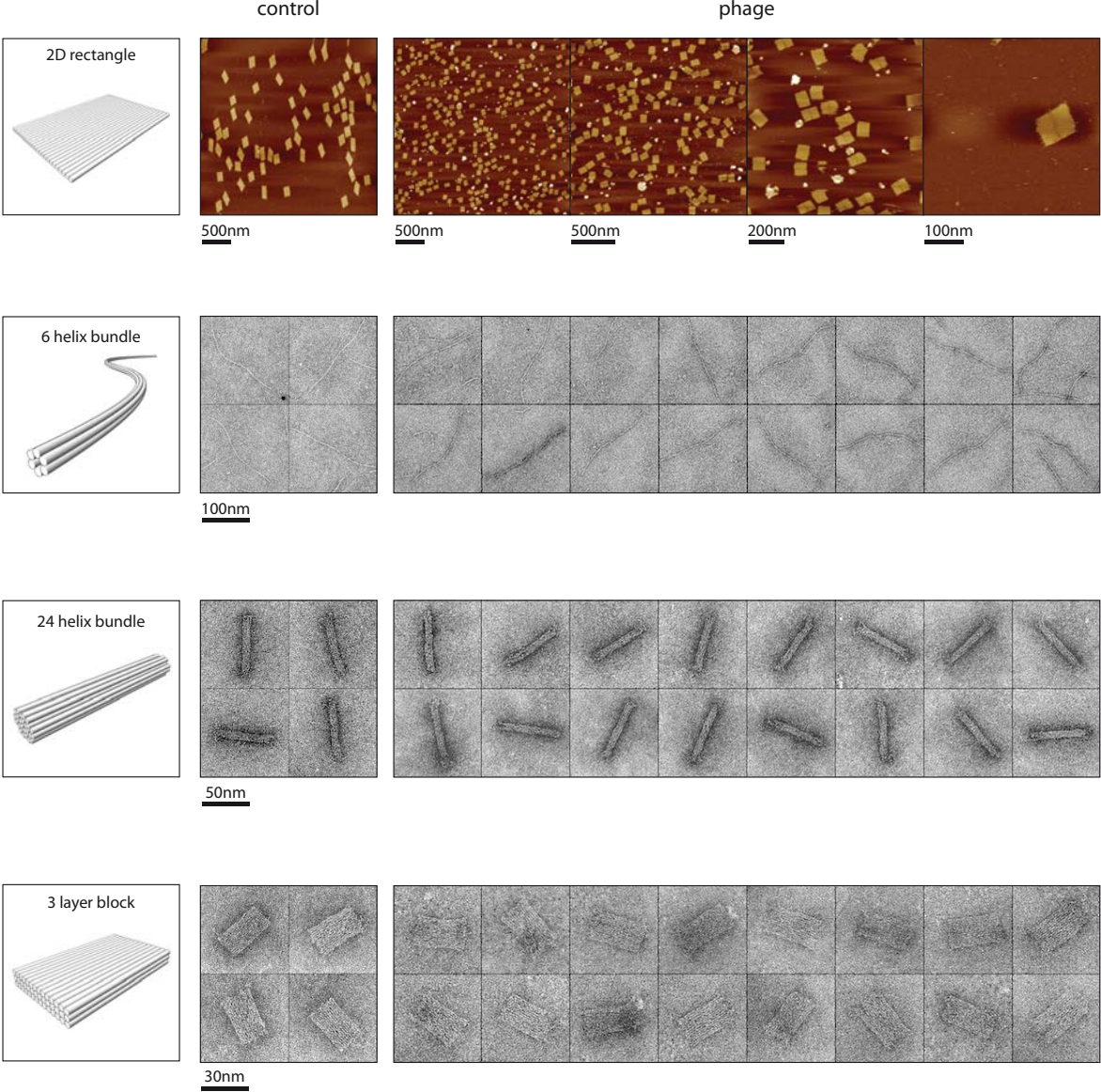
For TEM imaging, 3µL of the gel purified M13 origami solution was adsorbed onto glow-discharged formvar/carbon-coated TEM grids (Plano) and then stained using a 2% aqueous uranyl formate solution containing 25mM sodium hydroxide. Imaging was performed using

a JEM1011 transmission electron microscope (JEOL) operated at 100 kV equipped with a FastScan-F114 camera (TVIPS).

Note S1.6: Atomic Force Microscopy of M13 DNA Origami Structures

For AFM imaging, the folded M13 DNA origami structures (the 2D rectangle) were dialyzed against 500mL 1xTE buffer (10mM Tris-HCl pH=7.6, 1mM EDTA) containing 12mM MgCl₂ for 2 hours at room temperature in 3.5kDa MWCO dialysis units (Slide-A-Lyzer MINI Dialysis Unit 3.5kDa MWCO, Thermo scientific) to remove the SDS. Samples were imaged in tapping mode using a Multimode III AFM (Veeco Metrology Group, now Bruker AXS). Imaging was performed in 1xTAE buffer solution containing 12mM MgCl₂ with SNL-10 sharp nitride cantilevers (Veeco, now Bruker AFM Probes) using resonance frequencies between 7-9 kHz of the 0.24N/m force constant cantilever. 25μL of buffer solution was dropped onto a freshly cleaved mica surface (Plano). 5μL of the dialyzed origami solution was added to the buffer on the mica surface. Imaging parameters were optimized for best image quality while maintaining the highest possible set point to minimize damage to the samples. Images were post-processed by subtracting a 1st order polynomial from each scan line.

Figure S4: Additional AFM and TEM Data of M13 DNA Origami Structures



Supplementary Note S2: Folding from Bacteriophage λ

Note S2.1: Preparation of λ Phages

Bacteriophage λ particles were prepared as follows: wild-type λ -DNA was packaged using a commercially available packaging extract (MaxPlax™ Lambda Packaging Extract, EPICENTRE® Biotechnologies) following the manufacturers instructions. This packaging reactions yielded a packaging efficiency of $> 10^9$ pfu/ μ g of the wild-type λ -DNA. A high titer stock of λ phages for long term storage was prepared via plate lysis and elution. DMSO was added to the phage suspension (final concentration of 7% (v/v)), aliquots were plunged in liquid nitrogen and afterwards stored at -80°C .

Phage particles for folding experiments were prepared via a small scale liquid culture. A 50mL LB culture (supplemented with 0.2% (v/v) maltose and 10mM MgSO_4) of *E.coli* XL-1 Blue cells (Agilent Technologies) was incubated at 30°C with shaking overnight (the low temperature ensures that the cells will not overgrow: phages can adhere to nonviable cells resulting in a decreased titer of the prep). The bacterial cells were pelleted via centrifugation (600rcf for 10min at room temperature) and the supernatant was discarded. The cells were re-suspended and diluted to an OD_{600} of 0.5 with 10mM MgSO_4 . 100 μ L of the prepared cells were mixed with 1×10^6 pfu (100 μ L of a 10^7 pfu/mL dilution of the high titer long term stock) and incubated at 37°C for 20min. 4mL of pre-warmed LB medium was added followed by incubation at 37°C with vigorous shaking (300rpm). After 5 hours, one drop of chloroform was added (about 50 μ L) and the suspension was incubated for another 15min at 37°C with shaking. The debris of the lysed bacterial cells was removed via centrifugation at 13,000rcf, 4°C for 15min. DNaseI was added to a final concentration of 20 μ g/mL, RNaseA to a final concentration of 8 μ g/mL, CaCl_2 to a final concentration of 10mM. The suspension was incubated at 37°C for 30min. Afterwards the suspension was filtered using a sterile 0.45 μ m syringe filter. The phage particles were precipitated (using 10% PEG-8000, 1M NaCl and incubation in ice water for 90min) and subsequently pelleted via centrifugation at 16,000rcf, 4°C for 20min. The pelleted phage was re-suspended in SM buffer (100mM NaCl, 8mM MgSO_4 , 50mM Tris-HCl pH 7.6, autoclaved). PEG was removed via addition of an equal volume of chloroform followed by slow vortexing and

centrifugation at 3,000rcf, 4°C for 10min. The purified phage suspension was stored at 4°C until further use as scaffold material. [2]

Figure S5a shows a transmission electron micrograph of a purified λ phage particle. Figure S5b shows an agarose gel assay of the different steps of the phage purification procedure after the small scale liquid lysate prep. The concentration of the purified phages was estimated as described in Note S1.1 for the M13 phages. We compared the fluorescence intensity of the purified λ phage band to the intensity of the standard DNA marker with known mass value.

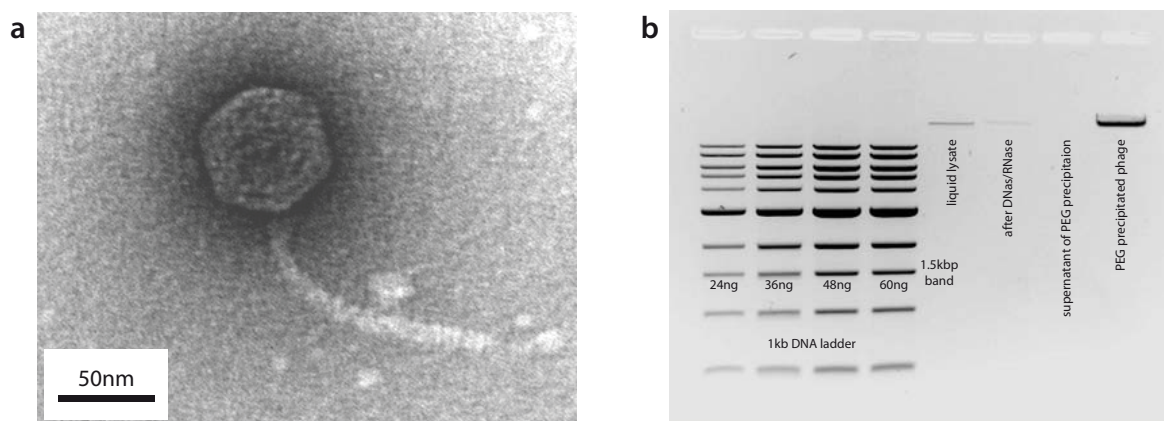


Figure S5: (a) Transmission electron micrograph of a purified λ phage particle. (b) 0.7% agarose gel containing 0.5xTBE and 0.5 μ g/mL ethidium bromide run for 3 hours at 70V. We used 4 different concentrations of the 1kb DNA ladder. For each concentration we measured the intensity of the 1.5kbp band and together with the known mass value we derived an intensity-mass plot. Based on this intensity-mass plot we estimated the concentration of the phage particles using the intensity of the PEG precipitated λ phage band.

Note S2.2: Denaturing Agarose Gel Electrophoresis of λ -DNA and Phages

Native and denatured λ -DNA (commercially available from New England Biolabs (NEB) as well as our own) and λ phage particles were compared on a 0.7% agarose gel containing 1xTAE buffer (40mM Tris, 40mM acetic acid, 1mM EDTA) containing 1M urea and 0.5 μ g/mL ethidium bromide. Denatured samples contained 8M urea and were incubated at 80°C for 5min prior to loading.[3] The gel was run for 3 hours at 5.5V/cm cooled in an ice water bath and bands were visualized with ultraviolet light (image shown in figure S6).

The native NEB λ -DNA results in a nice single band (lane 1). The denatured NEB λ -DNA smears over a range of more than 10kbp (lane 2). This indicates the high amount of nicks in the commercially available λ -DNA molecules, most likely due to mechanical degradation from pipetting and storage. We ligated the NEB λ -DNA with *E.coli* DNA Ligase (New England Biolabs) to repair the backbone (4 hours incubation at 16°C followed by heat inactivation at 65°C for 20min). To prevent the creation of long concatamers we added and thermally annealed a 5-T overhang oligo complementary to one of the cohesive ends to the λ -DNA. Ligation was partly successful: less smearing was observed as well as a high amount of material not entering the gel (lane 3). This indicates that the strategy to prevent concatamers did not work sufficiently. Our own purified λ -DNA (lane 4) as well as the denatured phage particles (lane 5) show a nice single-stranded band. Note that there is a band migrating at the same speed as the native λ -DNA occurring in most denatured samples. This might indicate that not 100% of the dsDNA molecules denature via the 5min incubation step or a fraction of the DNA re-anneals afterwards.

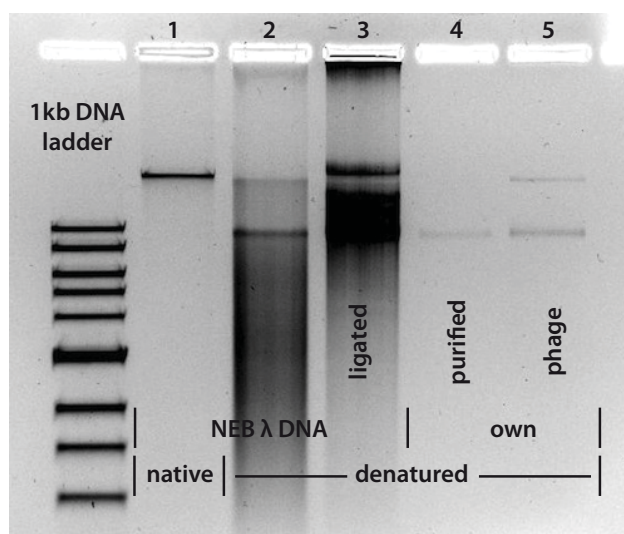


Figure S6: 0.7% agarose denaturing gel containing 1M urea. **Lane 1:** native NEB λ - DNA. **Lane 2:** denatured NEB λ -DNA. **Lane 3:** denatured NEB λ -DNA after ligation. **Lane 4:** denatured purified homemade λ -DNA. **Lane 5:** denatured λ -DNA directly from phage particles. (Denatured samples contained 8M urea and were heated to 65°C for 5min prior to loading on to the gel.)

Note S2.3: λ -DNA Melting Curves

We measured the melting behavior of λ -DNA in the presence of six different formamide concentrations (figure S7). Each sample contained 5 μ g of λ -DNA (Invitrogen), 1xTE buffer (10mM Tris-HCl pH=7.6, 1mM EDTA), and 12mM MgCl₂. Due to the spectral overlay of formamide and DNA at 260nm we recorded the absorption at 270nm in a UV/Vis spectrophotometer (JASCO V-650). The samples were heated to 97°C, cooled to 25°C and again heated to 97°C in intervals of 0.1°C at a rate of 0.5°C per min. The shift of the melting temperature in the presence of formamide to lower temperatures corresponds nicely with the reported value of 0.64°C per volume percent of formamide.^[4]

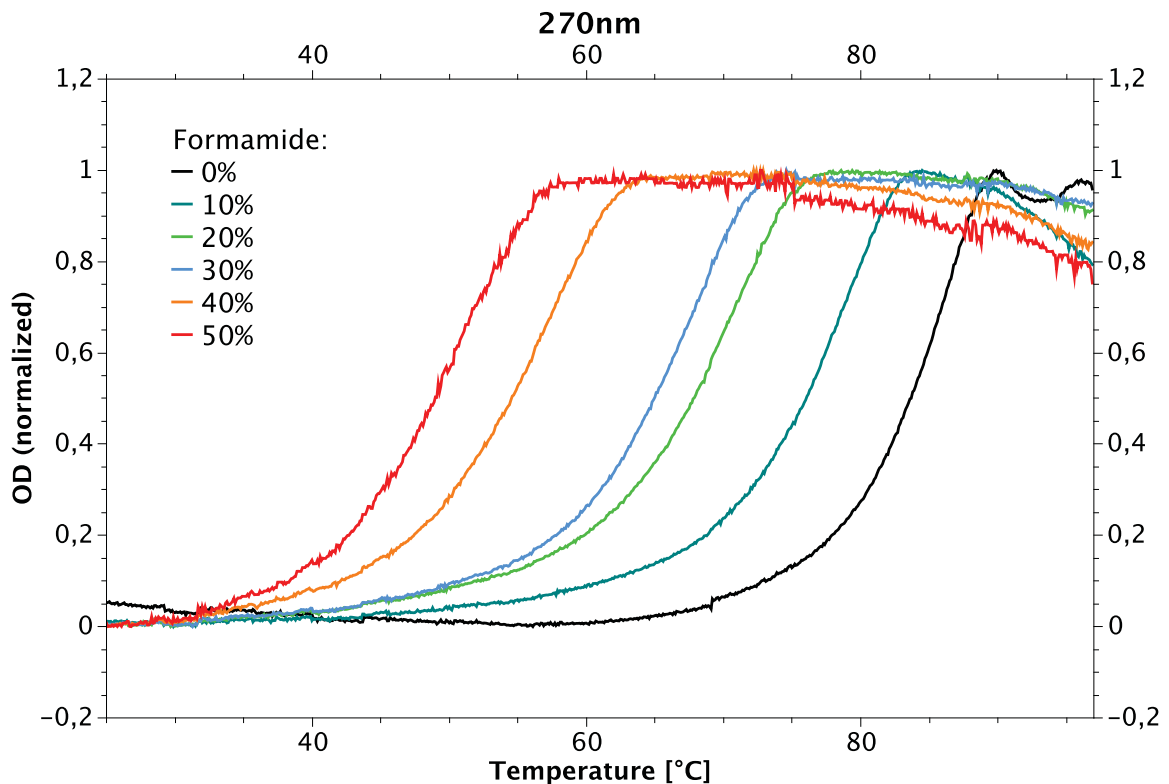


Figure S7: Melting curves of λ -DNA in the presence of different formamide concentrations. The fact that the blue curve is not showing the melting temperature as expected for 30% formamide is most likely due to a pipetting error.

Note S2.4: Assembling Structures from λ Phage Particles

Assembly of λ DNA origami structures was accomplished in a one-pot reaction. 0.2nM bacteriophage λ particles were mixed with 10nM of every oligonucleotide staple strand (reverse-phase cartridge purified, Bioneer Inc.) in 1xTE buffer (10mM Tris-HCl pH=7.6, 1mM EDTA) containing 12mM $MgCl_2$, 0.1% SDS, and 40% formamide. For the control samples between 0.2 and 2nM of commercially available λ -DNA (New England Biolabs) was used instead of the phage particles. The mixture was subjected to a thermal annealing ramp (using a PTC-225 DNA Engine Tetrad, MJ Research) as described in figure S7. The samples were dialyzed against 500mL 1xTE buffer (10mM Tris-HCl pH=7.6, 1mM EDTA) containing 12mM $MgCl_2$ at 4°C overnight in 3.5kDa MWCO dialysis units (Slide-A-Lyzer MINI Dialysis Unit 3.5kDa MWCO, Thermo scientific) with gentle mixing using a magnetic stirrer.

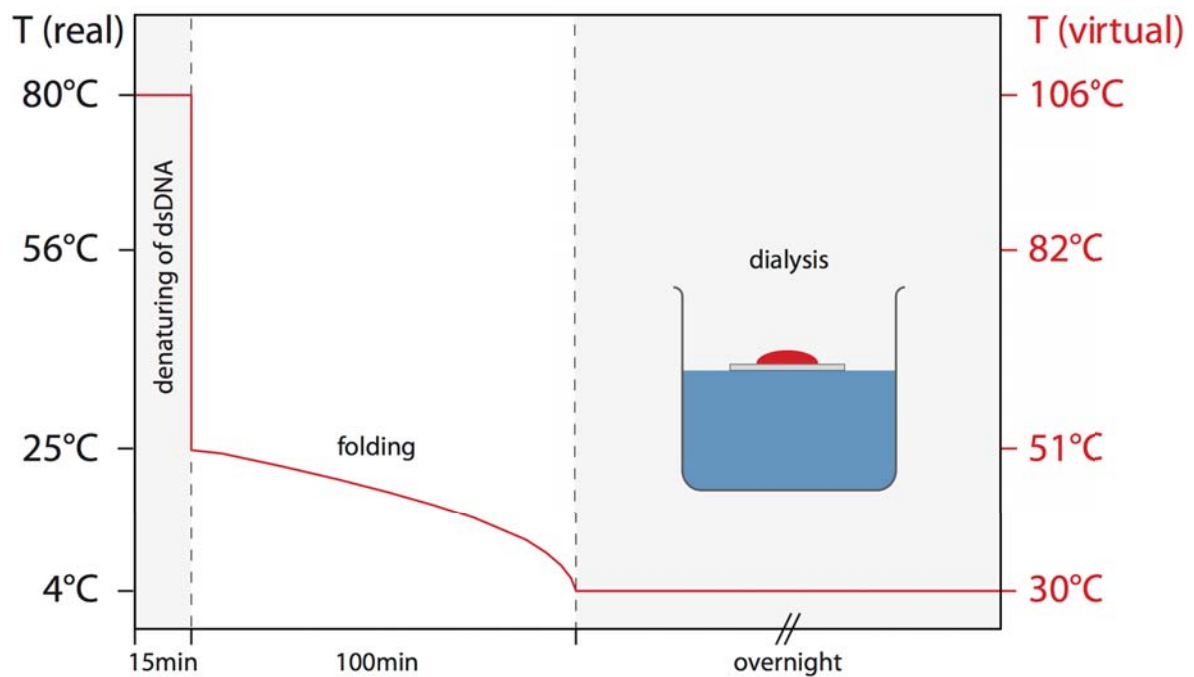


Figure S8: The sample is heated to 80°C for 15min to denature the phage particles, release the genomic DNA and melt the dsDNA. A temperature drop to 25°C in the presence of the high excess of staple strands prevents re-annealing of the dsDNA. A nonlinear temperature ramp to 4°C over the course of 100min is applied to assemble the structures. Overnight dialysis at 4°C is used to remove the formamide as well as the SDS.

Note S2.5: Agarose Gel Electrophoresis of λ DNA Origami Structures

Folded constructs were electrophoresed on 0.7% agarose gels containing 0.5xTBE buffer (45mM Tris, 45mM boric acid, 1mM EDTA), 11mM MgCl₂ and 0.5 μ g/mL ethidium bromide for 3 hours at 5.5 V/cm cooled in an ice water bath. Bands were visualized with ultraviolet light.

Note S2.6: Atomic Force Microscopy of λ DNA Origami Structures

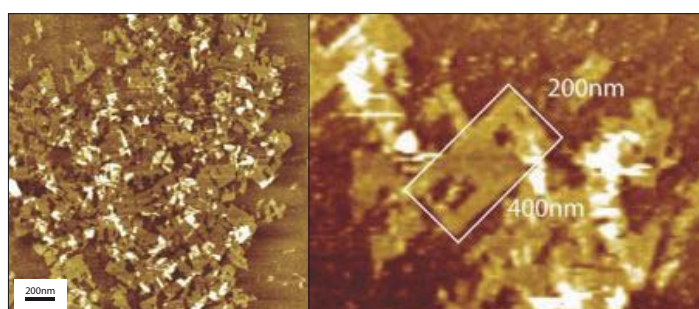
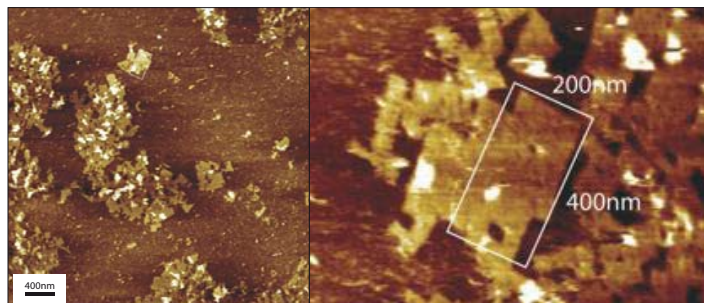
Samples were imaged in tapping mode using a Multimode III AFM (Veeco Metrology Group, now Bruker AXS). Imaging was performed in 1xTAE buffer solution containing 12mM MgCl₂ with SNL-10 sharp nitride cantilevers (Veeco, now Bruker AFM Probes) using resonance frequencies between 7-9 kHz of the 0.24 N/m force constant cantilever. 5 μ L of the dialyzed origami solution was dropped onto a freshly cleaved mica surface (Plano). After 5min, 25 μ L of buffer solution was added to the sample on the mica surface. Imaging parameters were optimized for best image quality while maintaining the highest possible set point to minimize damage to the samples. Images were post-processed by subtracting a 1st order polynomial from each scan line.

Note S2.7: Transmission Electron Microscopy of λ DNA Origami Structures

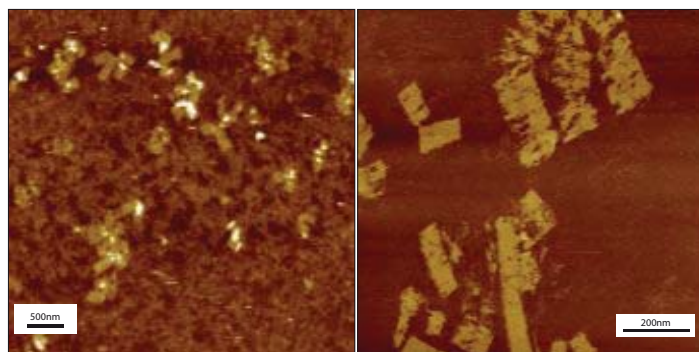
For TEM imaging, 3 μ L of the dialyzed origami solution was adsorbed onto glow-discharged formvar/carbon-coated TEM grids (Plano) and then stained using a 2% aqueous uranyl formate solution containing 25mM sodium hydroxide. Imaging was performed using a JEM1011 transmission electron microscope (JEOL) operated at 100 kV equipped with a FastScan-F114 camera (TVIPS).

Figure S9: Additional AFM and TEM Images of λ DNA Origami Structures

a) AFM: folded from commercially available λ DNA:



b) AFM: folded directly from bacteriophage λ



c) TEM: folded directly from bacteriophage λ

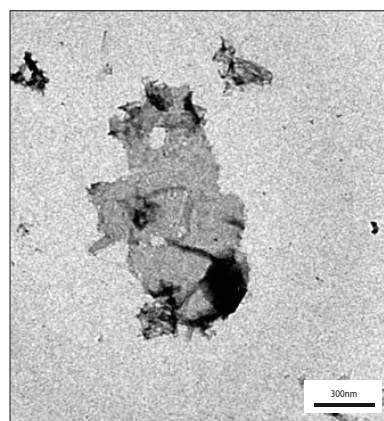
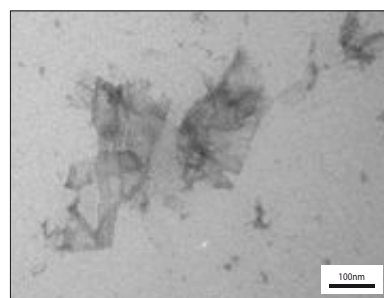
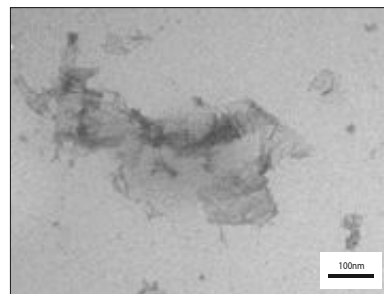


Figure S9: (a) AFM images of samples prepared with commercially available λ -DNA. **Left:** Structures folded with 2nM λ -DNA. (Note: the small M13 based triangular structures in the upper most left image result from a tip used before to image these triangles. However, they serve as a nice physical scale bar.) **Right:** The same sample imaged with higher magnification. (b) AFM data of structures folded directly from λ phage particles. The high amount of phage protein debris covering the surface is clearly visible. (c) Negative stain TEM images of structures folded directly from λ phage particles.

Supplementary Note S3: DNA Origami Designs and DNA Sequences

Note S3.1: Design of M13 DNA Origami Structures

All M13 based structures were designed using the software package caDNAno (version 0.23, <http://www.cadnano.org/legacy>).^[5] The 2D rectangle was slightly modified from the original version described by Rothemund: the scaffold was permuted and the global twisting was reduced by the introduction of targeted deletions.^[6,7] The 'M13' writing was realized by inserting dumbbell shaped hairpins at the positions indicated in figure S10 (see reference [6] for the hairpin sequence). The scaffold routing of the six helix bundle was as well permuted compared to the original version described by Douglas et al.^[1] The 24 helix bundle as well as the three layer block were used as previously described without any changes.^[8,9] The four designs are shown in figures S10-13.

Note S3.2: Design of the λ DNA Origami Structure

For each of the two single strands of the double-stranded molecule we designed a separate structure. These two structures are geometrically identical but chemically distinct rectangles, each 100x400nm in size. Each of these monomers consists of 154 adjacent antiparallel double helices of 320bp in length and is folded by an individual set of staples (3150 individual oligonucleotides of 32nt length in total). The two monomers are connected via an extra set of staples and together form the complete 200x400nm large rectangular object. The scaffold is routed through the λ DNA origami structure similar to the M13 based 2D rectangle. Staple double crossovers are implemented every 32 base pairs. A python script (appendix S1) which uses the scheme shown in figure S14 was used to draw the entire design of the λ DNA origami structure (figure S16), to save a caDNAno compatible file and compute all the staple sequences. Since the caDNAno software was not able to open the generated file (the software crashed due to the high number of bases populated), we used the script to generate a truncated design with only 12 double helices as a control. The staple sequences generated by the script matched perfectly with the sequences generated independently by caDNAno. Figure S15 shows the caDNAno design of the truncated 12 helix tall structure. (A complete list of all staple sequences used is available upon request.)

References

- [1] S. M. Douglas, J. J. Chou, W. M. Shih, *Proceedings of the National Academy of Sciences* **2007**, *104*, 6644–6648.
- [2] J. Sambrook, *Molecular Cloning: a Laboratory Manual, Third Edition*, Cold Spring Harbor Laboratory Press, **2001**.
- [3] E. Hegedus, E. Kokai, A. Kotlyar, V. Dombradi, G. Szabo, *Nucleic Acids Research* **2009**, *37*, e112–e112.
- [4] R. D. Blake, S. G. Delcourt, *Nucleic Acids Research* **1996**, *24*, 2095–2103.
- [5] S. M. Douglas, A. H. Marblestone, S. Teerapittayanon, A. Vazquez, G. M. Church, W. M. Shih, *Nucleic Acids Research* **2009**, *37*, 5001–5006.
- [6] P. W. K. Rothmund, *Nature* **2006**, *440*, 297–302.
- [7] Y. Ke, S. Douglas, M. Liu, J. Sharma, A. Cheng, A. Leung, Y. Liu, W. Shih, H. Yan, *Journal of the American Chemical Society* **2009**, *131*, 15903–15908.
- [8] A. Kuzyk, R. Schreiber, Z. Fan, G. Pardatscher, E.-M. Roller, A. Högele, F. C. Simmel, A. O. Govorov, T. Liedl, *Nature* **2012**, *483*, 311–314.
- [9] I. H. Stein, V. Schüller, P. Böhm, P. Tinnefeld, T. Liedl, *Chem. Eur. J. of Chem. Phys.* **2011**, *12*, 689–695.

Figure S10:
Design of the 2D Rectangle

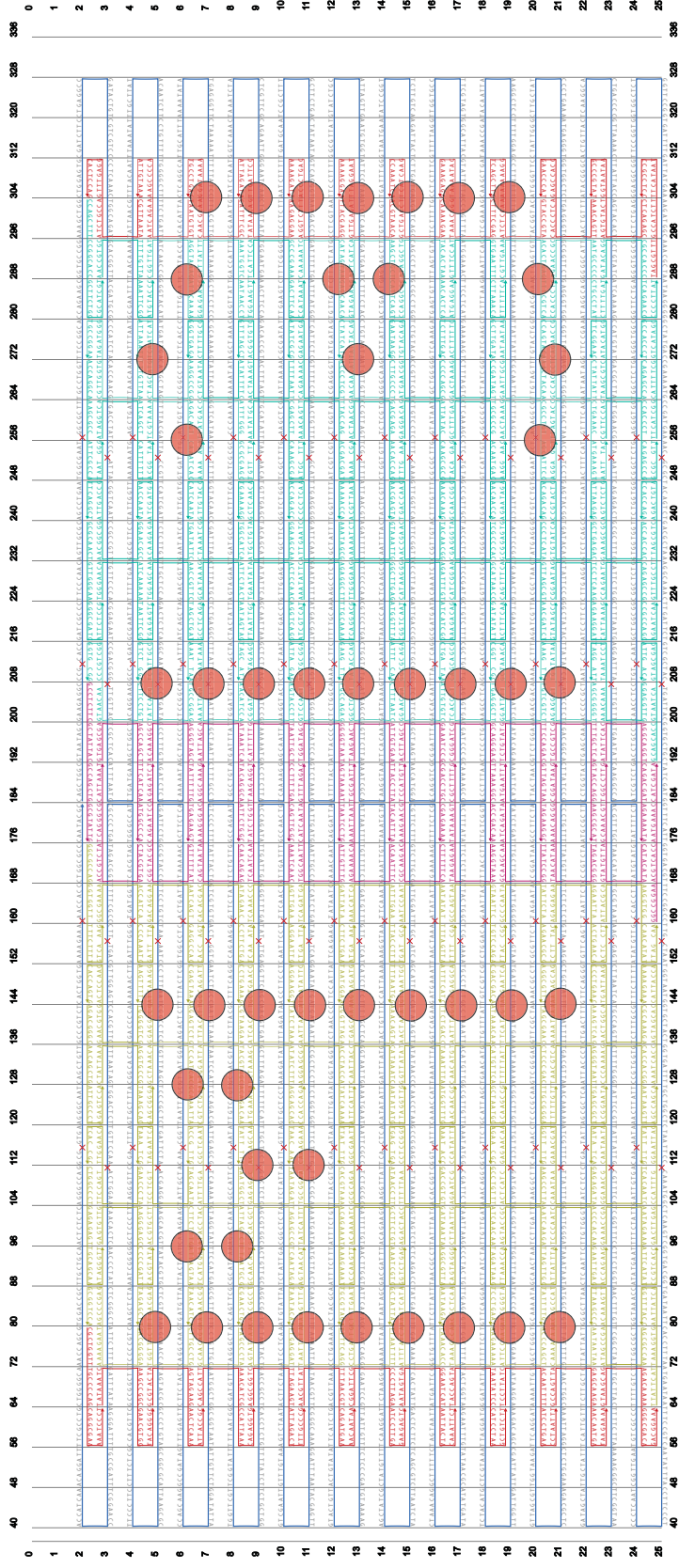
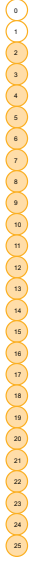


Figure S11:
Design of the 6 Helix Bundle



Figure S13:
Design of the 3 Layer Block

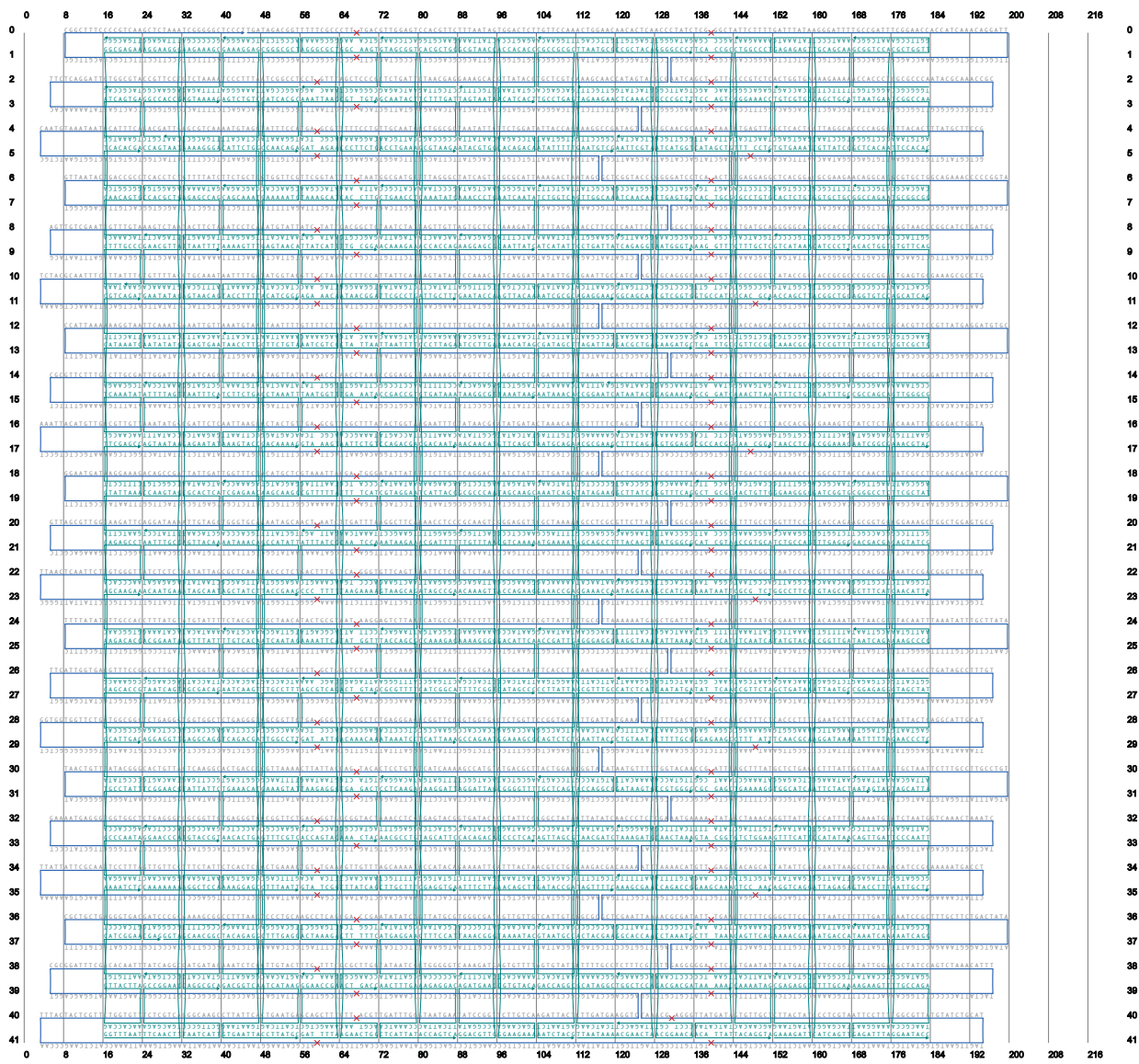


Figure S15: Truncated λ DNA Origami Design

The caDNAno file generated by the python script (Appendix S1) is too big to be opened with the caDNAno software. This truncated design with only 12 double helices instead of 154 was generated to check if the design as well as the computed sequences are correct.

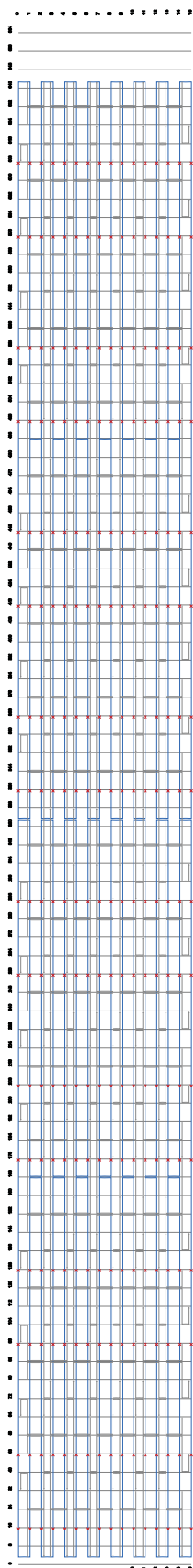


Figure S16: Entire Design Schematics of the λ DNA Origami Structure



Appendix S1: Python code used to draw the design of the λ DNA origami structure and compute the staple sequences

```
#!/usr/bin/env python
# encoding: utf-8
...
Coded by B. Hogberg

Draws the design for the lambda double-rectangle, saves a caDNAnc-compatible file and
computes the staple sequences.

For a 12 helices tall rectangle, the staples generated by caDNAnc and this script matches
perfectly.
...

# Python standard libraries
import string
import os
import sys

import caDNAncFileHandlerClass as caDNAnc

def caDNAncifyScaffold(fragments,VirtStrands):
    # Describing each fragment like this:
    # [ [at this helix,at this base], [coming from helix,base], [at this helix,go to this
    base],[continued by this helix, this base] ]
    #
    # So a list of fragments will be:
    # [ [[helix1,base1], [fromHelix1,fromBase1], [goToHelix1,goToBase1], [toHelix1,
    toBase1] ],
    # [[helix2,base2], [fromHelix2,fromBase2], [goToHelix2,goToBase2], [toHelix2,
    toBase2] ] ]
    for frag in fragments:
        currStrandIndex=frag[0][0]
        nextStrandIndex=frag[2][0]
        prevStrandIndex=frag[1][0]
        if currStrandIndex%2==0:
            evenStrand=True
        else:
            evenStrand=False
        currBpIndex=frag[0][1]
        if evenStrand:
            nextBpIndex=frag[0][1]+1
        else:
            nextBpIndex=frag[0][1]-1
        prevBpIndex=frag[1][1]
        # Defining indices to loop through if even strand left to right
        # if odd strand right to left.
        if evenStrand:
            indices=range(frag[0][1],frag[2][1])
        else:
            indices=range(frag[2][1],frag[0][1][::-1])
        for bp in indices:
            VirtStrands[currStrandIndex]
            [currBpIndex]=[prevStrandIndex,prevBpIndex,nextStrandIndex,nextBpIndex]
            prevStrandIndex=currStrandIndex
            prevBpIndex=currBpIndex
            currBpIndex=nextBpIndex
            if evenStrand:
                nextBpIndex=currBpIndex+1
            else:
                nextBpIndex=currBpIndex-1
        # Last bp:
        VirtStrands[frag[2][0]][frag[2][1]]=[prevStrandIndex,prevBpIndex,frag[3]
        [0],frag[3][1]]
```

```
def caDNAncifyStaples(fragments,VirtStrands,printOut=False):
    #
    # Same as above but with changed directions of odd and even strands
    #
    #
    #
    for frag in fragments:
        currStrandIndex=frag[0][0]
        nextStrandIndex=frag[2][0]
        prevStrandIndex=frag[1][0]
        if currStrandIndex%2==0:
            evenStrand=True
            if not frag[0][1]>frag[2][1]:
                print 'Strand in wrong direction!'
                return
        else:
            evenStrand=False
            if not frag[0][1]<frag[2][1]:
                print 'Strand in wrong direction!'
                return
        currBpIndex=frag[0][1]
        if evenStrand:
            nextBpIndex=frag[0][1]-1
        else:
            nextBpIndex=frag[0][1]+1
        prevBpIndex=frag[1][1]
        # Defining indices to loop through if even strand left to right
        # if odd strand right to left.
        if evenStrand:
            indices=range(frag[2][1],frag[0][1][::-1])
        else:
            indices=range(frag[0][1],frag[2][1])
        for bp in indices:
            VirtStrands[currStrandIndex]
            [currBpIndex]=[prevStrandIndex,prevBpIndex,nextStrandIndex,nextBpIndex]
            if printOut:
                print [prevStrandIndex,prevBpIndex,nextStrandIndex,nextBpIndex]
            prevStrandIndex=currStrandIndex
            prevBpIndex=currBpIndex
            currBpIndex=nextBpIndex
            if evenStrand:
                nextBpIndex=currBpIndex-1
            else:
                nextBpIndex=currBpIndex+1
        # Last bp:
        VirtStrands[frag[2][0]][frag[2][1]]=[prevStrandIndex,prevBpIndex,frag[3]
        [0],frag[3][1]]
        if printOut:
            print VirtStrands[currStrandIndex][currBpIndex]

#####
# Variables
#
#####
lastBpIndex=671
lastStrandIndex=155
leftBrPt=[0,168] # 5'-end of strand is at [helix, base]
rightBrPt=[lastStrandIndex,487]

#####
#
```

```
# Some Initialization...
#####
obj=caDNAnc.caDNAncFileHandler()
obj.initializeEmpty()
# Make empty virtual scaffold strands:
scaffVirtStrands=[[[-1,-1,-1,-1] for i in range(lastBpIndex+1)] for s in
range(lastStrandIndex+1)]
# Make empty virtual staple strands:
stapVirtStrands=[[[-1,-1,-1,-1] for i in range(lastBpIndex+1)] for s in
range(lastStrandIndex+1)]

#####
#
# Scaffold Routing
#
#####
# Make a list of deletion positions
bp=-1
deletions=[]
while bp+5*16 < lastBpIndex:
    insertedDeletions=0
    for i in range(5):
        bp=bp+16
        if i%2==0 and insertedDeletions<2:
            deletions.append(bp)
            insertedDeletions+=1
skipMaster=[0 for i in range(lastBpIndex+1)]
for deletion in deletions:
    skipMaster[deletion]=1
skipVirtStrands=[skipMaster for i in range(lastStrandIndex+1)]

# First two strand fragments:
firstStrandFragments=[[ [0,88], [1,88], [0,322],[1,322]],
[[0,408],[1,408], [0,631],[1,631]]]
caDNAncifyScaffold(firstStrandFragments0,scaffVirtStrands)
firstStrandFragments1=[[ [1,631],[0,631], [1,488], [2,488]],
[[1,487],[2,487], [1,408], [0,408]],
[[1,322],[0,322], [1,168], [2,168]],
[[1,167],[2,167], [1,88], [0,88]]]
caDNAncifyScaffold(firstStrandFragments1,scaffVirtStrands)

# Last strand fragments:
lastStrandFragments=[[ [lastStrandIndex,642],[lastStrandIndex-1,642], [lastStrandIndex,
323],[lastStrandIndex-1,323]],
[[lastStrandIndex,322],[lastStrandIndex-1,322], [lastStrandIndex,3],
[lastStrandIndex-1,3]]]

caDNAncifyScaffold(lastStrandFragments,scaffVirtStrands)

# All the other strands
for s in range(2,lastStrandIndex):
    if s%2==0:
        # Even strands
        betweenFragments=[
            [[s,3], [s+1,3], [s,167], [s-1,167]],
            [[s,168], [s-1,168], [s,322], [s+1,322]],
            [[s,323], [s+1,323], [s,487], [s-1,487]],
            [[s,488], [s-1,488], [s,642], [s+1,642]]
        ]
    else: # Odd strands
```

```
betweenFragments=[
    [[s,642], [s-1,642], [s,488], [s+1,488]],
    [[s,487], [s+1,487], [s,323], [s-1,323]],
    [[s,322], [s-1,322], [s,168], [s+1,168]],
    [[s,167], [s+1,167], [s,3], [s-1,3]]
]
caDNAncifyScaffold(betweenFragments,scaffVirtStrands)

# Insert breakpoints
scaffVirtStrands[leftBrPt[0]][leftBrPt[1]][0]=-1
scaffVirtStrands[leftBrPt[0]][leftBrPt[1]][1]=-1
if leftBrPt[0]%2==0:
    mod=-1
else:
    mod=+1
scaffVirtStrands[rightBrPt[0]][rightBrPt[1]][0]=-1
scaffVirtStrands[rightBrPt[0]][rightBrPt[1]][1]=-1

# Staple strands
#####
# Regular ones:
regularStartBases=[5*8,9*8,13*8,25*8,29*8,33*8,45*8,49*8,53*8,65*8,69*8,73*8]
for startBase in regularStartBases:
    n=startBase
    topStaple=[
        [[0,n+23],[-1,-1],[0,n],[1,n]],
        [[1,n],[0,n],[1,n+7],[-1,-1]]
    ]
    caDNAncifyStaples(topStaple,stapVirtStrands)
    bottomStaple=[
        [[lastStrandIndex,n+8],[-1,-1],[lastStrandIndex,n+31],
        [lastStrandIndex-1,n+31]],
        [[lastStrandIndex-1,n+31],[lastStrandIndex,n+31],[lastStrandIndex-1,n
        +24],[-1,-1]]
    ]
    caDNAncifyStaples(bottomStaple,stapVirtStrands)

for y in range(2,lastStrandIndex,2):
    n=startBase
    staple1=[
        [[y,n+23], [-1,-1], [y,n+16], [y-1,n+16]],
        [[y-1,n+16], [y,n+16], [y-1,n+31], [y-2,n+31]],
        [[y-2,n+31], [y-1,n+31], [y-2,n+24], [-1,-1]]
    ]
    caDNAncifyStaples(staple1,stapVirtStrands)
    staple2=[
        [[y-1,n+8],[-1,-1], [y-1,n+15], [y,n+15]],
        [[y,n+15], [y-1,n+15], [y,n], [y+1,n]],
        [[y+1,n], [y,n], [y+1,n+7], [-1,-1]]
    ]
```

```

    ]
    caDNAnifyStaples(staple2, stapVirtStrands)

# Left edge
topLeftCorner=[[2,31],[-1,-1],[2,3],[-1,-1]]
caDNAnifyStaples(topLeftCorner, stapVirtStrands)

botLeftCorner=[
    [[lastStrandIndex,3],[-1,-1],[lastStrandIndex,39],[lastStrandIndex-1,39]],
    [[lastStrandIndex-1,39],[lastStrandIndex,39],[lastStrandIndex-1,32],
    [-1,-1]]
]
caDNAnifyStaples(botLeftCorner, stapVirtStrands)

for y in range(4, lastStrandIndex, 2):
    n=8
    snakeStaple=[
        [[y,n+23], [-1,-1], [y,n+16], [y-1,n+16]],
        [[y-1,n+16], [y,n+16], [y-1,n+31], [y-2,n+31]],
        [[y-2,n+31], [y-1,n+31], [y-2,n+24], [-1,-1]]
    ]
    caDNAnifyStaples(snakeStaple, stapVirtStrands)

    stapleStaple=[
        [[y-1,3], [-1,-1], [y-1,23], [y,23]],
        [[y,23], [y-1,23], [y,3], [-1,-1]]
    ]
    caDNAnifyStaples(stapleStaple, stapVirtStrands)

# At seams
seamPositions=[168,488]
for n in seamPositions:
    top1 = [ [0,n+23],[-1,-1],[0,n-8],[-1,-1] ]
    caDNAnifyStaples(top1, stapVirtStrands)

    top2 = [
        [[0,n-9],[-1,-1],[0,n-32],[1,n-32]],
        [[1,n-32],[0,n-32],[1,n-25],[-1,-1]]
    ]
    caDNAnifyStaples(top2, stapVirtStrands)

    bot1 = [ [lastStrandIndex,n-24],[-1,-1],[lastStrandIndex,n+7],[-1,-1] ]
    caDNAnifyStaples(bot1, stapVirtStrands)

    bot2 = [
        [[lastStrandIndex,n+8],[-1,-1],[lastStrandIndex,n+31],[lastStrandIndex-1,n
+31]],
        [[lastStrandIndex-1,n+31],[lastStrandIndex,n+31],[lastStrandIndex-1,n+24],
        [-1,-1]]
    ]
    caDNAnifyStaples(bot2, stapVirtStrands)

    for y in range(2, lastStrandIndex, 2):
        leftSnake=[
            [[y-1,n-24], [-1,-1], [y-1,n-17], [y,n-17]],
            [[y,n-17], [y-1,n-17], [y,n-32], [y+1,n-32]],
            [[y+1,n-32], [y,n-32], [y+1,n-25], [-1,-1]]
        ]
        caDNAnifyStaples(leftSnake, stapVirtStrands)

        leftRound=[
            [[y,n+7], [-1,-1], [y,n-16], [y-1,n-16]],
            [[y-1,n-16], [y,n-16], [y-1,n-9], [-1,-1]]
        ]
        caDNAnifyStaples(leftRound, stapVirtStrands)

```

```

    rightRound=[
        [[y-1,n-8],[-1,-1],[y-1,n+15],[y,n+15]],
        [[y,n+15],[y-1,n+15],[y,n+8],[-1,-1]]
    ]
    caDNAnifyStaples(rightRound, stapVirtStrands)

    rightSnake=[
        [[y,n+23], [-1,-1], [y,n+16], [y-1,n+16]],
        [[y-1,n+16], [y,n+16], [y-1,n+31], [y-2,n+31]],
        [[y-2,n+31], [y-1,n+31], [y-2,n+24], [-1,-1]]
    ]
    caDNAnifyStaples(rightSnake, stapVirtStrands)

# Stitch
n=328
top1 = [ [0,n+23],[-1,-1],[0,n-8],[-1,-1] ]
caDNAnifyStaples(top1, stapVirtStrands)

top2 = [
    [[0,n-9],[-1,-1],[0,n-32],[1,n-32]],
    [[1,n-32],[0,n-32],[1,n-25],[-1,-1]]
]
caDNAnifyStaples(top2, stapVirtStrands)

bot1 = [ [lastStrandIndex,n-24],[-1,-1],[lastStrandIndex,n+7],[-1,-1] ]
caDNAnifyStaples(bot1, stapVirtStrands)

bot2 = [
    [[lastStrandIndex,n+8],[-1,-1],[lastStrandIndex,n+31],[lastStrandIndex-1,n+31]],
    [[lastStrandIndex-1,n+31],[lastStrandIndex,n+31],[lastStrandIndex-1,n+24],
    [-1,-1]]
]
caDNAnifyStaples(bot2, stapVirtStrands)
for y in range(2, lastStrandIndex, 2):
    leftSnake=[
        [[y-1,n-24], [-1,-1], [y-1,n-17], [y,n-17]],
        [[y,n-17], [y-1,n-17], [y,n-32], [y+1,n-32]],
        [[y+1,n-32], [y,n-32], [y+1,n-25], [-1,-1]]
    ]
    caDNAnifyStaples(leftSnake, stapVirtStrands)

    leftRound=[
        [[y,n-1], [-1,-1], [y,n-16], [y-1,n-16]],
        [[y-1,n-16], [y,n-16], [y-1,n-11], [-1,-1]]
    ]
    caDNAnifyStaples(leftRound, stapVirtStrands)

    rightRound=[
        [[y-1,n],[-1,-1],[y-1,n+15],[y,n+15]],
        [[y,n+15],[y-1,n+15],[y,n],[-1,-1]]
    ]
    caDNAnifyStaples(rightRound, stapVirtStrands)

    rightSnake=[
        [[y,n+23], [-1,-1], [y,n+16], [y-1,n+16]],
        [[y-1,n+16], [y,n+16], [y-1,n+31], [y-2,n+31]],
        [[y-2,n+31], [y-1,n+31], [y-2,n+24], [-1,-1]]
    ]
    caDNAnifyStaples(rightSnake, stapVirtStrands)

# Right edge
topRightCorner=[
    [[0,642],[-1,-1],[0,616],[1,616]],

```

```

    [[1,616],[0,616],[1,623],[-1,-1]]
]
caDNAnifyStaples(topRightCorner, stapVirtStrands)

botRightCorner=[ [lastStrandIndex,624],[-1,-1],[lastStrandIndex,642],[-1,-1] ]
caDNAnifyStaples(botRightCorner, stapVirtStrands)

for y in range(2, lastStrandIndex, 2):
    n=616
    snake=[
        [[y-1,n+8],[-1,-1], [y-1,n+15], [y,n+15]],
        [[y,n+15], [y-1,n+15], [y,n], [y+1,n]],
        [[y+1,n], [y,n], [y+1,n+7], [-1,-1]]
    ]
    caDNAnifyStaples(snake, stapVirtStrands)

    stapleStaple=[
        [[y,642],[-1,-1],[y,632],[y-1,632]],
        [[y-1,632],[y,632],[y-1,642],[-1,-1]]
    ]
    caDNAnifyStaples(stapleStaple, stapVirtStrands)

# Erase staples at top to make room for notches.
# Then edit the bases that needs change.
for i in range(88):
    stapVirtStrands[0][i]=[-1,-1,-1,-1]
    stapVirtStrands[1][i]=[-1,-1,-1,-1]
for i in range(323,408):
    stapVirtStrands[0][i]=[-1,-1,-1,-1]
    stapVirtStrands[1][i]=[-1,-1,-1,-1]

# A
notchChangeA=[ [2,63],[-1,-1],[2,55],[2,54] ]
caDNAnifyStaples(notchChangeA, stapVirtStrands)
# B
stapVirtStrands[2][87]=[-1,-1,2,86]
# C
notchChangeB=[ [0,103],[1,103],[0,88],[-1,-1] ]
caDNAnifyStaples(notchChangeB, stapVirtStrands)
# D
notchChangeD=[ [0,322],[-1,-1],[0,296],[1,296] ]
caDNAnifyStaples(notchChangeD, stapVirtStrands)
# E
notchChangeE=[ [1,312],[2,312],[1,322],[-1,-1] ]
caDNAnifyStaples(notchChangeE, stapVirtStrands)
# F
notchChangeF=[ [2,351],[-1,-1],[2,328],[-1,-1] ]
caDNAnifyStaples(notchChangeF, stapVirtStrands)
# G
notchChangeG=[ [2,407],[-1,-1],[2,392],[3,392] ]
caDNAnifyStaples(notchChangeG, stapVirtStrands)
# H
notchChangeH=[ [0,423],[1,423],[0,408],[-1,-1] ]
caDNAnifyStaples(notchChangeH, stapVirtStrands)
# I
notchChangeI=[ [2,383],[-1,-1],[2,360],[3,360] ]
caDNAnifyStaples(notchChangeI, stapVirtStrands)

# J - scaffold
for i in range(13):
    scaffVirtStrands[2][i]=[-1,-1,-1,-1]
    scaffVirtStrands[3][i]=[-1,-1,-1,-1]
scaffVirtStrands[2][13]=[3,13,2,14]
scaffVirtStrands[3][13]=[3,12,2,13]
# J - staples

```

```

for i in range(13):
    stapVirtStrands[2][i]=[-1,-1,-1,-1]
    stapVirtStrands[3][i]=[-1,-1,-1,-1]
    stapVirtStrands[2][13]=[2,12,-1,-1]
    stapVirtStrands[3][13]=[-1,-1,3,14]

# K - scaffold
for i in range(632,643):
    scaffVirtStrands[0][i]=[-1,-1,-1,-1]
    scaffVirtStrands[1][i]=[-1,-1,-1,-1]
scaffVirtStrands[0][631]=[0,630,1,631]
scaffVirtStrands[1][631]=[0,631,1,630]
# K - staples
for i in range(632,643):
    stapVirtStrands[0][i]=[-1,-1,-1,-1]
    stapVirtStrands[1][i]=[-1,-1,-1,-1]
    stapVirtStrands[0][631]=[-1,-1,0,630]
    stapVirtStrands[2][632]=[2,633,-1,-1]

#####
# Writing caDNA compatible file
#####
for i in range(lastStrandIndex+1):
obj.appendStrand(num=i,scaf=scaffVirtStrands[i],stap=stapVirtStrands[i],skip=skipVirtStrands[i],row=i,col=1)

obj.printBasicData()
obj.writeCaDNAFile('lambdaRectangle.json')

#####
# Printing out the staple sequences
#####
def reverse(sequence):
    """Returns the bases in reverse order"""
    return sequence[::-1]

def complement_to(sequence):
    """Returns the wc-complement to the sequence"""
    comp = {'a':'T', 'A':'A', 'c':'G', 'C':'G', 'g':'C', 'G':'C', 't':'A', 'T':'A',
    'd':'B', 'B':'?'}
    temp_complement = ''
    for letter in sequence:
        if letter in comp:
            temp_complement = temp_complement + comp[letter]
    return reverse(temp_complement)

def stripped_seq(raw_sequence):
    """Clean the input sequence from unnecessary characters
    and makes the bases uppercase"""
    uppercase = {'a':'A', 'A':'A', 'c':'C', 'C':'C', 'g':'G', 'G':'G', 't':'T', 'T':'T'}
    temp_seq_ra = ''
    for letter in raw_sequence:
        if letter in uppercase:
            temp_seq_ra = temp_seq_ra + uppercase[letter]
    return temp_seq_ra

# First populate the virtual scaffold strands:

```

```

# make an empty ('?') set of virtual strands
wSeqVirtStrs=[['?' for i in range(lastBpIndex+1)] for s in range(lastStrandIndex+1)]

input_file = file('LambdaForwardStrand.txt', 'r')
scaffoldLeftStr = stripped_seq(input_file.read())
input_file.close()
input_file2 = file('LambdaReverseStrand.txt', 'r')
scaffoldRightStr = stripped_seq(input_file2.read())
input_file2.close()

scaffoldLeft=list(scaffoldLeftStr)
scaffoldRight=list(scaffoldRightStr)

# Left Part:
lenBefore=len(scaffoldLeft)
currBase=scaffVirtStrands[lftBrPt[0]][lftBrPt[1]]
currBaseIn=lftBrPt[1]
currStrIn=lftBrPt[0]
lastPointAdded=False
while not lastPointAdded:
    if skipVirtStrands[currStrIn][currBaseIn]==1:
        # Here a deletion should be added, marked by 'D'
        wSeqVirtStrs[currStrIn][currBaseIn]='D'
    else:
        wSeqVirtStrs[currStrIn][currBaseIn]=scaffoldLeft.pop(0)
        currBaseIn=currBase[3]
        currStrIn=currBase[2]
        if currBaseIn==1 and currStrIn==-1:
            lastPointAdded=True
        else:
            currBase=scaffVirtStrands[currStrIn][currBaseIn]
lenAfter=len(scaffoldLeft)
print 'In left part '+str(lenBefore-lenAfter)+' bases were added and '+str(lenAfter)+'
bases are left over'

# Right Part:
lenBefore=len(scaffoldRight)
currBase=scaffVirtStrands[rhtBrPt[0]][rhtBrPt[1]]
currBaseIn=rhtBrPt[1]
currStrIn=rhtBrPt[0]
lastPointAdded=False
while not lastPointAdded:
    if skipVirtStrands[currStrIn][currBaseIn]==1:
        # Here a deletion should be added, marked by 'D'
        wSeqVirtStrs[currStrIn][currBaseIn]='D'
    else:
        wSeqVirtStrs[currStrIn][currBaseIn]=scaffoldRight.pop(0)
        currBaseIn=currBase[3]
        currStrIn=currBase[2]
        if currBaseIn==1 and currStrIn==-1:
            lastPointAdded=True
        else:
            currBase=scaffVirtStrands[currStrIn][currBaseIn]
lenAfter=len(scaffoldRight)
print 'In right part '+str(lenBefore-lenAfter)+' bases were added and '+str(lenAfter)+'
bases are left over'

#####
# OUTPUT TABLE STRANDS
# Go through the virtual staple strands and look for
# staple startpoints. Horizontally, through each of the two
# sub-structures.
#####
stapBcount=0

```

```

stapCount=0
output=[]
strippedOut=[]
rows=['A','B','C','D','E','F','G','H']
plateNum=774
for subStructure in range(2):
    if subStructure==0:
        print 'Forward strand staples starting w. index '+str(stapCount)
        output.append(',,Forward Strand\n')
        strtBase=0
        endBase=323
    else:
        print 'Reverse strand staples starting w. index '+str(stapCount)
        output.append(',,Reverse Strand\n')
        strtBase=328
        endBase=643
    plateNum+=1
    r=-1
    for sI in range(lastStrandIndex+1):
        r+=1
        if r==8: # Reset row numbering and start new plate
            plateNum+=1
            r=0
        c=1 # Reset column numbering
        for bI in range(strtBase,endBase):
            if stapVirtStrands[sI][bI][0]==-1 and stapVirtStrands[sI][bI][1]==-1 and
stapVirtStrands[sI][bI][2]>-1:
                # A staple start point
                stapleSeq=[]
                currBase=stapVirtStrands[sI][bI]
                currBaseIn=bI
                currStrIn=sI
                lastPointAdded=False
                while not lastPointAdded:
                    if skipVirtStrands[currStrIn][currBaseIn]==0: # only add bases if no
deletion
                        stapleSeq.append( complement_to(wSeqVirtStrs[currStrIn]
[currBaseIn]) )
                        stapBcount+=1
                        currBaseIn=currBase[3]
                        currStrIn=currBase[2]
                        if currBaseIn==1 and currStrIn==-1:
                            lastPointAdded=True
                        else:
                            currBase=stapVirtStrands[currStrIn][currBaseIn]
                stringoligo=''.join(stapleSeq)
                output.append(str(plateNum)+' '+rows[r]+str(c)+' '+stringoligo+'\n')
                strippedOut.append(stringoligo+'\n')
                stapCount+=1
                c+=1
                if c==14:
                    print 'Warning, col number was too high in plate '+str(plateNum)
                    while c<13:
                        # fill all columns
                        output.append(str(plateNum)+' '+rows[r]+str(c)+' '+'\n')
                        c+=1

# Connector staples
print 'Connector staples starting w. index '+str(stapCount)
plateNum+=1
#
r=0
c=0
output.append(',,Connector staples\n')
for sI in range(lastStrandIndex+1):
    if stapVirtStrands[sI][327][0]==-1 and stapVirtStrands[sI][327][1]==-1 and
stapVirtStrands[sI][327][2]>-1:

```

```

# A staple start point
c+=1
if c==13:
    c=1
    r+=1
    stapleSeq=[]
    currBase=stapVirtStrands[sI][327]
    currBaseIn=327
    currStrIn=sI
    lastPointAdded=False
    while not lastPointAdded:
        if skipVirtStrands[currStrIn][currBaseIn]==0: # only add bases if no deletion
            stapleSeq.append( complement_to(wSeqVirtStrs[currStrIn][currBaseIn]) )
            stapBcount+=1
            currBaseIn=currBase[3]
            currStrIn=currBase[2]
            if currBaseIn==1 and currStrIn==-1:
                lastPointAdded=True
            else:
                currBase=stapVirtStrands[currStrIn][currBaseIn]
    stringoligo=''.join(stapleSeq)
    output.append(str(plateNum)+' '+rows[r]+str(c)+' '+stringoligo+'\n')
    strippedOut.append(stringoligo+'\n')
    stapCount+=1

print 'The total number of staple bases calculated is '+str(stapBcount)+' on a total of
'+str(stapCount)+' staple strands.'

output_file=file('./LambdaStaples.csv', 'w')
output_file.write(''.join(output))
output_file.close()

output_file2=file('./strippedLambdaStaples.txt', 'w')
output_file2.write(''.join(strippedOut))
output_file2.close()

```


A.2 SUPPORTING INFORMATION FOR ASSOCIATED PUBLICATION P2

Supporting Information

**DNA Origami Seesaws as Comparative
Binding Assay**

By

Philipp C. Nickels, Hans C. Høiberg, Stephanie S. Simmel, Phil
Holzmeister, Philip Tinnefeld, and Tim Liedl

published in

ChemBioChem (2016), 17, 1093 - 1096 [188]

CHEM**BIO**CHEM

Supporting Information

DNA Origami Seesaws as Comparative Binding Assay

Philipp C. Nickels,^[a] Hans C. Høiberg,^[a] Stephanie S. Simmel,^[a] Phil Holzmeister,^[b]
Philip Tinnefeld,^[b] and Tim Liedl^{*[a]}

cbic_201600059_sm_miscellaneous_information.pdf

DNA Origami Design

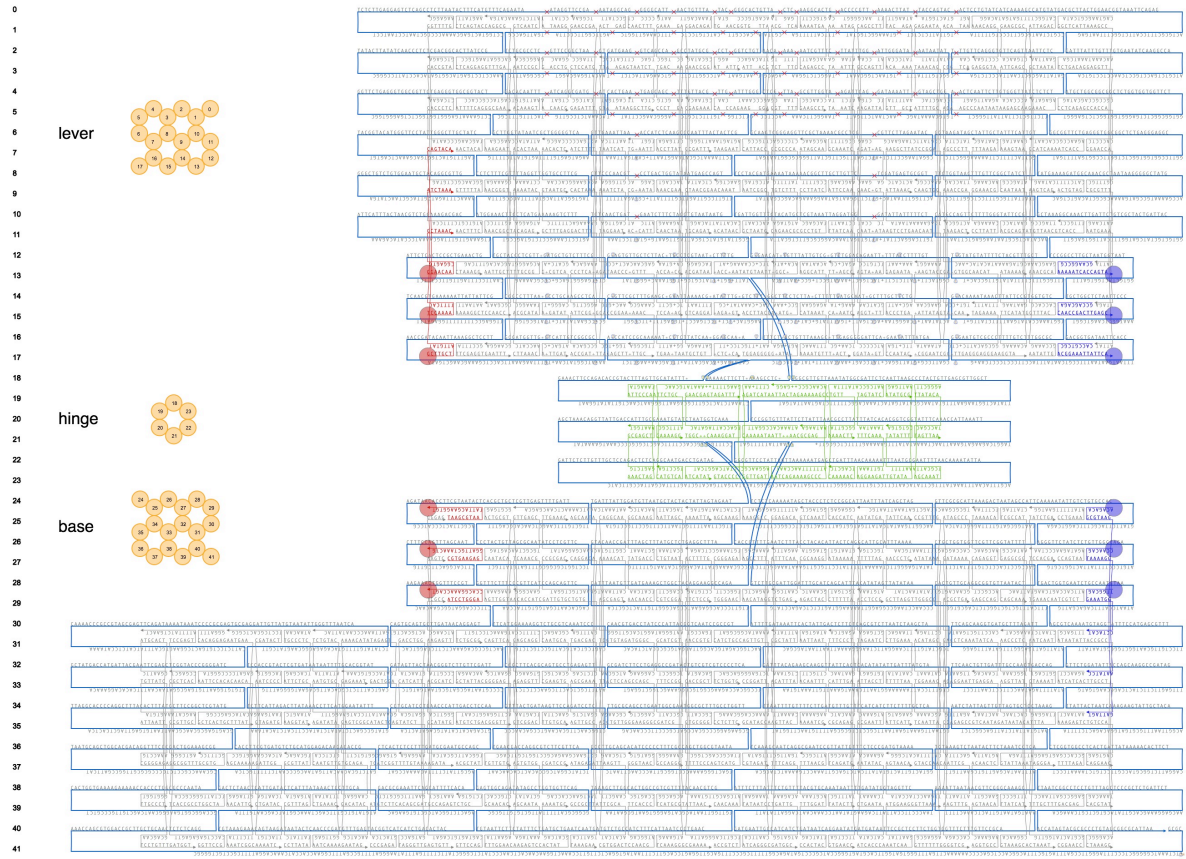


Figure S1: Design schematics of the seesaw structure. The extension positions are highlighted by red (left) and blue (right) circles. The staples forming the hinge are coloured green. Base deletions are marked by red crosses and base insertions are marked by blue loops.

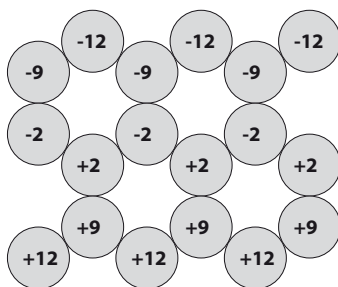


Figure S2: Number of deleted and inserted bases in a region of 98 base pairs to achieve the 60° bending of the lever.

Sequences of ssDNA Extensions

name	left	right
20 nt: lever 20 nt: base	5'-TACGAGTCCATGGGATCTGA-staple-3' 3'-ATGCTCAGGTACCTTAGACT-staple-5'	5'-staple-AGTCTAGGGTACCTGAGCAT-3' 3'-staple-TCAGATCCCATGGACTCGTA-5'
15vs30: lever 15vs30: base input:	5'-GTCCATGGGATCTGA-staple-3' 3'-CAGGTACCTTAGACT-staple-5'	5'-staple-GACCTCTAGCTCCTTTACAAAGTACAGGTT-3' 3'-staple-CTGGAGATCGAGGAAATGTTTCATGTCCAACCTGATAG-5' 5'-GACCTCTAGCTCCTTTACAAAGTACAGGTTGGACTATC-3'

Theoretical prediction of expected distribution

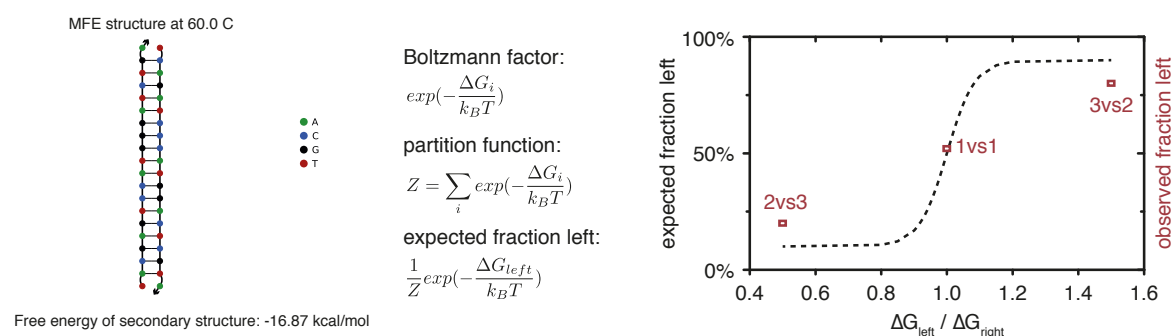


Figure S3: The Gibbs free energy ΔG for the 20 basepair duplex formed by the ssDNA extensions was calculated for 60°C (calculated T_M) using the NUPACK web server. These values were used to assign a Boltzmann factor for the states *left* and *right*. The expected fraction of structures in the *left* state was calculated for ratios of $\Delta G_{left}/\Delta G_{right}$ ranging between 0.5 (corresponds to the 2vs3 sample) and 1.5 (corresponds to the 3vs2 sample). The calculated expected fraction was then normalized to the observed values for the minimum (0vs3 sample) and maximum (3vs0 sample) concentration of *left* structures and plotted (dashed line).

Thermal Annealing Protocol

temperature [°C]	time [s]	time [min]
65	120	2
64	180	3
63	180	3
62	180	3
61	180	3
60	900	15
59	900	15
58	1800	30
57	2700	45
56	3600	60
55	4500	75
54	5400	90
53	5400	90
52	5400	90
51	5400	90
50	5400	90
49	5400	90
48	5400	90
47	5400	90
46	5400	90
45	5400	90
44	4500	75
43	3600	60
42	2700	45
41	1800	30
40	1800	30
39	1800	30
38	900	15
37	900	15
36	480	8
35	480	8
34	480	8
33	480	8
32	480	8
31	480	8
30	480	8
29	120	2
28	120	2
27	120	2
26	120	2
25	120	2

Agarose gel analysis

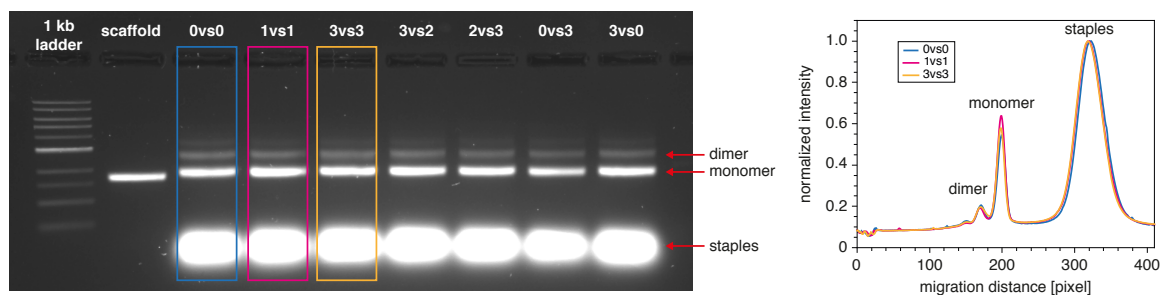
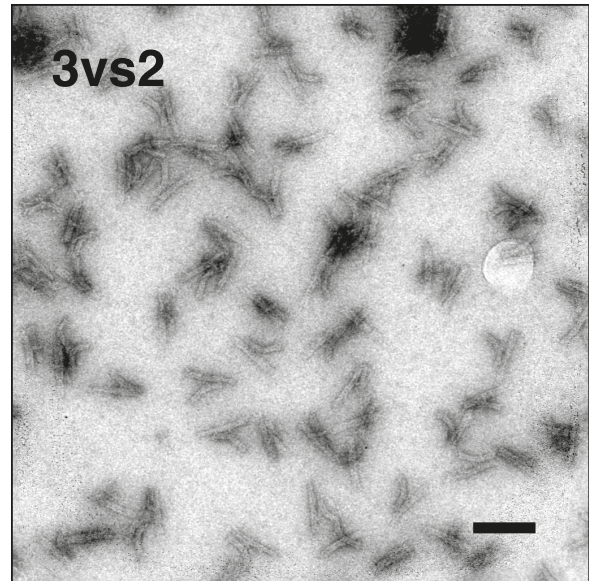
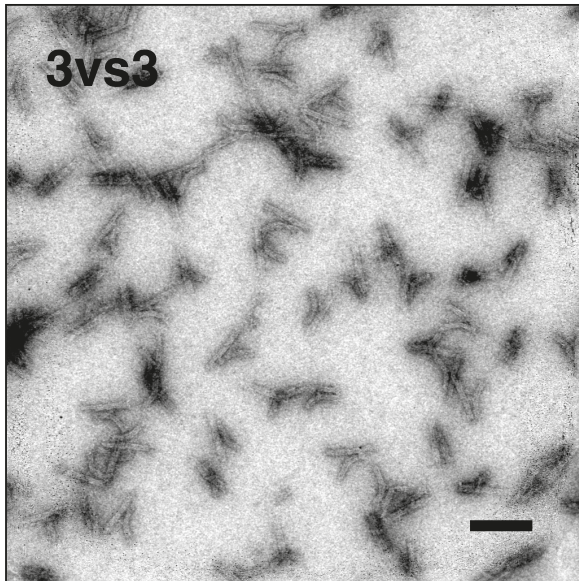
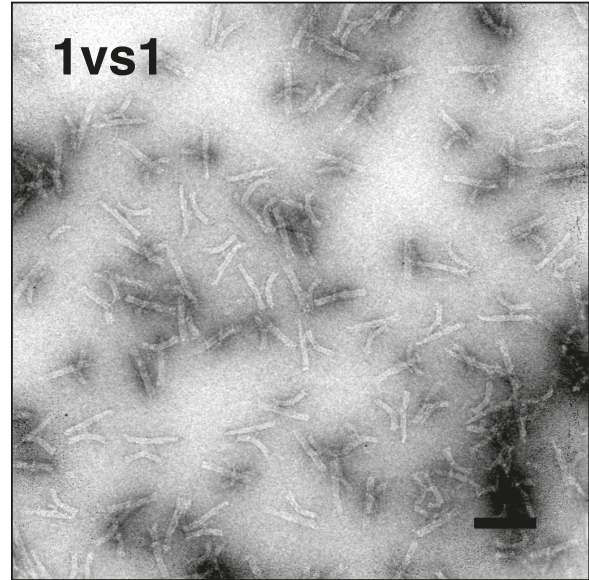
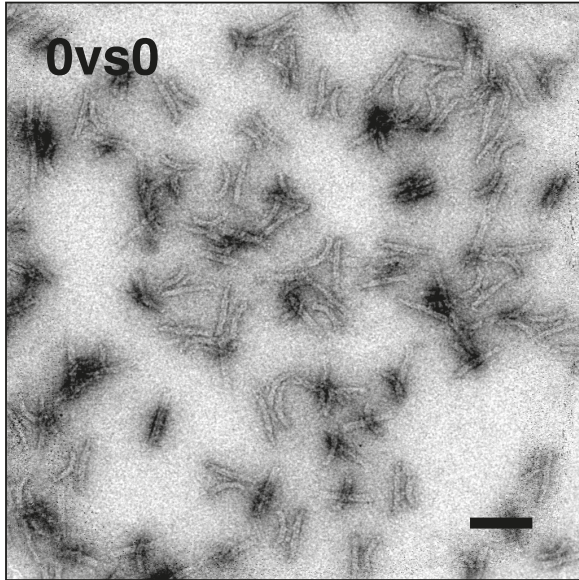


Figure S4: Agarose gel analysis of the folded samples from figure 2 (1% agarose gel, 1xTAE buffer + 11mM $MgCl_2$, run for 2 hours at 5.5 V/cm, cooled in ice water bath, stained with SybrSafe). A small fraction of the folded structures form dimers. This dimer formation is most likely unspecific and a result from base stacking. There is no significant increase in dimerization from specific intermolecular binding after closing of the structure via intramolecular binding. A comparison of the intensity profile of the 0vs0 (blue) sample (no specific intermolecular dimerization) with the intensity profile of the 1vs1 (magenta) and 3vs3 (orange) samples shows that there is no difference in the relative percentage of monomers and dimers. If specific dimerization via the complementary extensions occurs, it should be most pronounced in the 3vs3 sample.

Zoom-out TEM images



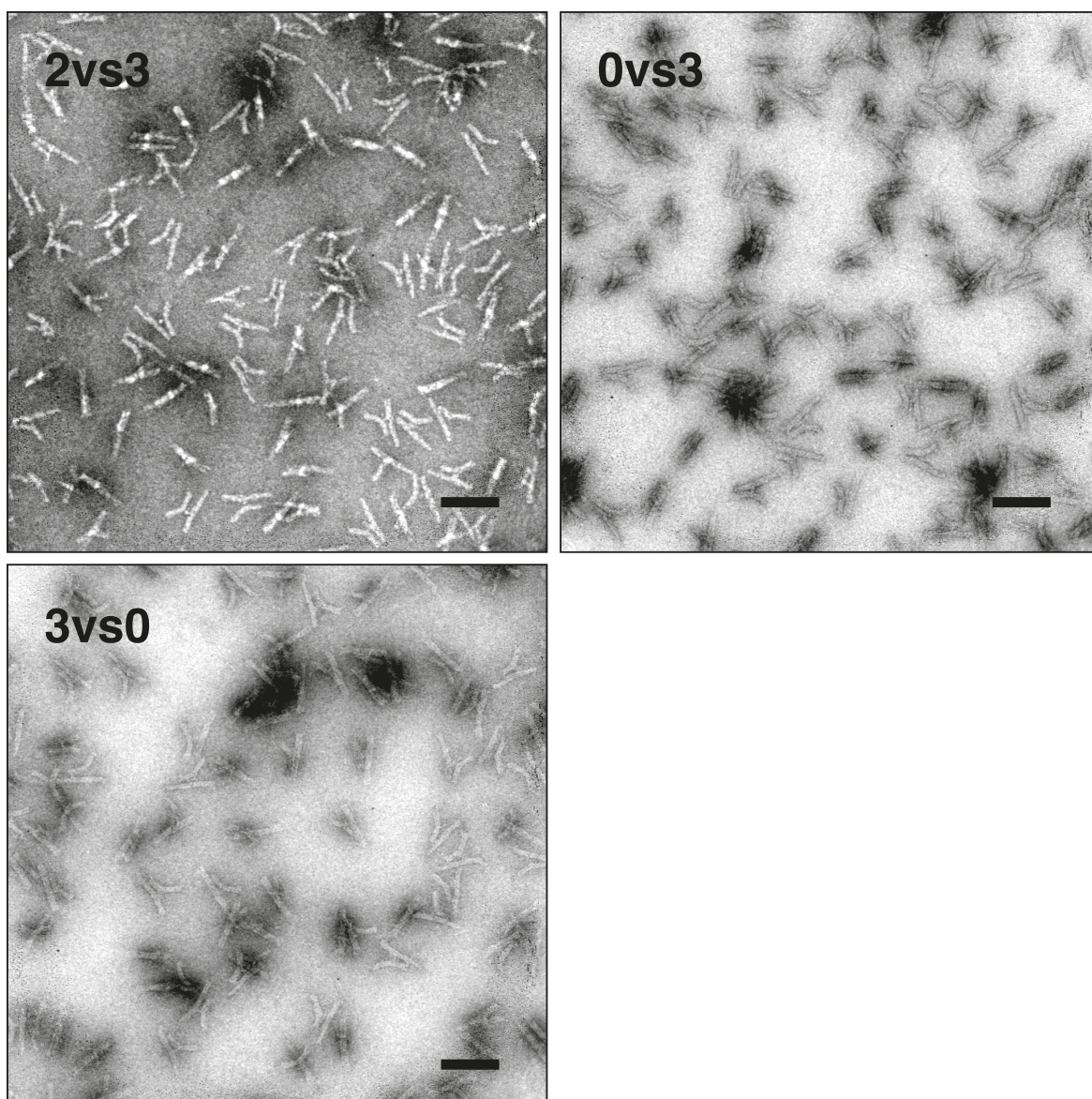


Figure S5: Exemplary zoom out TEM images (imaged at 12.000 x magnification) of all samples shown in figure 2. Only structures lying on their side were included in the analysis. Scale bars are 100nm.

Exemplary Set of Particles (0vs3 sample)

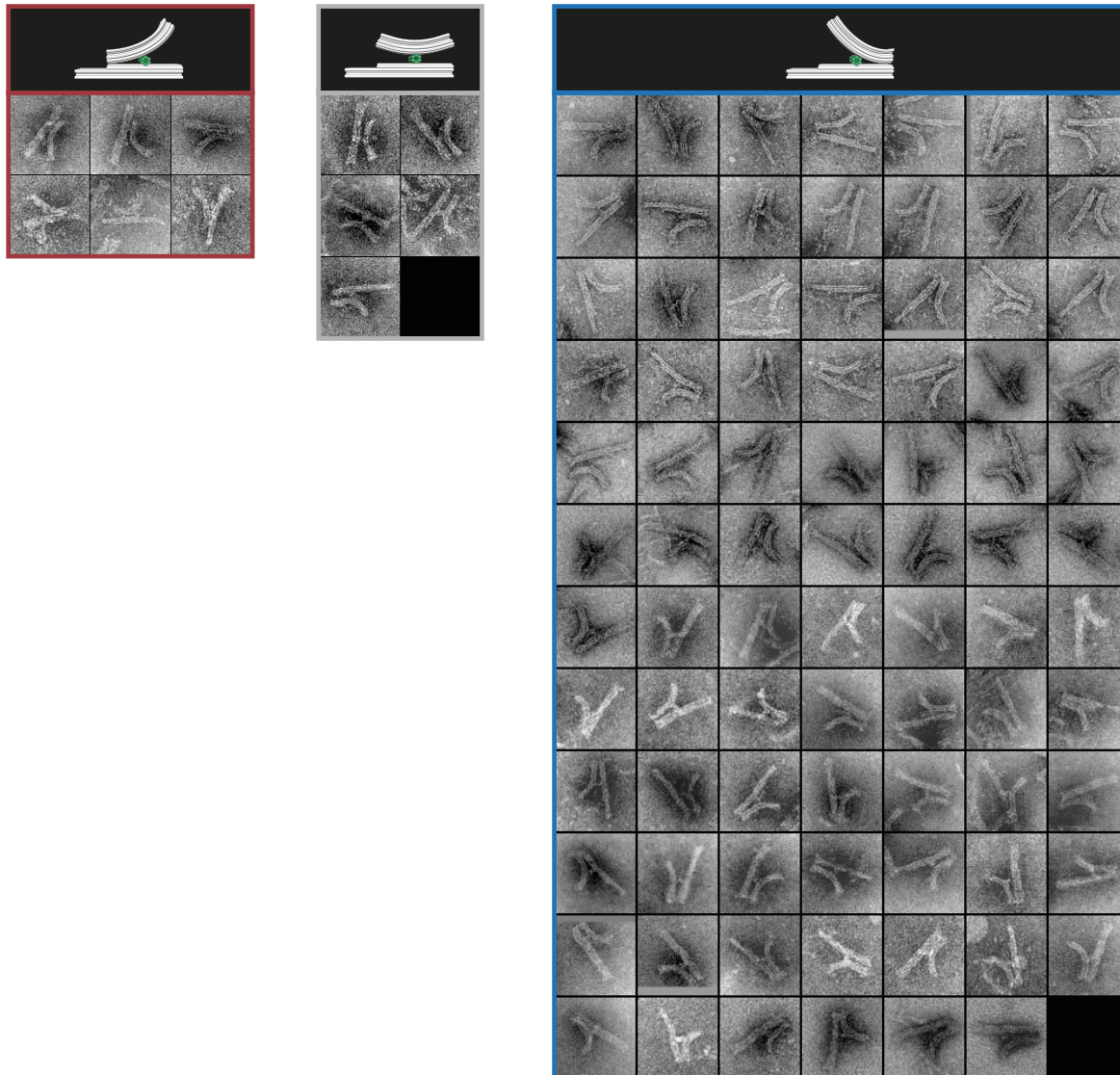


Figure S6: Three groups (*left*, *open*, and *right*) of TEM images of in total 94 particles of the 0vs3 sample. Particles were identified and boxed (300x300 pixel) from TEM micrographs taken at 30.000x magnification.

A.3 SUPPORTING INFORMATION FOR ASSOCIATED PUBLICATION P3

Supporting Information

**Molecular force spectroscopy with a DNA
origami based nanoscopic force clamp**

By

Philipp C. Nickels, Bettina Wunsch, Phil Holzmeister, Wooli Bae,
Luisa M. Kneer, Dina Grohmann, Philip Tinnefeld, and Tim Liedl

published in

Science (2016), 354, 305 - 307

Reprinted with permission from ref. [200]. Copyright 2016 AAAS.



www.sciencemag.org/content/354/6310/305/suppl/DC1

Supplementary Materials for

Molecular force spectroscopy with a DNA origami–based nanoscopic force clamp

Philipp C. Nickels, Bettina Wünsch, Phil Holzmeister, Wooli Bae, Luisa M. Kneer, Dina Grohmann, Philip Tinnefeld,* Tim Liedl*

‡Corresponding author. Email: p.tinnefeld@tu-braunschweig.de (P.T.); tim.liedl@physik.lmu.de (T.L.)

Published 21 October 2016, *Science* **354**, 305 (2016)

DOI: 10.1126/science.aah5974

This PDF file includes:

- Materials and Methods
- Supplementary Text
- Figs. S1 to S42
- Custom M13mp18-Based Scaffold Sequences
- References

Materials and Methods

Preparation of custom M13mp18-based scaffolds

The force-clamp origami design is based on the 7249 nt long M13mp18 ssDNA with the multiple-cloning-site located in the middle of the ssDNA spring region. To study the two systems of interest, we made two custom scaffold variants: a 7253 nt long variant for the Holliday junction measurements (7253_HJ) and a 7283 nt long variant including the SSV T6 promoter for TBP bending (7283_SSV). Recombinant M13 filamentous bacteriophage was prepared by replacing the BamHI - HindIII segment of M13mp18 with the corresponding insert. The sense and antisense strand of the inserts were chemically synthesized (5'-PHO, HPLC purified, MWG Eurofins Operon). The replicative form of the bacteriophage M13 DNA with the insert was prepared as described earlier (30). Successful cloning was verified by sequencing (MWG Eurofins Operon). The full sequences of the 7253_HJ and 7283_SSV scaffolds are shown at the end of this document. High titer inoculation stocks and single-stranded M13 DNA for DNA origami assembly was produced as described earlier (30, 31).

DNA origami sample preparation

The DNA origami structures were designed using caDNAno (version 0.2.3, design schematics in Figures S2 - 3, S16 - 18, and S29 - 33). For the 0 pN samples, the scaffold was first annealed with a 20 nt long oligo complementary to the BamHI restriction site (plus the 7 bases on both sides) in 1 x enzyme reaction buffer over the course of 1 hour (from 65°C to 25°C). After annealing, BamHI (Fast Digest BamHI, ThermoFisher Scientific) was added and the mixture was incubated at 37°C for 30 min. BamHI was heat inactivated at 80°C for 5 min and the linearized scaffold stored unpurified at -20°C until usage for folding. Scaffold DNA was mixed with all staples (unmodified: high purity salt, MWG Eurofins Operon; modified: HPLC purified, Biomers) in folding buffer (10 mM Tris pH 7.6, 1 mM EDTA, 20 mM MgCl₂, 5 mM NaCl) at the following final concentrations:

7253_HJ samples	Concentration (nM)
scaffold	20
core staples	100
spring subset	200
biotin handles	200
biotin oligos	2000
HJ_b	40
HJ_r	40
HJ_h	200

7283_SSV samples	Concentration (nM)
scaffold	20
core staples	100
spring subset	200
biotin handles	200
biotin oligos	2000
SSV complement	40

For the SSV complement, we ordered two separate strands (*SSV_compl_1* with the acceptor and *SSV_compl_2* with the donor, fig. S27). We thermally annealed the two strands with a complementary 30 nt long strand (*SSV_lig*) over the course of 1 hour (from 65°C to 25°C) in 150 mM NaCl and ligated the strands with T4 DNA ligase (New England Biolabs) for 2 hours at 16°C. The ligated product was separated from remaining un-ligated strands and the complementary 30-mer by denaturing polyacrylamide gel electrophoresis.

The folding mixtures were subjected to the following nonlinear thermal annealing ramp:

Temperature (°C)	Time per °C (min)	Temperature (°C)	Time per °C (min)
65	2	44	75
64-61	3	43	60
60-59	15	42	45
58	30	41-39	30
57	45	38-37	15
56	60	36-30	8
55	75	29-25	2
54-45	90	4	storage

Folded samples were purified to remove excess staple strands *via* two rounds of polyethylene glycol (PEG) precipitation (31, 32). In detail, samples were mixed with an equal volume of 2 x PEG precipitation buffer (10 mM Tris pH 7.6, 1 mM EDTA, 15 % (w/v) PEG-8000, 500 mM NaCl) and centrifuged at 17,900 ref for 30 min at 4°C. The pellet was re-suspended in 1 x folding buffer and placed on a shaker at 30°C for 30 min. The purified samples were stored in 1 x folding buffer at 4°C until further use.

Holliday junction sequences:

x: 5' -CCCAGTTGAGCGCTTGCTAGGG-3'
r: 5' -CCCACCGCTCGGCTCAACTGGG-3'
b: **Cy5**-5' -CCCTAGCAAGCCGCTGCTACGG-3'
h: **Cy3**-5' -CCGTAGCAGCGCGAGCGGTGGG-3'

SSV promotor and SSV complement sequences:

SSV: 5'-CGGACCGAAAGCGCGACCATCGCCGGAGATTGGAGTAAAGTTTAAATACTG-3'

SSV_compl_1: Atto647n-5'-CAGTATTTAAAC-3'

SSV_compl_2: PHO-5'-TTTACdT_Atto532CCAATCTCCGGCGATGGTCGCGCTTTCGGTCCG-3'

SSV_lig: 5'-CGCCGGAGTTGGAGTAAAGTTTAAATACTG-3'

Biotin oligo sequence:

3'-staple-AACATTCTCCTATTACTA-5'
5'-GGTAGTAATAGGAGAATGTT-3'-biotin-TEG

Agarose gel electrophoresis

Samples were analyzed in 1 % and 2 % agarose gels containing 1 x Tris-acetate buffer (40 mM Tris, 40 mM acetic acid), 10 mM MgCl₂, and 1 x SybrSafe (Thermo Fisher Scientific) if not specified otherwise. Samples were separated for 2 - 3 hours at 5.5 V/cm. The gel box was cooled in an ice water bath. Bands in SybrSafe stained gels were visualized *via* ultraviolet light excitation. Bands in unstained gels were visualized by exciting the corresponding fluorescence dye in the sample with a laser gel scanner (Tecan LS300).

TEM imaging

5 μL of purified origami solution was adsorbed onto glow-discharged TEM grids (formvar/carbon, 300 mesh Cu ; Ted Pella, Redding, CA) at room temperature and then stained with aqueous uranyl formate solution (2 %) containing sodium hydroxide (25 mM). Imaging was performed at 25,000 x magnification with a JEM1011 transmission electron microscope (JEOL) operated at 80 kV, equipped with a FastScan-F114 camera (TVIPS, Gauting, Germany). Generation of aligned and averaged TEM images was performed by picking particles with the manual boxing routine followed by iterative 2D alignment and averaging (ml_align2D) of the Xmipp 3.1 software package (33).

Single-molecule ALEX setup

For single-molecule experiments, a custom built confocal microscope based on an Olympus IX-71 inverted microscope was used. An 80 MHz pulsed laser with an emission at 640 nm (LDH-D-C-640, Picoquant) and a continuous wave diode laser at 532 nm (Sapphire LP 532 nm 100 mW) were alternated by an acousto-optical tunable filter (AOTFnc-VIS, AA optoelectronic) with a 100 μs period. The laser beam was focused into the sample by an oil-immersion objective (UPLSAPO100XO, NA 1.40, Olympus). The emission was collected by the same objective, separated from the excitation beam by

a dichroic mirror (Dualband z532/633, AHF) and focused onto a 50 μm pinhole (Linos). The emission light was split by a dichroic mirror (640DCXR, AHF) and focused onto two avalanche photo diodes (t-SPAD-100, Picoquant) after appropriate spectral filtering (Brightline HC582/75, Bandpass ET 700/75 nm, both AHF, RazorEdge LP 532, RazorEdge LP 647, both Semrock). The signals were registered by a TCSPC system (SPC-830, Becker&Hickl) and analyzed using custom-made LabVIEW software (National Instruments).

Single-molecule ALEX measurements of the Holliday junction

Single-molecule FRET measurements of immobilized 7235_HJ force clamps were performed in LabTek chamber slides (Thermo Scientific), which were cleaned with 1 M KOH and functionalized with biotin-labeled BSA (Sigma-Aldrich). Purified DNA origami force clamp structures were bound *via* neutravidin (Sigma-Aldrich) to the BSA-biotin surface. Measurements were carried out in a buffer consisting of 1 x PBS at pH 7, 2 mM trolox/troloxquinone, 1 % (w/w) glucose, and 10 % (v/v) of GOC (1 mg/mL glucose oxidase, 0.4 % (v/v) catalase (50 $\mu\text{g}/\text{mL}$), 30 % glycerol, 12.5 mM KCl in 50 mM TRIS pH 7.5) for stabilization of the fluorophores (34) and 100 mM MgCl_2 .

Single-molecule ALEX measurements of TBP-induced DNA bending

Single-molecule FRET measurements of diffusing 7283_SSV force clamps were performed in home-built sample chambers with a total volume of about 30 μL on cover slips (Roth), which were cleaned with 1 M KOH and passivated with BSA (10 mg/mL). Measurements were carried out in a buffer consisting of 1 x PBS at pH 7, 1 M NaCl, and 12.5 mM MgCl_2 . In order to identify fluorescence bursts from single molecules, the concentration of force clamp structures was adjusted to less than one molecule per confocal volume (typically in the low picomolar range). The sample was heated up to a temperature of about 35°C *via* the objective. The activity of MjTBP increases with increasing temperature (the optimal growth temperature of the organism of origin is 85°C) (27). However, 35°C was the maximum temperature we could achieve with the experimental setup used here. To analyze the recorded fluorescence bursts, a burst search algorithm according to reference (35) was applied (parameters: $t = 500 \mu\text{s}$, $M = 30$, $L = 100$). For the calculation of the FRET efficiency, the intensities were corrected for leakage from the donor into the red detection channel (14 %) and the direct excitation of the acceptor by the 532 nm laser excitation (11 %). The ALEX-2CDE filter was used to filter the E-S-histograms as described in reference (36) (ALEX-2CDE < 12).

Supplementary Text

S1: Entropic force of single-stranded DNA

Single-stranded DNA can be well described as a freely-jointed chain (FJC) (3). The FJC models polymer chains as a random walk of the chain's segments. The model neglects self avoidance of the segments and treats the orientation of each segment independent of its neighbors. The polymer chain is formed by N monomers with a total contour length L_C of:

$$L_C = N * l$$

where l is the length of each monomer. The average end-to-end distance d of the polymer is described as:

$$\langle d^2 \rangle = N * l^2$$

The realistic length of one chain segment is called Kuhn length l_K ($l_K \geq l$). For semiflexible polymers such as ssDNA, l_K equals twice the persistence length (37).

A polymer can adopt each possible end-to-end distance by several conformations. The number of possible conformations the polymer can adopt in space increases with a decreasing end-to-end distance. Hence, the polymer more likely adopts a coiled conformation with a short end-to-end distance instead of a stretched conformation with a long end-to-end distance. The force F exerted on each end of a long polymer ($L_C \gg l_K$) can be expressed as:

$$\langle F \rangle = \frac{-3k_B T L_C}{N_K l_K^2}$$

with N_K as the number of Kuhn segments.

Smith et al. showed that a FJC modified with stretchable Kuhn segments that can align under force (mFJC) describes the force-extension behavior of ssDNA well (3):

$$d(F) = L_C * \left[\coth \left(\frac{F l_K}{k_B T} \right) - \frac{k_B T}{F l_K} \right] * \left(1 + \frac{F}{S} \right)$$

with S being the stretch modulus and the contour length L_C being the number of nucleotides N of the ssDNA times the length per single base L_B :

$$L_C = N * L_B$$

We used the following parameters to calculate the resulting entropic force for a fixed end-to-end distance d (d is given by the force-clamp design as described in figs. S1, S15, and S28):

Parameter	Value
L_B	$6.3 \text{ \AA} \pm 0.8 \text{ \AA}$
l_K	1.5 nm
S	800 pN
$k_B T$	4.114 pNnm

The $6.3 \text{ \AA} \pm 0.8 \text{ \AA}$ for L_B were taken from a length comparison of five different crystal structures of ssDNA segments from reference 24. The parameters for l_K and S were taken from reference 3.

Here, we approximate the entropic force as being constant over time and thus call our device a force clamp, analog to the constant force experiments with conventional force spectroscopy techniques. However, the two molecular systems studied here (the Holliday junction and the TBP-induced DNA bending) undergo a conformational transition that changes the end-to-end distance of the ssDNA spring. These changes in distance result in a minor change in entropic force acting on the molecular systems. For the force calculation, we always used the average distance (see figs. S15 and S28 for more details). The maximum change in force resulting from this conformational distance change is less than 10 % for the 7253_HJ samples and less than 17 % for the 7283_SSV samples.

One assumption we make is that ssDNA behaves like a purely entropic spring with ideal elasticity at low forces at the salt concentrations we used for our experiments (100 mM MgCl_2 for the Holliday junction and 1 M NaCl + 12.5 mM MgCl_2 for the TBP). We assume that these salt concentrations provide Θ solvent conditions (38).

Another simplifying assumption is that the formation of secondary structures in the ssDNA spring region can be ignored. To justify this assumption further, we could use secondary structure-free sequences in the spring region in future experiments (for example by using scaffold inserts programmed to consist only of the bases A, C, and T).

We also assume that force fluctuations over time can be neglected. The relaxation time τ_R (a measure of the timescale over which the chain undergoes conformational reconfigurations) is described by the Rouse model extended with hydrodynamic interactions mediated by the solvent (39):

$$\tau_R = \frac{\eta_S (\sqrt{N} l_K)^3}{\sqrt{3\pi} k_B T}$$

with N as the number of monomers in the polymer chain and η_S the viscosity of the solvent. Depending on the length of the ssDNA spring regions in our design, the relaxation time τ_R is between 0.2 μs and 2.0 μs . This fluctuation is 100 – 1000 times

faster than the duration of a fluorescence burst (> 1 ms) as well as the timescale of the Holliday junction fluctuation and the TBP-DNA complex (both on the order of milliseconds to seconds).

S2: Nicks in circular scaffold molecules

M13 bacteriophage derived ssDNA is a circular molecule. However, a certain fraction of the molecules are linearized during the purification process. These nicks should be randomly distributed along the contour length of the molecule. One commercial supplier of M13mp18 ssDNA, New England Biolabs, claims that more than 90 % of the molecules are in the circular form. We assume that our M13 ssDNA contains also roughly 10 % linearized molecules. In order to successfully exert a force on the mounted system of interest, we need the scaffold molecule to be intact and not contain any nicks in the section spanning the gap in the force clamp. The longest ssDNA section used in this study is 400 nt long (7253_HJ_1.2pN). Adding another 50 nt on each side for efficient anchorage in the structure gives 500 nt, a fraction of less than 7 % of the scaffold material. An overall 10 % chance of having a scaffold nick in one origami structure thus results in a probability of less than 1 % of this nick being in the important spring region. All other nicks do not affect the performance of the force clamp, as long as only one nick per scaffold molecule occurs.

In the 0 pN control samples, we observed a fraction of partially assembled structures (examples are highlighted in figs. S8, S20 & S35 by red arrows). This is most likely a result of scaffold molecules that were nicked already before the enzymatic scaffold linearization was performed for the 0 pN samples. However, this should not have any influence on the 0 pN force measurements as long as the system of interest is successfully tethered to the force clamp structure.

S3: TBP-induced bending probability - Boltzmann distribution

We calculated the force-dependent probability of the bent state P_{bent} by comparing the areas of the Gaussian fits of the two sub-populations in the bimodal FRET distribution:

$$P_{bent} = \frac{\text{area}(\text{high FRET})}{\text{area}(\text{low FRET}) + \text{area}(\text{high FRET})}$$

P_{bent} is related to the change in free energy ΔG between the undistorted state (at 0 pN) and the bent state through the Boltzmann distribution:

$$P_{bent} = \frac{\exp\left(\frac{\Delta G - F * \Delta x}{k_B T}\right)}{1 + \exp\left(\frac{\Delta G - F * \Delta x}{k_B T}\right)}$$

where F is the applied force to the promotor DNA and Δx is the distance change along a one-dimensional reaction coordinate.

S4: Dynamic range of the DNA origami force clamp

The ssDNA section of the scaffold exits the origami structure in a shear geometry. Single-molecule force spectroscopy experiments revealed that the unbinding force of DNA duplexes in the shear geometry is about 50 pN (at room temperature in PBS buffer), more than three times higher than in the zipper geometry (40). We assume that it is possible to generate forces of up to 50 pN with our origami force clamp. However, the uncertainty of the parameter for the length per single base used in this study and the nonlinear dependency of the contour length on the entropic force lead to an error of the calculated force that increases drastically with a decreasing contour length. An improved theoretical modeling of the ssDNA in the future will lead to a more precise adjustment of higher forces and to access to the whole potential dynamic range of our force clamp.

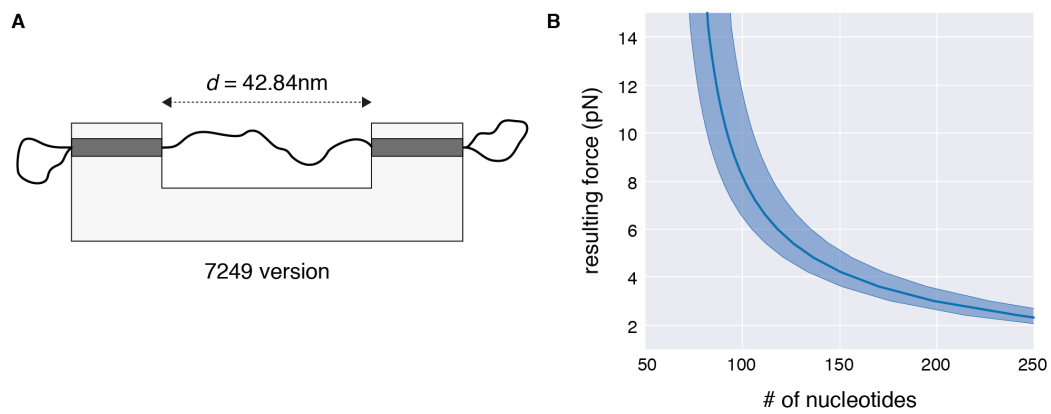


Fig. S1

(A) Geometric model of the 7249 based variant of the force clamp structure with the ssDNA spanning the gap distance d . The dark gray region represents the subset of 10 staple strands that need to be changed to adjust the ssDNA spring length. (B) Resulting entropic force as a function of the number of nucleotides spanning the gap distance d . The shaded blue region is the margin of error resulting from the standard deviation of the single base length.

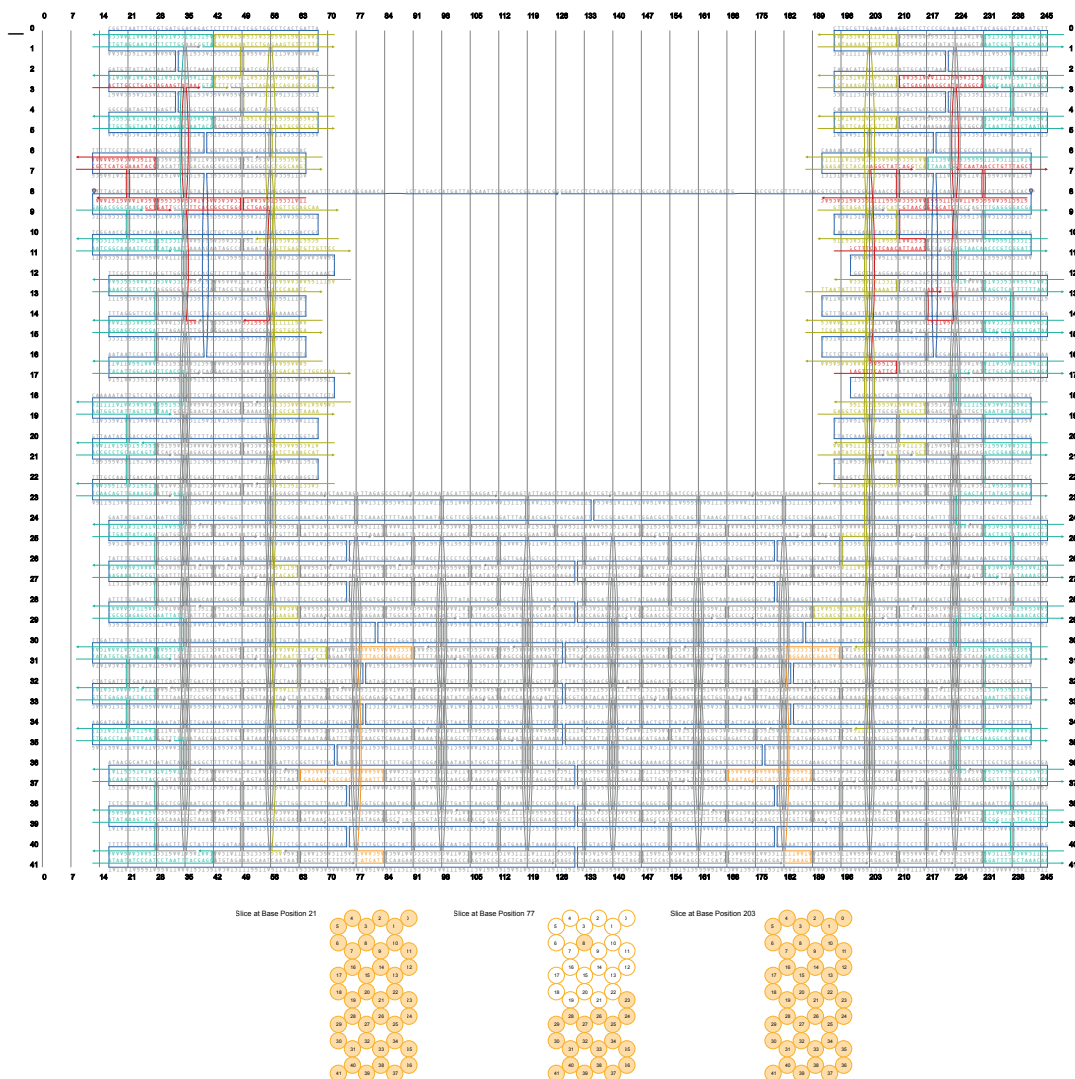


Fig. S2

Scaffold/staple layout of the 7249_6pN version. The number of nucleotides in the ssDNA spring is 116. The scaffold starting point (in the middle of the gap) is the BamHI site. Core staples are gray. The subset of 10 staples to adjust the length of the ssDNA spring is colored red. Biotin modified strands were attached to complementary 5'-end extensions on the orange staples. Thymidine-tails (4 x T) were added to all edge staples (cyan and yellow) to prevent unspecific stacking and aggregation.

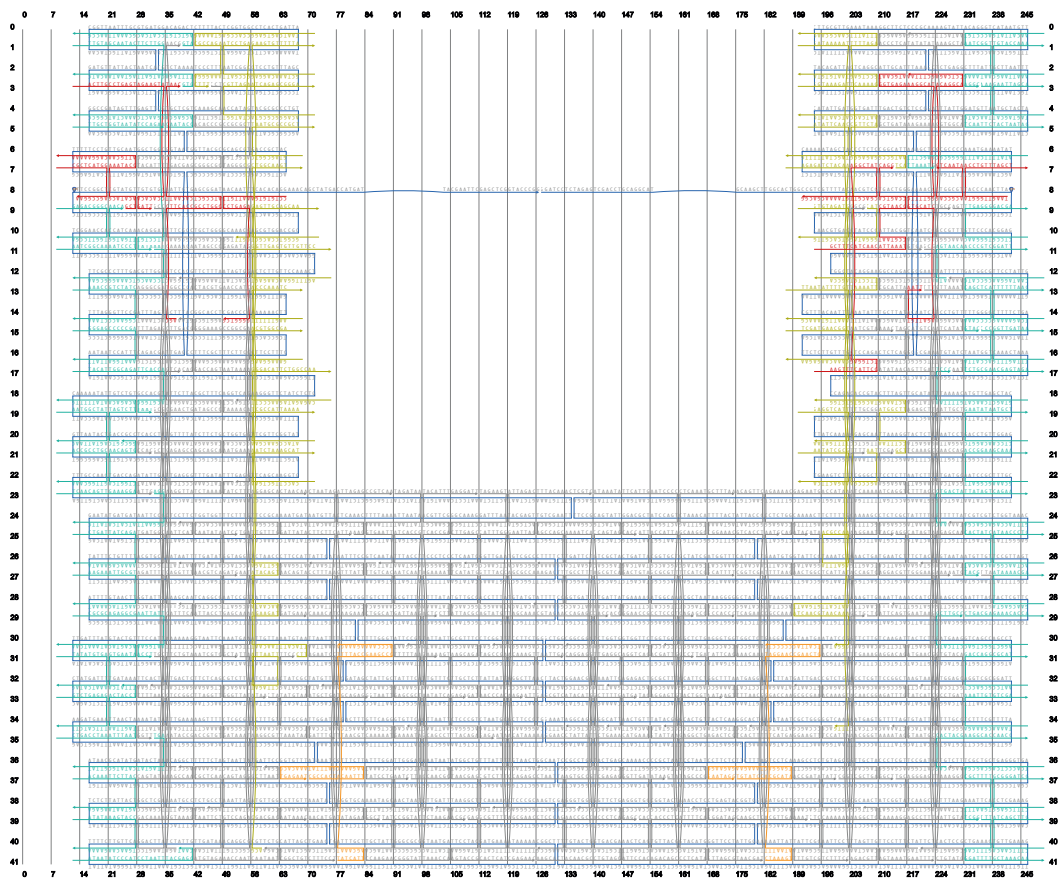


Fig. S3

Scaffold/staple layout of the 7249_12pN version. The number of nucleotides in the ssDNA spring is 87. The same subset of staples was used for the 0 pN version folded with the enzymatically-linearized scaffold.

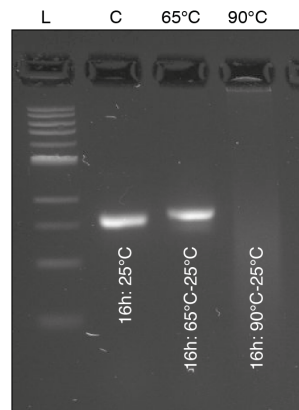


Fig. S4

2 % agarose gel of the 7249 scaffold after thermal annealing in the presence of 1x folding buffer but without staples. **L**: 1kb DNA ladder; **C**: Control (16 hours at room temperature); **65°C**: 16 hour nonlinear annealing ramp as used for force clamp origami folding; **90°C**: Linear annealing ramp from 90°C to 25°C in steps of 15 min per °C. Thermal degradation of the scaffold is clearly visible in the 90°C sample.

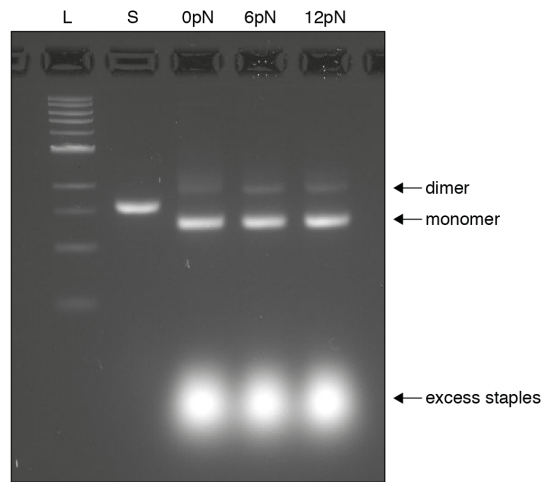


Fig. S5

2 % agarose gel of the three different 7249 variants after folding. **L:** 1kb DNA ladder; **S:** 7249 scaffold control. The monomer (M) and dimer band (D) of the origami structure are highlighted. The formation of origami dimers occurs most likely due to unspecific stacking interactions of the helix blunt ends on both sides of the clamp structure (42 blunt ends on each side).

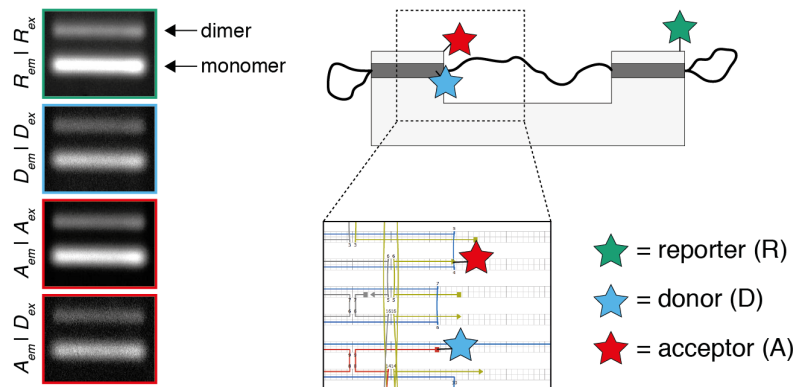


Fig. S6

We used a bulk FRET assay to evaluate whether the ssDNA spring is adjusted to the designed length and the subset of staple strands used for the adjustment is correctly incorporated. A donor (Atto550) was attached to the 5'-end of the last staple strand before the scaffold exits the structure on the left side (red staple). The acceptor (Atto647n) was placed in close proximity at the 3'-end of one of the core staple strands (yellow staple). A reporter dye (Atto488) was placed on the opposite side of the structure to confirm that the donor-acceptor pair is incorporated into the folded origami structure. The annealed sample (7249_12pN) was separated on a 1 % agarose gel and the dyes were excited in a laser scanner. Both donor and acceptor dyes are present and the FRET signal (acceptor emission upon donor excitation, $A_{em} | D_{ex}$) indicates that the length-adjustment staples were incorporated successfully.

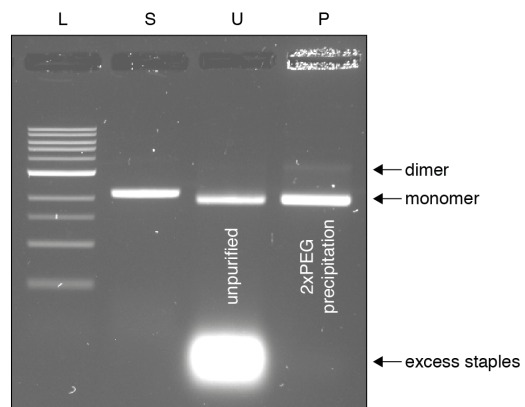


Fig. S7

1 % agarose gel of the 7249_6pN version before and after purification. **L:** 1kb DNA ladder; **S:** 7249 scaffold control. **U:** unpurified sample. **P:** purified sample.

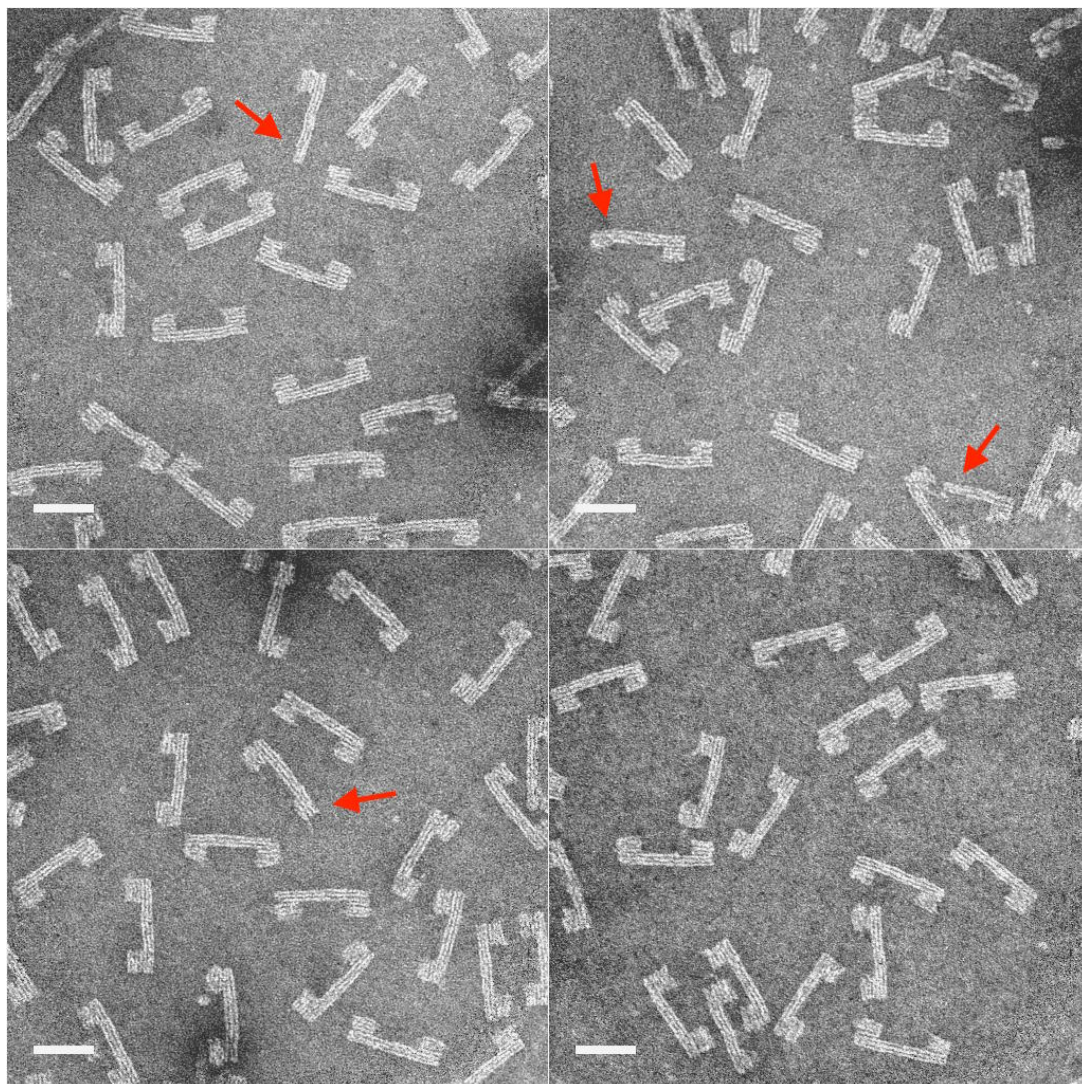


Fig. S8

TEM images of the 7249_0pN sample. The red arrows point at partially assembled structures. These were most likely folded from the fraction of scaffold that was already nicked at positions randomly distributed along the sequence before the enzymatic linearization. Scale bars: 50 nm.

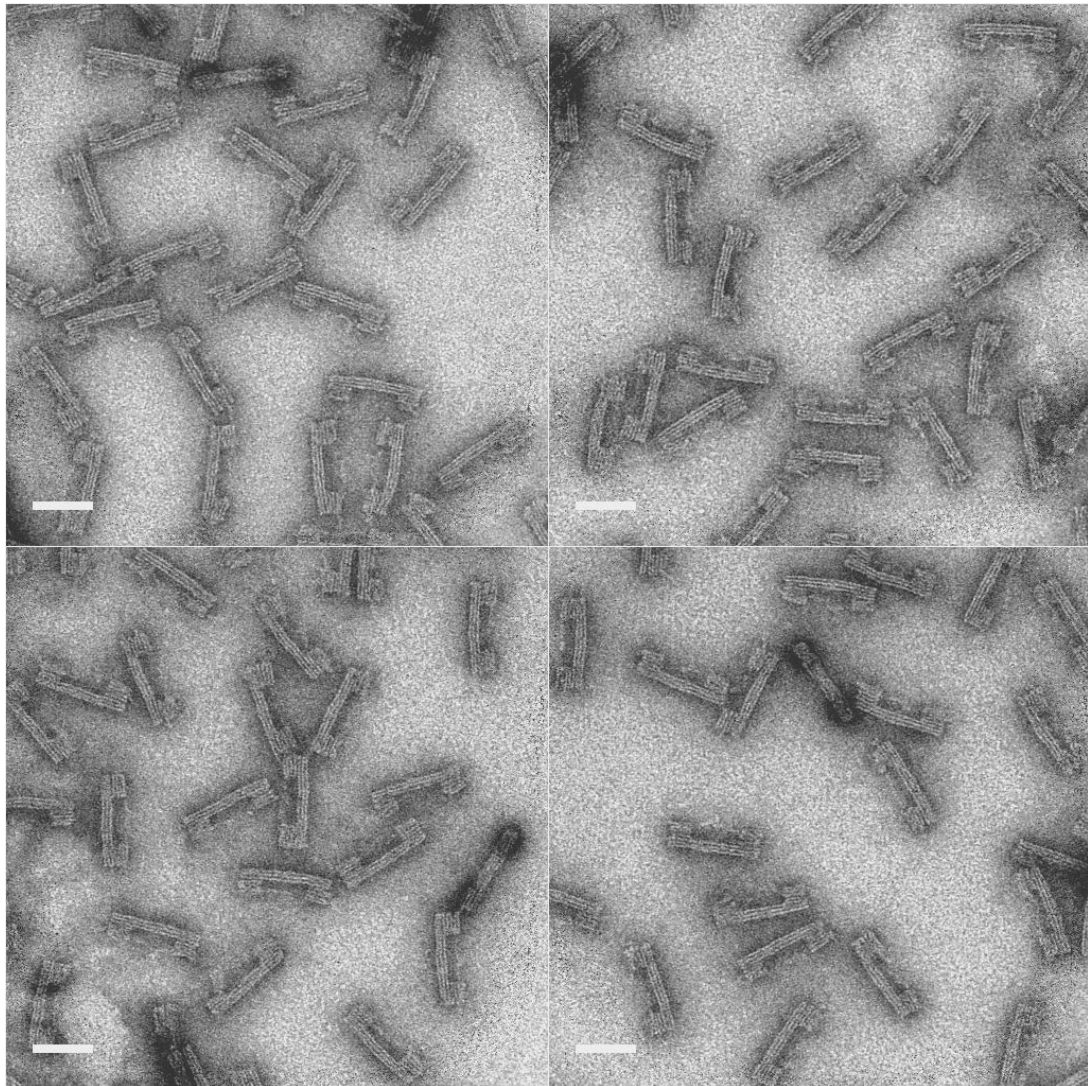


Fig. S9
TEM images of the 7249_6pN sample. Scale bars: 50 nm.

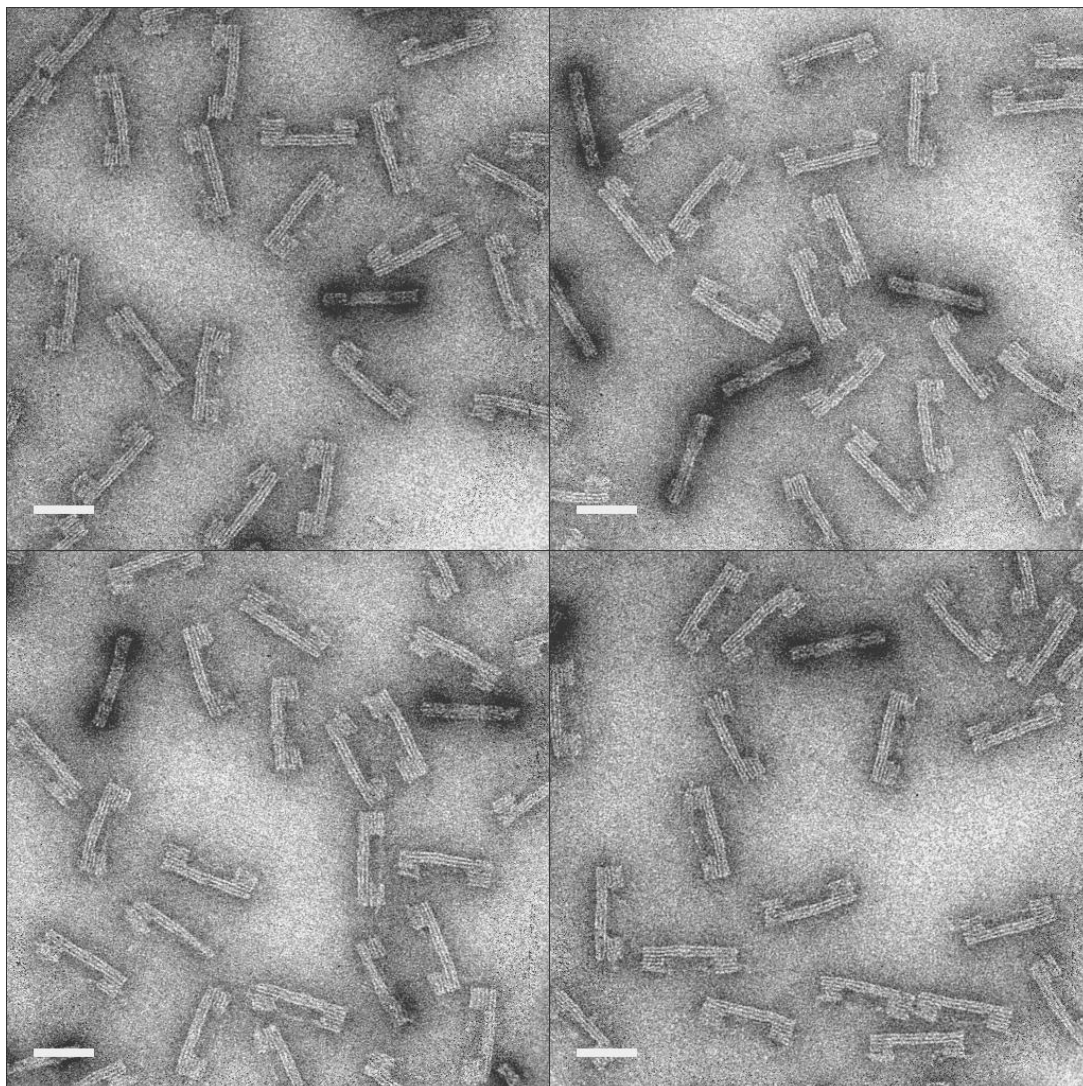


Fig. S10

TEM images of the 7249_12pN sample. Scale bars: 50 nm.

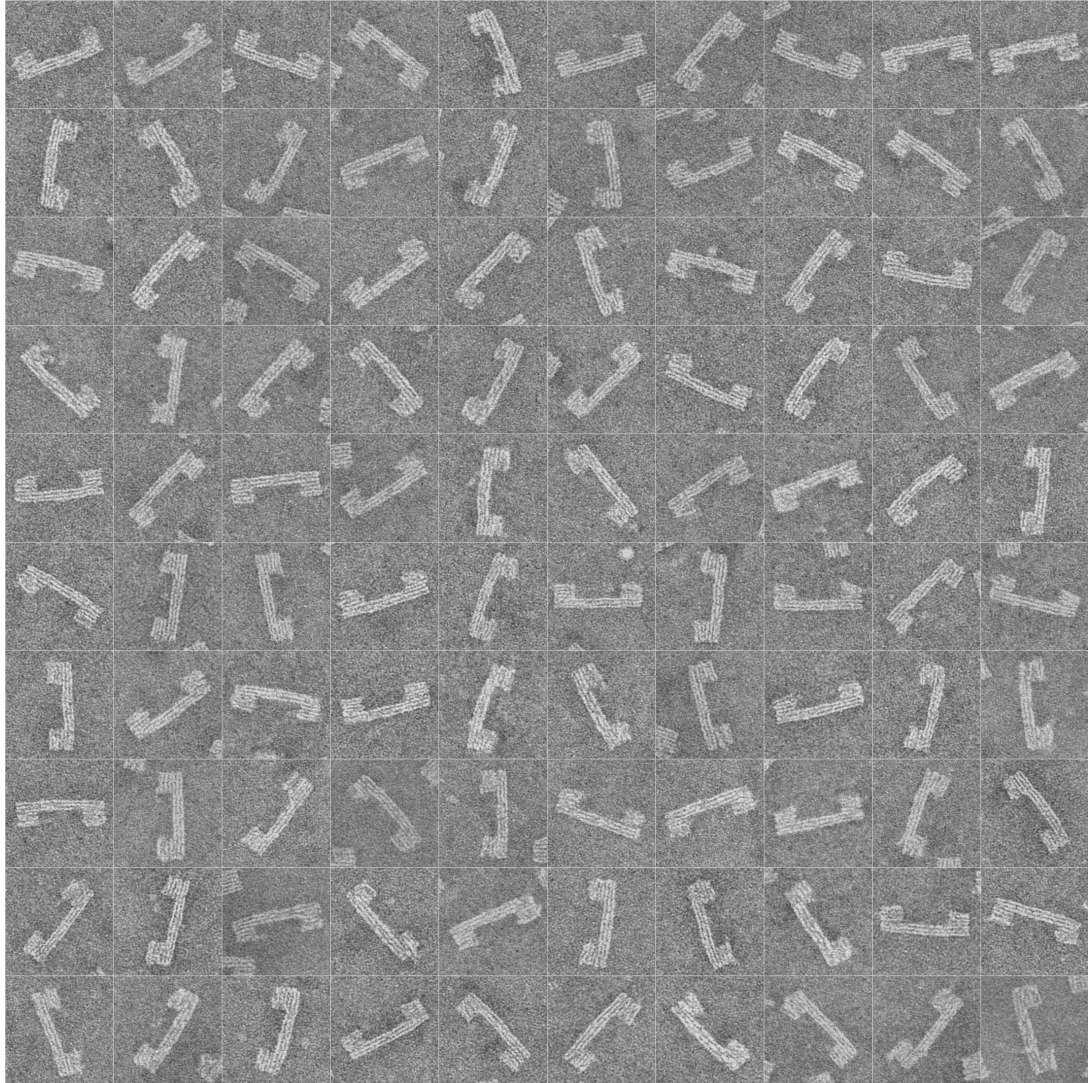


Fig. S11

All 100 single particles used to construct the average TEM image of the 7249_0pN sample shown in figure 1E. Each single image is 96 nm x 96 nm.

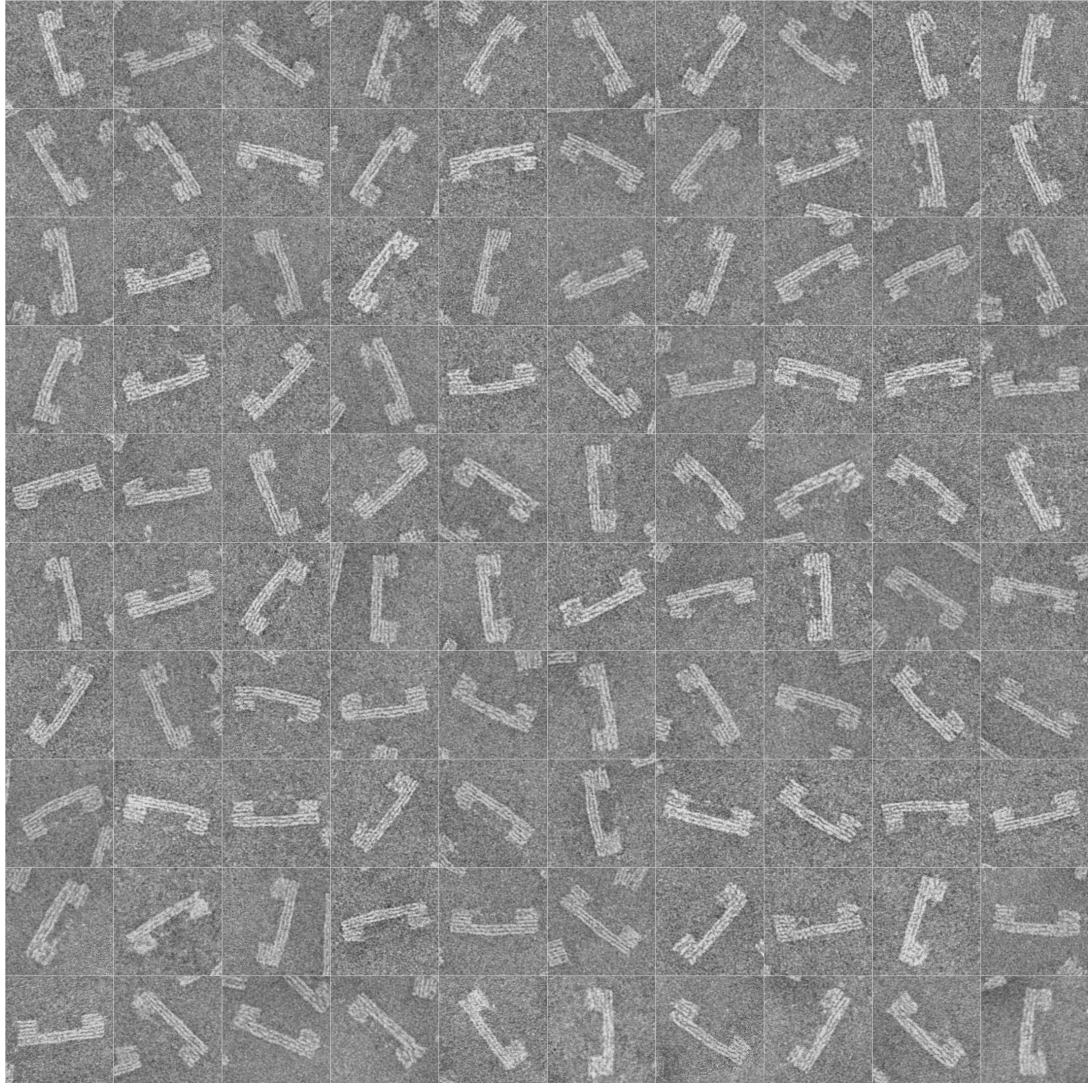


Fig. S12

All 100 single particles used to construct the average TEM image of the 7249_6pN sample shown in figure 1E. Each single image is 96 nm x 96 nm.

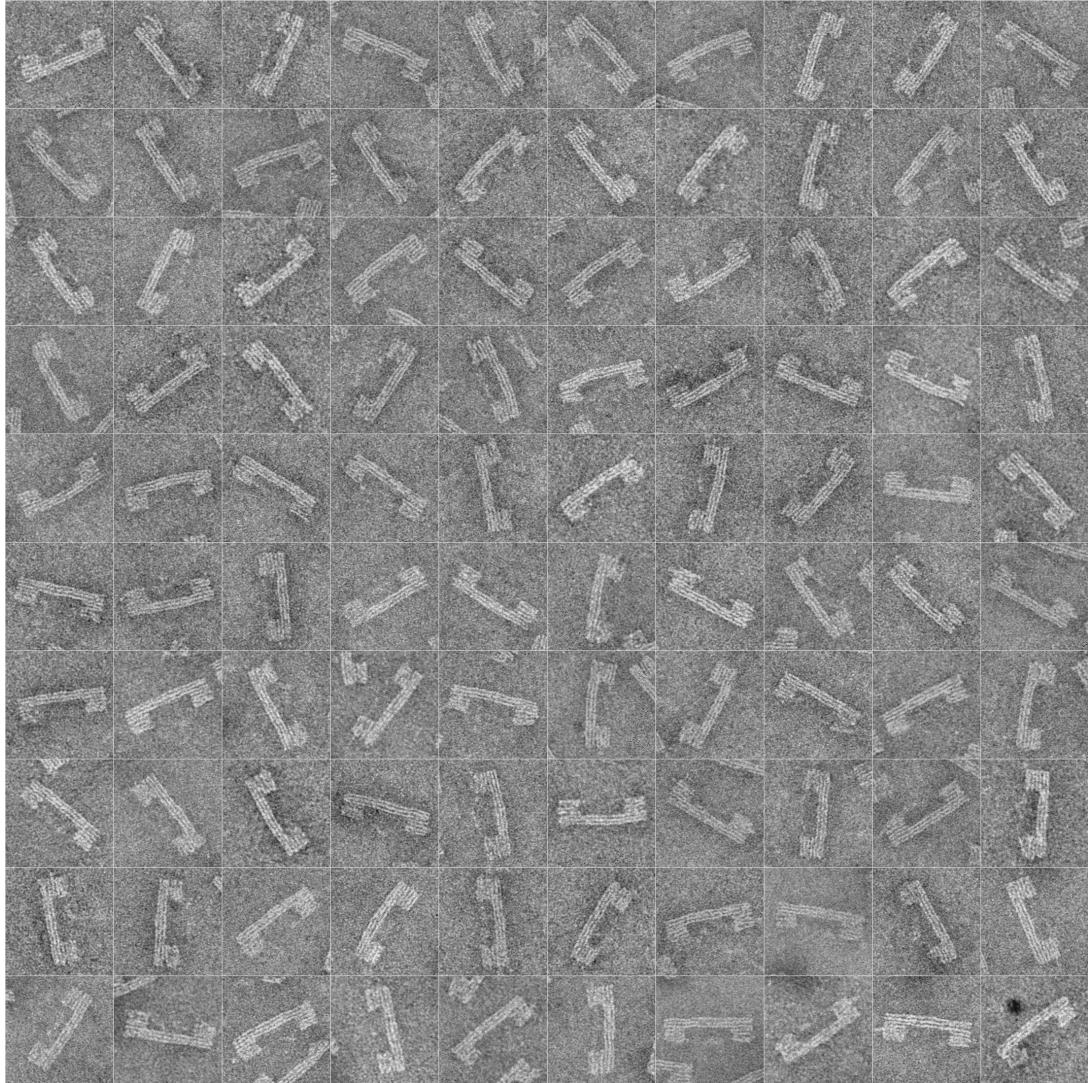


Fig. S13

All 100 single particles used to construct the average TEM image of the 7249_12pN sample shown in figure 1E. Each single image is 96 nm x 96 nm.

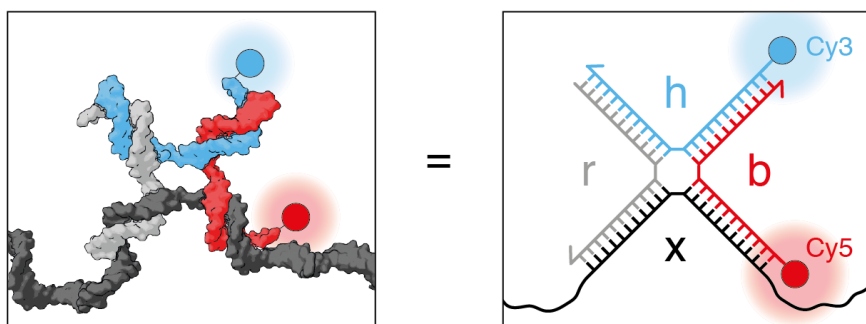


Fig. S14

Schematics of the Holliday junction with the basepairing between the four strands in detail. The donor (Cy3) is positioned at the 5' end of strand *h* (blue). The acceptor (Cy5) is positioned at the 5' end of strand *b* (red). Strand *x* is part of the scaffold (black). Strand *r* is unmodified. All four arms of the HJ are 11 base pairs long.

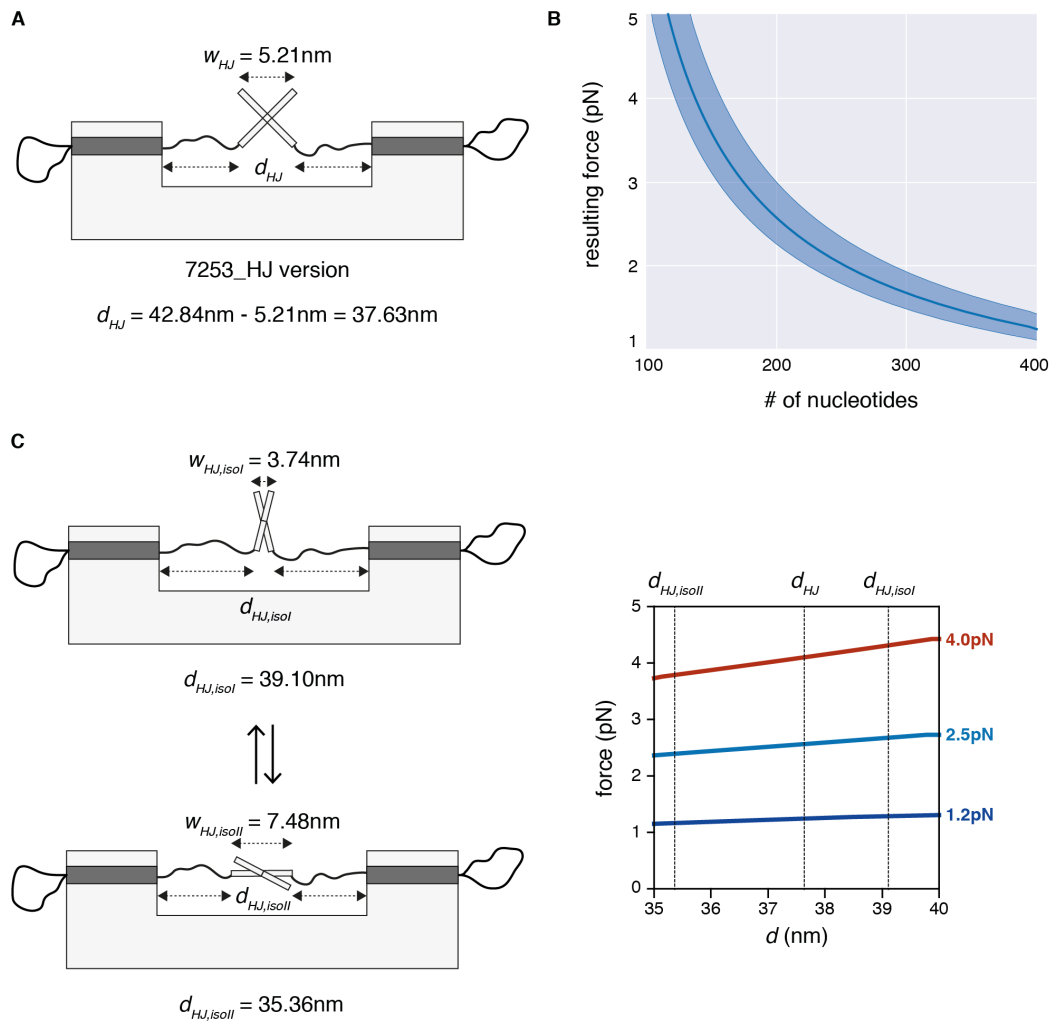


Fig. S15

(A) Geometric model of the 7253_HJ based variant of the force clamp structure with the ssDNA spanning the gap distance d_{HJ} . The dark gray region represents the subset of 10 staple strands that need to be changed to adjust the ssDNA spring length. Because of the constant switching of the HJ between the two stacked isomers, we used the open conformation to calculate the average width of the junction w_{HJ} . The HJ switches from one to the other isomer via this open conformation where every of the four arms points towards a different corner of a square. (B) Resulting entropic force as a function of the total number of nucleotides in the ssDNA spring spanning the gap distance d_{HJ} . The shaded blue region is the margin of error resulting from the standard deviation of the single base length. (C) The conformer transition of the HJ leads to a change of the distance d_{HJ} . The effect of this distance change on the resulting force is plotted on the right. The maximum fluctuation of the exerted force on the switching HJ is less than 10 %.

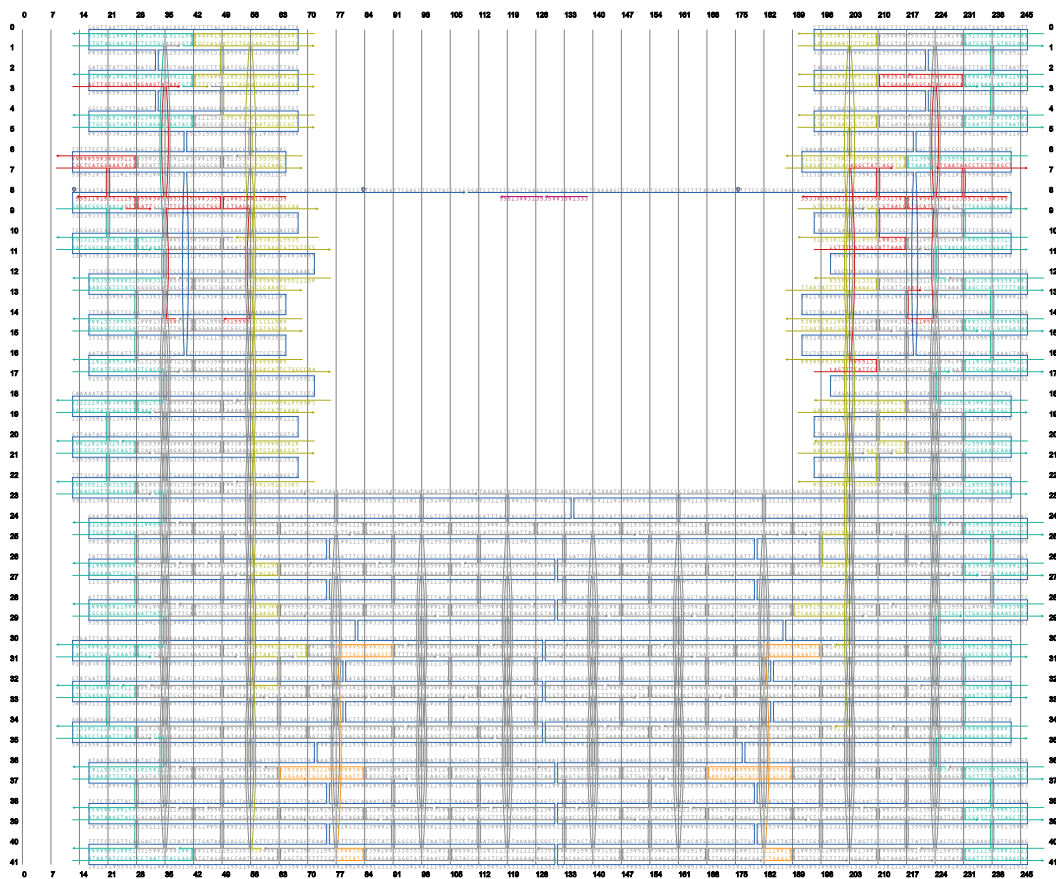


Fig. S16

Scaffold/staple layout of the 7253_HJ_1.2pN version. The number of nucleotides in the ssDNA spring is 400. Parts of the HJ complementary to the scaffold are purple.

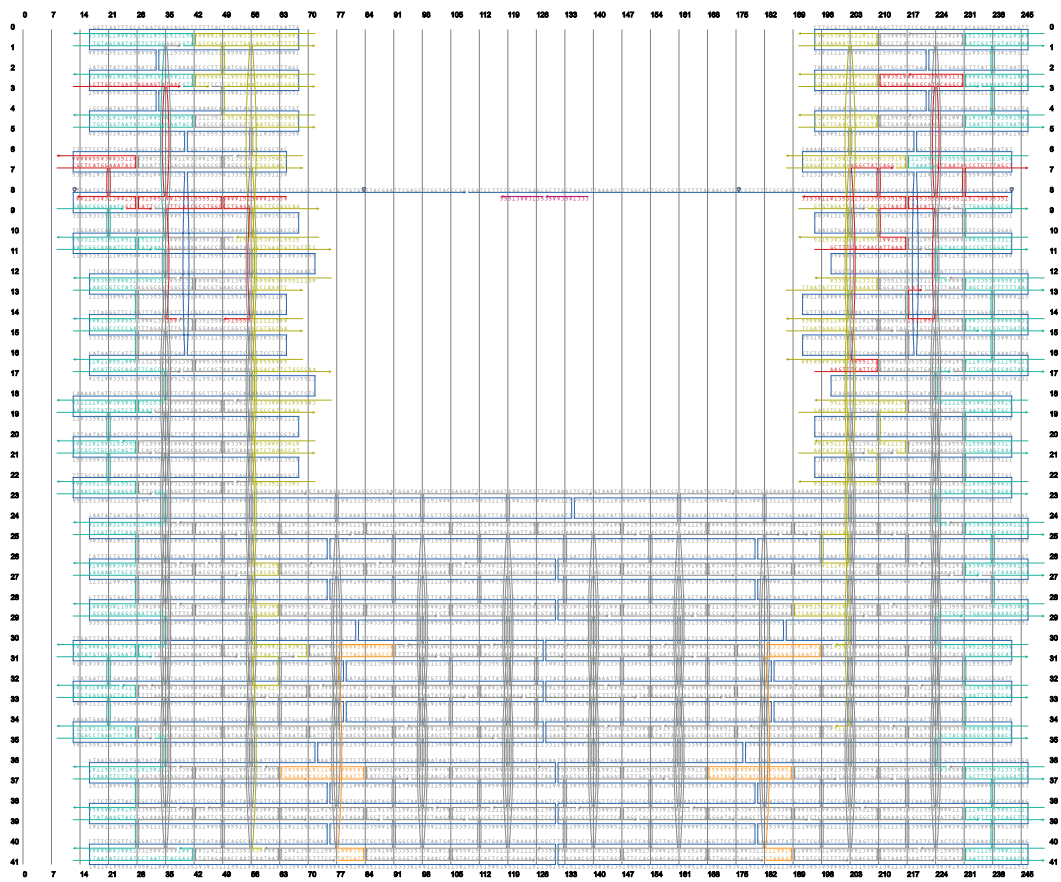


Fig. S17

Scaffold/staple layout of the 7253_HJ_2.5pN version. The number of nucleotides in the ssDNA spring is 202.

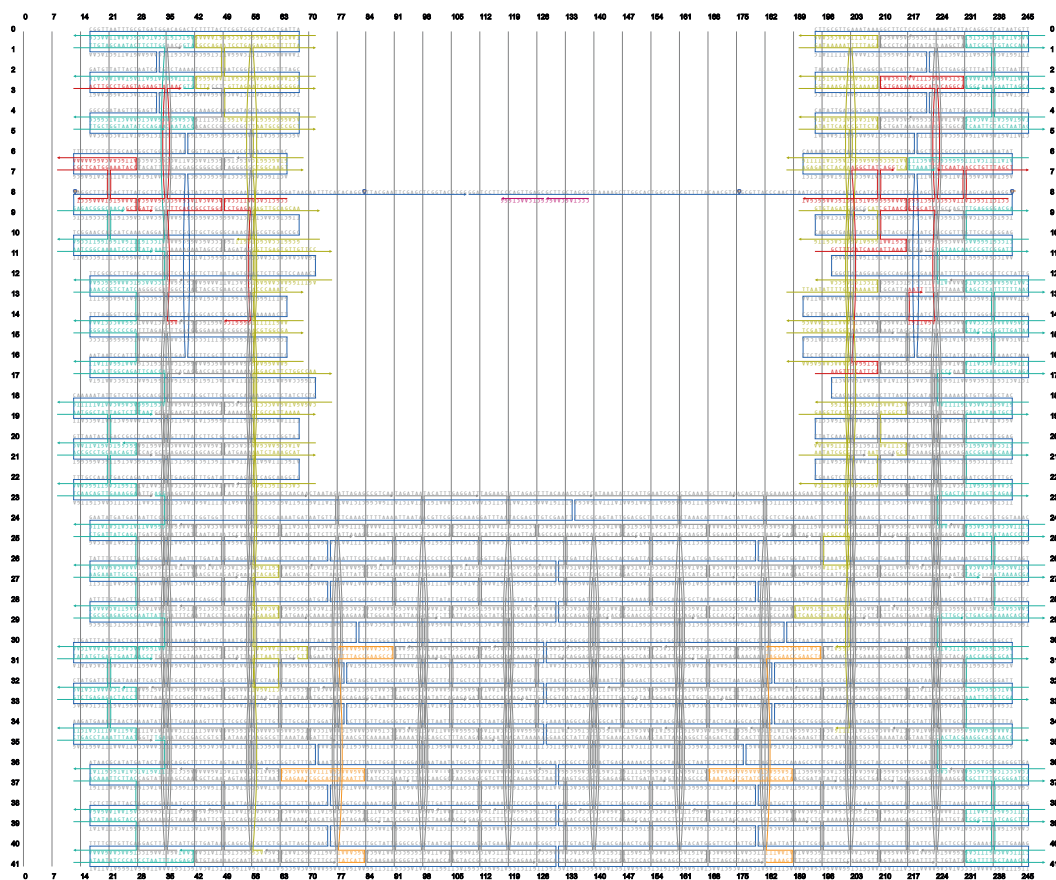


Fig. S18

Scaffold/staple layout of the 7253_HJ_4.0pN version. The number of nucleotides in the ssDNA spring is 136. The same subset of staples was used for the 0 pN version folded with the enzymatically-linearized scaffold.

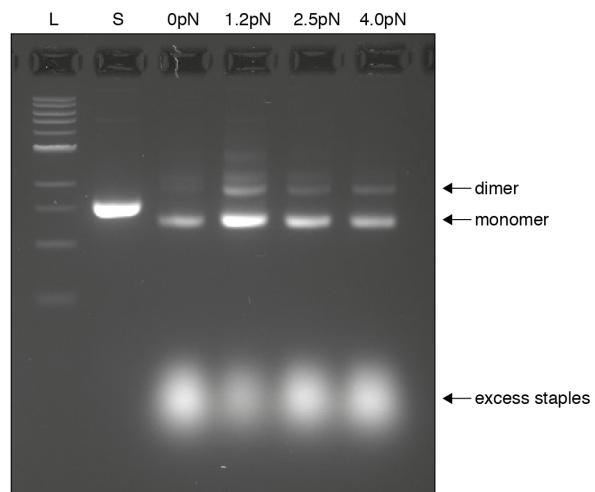


Fig. S19

2 % agarose gel of the four different 7253_HJ variants after folding. **L:** 1kb DNA ladder; **S:** 7253_HJ scaffold control.

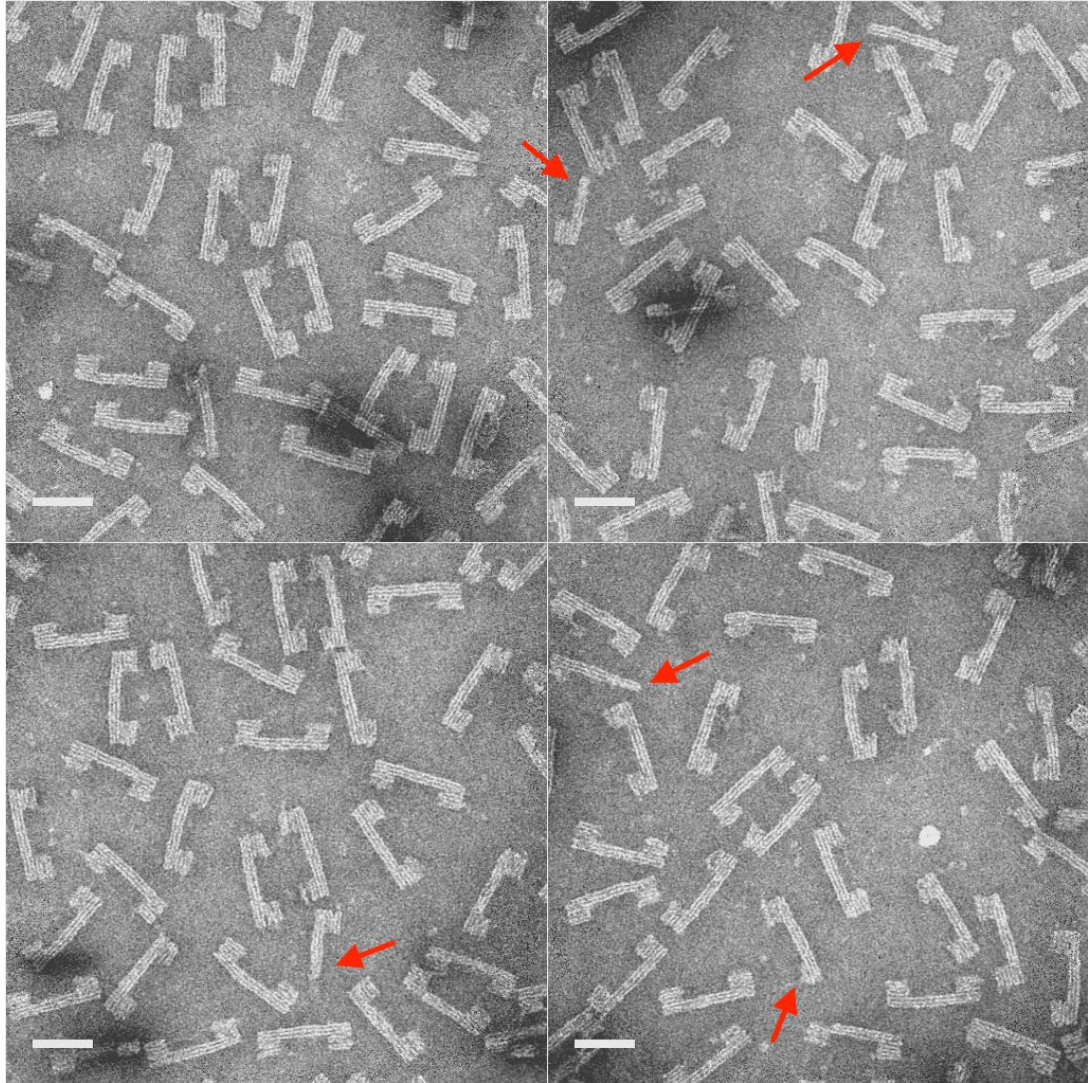


Fig. S20

TEM images of the 7253_HJ_0pN sample. The red arrows point at partially assembled structures. These were most likely folded from the fraction of scaffold that was already nicked at positions randomly distributed along the sequence before the enzymatic linearization. Scale bars: 50 nm.

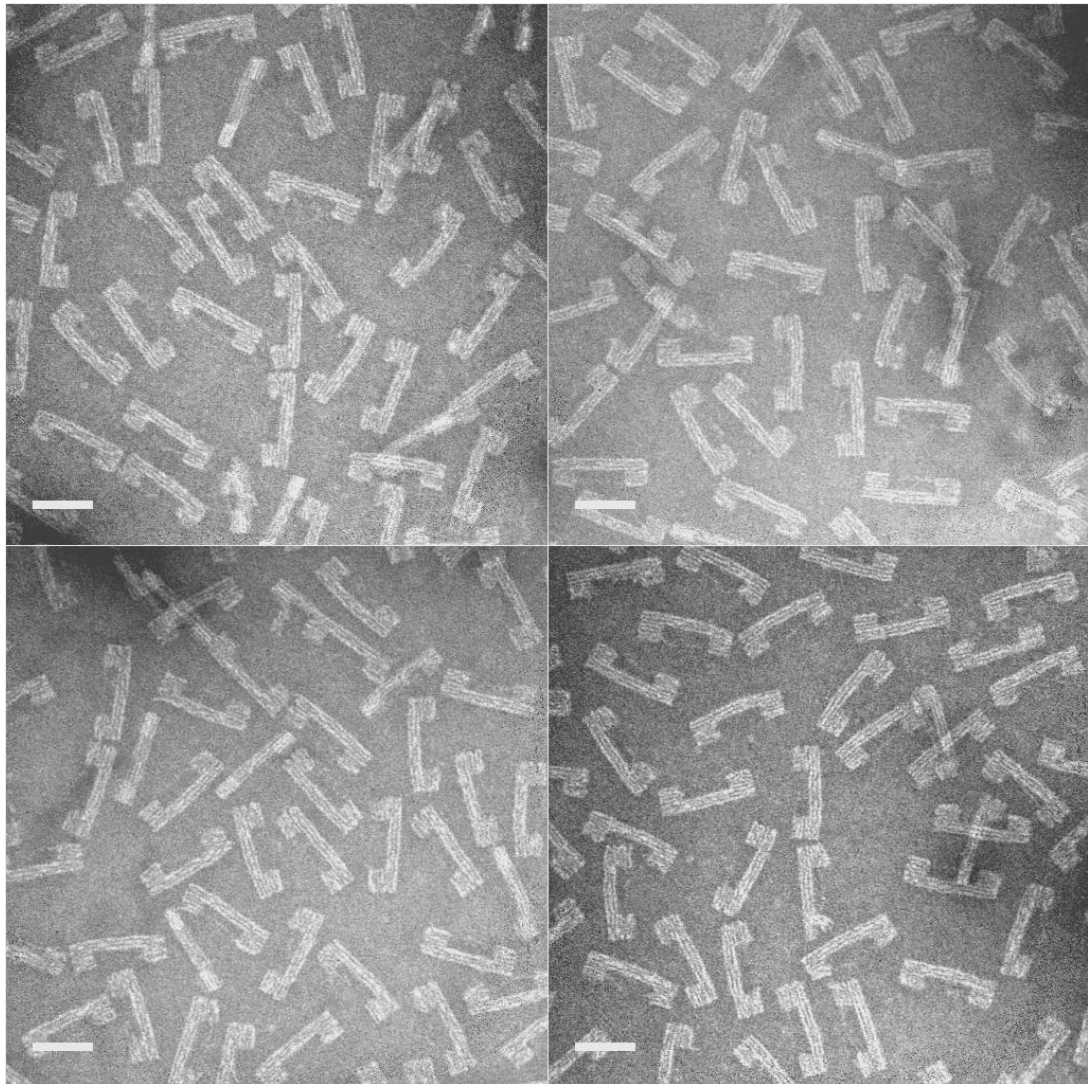


Fig. S21

TEM images of the 7253_HJ_1.2pN sample. Scale bars: 50 nm.

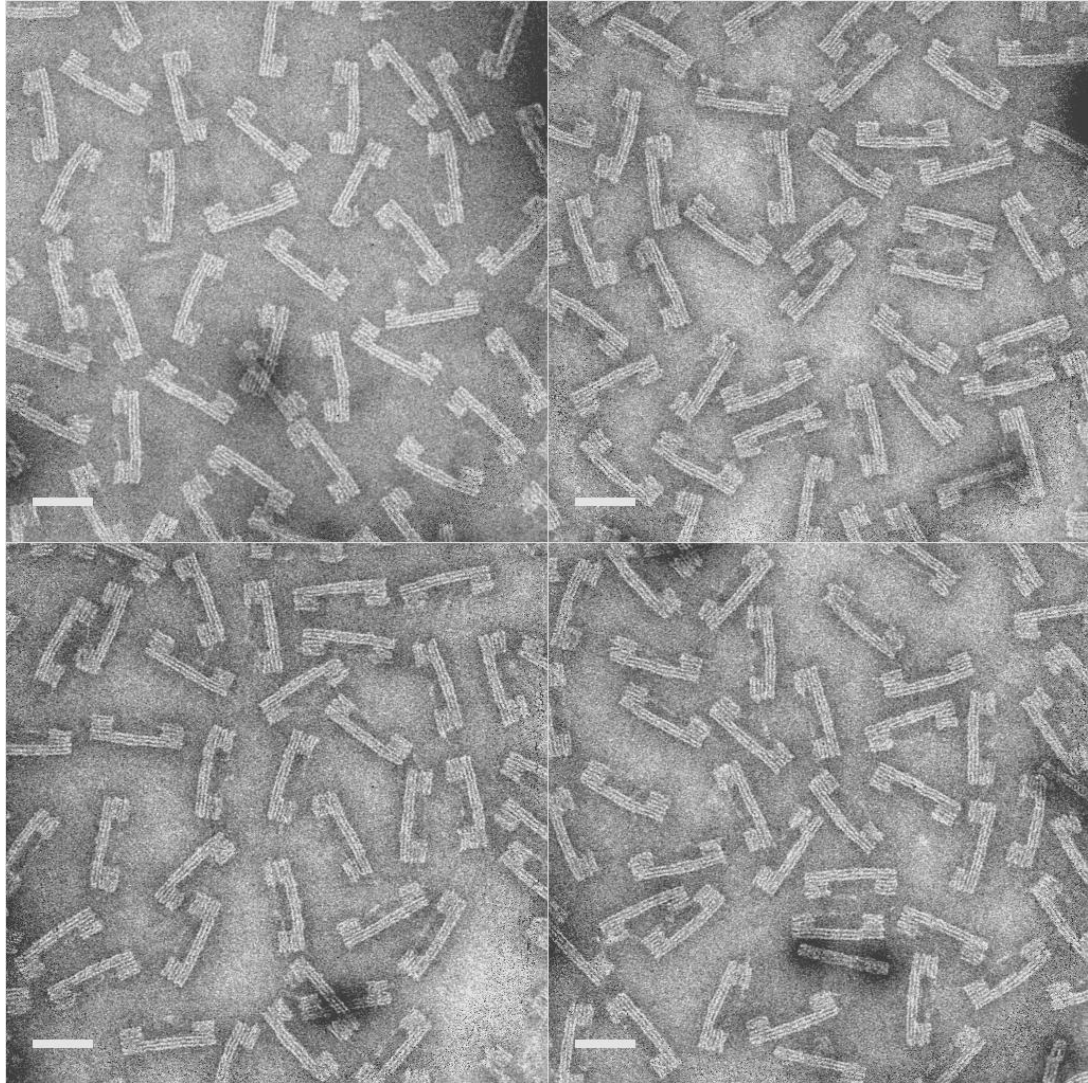


Fig. S22

TEM images of the 7253_HJ_2.5pN sample. Scale bars: 50 nm.

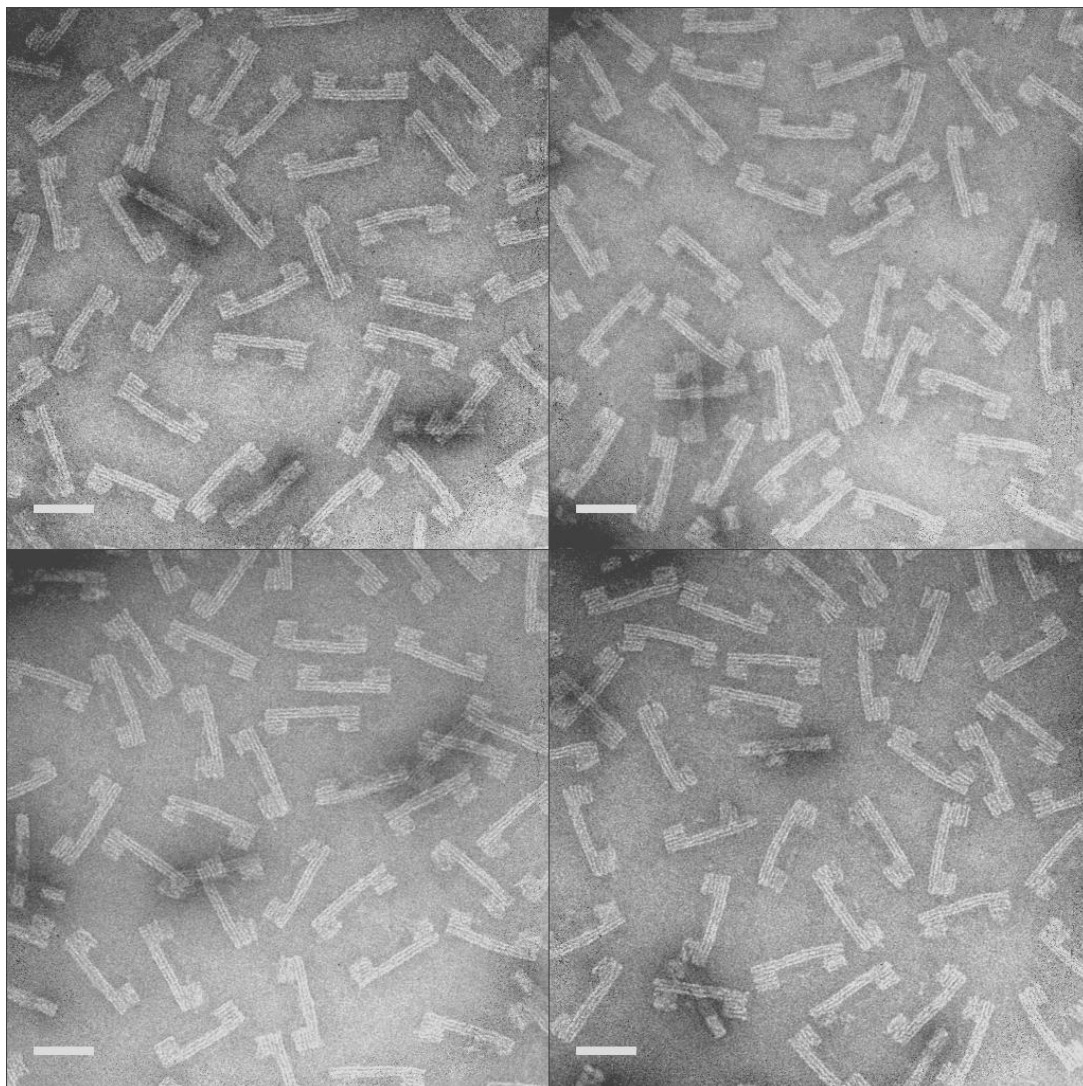


Fig. S23

TEM images of the 7253_HJ_4.0pN sample. Scale bars: 50 nm.

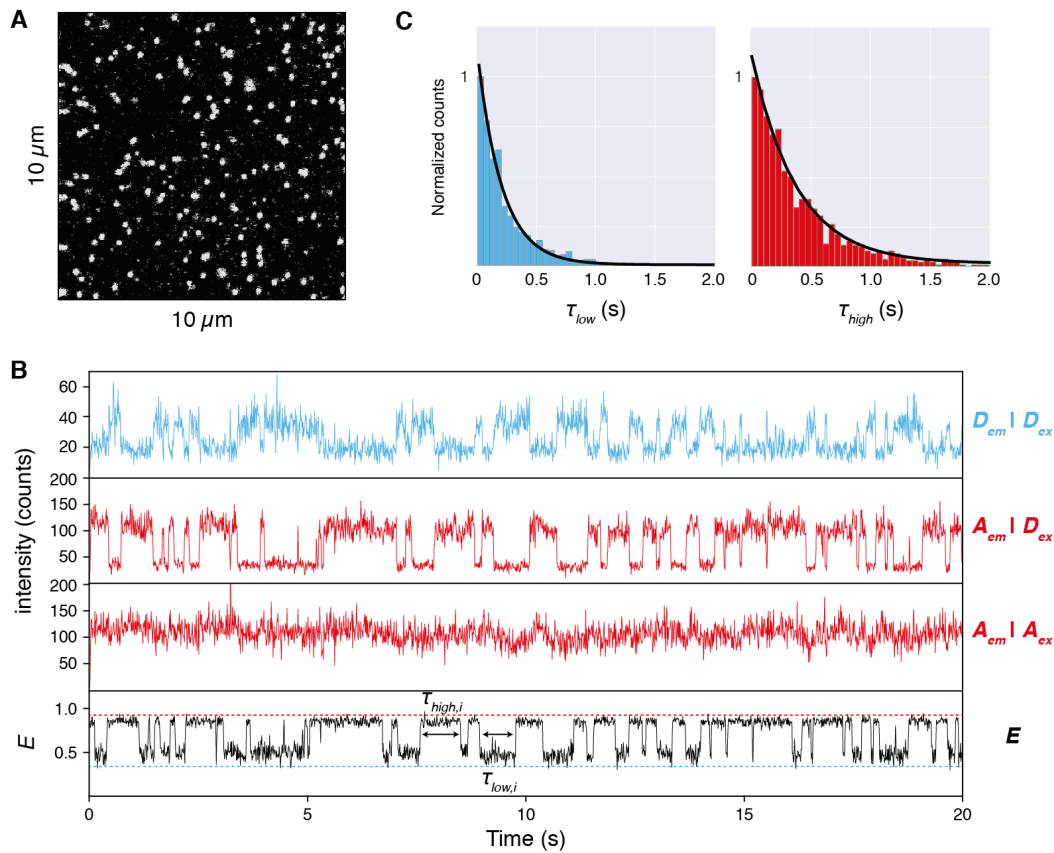


Fig. S24

Single-molecule ALEX measurement of surface-immobilized 7253_HJ_0pN sample. (A) Confocal scan of a 10 μm x 10 μm section of the surface. The bright spots are co-localized force clamp structures (the acceptor emission upon donor excitation $A_{em} | D_{ex}$ was measured). After scanning such a section, the fluorescence of each co-localized structure was monitored over time with alternating laser excitation until bleaching of the dyes. (B) Section of a time trace of one of the spots in panel A: donor intensity upon donor excitation ($D_{em} | D_{ex}$) in blue; acceptor intensity upon donor excitation ($A_{em} | D_{ex}$) and acceptor intensity upon acceptor excitation ($A_{em} | A_{ex}$) in red; calculated FRET efficiency (E) in black. The HJ is constantly switching between *isoI* (low FRET) and *isoII* (high FRET). (C) Dwell time histograms of the low- and high-FRET state for all traces from the 7253_HJ_0pN traces combined. The black line is a mono-exponential decay fit. Switching rates were extracted from the fit for each trace individually. Only traces with more than 20 transition events were included in the dwell time analysis.

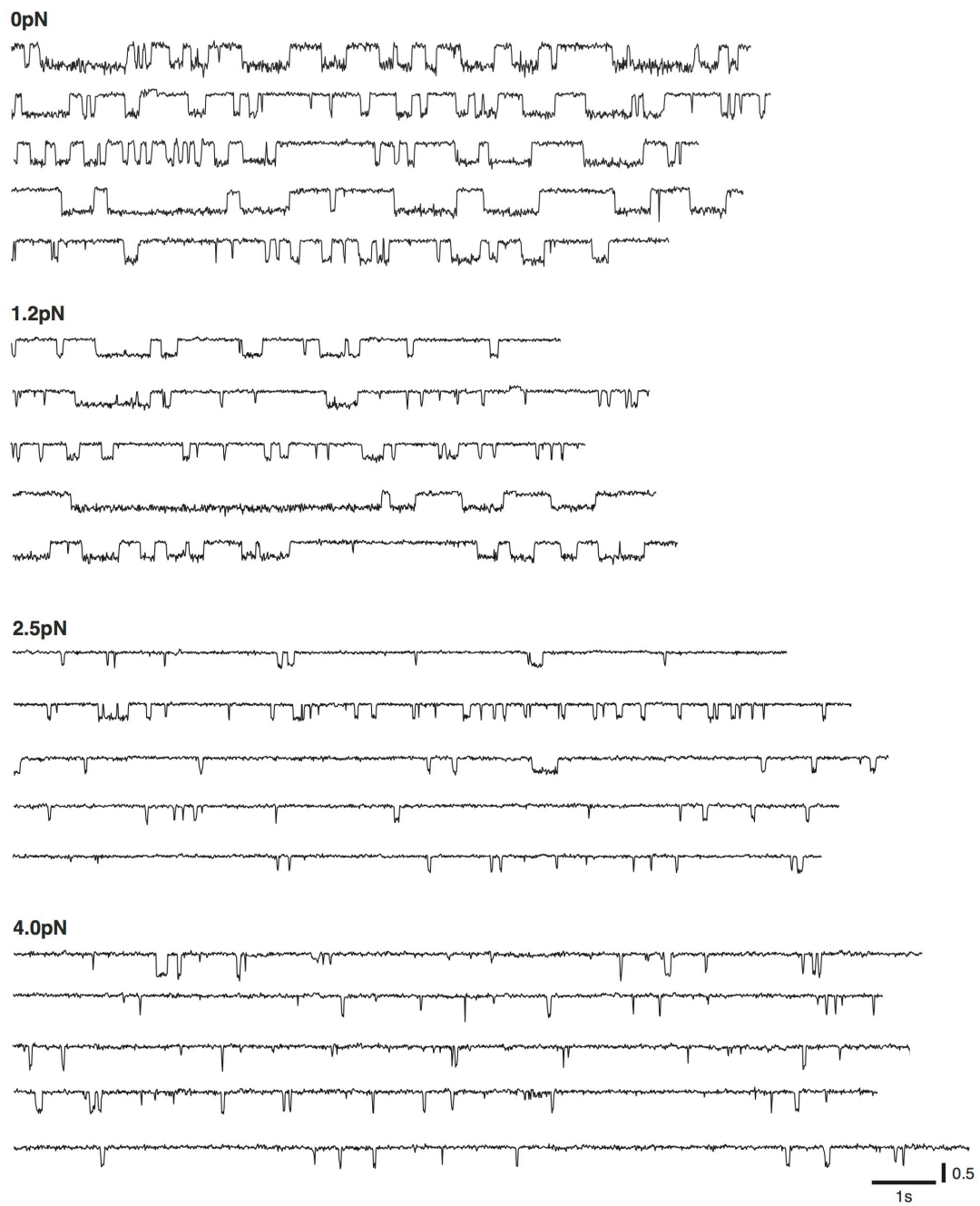


Fig. S25

5 randomly selected FRET time traces for each of the four 7253_HJ variants.

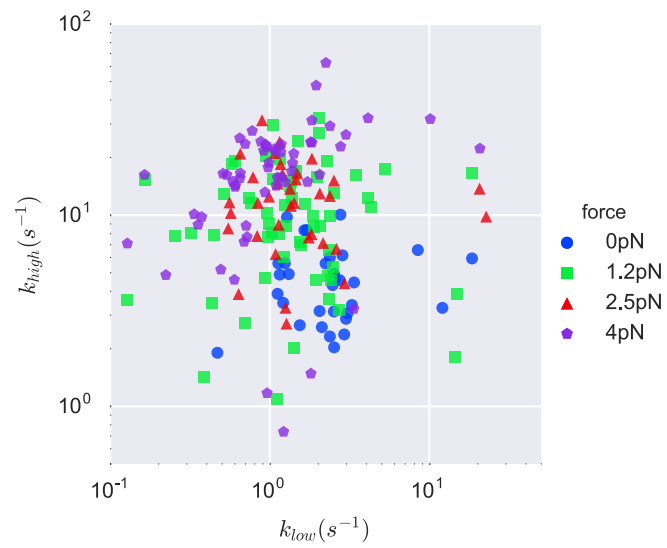


Fig. S26

Log-log plot of the distribution of transition rates of all individual Holliday junctions. We extracted the rates for each dwell time histogram individually to acquire information about the level of heterogeneity. The Holliday junction is known to have a very distinct molecule-to-molecule variation in its switching dynamics (26). This heterogeneity is well preserved in the force clamp.

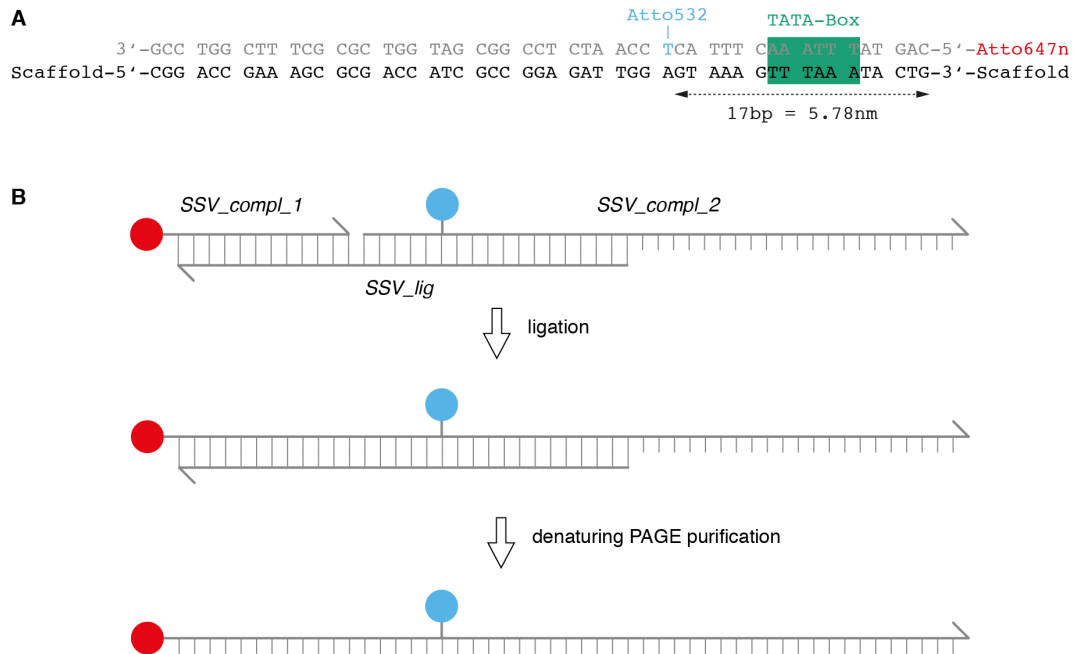


Fig. S27

(A) T6 gene promoter sequence of the Sulfolobus spindle-shaped virus 1 (SSV) in the 7283_SSV scaffold (black) and its complementary strand (gray). The TATA-box is flanked by a donor-acceptor pair (Atto532 & Atto647n) on the complementary strand spaced 17 base pairs apart. (B) Scheme of the ligation of *SSV_compl_1* and *SSV_compl_2* to prepare the full complementary strand *SSV_compl* carrying both donor and acceptor.

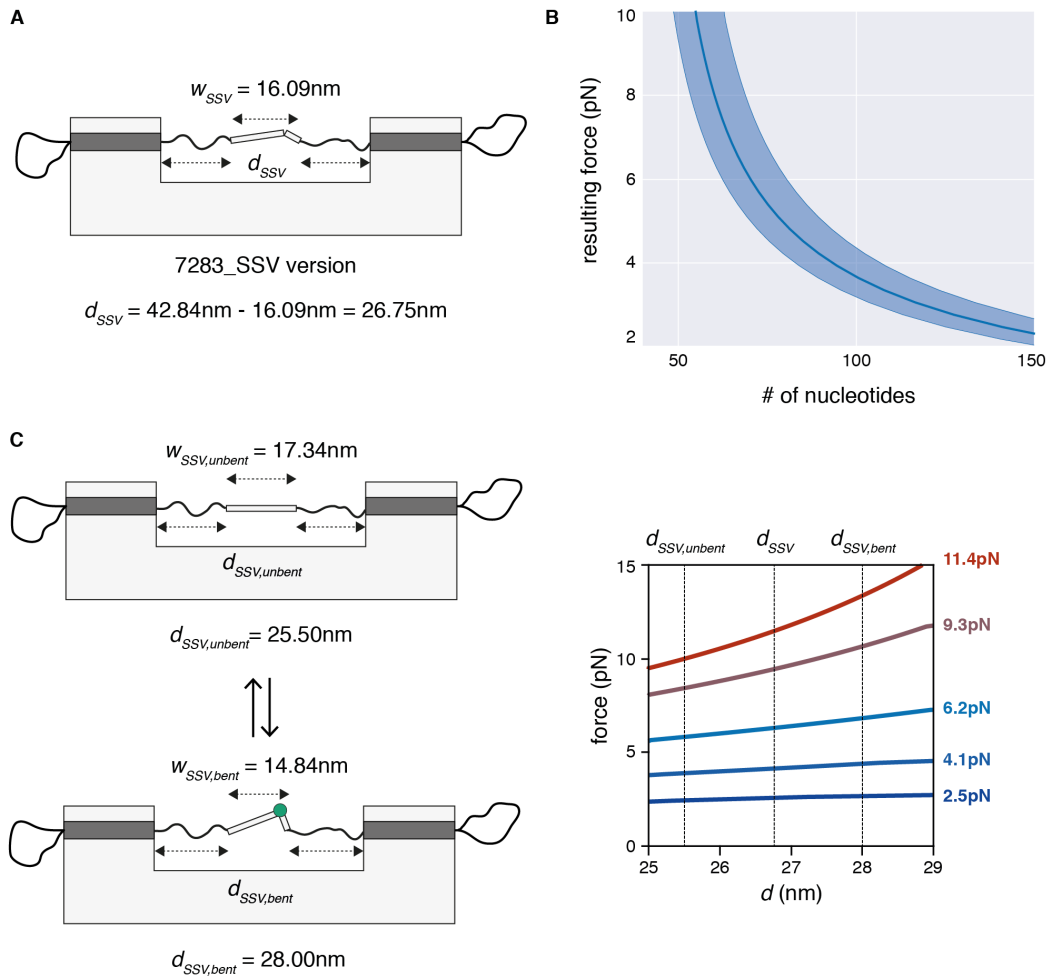


Fig. S28

(A) Geometric model of the 7283_SSV based variant of the force clamp structure with the ssDNA spanning the gap distance d_{SSV} . The dark gray region represents the subset of 10 staple strands that need to be changed to adjust the ssDNA spring length. As a width of the double-stranded SSV promoter, we used the average value of the unbent and bent state (resulting in an average width of the SSV promoter w_{SSV} of 16.09 nm). (B) Resulting entropic force as a function of the total number of nucleotides in the ssDNA spring spanning the gap distance d_{SSV} . The shaded blue region is the margin of error resulting from the standard deviation of the single base length. (C) Similar to the 7253_HJ samples, the bending of the SSV promoter leads to a change of the distance d_{SSV} . To calculate the change in distance, we treated the 51 base pair long SSV promoter DNA as two connected rigid rods with a hinge in the middle of the TATA-box and a length per base pair of 0.34 nm. The TBP induces a 90° bending angle. The effect of this distance change on the resulting force is plotted on the right. The maximum fluctuation of the exerted force on the SSV promoter is around 17 %.

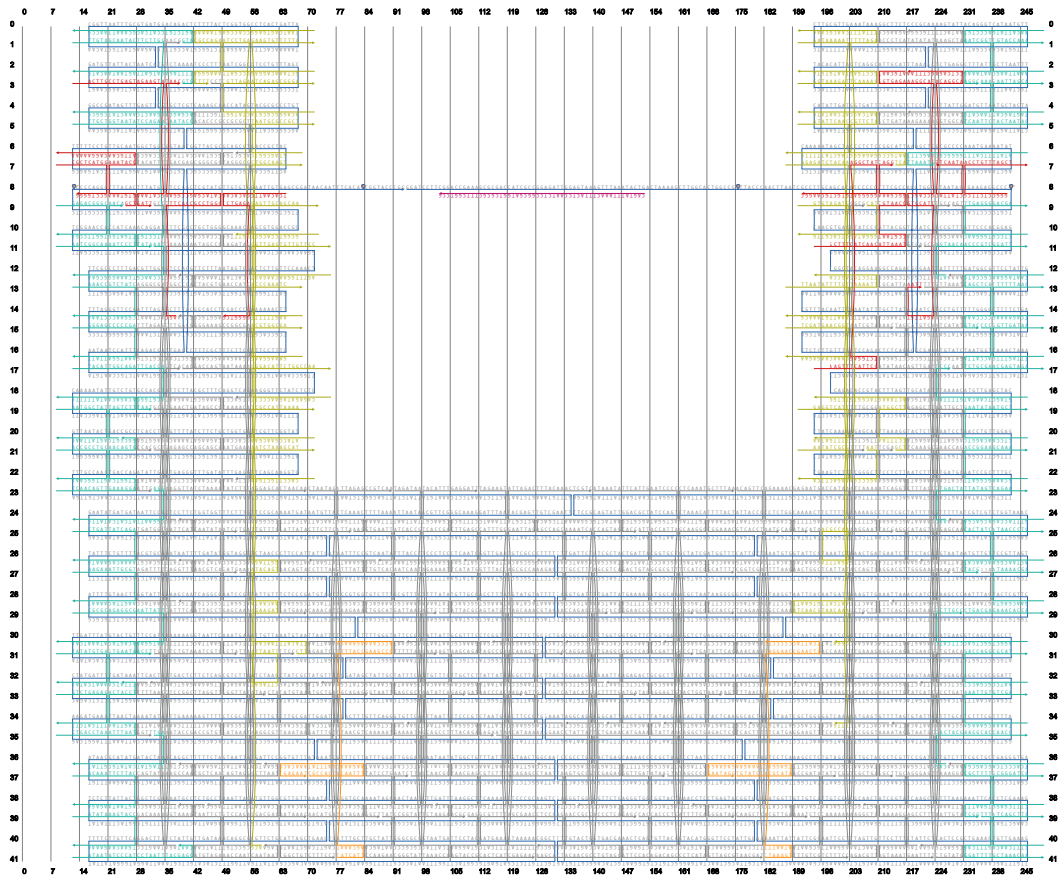


Fig. S29

Scaffold/staple layout of the 7283_SSV_2.5pN version. The number of nucleotides in the ssDNA spring is 143. The complementary strand of the SSV promoter region in the scaffold is purple.

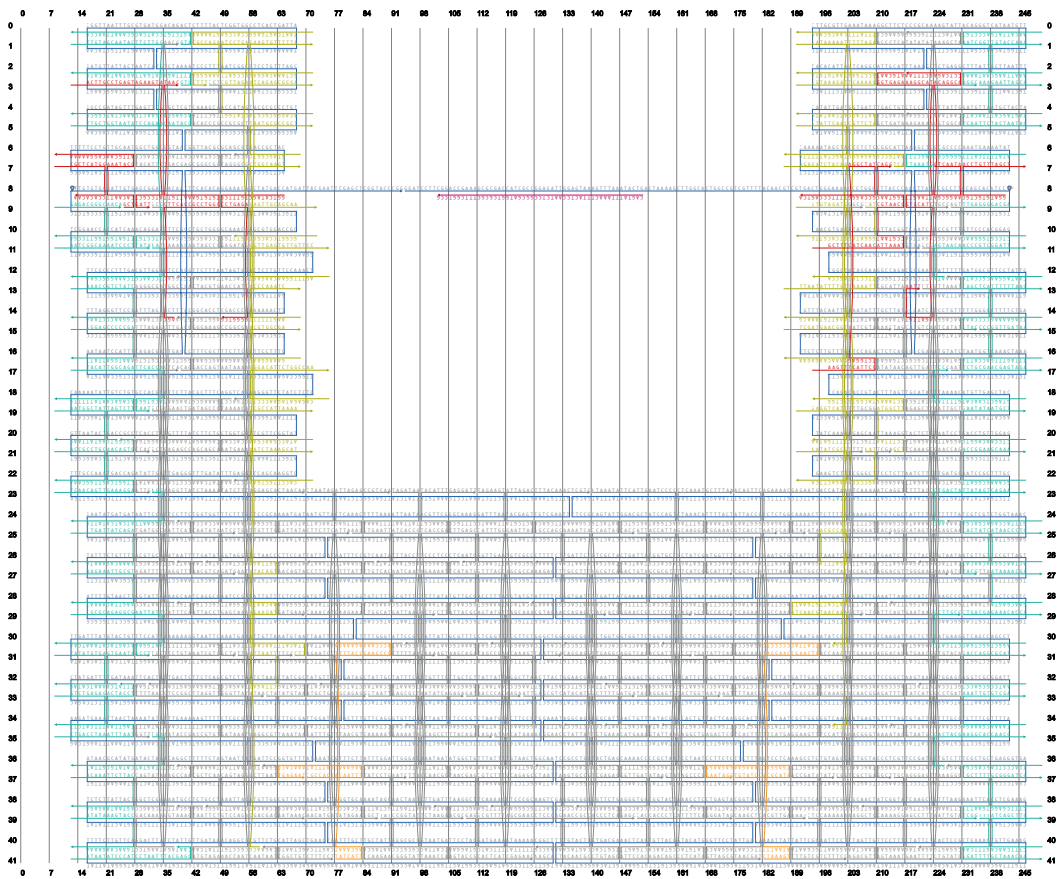


Fig. S31

Scaffold/staple layout of the 7283_SSV_6.2pN version. The number of nucleotides in the ssDNA spring is 72.

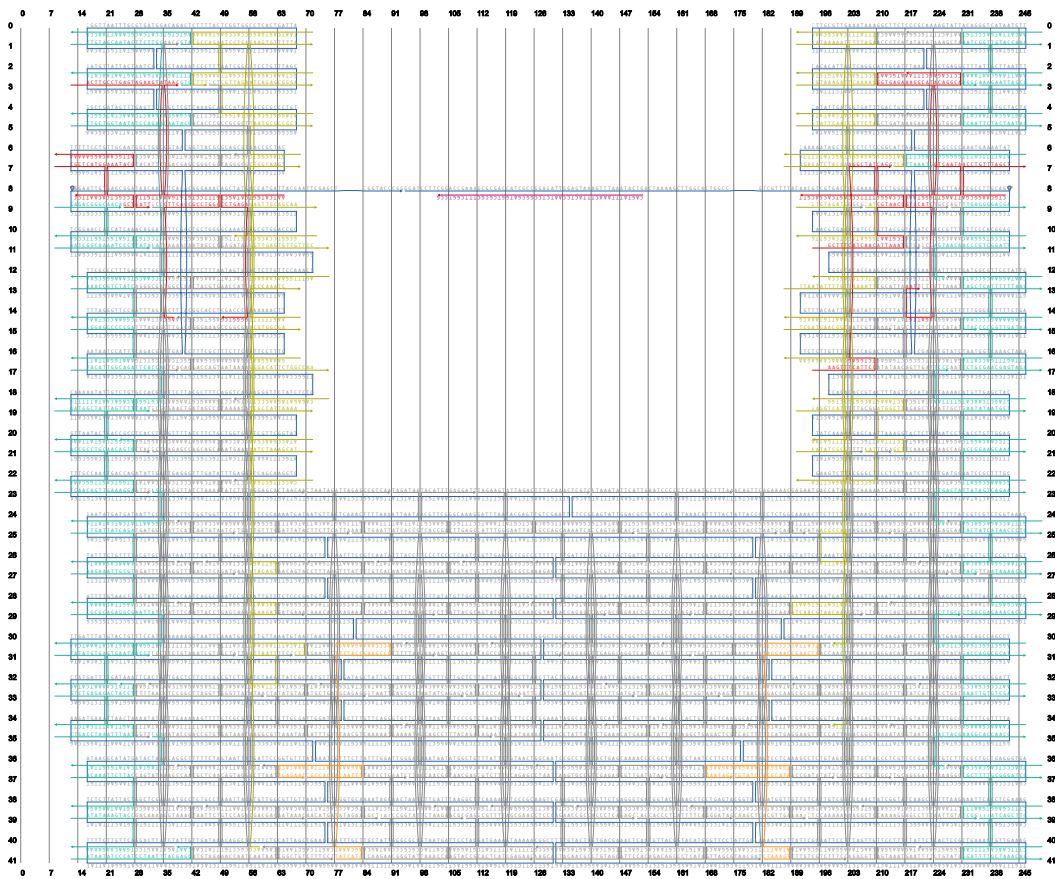


Fig. S32

Scaffold/staple layout of the 7283_SSV_9.3pN version. The number of nucleotides in the ssDNA spring is 59.

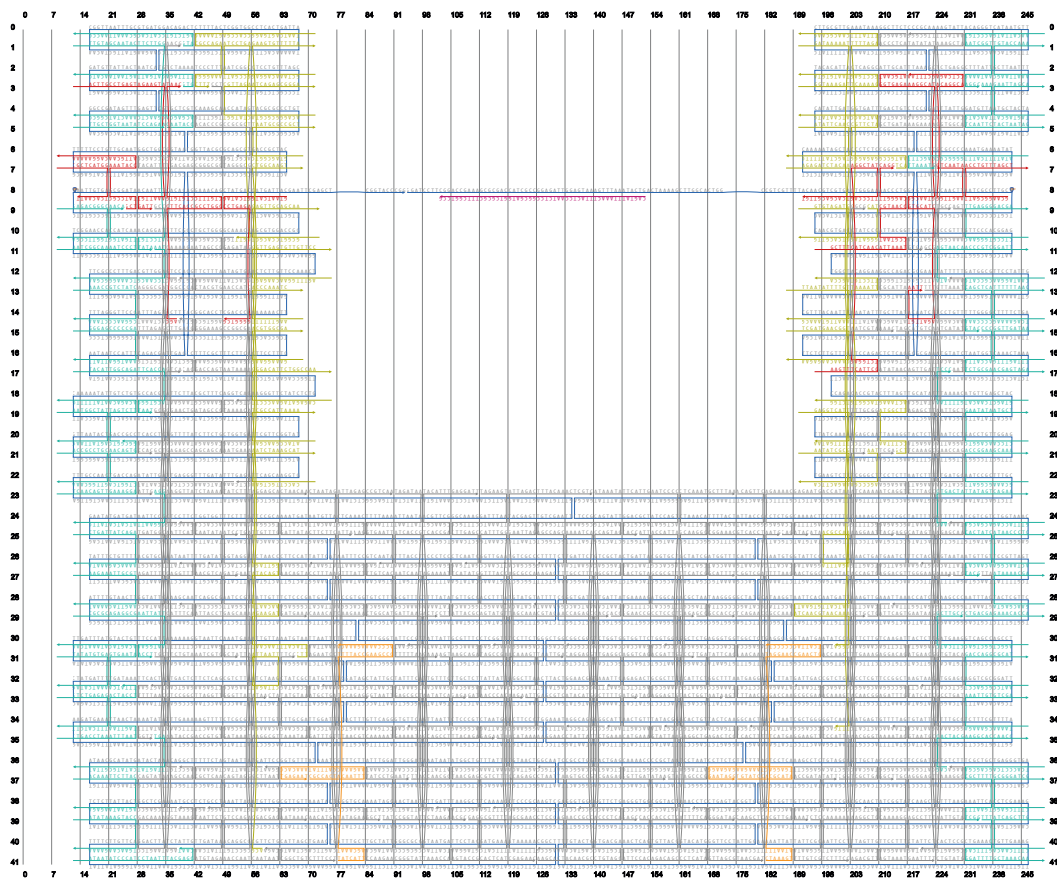


Fig. S33

Scaffold/staple layout of the 7283_SSV_11.4pN version. The number of nucleotides in the ssDNA spring is 55. The same subset of staples was used for the 0 pN version folded with the enzymatically-linearized scaffold.

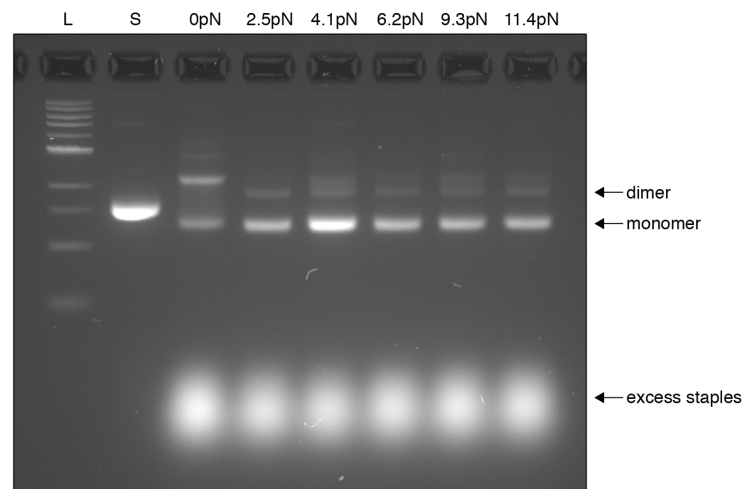


Fig. S34

2 % agarose gel of the six different 7283_SSV variants after folding. **L:** 1kb DNA ladder; **S:** 7283_SSV scaffold control.

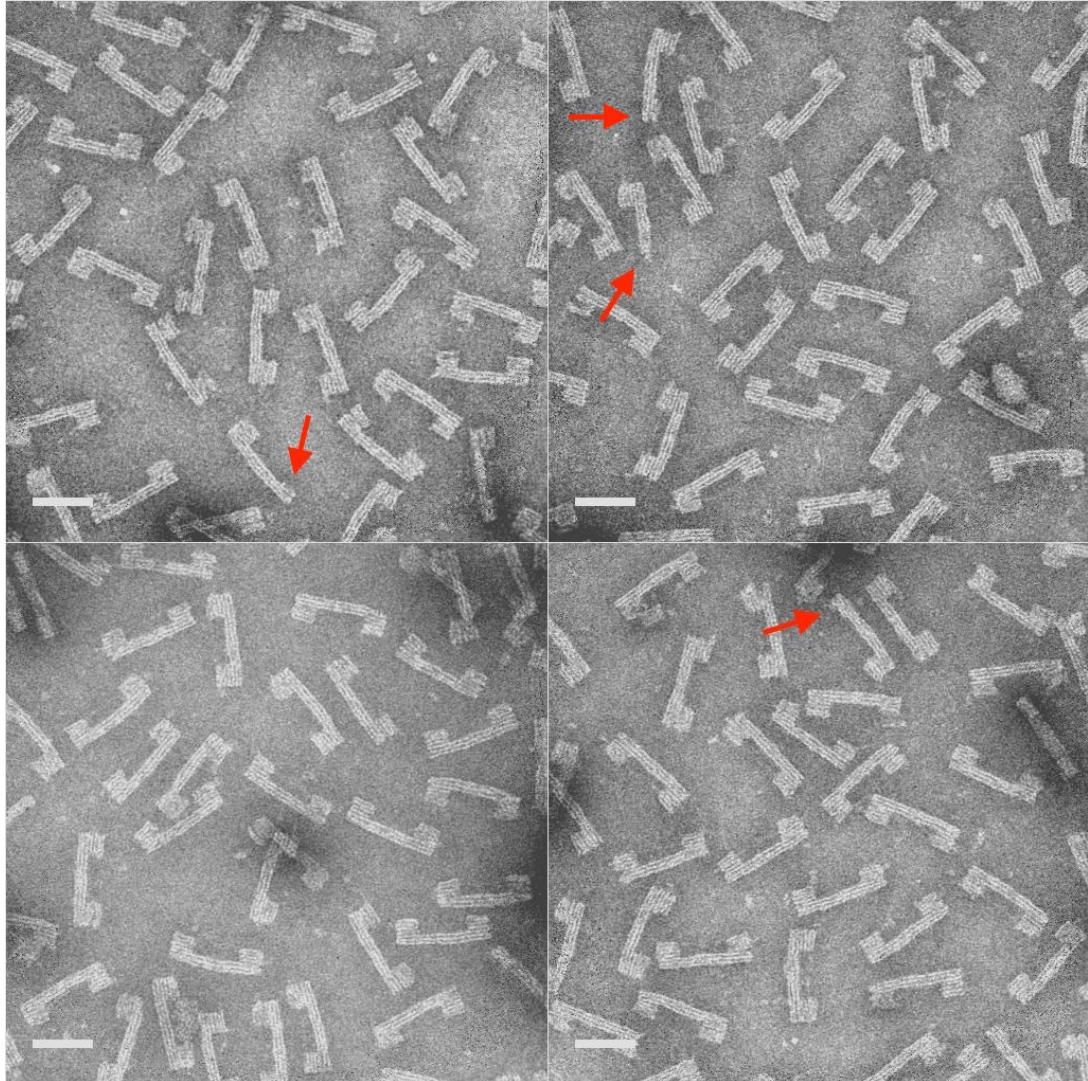


Fig. S35

TEM images of the 7283_SSV_0pN sample. The red arrows point at partially assembled structures. These were most likely folded from the fraction of scaffold that was already nicked at positions randomly distributed along the sequence before the enzymatic linearization. Scale bars: 50 nm.

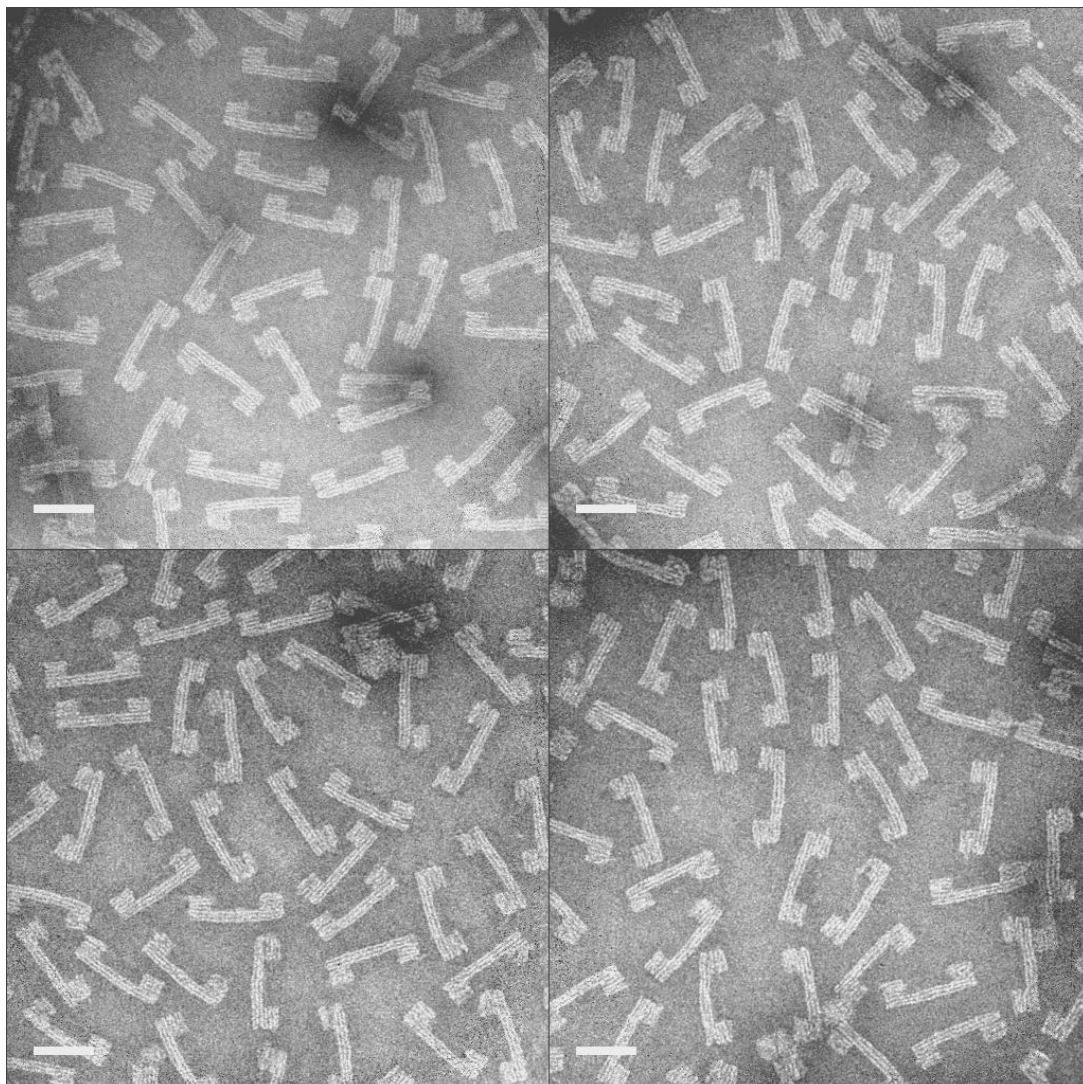


Fig. S36

TEM images of the 7283_SSV_2.5pN sample. Scale bars: 50 nm.



Fig. S37

TEM images of the 7283_SSV_4.1pN sample. Scale bars: 50 nm.

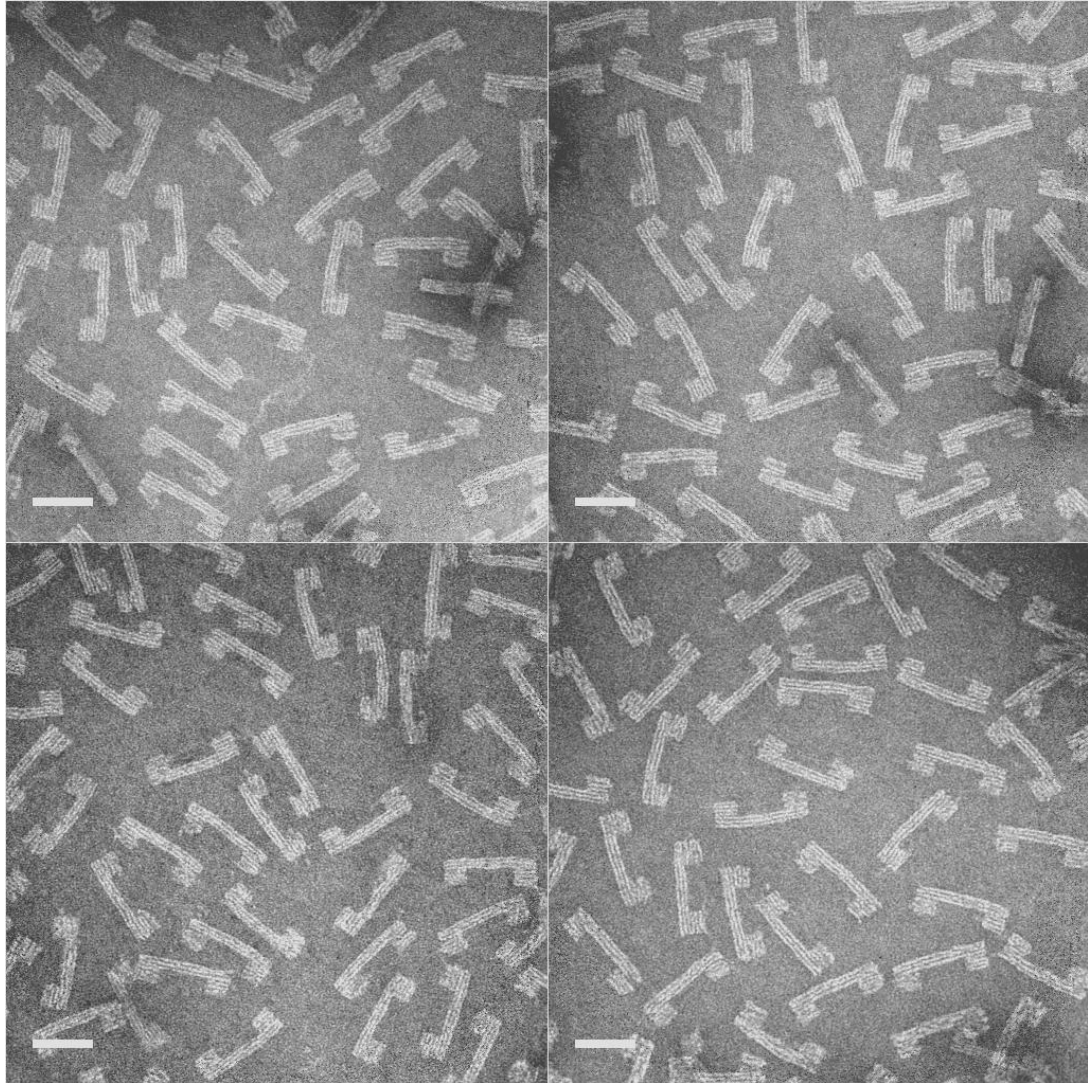


Fig. S38

TEM images of the 7283_SSV_6.2pN sample. Scale bars: 50 nm.

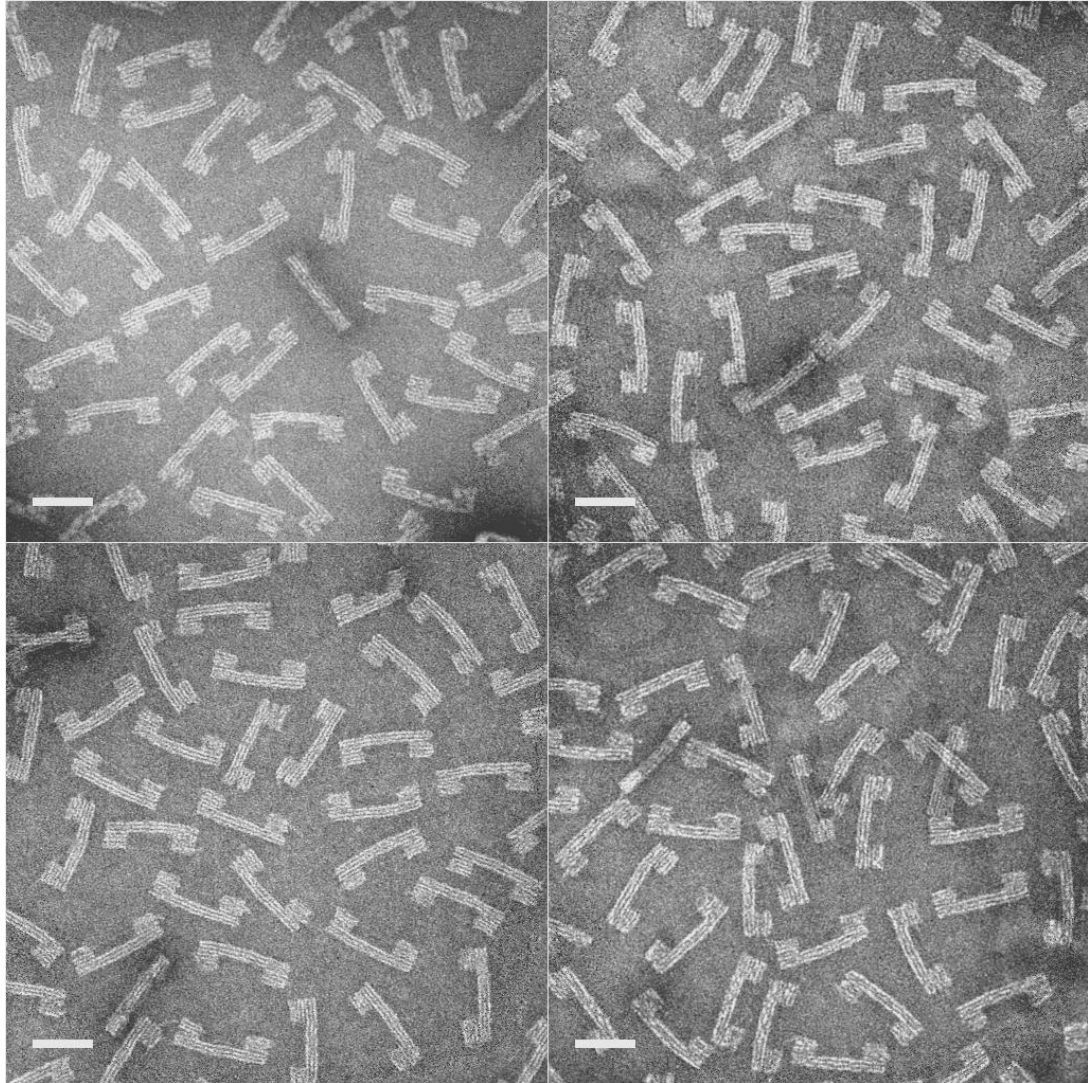


Fig. S39

TEM images of the 7283_SSV_9.3pN sample. Scale bars: 50 nm.

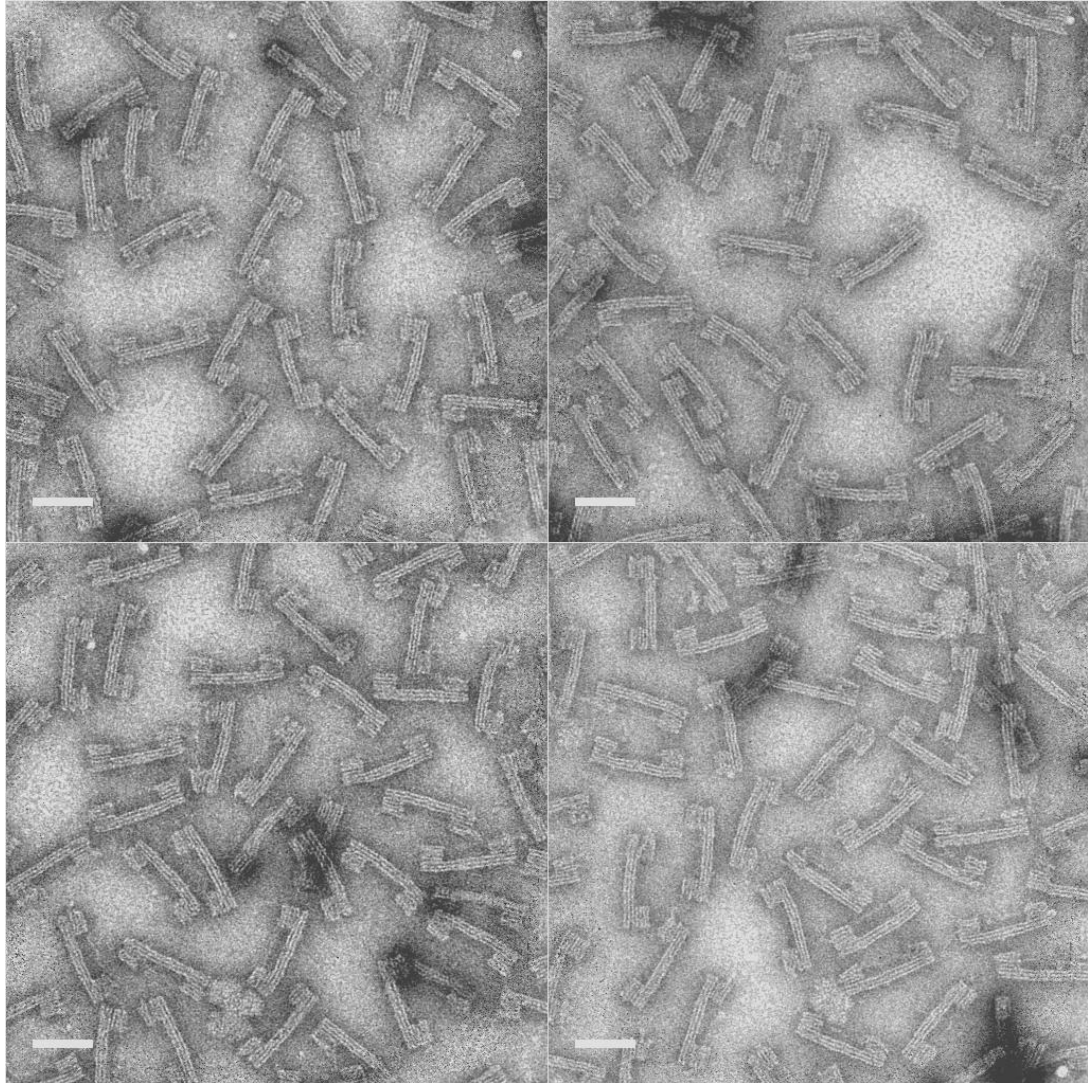


Fig. S40

TEM images of the 7283_SSV_11.4pN sample. Scale bars: 50 nm.

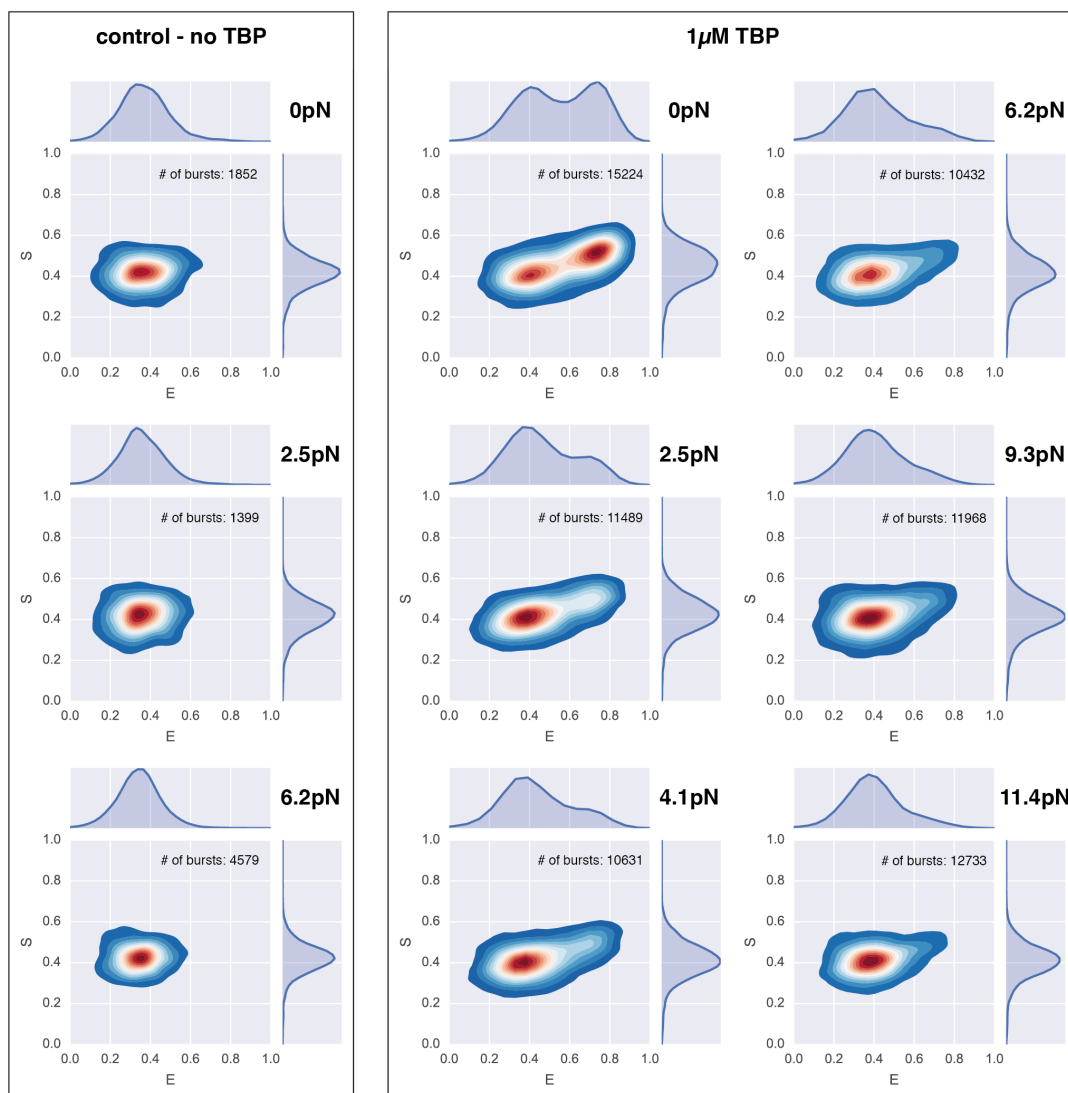


Fig. S41

E - *S* histograms of the 7283_SSV samples (ALEX-2CDE < 12). **(Left)** Control measurements of three force versions without TBP added. Only the low-FRET population (corresponding to the undistorted state) is present at all three forces. **(Right)** Measurements after the addition of 1 μ M MjTBP. Average measurement time per sample was \sim 30 min.

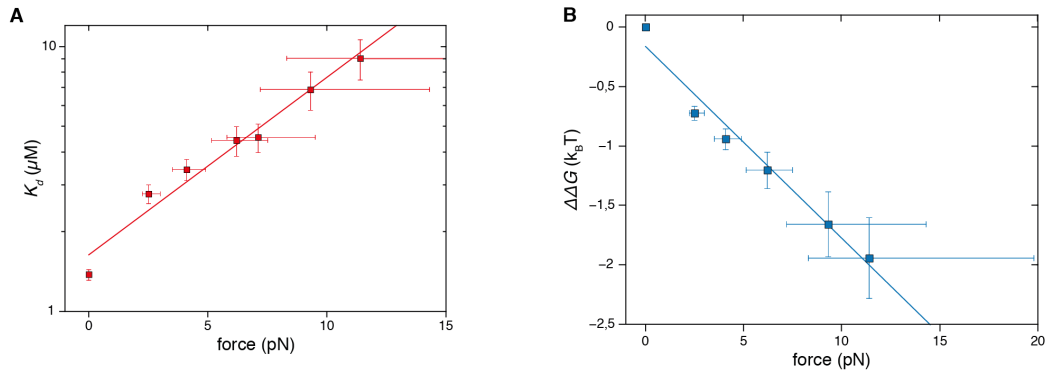


Fig. S42

(A) Dissociation equilibrium constant K_d plotted as a function of force in a semi-log plot. To calculate K_d we assumed the following reversible, bimolecular binding reaction with concurrent binding and bending:



At equilibrium, K_d is given by:

$$K_d = [TBP] * \frac{[DNA]}{[TBP-DNA]}$$

The TBP concentration $[TBP]$ was constant for all measurements ($1\mu\text{M}$). The solid line is an exponential fit. The ratio of free DNA and TBP–DNA complex was calculated from the bimodal FRET efficiency distribution. The initial value for K_d at 0 pN is with $1.37\mu\text{M}$ higher than the $\sim 50\text{ nM}$ reported earlier (27). We attribute this mainly to the significantly lower temperature of 35°C at which we measure (compared to 55°C in ref. 27 and the optimal growth temperature of *M.jannashii* of 85°C) and the low salt concentration used in our measurements.

(B) Change in the molar Gibbs free energy $\Delta\Delta G$ plotted as a function of force. The solid line is a linear fit.

Sequence of 7253_HJ scaffold:

insert sequences:

HJ_insert:

5' -GATCCTTCCCAGTTGAGCGCTTGCTAGGGTTAAA-3'

HJ_insert_complement

5' -AGCTTTTAAACCCTAGCAAGCGCTCAACTGGGAAG-3'

full sequence:

BamHI site: red
Holliday Junction strand x: green
HindIII site: blue

GGATCCTTCCCAGTTGAGCGCTTGCTAGGGTTAAAAGCTTGGCAC TGGCCGTCGTTTTACAACGTCGTGAC
TGGGAAAACCTGGCGTTACCCAACTTAATCGCCTTGCAGCACATCCCCCTTTCGCCAGCTGGCGTAATAG
CGAAGAGCCCGCACCGATCGCCCTTCCCAACAGTTGCGCAGCCTGAATGGCGAATGGCGCTTTGCCTGGT
TTCCGGCACCAGAAGCGGTGCCGAAAGCTGGCTGGAGTGCATCTTCCCTGAGGCCGATACTGTCGTGTC
CCCTCAAAC TGGCAGATGCACGGTTACGATGGCCCATCTACACCAACGTGACCTATCCATTACGGTCAA
TCCGCGCTTTGTTCCACGGAGAATCCGACGGGTTGTTACTCGCTCACATTTAATGTTGATGAAAGCTGGC
TACAGGAAGGCCAGACGCGAATTAATTTTGGATGGCGTTCCCTATTGGTTAAAAAATGAGCTGATTTAACAAA
AATTTAATGCGAATTTTAAACAAAATATTAACGTTTACAATTTAAATATTTGCTTATACAATCTTCTGT
TTGGGGCTTTTCTGATTATCAACCGGGGTACATATGATTGACATGCTAGTTTTACGATTACCGTTCATCGA
TTCTCTTGTTTGCTCCAGACTCTCAGGCAATGACCTGATAGCCTTTGTAGATCTCTAAAAATAGCTACCC
TCTCCGGCATTAAATTTATCAGCTAGAACGGTTGAATATCATATTGATGGTGATTTGACTGTCTCCGGCCTT
TCTCACCTTTTGAATCTTTACCTACACATTA CTAGGCATTTGCATTTAAAAATATATGAGGGTCTAAAAA
TTTTTATCCTTGCCTTGAATAAAGGCTTCTCCCGCAAAAGTATTACAGGGTCATAATGTTTTTGGTACAA
CCGATTTAGCTTTATGCTCTGAGGCTTATTGCTTAATTTTGCATAATCTTTGCCTTGCCTGTATGATTTA
TTGGATGTTAATGCTACTACTATTAGTAGAATTGATGCCACCTTTTCAGCTCGCGCCCCAAATGAAAAAT
AGCTAAACAGGTTATTGACCATTTGCGAAATGTATCTAATGGTCAAAC TAAATCTACTCGTTCGCAGAATT
GGGAATCAACTGTTATATGGAATGAACTTCCAGACACCGTACTTTAGTTGCATATTTAAAAATAGTTGAG
CTACAGCAATTAAGCTCTAAGCCTAAGCCATCCGCAAAAAATGACCTCTTATCAAAGGAGCAATT
AAAGTACTCTCTAATCCTGACCTGTTGGAGTTTGTCTCCGGTCTGGTTTCGCTTTGAAGCTCGAATTTAAA
CGCGATATTTGAAGTCTTTCCGGCTTCTCTTAATCTTTTTGATGCAATCCGCTTTGCTTCTGACTATAAT
AGTCAGGTTAAAGACCTGATTTTTGATTTATGGTCATTCTCGTTTTCTGAACTGTTTAAAGCATTGAGGG
GGATTC AATGAATATTTATGACGATTCGCGAGTATTGGACGCTATCCAGTCTAAACATTTTACTATTAACC
CCTCTGGCAAACTTCTTTTGCAAAAGCCTCTCGCTATTTTGGTTTTTATCGTCTGCTGGTAAACGAGGGT
TATGATAGTGTGCTCTTACTATGCCCTGTAATTCCTTTTGGCGTTATGTATCTGCATTAGTTGAATGTGG
TATTC TAAATCTCAACTGATGAATCTTTCTACCTGTAATAATGTTGTTCCGTTAGTTCCGTTTTATTAACG
TAGATTTTCTTCCCAACGTCCTGACTGGTATAATGAGCCAGTTC TAAAAATCGCATAAGGTAATTCACAA
TGATTAAGTTGAAATTA AACCATCTCAAGCCCAATTTACTACTCGTTCGGTGTCTCTCGTCAGGGCAAG
CCTTAT TCACTGAATGAGCAGCTTTGTTACGTTGATTTGGGTAATGAATATCCGGTCTTGTCAAGATTAC
TCTTGATGAAGGTGAGCCAGCCTATGCGCCTGGTCTGTACACCGTTCATCTGTCCTCTTTCAAAGTTGGTC
AGTTCGGTTCCTTATGATTGACCGTCTGCGCCTCGTTCGGGCTAAGTAAACATGGAGCAGGTCGCGGATTT
CGACACAATTTATCAGGCGATGATACAAATCTCCGTTGTACTTTGTTTCGCGCTTGGTATAATCGCTGGGG
GTCAAAGATGAGTGTTTTAGTGTATCTTTTGCCTCTTTTCGTTTTAGGTTGGTGCCTTCGTAGTGGCATT
CGTATTTTACCCGTTTAAATGAAACTTCTCATGAAAAAGTCTTTAGTCTCAAAGCCTCTGTAGCCGTTG
CTACCCCTCGTTCGGATGCTGTCTTTCGCTGCTGAGGGTACGATCCCGCAAAAGCGGCCCTTTAACTCCCTG
CAAGCCTCAGCACC GAATATATCGGTTATGCGTGGCGGATGGTTGTTGTCATTGTCGGCGCAACTATCGG
TATCAAGCTGTTTAAAGAAATTCACCTCGAAAGCAAGCTGATAAACCGATACAATTAAGGCTCCTTTTGG
GCCTTTT TTTTGGAGATTTTCAACGTGAAAAAATTATTATTCGCAATTCCTTTAGTTGTTCTTCTATTC
TCACTCCGCTGAAACTGTTGAAAGTTGTTTAGCAAAATCCCATACAGAAAATTCATTTACTAACGCTCTGGA
AAGACGCAAAACTTTAGATCGTTACGCTAACTATGAGGGCTGTCTGTGGAATGCTACAGGCGTTGATGTT
TGTACTGGTGACGAAACTCAGTGTACGGTACATGGGTTCC TATTGGGCTTGCTATCCCTGAAAAATGAGGG

TGGTGGCTCTGAGGGTGGCGGTCTGAGGGTGGCGGTACTAAACCTCCTGAGTACG
GTGATACACCTATTCGGGGCTATACCTTATATCAACCCTCTCGACGGCACTTATCCGCCTGGTACTGAGCAA
AACCCCGTAATCCTAATCCTTCTCTGAGGAGTCTCAGCCTCTTAATACTTTCATGTTTCAGAATAATAG
GTTCCGAAATAGGCAGGGGGCATTAACTGTTTATACGGGCACTGTTACTCAAGGCACTGACCCCGTAAAA
CTTATTACCAGTACACTCCTGTATCATCAAAAGCCATGTATGACGCTTACTGGAACGGTAAATTCAGAGAC
TGCCTTTCCATTCTGGCTTTAATGAGGATTTATTTGTTTGTGAATATCAAGGCCAATCGTCTGACCTGCC
TCAACCTCCTGTCAATGCTGGCGGGCTCTGGTGGTGGTTCGGTGGCGGCTCTGAGGGTGGTGGCTCTG
AGGGTGGCGGTCTGAGGGTGGCGGCTCTGAGGGAGGCGGTTCGGTGGTGGCTCTGGTTCGGGTGATTTT
GATTATGAAAAGATGGCAAACGCTAATAAGGGGGCTATGACCGAAAAATGCCGATGAAAACGGCTACAGTC
TGACGCTAAAGGCAAACCTTGATTCTGTCGCTACTGATTACGGTGTGCTATCGATGGTTTCATTGGTGCAG
TTTCCGGCCTTGCTAATGGTAATGGTCTACTGGTGAATTTGCTGGCTCTAATTCCAAATGGCTCAAGTC
GGTGACGGTGATAATCACCTTAAATGAATAATTTCCGTCAATATTTACCTTCCCTCCCTCAATCGGTTGA
ATGTCGCCCTTTTGTCTTTGGCGCTGGTAAACCATATGAATTTTCTATTGATTGTGACAAAATAAACTTAT
TCCGTGGTGTCTTTGCGTTTCTTTTATATGTTGCCACCTTTATGTATGTATTTTCTACGTTTGTAAACATA
CTGCGTAAATAAGGAGTCTTAAATCATGCCAGTTCCTTTGGGTATTCCGTTATTATTGCGTTTCTCGGTTT
CTTCTGGTAACTTTGTTCCGGCTATCTGCTTACTTTTCTAAAAAGGGCTTCGGTAAAGATAGCTATTGCTAT
TTCATTGTTTCTTGCTCTTATTATTGGGCTTAACTCAATTTCTTGTGGGTATCTCTCTGATTTAGCGCTC
AATTAGCCTCTGACTTTGTTTCCAGGTGTTTTCAGTTAATTTCCCGTCTAATGCGCTTCCCTTCCCTTATGTT
ATTCTCTCTGTAAAGGCTGCTATTTTCAATTTTGGCGTAAACAAAAAATCGTTTCTTATTTGGATTGGGA
TAAATAATATGGCTGTTTATTTTGTAACTGGCAAATTAGGCTCTGGAAAGACGCTCGTTAGCGTTGGTAAG
ATTCAGGATAAAATTTGTAGCTGGGTGCAAATAGCAACTAATCTTGATTAAAGGCTTCAAACCTCCCGCA
AGTCCGGAGGTTTCGCTAAAACGCCCTCGCTTCTTAGAATACCGGATAAGCCTTCTATATCTGATTTGCTTG
CTATTGGGCGCGGTAATGATTCCTACGATGAAAATAAAAACGGCTTGCTTGTCTCGATGAGTGGCGTACT
TGGTTTAAATACCCGTTCTTGGAAATGATAAGGAAAGACAGCCGATTATGATTGGTTTCTACATGCTCGTAA
ATTAGGATGGGATATTATTTTCTTGTTCAGGACTTATCTATTGTTGATAAACAGGCGGCTTCTGCATTAG
CTGAACATGTTGTTTATTGTCTGCTGCTGGACAGAATTACTTTTACCTTTTGTGGTACTTTTATATTTCTCTT
ATTACTGGCTCGAAAATGCCTCTGCCATAATTACATGTTGGCGTTGTTAAATATGGCGATTCTCAATTAAG
CCCTACTGTTGAGCGTTGGCTTTTACTGGTAAGAATTTGTATAACGCATATGATACTAAACAGGCTTTTT
CTAGTAAATATGATTCCGGTGTATTTCTTATTTAACGCCCTTATTTATCACACGGTCCGTTATTTCAAACCA
TTAAATTTAGGTCAGAAGATGAAATTAATAAAATATATTTGAAAAAGTTTTCTCGCGTCTTTTGTCTTGC
GATTGGATTTGCATCAGCAATTTACATATAGTTATATAACCCAACTAAGCCGGAGGTTAAAAAGGTAGTCT
CTCAGCCTATGATTTGATAAATCATTACTTACTTCTCAGCGCTTAAATCTAAGCTTAAATCTGATGTT
TTCAAGGATTCTAAGGGAAAATTAATTAATAGCGACGATTTACAGAAAGCAAGGTTATTACTCACATATAT
TGATTTATGTAAGTTTCCATTAATAAAGGTAATCAAATGAAATGTTAAATGTAATTAATTTGTTTTCT
TTGATGTTTGTTCATCATCTTCTTTTGTCTCAGGTAATTGAAATGAATAATTCGCCTCTGCGCGATTTTGT
AACTTGGTATTCAAAGCAATCAGGCGAATCCGTTATTGTTTTCTCCGATGTAAGGTTACTGTTACTGTAT
ATTCATCTGACGTTAAACCTGAAAATCTACGCAATTTCTTTATTTCTGTTTTACGTGCAATAATTTTGTAT
ATGGTAGGTTCTAACCTTCCATTTATTCAGAAGTATAATCCAAACAATCAGGATTATATTGATGAATTTGCC
ATCATCTGATAATCAGGAATATGATGATAATTCGGCTCCTTCTGGTGGTTTCTTTGTTCCGCAAAATGATA
ATGTTACTCAAACCTTTTAAATTAATAACGTTTCGGGCAAAGGATTTAATACGAGTTGTCGAATTTGTTGTA
AAGTCTAATACTTCTAAATCCTCAAATGTATTATCTATTGACGGCTCTAATCTATTAGTTGTTAGTGCTCC
TAAAGATATTTAGATAACCTTCCCTCAATTCCTTTCAACTGTTGATTGCAACTGACCAGATAATTGATTG
AGGGTTTGTATTTGAGGTTTCAGCAAGGTGATGCTTTAGATTTTTCTATTGCTGCTGGCTCTCAGCGTGGC
ACTGTTGACGGCGGTGTTAATACTGACCGCCTCACCTCTGTTTTATCTTCTGCTGGTGGTTCGTTCCGTTAT
TTTTAATGGCGATGTTTTAGGGCTATCAGTTTCGGCATTAAAGACTAATAGCCATTCAAAAATATTGCTCTG
TGCCACGTATCTTACGCTTTCAGGTCAGAAGGTTCTATCTCTGTTGGCCAGAATGTCCCTTTTATTAAT
GGTCGTGACTGGTGAATCTGCCAATGTAATAATCCATTTTCAGACGATTGAGCGTCAAATGTTAGGTAT
TTCCATGAGCGTTTTTCTGTTGCAATGGCTGGCGGTAATATTGTTCTGGATATTACCAGCAAGGCCGATA
GTTTGAGTTCTTACTACTCAGGCAAGTGATGTTATTAATAATCAAAGAAGTATTGCTACAACGGTTAATTTG
CGTGATGGACAGACTCTTTTACTCGGTGGCCTCACTGATTATAAAAAACCTTCTCAGGATTTCTGGCGTACC
GTTCCGTCTAAAATCCCTTAAATCGGCCTCCTGTTTAGCTCCCGCTCTGATTCTAACGAGGAAAGCACGT
TATACGTGCTCGTCAAAGCAACCATAGTACGCGCCCTGTAGCGGCGCATTAAGCGCGGGGGTGTGGTGGT
TACGCGCAGCGTACCCGCTACACTTGCCAGCGCCCTAGCGCCCGCTCCTTTGCTTTTCTCCCTTCCCTTCT
TCGCCAGCTTCTGCGGCTTTCCCGTCAAGCTCAAACTGGGGGCTCCCTTTAGGGTTCCGATTTAGTGTCT
TTACCGGCACTCGACCCAAAAAATTTGATTTGGGTGATGGTTCACGTAGTGGCCATCGCCCTGATAGAC
GGTTTTTCTGCCCTTTGACGTTGGAGTCCACGTTCTTTAATAGTGGACTCTTGTTCAAACTGGAACAACAC
TCAACCTTATCTCGGGCTATTTCTTTGATTTATAAGGGATTTTGGCGATTTCCGAACCACCATCAAACAGG
ATTTTCCGCTGCTGGGGCAAACAGCGTGGACCGCTTGTGCAACTCTCTCAGGGCCAGGCGGTGAAGGGC

AATCAGCTGTTGCCCGTCTCACTGGTGAAAAGAAAAACCACCCCTGGCGCCAATACGCAAACCGCCTCTCC
CCGCGCGTTGGCCGATTCATTAATGCAGCTGGCACGACAGGTTTCCCGACTGGAAAGCGGGCAGTGAGCGC
AACGCAATTAATGTGAGTTAGCTCACTCATTAGGCACCCCAGGCTTTACACTTTATGCTTCCGGCTCGTAT
GTTGTGTGGAATTGTGAGCGGATAACAATTTCACACAGGAAACAGCTATGACCATGATTACGAATTCGAGC
TCGGTACCCGG

Sequence of 7283_SSV scaffold:

insert sequences:

SSV_insert:

5' -GATCCTTCGGACCGAAAGCGCGACCATCGCCGGAGATTGGAGTAAAGTTTAAATACTGACTAAA-3'

SSV_insert_complement

5' -AGCTTTTAGTCAGTATTTAAACTTTACTCCAATCTCCGGCGATGGTCGCGCTTTCGGTCCGAAG-3'

full sequence:

BamHI site: red
SSV T6 promotor: green
HindIII site: blue

GGATCCTTTCGGACCGAAAGCGCGACCATCGCCGGAGATTGGAGTAAAGTTTAAATACTGACTAAAAGCTTG
GCACCTGGCCGTCGTTTTACAACGTCGTGACTGGGAAAACCCCTGGCGTTACCCAACCTTAATCGCCTTGCAGC
ACATCCCCTTTTCGCCAGCTGGCGTAATAGCGAAGAGGCCCGCACCGATCGCCCTTCCCAACAGTTGCGCA
GCCTGAATGGCGAATGGCGCTTTGCCCTGGTTTCCGGCACCAGAAGCGGTGCCGAAAGCTGGCTGGAGTGC
GATCTTCTGAGGCCGATACGTGTCGTCGTCCTCAAACGGCAGATGCACGGTTACGATGCGCCCATCTA
CACCAACGTGACCTATCCATTACGGTCAATCCGCCGTTTGTTCACGGAGAATCCGACGGGTTGTTACT
CGCTCACATTTAATGTTGATGAAAGCTGGCTACAGGAAGGCCAGACGCGAATTATTTTTGATGGCGTTCTT
ATTGGTTAAAAAATGAGCTGATTTAACAAAAATTTAATGCGAATTTTAAACAAAATATTAACGTTTACAATT
TAAATATTTGCTTATAACAATCTTCCGTGTTTTGGGGCTTTTCTGATTATCAACCGGGGTACATATGATTGA
CATGCTAGTTTTACGATTACCGTTCATCGATTCTCTTGGTTGCTCCAGACTCTCAGGCAATGACCTGATAG
CCTTTGTAGATCTCTCAAAAATAGCTACCCTCTCCGGCATTAAATTTATCAGCTAGAACGGTTGAATATCAT
ATTGATGGTGATTTGACTGTCTCCGGCTTTCTCACCTTTTGAATCTTTACCTACACATTACTCAGGCAT
TGCATTTAAAATATATGAGGGTCTAAAAATTTTTATCCTTGGCTGAAATAAAGGCTTCTCCCGCAAAG
TATTACAGGGTCATAATGTTTTTGGTACAACCGATTTAGCTTTATGCTCTGAGGCTTTATTGCTTAATTTT
GCTAATTTCTTTCCTTGCCCTGTATGATTTATTGGATGTTAATGCTACTACTATTAGTAGAATTGATGCCAC
CTTTTCAGCTCGCGCCCCAAATGAAAATATAGCTAAACAGGTTATTGACCATTTGCGAAATGATATCAATG
CTCAAACCTAAATCTACTCGTTCGCAGAAATGGGAATCAACTGTTATATGGAATGAAATCCGACACCGT
ACTTTAGTTGCATATTTAAACATGTTGAGCTACAGCATTATATTCAGCAATTAAGCTCTAAGCCATCCGC
AAAAATGACCTCTTATCAAAAGGAGCAATTAAGGTAAGTCTCTAATCCTGACCTGTTGGAGTTTGCCTCCG
GTCGGTTTCGCTTTGAAGCTCGAATTAACCGGATATTTGAAGTCTTTCGGGCTTCTCTAATCTTTTTT
GATGCAATCCGCTTTGCTTCTGACTATAATAGTCAGGGTAAAGACCTGATTTTTGATTTATGGTCAATCTC
GTTTTCTGAACTGTTTTAAAGCATTGAGGGGGATTCAATGAATATTTATGACGATTCCGCAGTATTGGACG
CTATCCAGTCTAAACATTTTACTATTACCCCTCTGGCAAACCTTCTTTTGCAAAGCCTCTCGCTATTTT
GGTTTTTATCGTCGTCGGTAAACGAGGGTTATGATAGTGTGCTCTTACTATGCCTCGTAATCTCCTTTT
GCGTTATGTATCTGCATTAGTTGAATGTGGTATTCTAAATCTCAACTGATGAATCTTTCTACCTGTAATA
ATGTTGTTCGTTAGTTCGTTTTATTAACGTAGATTTTTCTTCCCAACGTCCTGACTGGTATAATGAGCCA
GTTCTTAAAATCGCATAAGGTAATTCACAATGATTAAGTTGAAATTAACCATCTCAAGCCCAATTTACT
ACTCGTTCTGGTGTTCCTCGTCAGGGCAAGCCTTATTCAGTGAATGAGCAGCTTTGTTACGTTGATTTGGG
TAATGAATATCCGTTCTTGTCAAGATTAATCTTGTGATGAAGGTCAGCCAGCCTATGCGCCTGGTCTGTACA
CCGTTCACTGTCTCTTTCAAAGTTGGTCAGTTCGGTTCCCTTATGATTGACCGTCTGCGCCTCGTTCCG
GCTAAGTAACATGGAGCAGGTCGCGGATTTTCGACACAATTTATCAGGCGATGATACAAATCTCCGTTGTAC
TTTTGTTTCGCGCTTGGTATAATCGCTGGGGTCAAAGATGAGTGTTTTAGTGATTTCTTTTGCCTCTTTTCG
TTTTAGTTGGTGCCTTCGTAGTGGCATTACGTATTTTTACCCGTTTAAATGGAAACTTCTCATGAAAAAGT
CTTTAGTCTCAAAGCCTCTGTAGCCGTTGCTACCCTCGTTCCGATGCTGTCTTTCGCTGCTGAGGGTGAC
GATCCCGCAAAGCGGCCTTTAACTCCCTGCAAGCCTCAGCGACCGAATATATCGGTTATGCGTGGGCGAT
GGTTGTTGTCATTGTGCGGCAACTATCGGTATCAAGCTGTTTAAAGAAATTCACCTCGAAAGCAAGCTGAT
AAACCGATACAATTAAGGCTCCTTTTGGAGCCTTTTTTTTTGGAGATTTTCAACGTGAAAAAATTTATTATT
CGCAATCTCTTTAGTTGTTCTTTCTATTTCTACTCCGCTGAAACTGTTGAAAGTTGTTTAGCAAAATCCC
ATACAGAAAATTCATTTACTAACGTCTGAAAGACGACAAAACTTTAGATCGTTACGCTAACCTATGAGGGC

TGTCGTGGAATGCTACAGGCGTTGTAGTTTGTACTGGTGACGAACTCAGTGTTACGGTACATGGGTTCC
TATTGGGCTTGCTATCCCTGAAAATGAGGGTGGTGGCTCTGAGGGTGGCGGTTCTGAGGGTGGCGGTTCTG
AGGGTGGCGGTACTAAACCTCCTGAGTACGGTGTACACCTATTCCGGGTATACTTATATCAACCTCTC
GACGGCACTTATCCGCTGGTACTGAGCAAAACCCGCTAATCCTAATCCTTCTCTTGAGGAGTCTCAGCC
TCTTAATACTTTCATGTTTCAGAATAATAGGTTCCGAAATAGGCAGGGGGCATTAACTGTTTATACGGGCA
CTGTTACTCAAGGCACTGACCCCGTTAAAACCTTATTACCAGTACACTCCTGTATCATCAAAAGCCATGTAT
GACGCTTACTGGAACGGTAAATTCAGAGACTGCGCTTTCATTCTGGCTTTAATGAGGATTTATTTGTTTG
TGAATATCAAGGCCAATCGTCTGACCTGCCTCAACCTCCTGTCAATGCTGGCGGGGCTCTGGTGGTGGTT
CTGGTGGCGGCTCTGAGGGTGGTGGCTCTGAGGGTGGCGGTTCTGAGGGTGGCGGCTCTGAGGGAGGCGGT
TCCGGTGGTGGCTCTGGTTCCGGTGATTTTGATTATGAAAAGATGGCAAACGCTAATAAGGGGGCTATGAC
CGAAAATGCCGATGAAAACGCGCTACAGTCTGACGCTAAAGGCAAACCTTGATTCTGTGCTACTGATTACG
GTGCTGCTATCGATGGTTTCATTGGTGACGTTTCCGGCCTTGCTAATGGTAATGGTGCTACTGGTGATTTT
GCTGGCTCAATTTCCCAAATGGCTCAAGTCGGTGACGGTGATAATTCACCTTAAATGAATAATTTCCGTCA
ATATTTACTTCCCTCCCTCAATCGTGAATGTGCGCCTTTTGTCTTTGGCGCTGGTAAACCATATGAAT
TTTCTATTTGATTGTGACAAAATAAACTTATTCCGTGGTGTCTTTGCGTTTCTTTTATATGTTGCCACCTTT
ATGTATGTATTTTCTACGTTTGTCAACATACTGCGTAATAAGGAGTCTTAATCATGCCAGTCTTTTGGGT
AAACGGCTTCGGTAAGATAGCTATTGCTAATTTGTTTCTTGGCTCTTATTATTGGGTTAACTCAATTC
TTGTGGGTTATCTCTGATATTAGCGCTCAATTACCCTCTGACTTTGTTTACGGGTGTTTCAATTCTC
CCGTCAATGCGCTTCCCTGTTTTATGTTATTCTCTCTGTAAAGGCTGCTATTTTCATTTTGACGTAA
ACAAAAATCGTTTCTTATTTGGATTGGGATAAATAATATGGCTGTTTATTTTGTAACTGGCAAATAGGC
TCTGGAAAGACGCTCGTTAGCGTTGGTAAGATTACAGGATAAAATTTAGCTGGGTGCAAAATAGCAACTAA
TCTTGATTTAAGGCTTCAAACCTCCCGCAAGTCGGGAGGTTGCTAAAACGCTCGCGTTCTTAGAATAC
CGGATAAGCCTTCTATATCTGATTTGCTTGTCTATTGGGCGCGGTAATGATTCCTACGATGAAAATAAAAC
GGCTTGGCTTGTCTCGATGAGTGCGGTACTTGGTTTAAATACCCGTTCTTGGAAATGATAAGGAAAGACAGC
GATTAATTGATTGGTTTTCTACATGCTCGTAAATAGGATGGGATATTATTTTTCTTGTTCAGGACTTATCTA
TTGTTGATAAACAGGCGGTTCTGCATTAGCTGAACATGTTGTTTATTTGTCGTCGCTGGACAGAATTACT
TTACCTTTTGTGCGTACTTTATATCTCTTATTACTGGCTCGAAAATGCCTCTGCCTAAATTACATGTTGG
CGTTGTTAAATATGGCGATTCTCAATTAAGCCCTACTGTTGAGCGTTGGCTTTATACTGGTAAGAAATTTGT
ATAACGCATATGATACTAAACAGGCTTTTTCTAGTAATTATGATTCCGGTGTTTATTTCTTATTTAACGCT
TATTTATCACACGGTTCGGTATTTCAAACCATAAATTTAGGTCAGAAGATGAAATTAACATAAAATATATTT
GAAAAGTTTCTCGCTTCTTGGTCTTGGCATTTGATTTGCATCAGCATTTACATATAGTTATATAATCCC
AACCTAAGCCGGAGGTTAAAAGGTACTCTCTCAGACCTATGATTTTGGATAAAATCACTATTGACTTCTCT
CAGCGTCTTAATCTAAGCTATCGCTATGTTTTCAAGGATTCTAAGGGAAAATTAATTAATAGCGACGATTT
ACAGAAGCAAGGTTATTTCACTCACATATATTGATTTATGTACTGTTTCCATTAATAAGGTAATTCAAATG
AAATTGTTAAATGTAATTAATTTTGTCTTGTGATGTTTGTTCATCATCTTCTTTTGTCTCAGGTAATTTGA
AATGAATAATTCGCTCTGCGGATTTTGTAACTTGGTATTCAAAGCAATCAGGCGAATCCGTTATTTGTTT
CTCCCGATGTAAGGTTACTGTTACTGTATATTATCTGACGTTAAACCTGAAAATCTACGCAATTTCTTT
ATTTCTGTTTACGTGCAAATAATTTGATATGGTAGGTTCTAACCTTCCATTATTACAGAGTATAATCC
AACAATCAGGATTATATTGATGAATTTGCCATCATCTGATAATCAGGAATATGATGATAATTCGGCTCCTT
CTGGTGGTTTTCTTGTTCGCAAAAATGATAATGTTACTCAAACTTTTAAAATTAATAACGTTCCGGGCAAAAG
GATTTAATACGAGTTGTGCAATTTGTTGTAAGTCTAATACTTCTAAATCCTCAAATGTATTATCTATTGA
CGGCTCAATCTATTAGTTGTTAGTGCTCCTAAAGATATTTTAGATAACCTTCCCTCAATTCCTTTCAACTG
TTGATTTGCCAACTGACCAGATATTGATTGAGGGTTTGATTTTGGAGGTTTACGCAAGGTGATGCTTTAGAT
TTTTCATTTGCTGCTGGCTCTCAGCGTGGCACTGTTGCAGGCGGTGTTAATACTGACCGCTCACCTCTGT
TTTATCTTCTGCTGGTGGTTGTTCCGGTATTTTAAATGGCGATGTTTTAGGGCTATCAGTTCGCGCATTA
AGACTAATAGCCATTCAAAAATATTGCTGTGCCACGATTTCTTACGCTTTTACGTTTACAGGTCAGAAGGGTCTATC
TCTGTTGGCCAGAATGTCCCTTTTATTACTGGTCTGTGACTGGTGAATCTGCCAATGTAATAATCCATT
TCAGACGATTGAGCGTCAAAATGTAGGATTTCCATGAGCGTTTTTCTGTTGCAATGGCTGGCGGTAATA
TTGTTCTGGATATTACCAGCAAGGCCGATAGTTTGGATTCTTCTACTCAGGCAAGTGATGTTATTACTAAT
CAAAGAAGTATTGCTACAACGGTTAATTTGCGTGTGACAGACTCTTTTACTCGGTGGCTCACCTGATTA
TAAAACACTTCTCAGGATTCTGGCGTACCGTTTCTGTCTAAAATCCCTTAAATCGGCTCCTGTTTAGCT
CCCGCTCTGATTCTCAACGAGGAAAGCACGTTATACGTGCTCGTCAAAGCAACCATAGTACGCGCCCTGTAG
CGCGCATTAAGCTCAGCGGGGTGTGGTGTACGCGACGCTGACCGCTACACTTGCAGCGCCCTAGCGC
CCGCTCCTTTGCTGCTTTCTTCCCTTCTTCTCGCCACGTTCCGCGGCTTTCCCGTCAAGCTCAAATCGG
GGGCTCCCTTTAGGGTTCCGATTTAGTGCTTTACGGCACCTCGACCCCAAAAAACTTGATTTGGGTGATGG
TTCACGTAGTGGGCCATCGCCCTGATAGACGGTTTTTTCGCCCTTTGACGTTGGAGTCCACGTTCTTAAATA
GTGGACTCTTGTTCCAAACCTGGAACAACACTCAACCTATCTCGGGTATTCTTTTATTATAAGGATT

TTGCCGATTCGGAACCACCATCAAACAGGATTTTCGCCTGCTGGGGCAAACCAGCGTGGACCGCTTGCTG
CAACTCTCTCAGGGCCAGGCGGTGAAGGGCAATCAGCTGTTGCCCGTCTCACTGGTGAAAAGAAAAACCAC
CCTGGCGCCAATACGCAAACCGCCTCTCCCCGCGCGTTGGCCGATTCATTAATGCAGCTGGCACGACAGG
TTTCCCGACTGGAAAAGCGGGCAGTGAGCGCAACGCAATTAATGTGAGTTAGCTCACTCATTAGGCACCCA
GGCTTTACACTTTATGCTTCCGGCTCGTATGTTGTGTGGAATTGTGAGCGGATAACAATTCACACAGGAA
ACAGCTATGACCATGATTACGAATTCGAGCTCGGTACCCGG

References and Notes

1. M. S. Kellermayer, S. B. Smith, H. L. Granzier, C. Bustamante, Folding-unfolding transitions in single titin molecules characterized with laser tweezers. *Science* **276**, 1112–1116 (1997). [Medline doi:10.1126/science.276.5315.1112](#)
2. M. Rief, M. Gautel, F. Oesterhelt, J. M. Fernandez, H. E. Gaub, Reversible unfolding of individual titin immunoglobulin domains by AFM. *Science* **276**, 1109–1112 (1997). [Medline doi:10.1126/science.276.5315.1109](#)
3. S. B. Smith, Y. Cui, C. Bustamante, Overstretching B-DNA: The elastic response of individual double-stranded and single-stranded DNA molecules. *Science* **271**, 795–799 (1996). [Medline doi:10.1126/science.271.5250.795](#)
4. J. M. Fernandez, H. Li, Force-clamp spectroscopy monitors the folding trajectory of a single protein. *Science* **303**, 1674–1678 (2004). [Medline doi:10.1126/science.1092497](#)
5. N. Ribbeck, O. A. Saleh, Multiplexed single-molecule measurements with magnetic tweezers. *Rev. Sci. Instrum.* **79**, 094301 (2008). [Medline doi:10.1063/1.2981687](#)
6. K. Halvorsen, W. P. Wong, Massively parallel single-molecule manipulation using centrifugal force. *Biophys. J.* **98**, L53–L55 (2010). [Medline doi:10.1016/j.bpj.2010.03.012](#)
7. K. C. Neuman, A. Nagy, Single-molecule force spectroscopy: Optical tweezers, magnetic tweezers and atomic force microscopy. *Nat. Methods* **5**, 491–505 (2008). [Medline doi:10.1038/nmeth.1218](#)
8. E. Pfitzner, C. Wachauf, F. Kilchherr, B. Pelz, W. M. Shih, M. Rief, H. Dietz, Rigid DNA beams for high-resolution single-molecule mechanics. *Angew. Chem. Int. Ed. Engl.* **52**, 7766–7771 (2013). [Medline doi:10.1002/anie.201302727](#)
9. H. Shroff, B. M. Reinhard, M. Siu, H. Agarwal, A. Spakowitz, J. Liphardt, Biocompatible force sensor with optical readout and dimensions of 6 nm³. *Nano Lett.* **5**, 1509–1514 (2005). [Medline doi:10.1021/nl050875h](#)
10. W. Shen, M. F. Bruist, S. D. Goodman, N. C. Seeman, A protein-driven DNA device that measures the excess binding energy of proteins that distort DNA. *Angew. Chem. Int. Ed. Engl.* **43**, 4750–4752 (2004). [Medline doi:10.1002/anie.200460302](#)
11. H. Gu, W. Yang, N. C. Seeman, DNA scissors device used to measure MutS binding to DNA mis-pairs. *J. Am. Chem. Soc.* **132**, 4352–4357 (2010). [Medline doi:10.1021/ja910188p](#)
12. C. Grashoff, B. D. Hoffman, M. D. Brenner, R. Zhou, M. Parsons, M. T. Yang, M. A. McLean, S. G. Sligar, C. S. Chen, T. Ha, M. A. Schwartz, Measuring mechanical tension across vinculin reveals regulation of focal adhesion dynamics. *Nature* **466**, 263–266 (2010). [Medline doi:10.1038/nature09198](#)
13. N. C. Seeman, DNA in a material world. *Nature* **421**, 427–431 (2003). [Medline doi:10.1038/nature01406](#)
14. P. W. K. Rothmund, Folding DNA to create nanoscale shapes and patterns. *Nature* **440**, 297–302 (2006). [Medline doi:10.1038/nature04586](#)

15. S. M. Douglas, A. H. Marblestone, S. Teerapittayanon, A. Vazquez, G. M. Church, W. M. Shih, Rapid prototyping of 3D DNA-origami shapes with caDNAo. *Nucleic Acids Res.* **37**, 5001–5006 (2009). [Medline doi:10.1093/nar/gkp436](#)
16. Y. Ke, S. M. Douglas, M. Liu, J. Sharma, A. Cheng, A. Leung, Y. Liu, W. M. Shih, H. Yan, Multilayer DNA origami packed on a square lattice. *J. Am. Chem. Soc.* **131**, 15903–15908 (2009). [Medline doi:10.1021/ja906381y](#)
17. E. S. Andersen, M. Dong, M. M. Nielsen, K. Jahn, R. Subramani, W. Mamdouh, M. M. Golas, B. Sander, H. Stark, C. L. Oliveira, J. S. Pedersen, V. Birkedal, F. Besenbacher, K. V. Gothelf, J. Kjems, Self-assembly of a nanoscale DNA box with a controllable lid. *Nature* **459**, 73–76 (2009). [Medline doi:10.1038/nature07971](#)
18. S. M. Douglas, H. Dietz, T. Liedl, B. Högberg, F. Graf, W. M. Shih, Self-assembly of DNA into nanoscale three-dimensional shapes. *Nature* **459**, 414–418 (2009). [Medline doi:10.1038/nature08016](#)
19. T. Liedl, B. Högberg, J. Tytell, D. E. Ingber, W. M. Shih, Self-assembly of three-dimensional prestressed tensegrity structures from DNA. *Nat. Nanotechnol.* **5**, 520–524 (2010). [Medline doi:10.1038/nnano.2010.107](#)
20. Materials and methods are available as supplementary materials on *Science Online*.
21. M. C. Murphy, I. Rasnik, W. Cheng, T. M. Lohman, T. Ha, Probing single-stranded DNA conformational flexibility using fluorescence spectroscopy. *Biophys. J.* **86**, 2530–2537 (2004). [Medline doi:10.1016/S0006-3495\(04\)74308-8](#)
22. S. Hohng, R. Zhou, M. K. Nahas, J. Yu, K. Schulten, D. M. Lilley, T. Ha, Fluorescence-force spectroscopy maps two-dimensional reaction landscape of the Holliday junction. *Science* **318**, 279–283 (2007). [Medline doi:10.1126/science.1146113](#)
23. J. Ross, P. Buschkamp, D. Fetting, A. Donnermeyer, C. M. Roth, P. Tinnefeld, Multicolor single-molecule spectroscopy with alternating laser excitation for the investigation of interactions and dynamics. *J. Phys. Chem. B* **111**, 321–326 (2007). [Medline doi:10.1021/jp066082g](#)
24. S. A. McKinney, C. Joo, T. Ha, Analysis of single-molecule FRET trajectories using hidden Markov modeling. *Biophys. J.* **91**, 1941–1951 (2006). [Medline doi:10.1529/biophysj.106.082487](#)
25. F. E. Kemmerich, M. Swoboda, D. J. Kauert, M. S. Grieb, S. Hahn, F. W. Schwarz, R. Seidel, M. Schlierf, Simultaneous single-molecule force and fluorescence sampling of DNA nanostructure conformations using magnetic tweezers. *Nano Lett.* **16**, 381–386 (2016). [Medline doi:10.1021/acs.nanolett.5b03956](#)
26. C. Hyeon, J. Lee, J. Yoon, S. Hohng, D. Thirumalai, Hidden complexity in the isomerization dynamics of Holliday junctions. *Nat. Chem.* **4**, 907–914 (2012). [Medline doi:10.1038/nchem.1463](#)
27. A. Gietl, P. Holzmeister, F. Blombach, S. Schulz, L. V. von Voithenberg, D. C. Lamb, F. Werner, P. Tinnefeld, D. Grohmann, Eukaryotic and archaeal TBP and TFB/TF(II)B follow different promoter DNA bending pathways. *Nucleic Acids Res.* **42**, 6219–6231 (2014). [Medline doi:10.1093/nar/gku273](#)

28. A. N. Kapanidis, T. A. Laurence, N. K. Lee, E. Margeat, X. Kong, S. Weiss, Alternating-laser excitation of single molecules. *Acc. Chem. Res.* **38**, 523–533 (2005). [Medline doi:10.1021/ar0401348](#)
29. N. Adachi, M. Senda, R. Natsume, T. Senda, M. Horikoshi, Crystal structure of *Methanococcus jannaschii* TATA box-binding protein. *Genes Cells* **13**, 1127–1140 (2008). [Medline](#)
30. J. Sambrook, D. W. Russell, *Molecular Cloning: A Laboratory Manual* (Cold Spring Harbor Laboratory Press, ed. 3, 2001).
31. S. M. Douglas, J. J. Chou, W. M. Shih, DNA-nanotube-induced alignment of membrane proteins for NMR structure determination. *Proc. Natl. Acad. Sci. U.S.A.* **104**, 6644–6648 (2007). [Medline doi:10.1073/pnas.0700930104](#)
32. E. Stahl, T. G. Martin, F. Praetorius, H. Dietz, Facile and scalable preparation of pure and dense DNA origami solutions. *Angew. Chem. Int. Ed. Engl.* **53**, 12735–12740 (2014). [Medline doi:10.1002/anie.201405991](#)
33. J. M. de la Rosa-Trevín, J. Otón, R. Marabini, A. Zaldívar, J. Vargas, J. M. Carazo, C. O. Sorzano, Xmipp 3.0: An improved software suite for image processing in electron microscopy. *J. Struct. Biol.* **184**, 321–328 (2013). [Medline doi:10.1016/j.jsb.2013.09.015](#)
34. T. Ha, P. Tinnefeld, Photophysics of fluorescent probes for single-molecule biophysics and super-resolution imaging. *Annu. Rev. Phys. Chem.* **63**, 595–617 (2012). [Medline doi:10.1146/annurev-physchem-032210-103340](#)
35. E. Nir, X. Michalet, K. M. Hamadani, T. A. Laurence, D. Neuhauser, Y. Kovchegov, S. Weiss, Shot-noise limited single-molecule FRET histograms: Comparison between theory and experiments. *J. Phys. Chem. B* **110**, 22103–22124 (2006). [Medline doi:10.1021/jp063483n](#)
36. T. E. Tomov, R. Tsukanov, R. Masoud, M. Liber, N. Plavner, E. Nir, Disentangling subpopulations in single-molecule FRET and ALEX experiments with photon distribution analysis. *Biophys. J.* **102**, 1163–1173 (2012). [Medline doi:10.1016/j.bpj.2011.11.4025](#)
37. G. R. Strobl, *The Physics of Polymers* (Springer, ed. 3, 2007)
38. D. B. McIntosh, O. A. Saleh, Salt species-dependent electrostatic effects on ssDNA elasticity. *Macromolecules* **44**, 2328–2333 (2011). [doi:10.1021/ma1028196](#)
39. B. H. Zimm, Dynamics of polymer molecules in dilute solution: Viscoelasticity, flow birefringence and dielectric loss. *J. Chem. Phys.* **24**, 269 (1956). [doi:10.1063/1.1742462](#)
40. T. Strunz, K. Oroszlan, R. Schäfer, H. J. Güntherodt, Dynamic force spectroscopy of single DNA molecules. *Proc. Natl. Acad. Sci. U.S.A.* **96**, 11277–11282 (1999). [Medline doi:10.1073/pnas.96.20.11277](#)

BIBLIOGRAPHY

- [1] M Reibold, P Paufler, A. A. Levin, W Kochmann, N Pätzke, and D. C. Meyer. “Materials: Carbon nanotubes in an ancient Damascus sabre.” In: *Nature* 444.7117 (2006), pp. 286–286 (cit. on pp. 1, 2).
- [2] The British Museum. *The Lycurgus Cup*. Museum number: 1958,1202.1. 4th Century (cit. on p. 2).
- [3] brewbooks (flickr username). *First Scanning Tunneling Microscope Deutsches Museum*. May 2006 (accessed January 25, 2017) (cit. on p. 2).
- [4] D. M. Eigler and E. K. Schweizer. “Positioning single atoms with a scanning tunnelling microscope.” In: *Nature* 344.6266 (1990), pp. 524–526 (cit. on p. 2).
- [5] R. Zsigmondy and J. Alexander. *Colloids and the ultramicroscope; a manual of colloid chemistry and ultramicroscopy*. New York, J. Wiley & Sons, 1909 (cit. on p. 1).
- [6] I. Langmuir. “The constitution and fundamental properties of solids and liquids. II. Liquids. 1.” In: *Journal of the American Chemical Society* 39.9 (1917), pp. 1848–1906 (cit. on p. 1).
- [7] G. E. Moore. “Cramming More Components onto Integrated Circuits.” In: *Electronics* (1965), pp. 114–117 (cit. on p. 2).
- [8] N. Taniguchi. “On the Basic Concept of ‘Nano-Technology’.” In: *Proc. Intl. Conf. Prod. Eng. Tokyo* (1974), pp. 18–23 (cit. on p. 2).
- [9] K. E. Drexler. *Engines of Creation. The Coming Era of Nanotechnology*. Anchor Books, 1986 (cit. on p. 2).
- [10] G Binnig, H Rohrer, C. Gerber, and E Weibel. “Tunneling through a controllable vacuum gap.” In: *Applied Physics Letters* 40.2 (1982), pp. 178–180 (cit. on p. 2).
- [11] G Binnig, H Rohrer, C. Gerber, and E Weibel. “Surface Studies by Scanning Tunneling Microscopy.” In: *Physical Review Letters* 49.1 (1982), pp. 57–61 (cit. on p. 2).
- [12] G Binnig, C Quate, and C Gerber. “Atomic force microscope.” In: *Physical Review Letters* 56.9 (1986), pp. 930–933 (cit. on pp. 2, 22).
- [13] H Kroto. “C₆₀: Buckminsterfullerene.” In: *Nature* 318.6042 (1985), pp. 162–163 (cit. on p. 3).

- [14] A. I. Ekimov and A. A. Onushchenko. “Quantum size effect in three-dimensional microscopic semiconductor crystals.” In: *JETP Letters* 34.6 (1981) (cit. on p. 3).
- [15] R. P. Feynman. “There’s Plenty of Room at the Bottom.” In: *Engineering and Science* 23:5 (1960), pp. 22–36 (cit. on p. 3).
- [16] C. P. Toumey. “Reading Feynman into nanotechnology.” In: *Techné: Research in Philosophy and Technology* 12.3 (2008), pp. 133–168 (cit. on p. 3).
- [17] D. Goodsell. *Ribosomal Subunits - Molecule of the Month*. Oct. 2000 (accessed January 25, 2017). DOI: [10.2210/rcsb_pdb/mom_2000_10](https://doi.org/10.2210/rcsb_pdb/mom_2000_10) (cit. on p. 4).
- [18] D. S. Goodsell, S. Dutta, C. Zardecki, M. Voigt, H. M. Berman, and S. K. Burley. “The RCSB PDB “Molecule of the Month”: Inspiring a Molecular View of Biology.” In: *PLOS Biology* 13.5 (2015), pp. 1–12 (cit. on p. 4).
- [19] P Traub and M Nomura. “Structure and function of E. coli ribosomes. V. Reconstitution of functionally active 30S ribosomal particles from RNA and proteins.” In: *Proceedings of the National Academy of Sciences of the United States of America* 59.3 (1968), pp. 777–784 (cit. on p. 5).
- [20] I. UniScience News Net. *NYU Chemist Nadrian Seeman Wins Feynman Prize*. accessed January 25, 2017 (cit. on pp. 5, 6).
- [21] N. Seeman. “DNA in a material world.” In: *Nature* 421.6921 (2003), pp. 427–431 (cit. on pp. 5–7).
- [22] W. W. Grabow and L. Jaeger. “RNA self-assembly and RNA nanotechnology.” In: *Accounts of Chemical Research* 47.6 (2014), pp. 1871–1880 (cit. on p. 5).
- [23] N. C. Seeman. “Nucleic acid junctions and lattices.” In: *Journal of theoretical biology* 99.2 (1982), pp. 237–247 (cit. on p. 6).
- [24] D. A. Jackson, R. H. Symons, and P Berg. “Biochemical method for inserting new genetic information into DNA of Simian Virus 40: circular SV40 DNA molecules containing lambda phage genes and the galactose operon of Escherichia coli.” In: *Proceedings of the National Academy of Sciences of the United States of America* 69.10 (1972), pp. 2904–2909 (cit. on p. 6).
- [25] J. H. Chen and N. C. Seeman. “Synthesis from DNA of a molecule with the connectivity of a cube.” In: *Nature* 350.6319 (1991), pp. 631–633 (cit. on p. 7).
- [26] E Winfree, F Liu, L. A. Wenzler, and N. C. Seeman. “Design and self-assembly of two-dimensional DNA crystals.” In: *Nature* 394.6693 (1998), pp. 539–544 (cit. on p. 7).

- [27] R. P. Goodman, I. A. T. Schaap, C. F. Tardin, C. M. Erben, R. M. Berry, C. F. Schmidt, and A. J. Turberfield. “Rapid chiral assembly of rigid DNA building blocks for molecular nanofabrication.” In: *Science* 310.5754 (2005), pp. 1661–1665 (cit. on p. 7).
- [28] W. M. Shih, J. D. Quispe, and G. F. Joyce. “A 1.7-kilobase single-stranded DNA that folds into a nanoscale octahedron.” In: *Nature* 427.6975 (2004), pp. 618–621 (cit. on p. 7).
- [29] J. Zheng, J. J. Birktoft, Y. Chen, T. Wang, R. Sha, P. E. Constantinou, S. L. Ginell, C. Mao, and N. C. Seeman. “From molecular to macroscopic via the rational design of a self-assembled 3D DNA crystal.” In: *Nature* 461.7260 (2009), pp. 74–77 (cit. on p. 7).
- [30] P. W. K. Rothemund. “Folding DNA to create nanoscale shapes and patterns.” In: *Nature* 440.7082 (2006), pp. 297–302 (cit. on pp. 7, 8, 15, 16, 19, 27).
- [31] S. M. Douglas, H. Dietz, T. Liedl, B. Högberg, F. Graf, and W. M. Shih. “Self-assembly of DNA into nanoscale three-dimensional shapes.” In: *Nature* 459.7245 (2009), pp. 414–418 (cit. on pp. 7, 17, 19).
- [32] H. Dietz, S. M. Douglas, and W. M. Shih. “Folding DNA into twisted and curved nanoscale shapes.” In: *Science* 325.5941 (2009), pp. 725–730 (cit. on pp. 7, 17).
- [33] T. Liedl, B. Högberg, J. Tytell, D. E. Ingber, and W. M. Shih. “Self-assembly of three-dimensional prestressed tensegrity structures from DNA.” In: *Nature Nanotechnology* 5.7 (2010), pp. 520–524 (cit. on pp. 7, 18, 39).
- [34] D Han, S Pal, J Nangreave, Z Deng, Y Liu, and H Yan. “DNA Origami with Complex Curvatures in Three-Dimensional Space.” In: *Science* 332.6027 (2011), pp. 342–346 (cit. on pp. 7, 17).
- [35] E. Benson, A. Mohammed, A. Bosco, A. I. Teixeira, P. Orponen, and B. Högberg. “Computer-Aided Production of Scaffolded DNA Nanostructures from Flat Sheet Meshes.” In: *Angewandte Chemie International Edition* 55.31 (2016), pp. 8869–8872 (cit. on pp. 7, 18).
- [36] E. Benson, A. Mohammed, J. Gardell, S. Masich, E. Czeizler, P. Orponen, and B. Högberg. “DNA rendering of polyhedral meshes at the nanoscale.” In: *Nature* 523.7561 (2015), pp. 441–444 (cit. on pp. 7, 18).
- [37] M. Matthies, N. P. Agarwal, and T. L. Schmidt. “Design and Synthesis of Triangulated DNA Origami Trusses.” In: *Nano Letters* 16.3 (2016), pp. 2108–2113 (cit. on pp. 7, 18).

- [38] R. Veneziano, S. Ratanalert, K. Zhang, F. Zhang, H. Yan, W. Chiu, and M. Bathe. “Designer nanoscale DNA assemblies programmed from the top down.” In: *Science* 352.6293 (2016), pp. 1534–1534 (cit. on pp. 7, 18).
- [39] C Geary, P. W. K. Rothmund, and E. S. Andersen. “A single-stranded architecture for cotranscriptional folding of RNA nanostructures.” In: *Science* 345.6198 (2014), pp. 799–804 (cit. on p. 8).
- [40] L. M. Hochrein, M. Schwarzkopf, M. Shahgholi, P. Yin, and N. A. Pierce. “Conditional Dicer Substrate Formation via Shape and Sequence Transduction with Small Conditional RNAs.” In: *Journal of the American Chemical Society* 135.46 (2013), pp. 17322–17330 (cit. on p. 7).
- [41] H. Ohno, T. Kobayashi, R. Kabata, K. Endo, T. Iwasa, S. H. Yoshimura, K. Takeyasu, T. Inoue, and H. Saito. “Synthetic RNA-protein complex shaped like an equilateral triangle.” In: *Nature Nanotechnology* 6.2 (2011), pp. 116–120 (cit. on p. 7).
- [42] C. J. Delebecque, A. B. Lindner, P. A. Silver, and F. A. Aldaye. “Organization of Intracellular Reactions with Rationally Designed RNA Assemblies.” In: *Science* 333.6041 (2011), pp. 470–474 (cit. on p. 7).
- [43] P. Wang, S. H. Ko, C. Tian, C. Hao, and C. Mao. “RNA-DNA hybrid origami: folding of a long RNA single strand into complex nanostructures using short DNA helper strands.” In: *Chemical communications (Cambridge, England)* 49.48 (2013), pp. 5462–5464 (cit. on p. 7).
- [44] M. Endo, S. Yamamoto, K. Tatsumi, T. Emura, K. Hidaka, and H. Sugiyama. “RNA-templated DNA origami structures.” In: *Chemical communications (Cambridge, England)* 49.28 (2013), pp. 2879–2881 (cit. on p. 7).
- [45] J.-M. Arbona, J.-P. Aimé, and J. Elezgaray. “Cooperativity in the annealing of DNA origamis.” In: *The Journal of Chemical Physics* 138.1 (2013), p. 015105 (cit. on pp. 8, 16, 17, 19).
- [46] X. Wei, J. Nangreave, S. Jiang, H. Yan, and Y. Liu. “Mapping the Thermal Behavior of DNA Origami Nanostructures.” In: *Journal of the American Chemical Society* 135.16 (2013), pp. 6165–6176 (cit. on pp. 8, 19).
- [47] K. E. Dunn, F. Dannenberg, T. E. Ouldrige, M. Kwiatkowska, A. J. Turberfield, and J. Bath. “Guiding the folding pathway of DNA origami.” In: *Nature* 525.7567 (2015), pp. 82–86 (cit. on pp. 8, 16).

- [48] J. Fern, J. Lu, and R. Schulman. “The Energy Landscape for the Self-Assembly of a Two-Dimensional DNA Origami Complex.” In: *ACS nano* 10.2 (2016), pp. 1836–1844 (cit. on p. 8).
- [49] C. Steinhauer, R. Jungmann, T. L. Sobey, F. C. Simmel, and P. Tinnefeld. “DNA origami as a nanoscopic ruler for super-resolution microscopy.” In: *Angewandte Chemie International Edition* 48.47 (2009), pp. 8870–8873 (cit. on pp. 8, 19).
- [50] N. V. Voigt, T. Tørring, A. Rotaru, M. F. Jacobsen, J. B. Ravnsbaek, R. Subramani, W. Mamdouh, J. Kjems, A. Mokhir, F. Besenbacher, et al. “Single-molecule chemical reactions on DNA origami.” In: *Nature Nanotechnology* 5.3 (2010), pp. 200–203 (cit. on p. 8).
- [51] H. Gu, J. Chao, S.-J. Xiao, and N. C. Seeman. “A proximity-based programmable DNA nanoscale assembly line.” In: *Nature* 465.7295 (2010), pp. 202–205 (cit. on p. 8).
- [52] R. Jungmann, C. Steinhauer, M. Scheible, A. Kuzyk, P. Tinnefeld, and F. C. Simmel. “Single-Molecule Kinetics and Super-Resolution Microscopy by Fluorescence Imaging of Transient Binding on DNA Origami.” In: *Nano Letters* 10.11 (2010), pp. 4756–4761 (cit. on pp. 8, 19).
- [53] A. Shaw, V. Lundin, E. Petrova, F. Fördös, E. Benson, A. Al-Amin, A. Herland, A. Blokzijl, B. Högberg, and A. I. Teixeira. “Spatial control of membrane receptor function using ligand nanocalipers.” In: *Nature Methods* 11.8 (2014), pp. 841–846 (cit. on p. 8).
- [54] J. B. Knudsen, L. Liu, A. L. Bank Kodal, M. Madsen, Q. Li, J. Song, J. B. Woehrstein, S. F. J. Wickham, M. T. Strauss, F. Schueder, et al. “Routing of individual polymers in designed patterns.” In: *Nature Nanotechnology* 10.10 (2015), pp. 892–898 (cit. on p. 8).
- [55] J. J. Funke and H. Dietz. “Placing molecules with Bohr radius resolution using DNA origami.” In: *Nature Nanotechnology* 11.1 (2016), pp. 47–52 (cit. on p. 8).
- [56] N. A. W. Bell, C. R. Engst, M. Ablay, G. Divitini, C. Ducati, T. Liedl, and U. F. Keyser. “DNA Origami Nanopores.” In: *Nano Letters* 12.1 (2011), pp. 512–517 (cit. on p. 8).
- [57] R. Wei, T. G. Martin, U. Rant, and H. Dietz. “DNA Origami Gatekeepers for Solid-State Nanopores.” In: *Angewandte Chemie International Edition* 51.20 (2012), pp. 4864–4867 (cit. on p. 8).

- [58] C. Plesa, A. N. Ananth, V. Linko, C. Gülcher, A. J. Katan, H. Dietz, and C. Dekker. “Ionic permeability and mechanical properties of DNA origami nanoplates on solid-state nanopores.” In: *ACS nano* 8.1 (2014), pp. 35–43 (cit. on p. 8).
- [59] M. Langecker, V. Arnaut, T. G. Martin, J. List, S. Renner, M. Mayer, H. Dietz, and F. C. Simmel. “Synthetic Lipid Membrane Channels Formed by Designed DNA Nanostructures.” In: *Science* 338.6109 (2012), pp. 932–936 (cit. on p. 8).
- [60] S. Krishnan, D. Ziegler, V. Arnaut, T. G. Martin, K. Kapsner, K. Henneberg, A. R. Bausch, H. Dietz, and F. C. Simmel. “Molecular transport through large-diameter DNA nanopores.” In: *Nature Communications* 7 (2016), p. 12787 (cit. on p. 8).
- [61] M. Langecker, V. Arnaut, J. List, and F. C. Simmel. “DNA nanostructures interacting with lipid bilayer membranes.” In: *Accounts of Chemical Research* 47.6 (2014), pp. 1807–1815 (cit. on p. 8).
- [62] J. List, M. Weber, and F. C. Simmel. “Hydrophobic actuation of a DNA origami bilayer structure.” In: *Angewandte Chemie International Edition* 53.16 (2014), pp. 4236–4239 (cit. on pp. 8, 39).
- [63] Y. Suzuki, M. Endo, Y. Yang, and H. Sugiyama. “Dynamic Assembly/Disassembly Processes of Photoresponsive DNA Origami Nanostructures Directly Visualized on a Lipid Membrane Surface.” In: *Journal of the American Chemical Society* 136.5 (2014), pp. 1714–1717 (cit. on p. 8).
- [64] A. Czogalla, D. J. Kauert, H. G. Franquelim, V. Uzunova, Y. Zhang, R. Seidel, and P. Schwille. “Amphipathic DNA Origami Nanoparticles to Scaffold and Deform Lipid Membrane Vesicles.” In: *Angewandte Chemie* 127.22 (2015), pp. 6601–6605 (cit. on p. 8).
- [65] Y. Yang, J. Wang, H. Shigematsu, W. Xu, W. M. Shih, J. E. Rothman, and C. Lin. “Self-assembly of size-controlled liposomes on DNA nanotemplates.” In: *Nature Chemistry* 8.5 (2016), pp. 476–483 (cit. on p. 8).
- [66] W. Liu, H. Zhong, R. Wang, and N. C. Seeman. “Crystalline Two-Dimensional DNA-Origami Arrays.” In: *Angewandte Chemie* 123.1 (2010), pp. 278–281 (cit. on p. 8).
- [67] S. Woo and P. W. K. Rothemund. “Programmable molecular recognition based on the geometry of DNA nanostructures.” In: *Nature Chemistry* 3.8 (2011), pp. 620–627 (cit. on p. 8).

- [68] A. Aghebat Rafat, T. Pirzer, M. B. Scheible, A. Kostina, and F. C. Simmel. “Surface-assisted large-scale ordering of DNA origami tiles.” In: *Angewandte Chemie International Edition* 53.29 (2014), pp. 7665–7668 (cit. on p. 8).
- [69] S. Kocabey, S. Kemper, J. List, Y. Xing, W. Bae, D. Schiffels, W. M. Shih, F. C. Simmel, and T. Liedl. “Membrane-Assisted Growth of DNA Origami Nanostructure Arrays.” In: *ACS nano* 9.4 (2015), pp. 3530–3539 (cit. on p. 8).
- [70] W. Liu, M. Tagawa, H. L. Xin, T. Wang, H. Emamy, H. Li, K. G. Yager, F. W. Starr, A. V. Tkachenko, and O. Gang. “Diamond family of nanoparticle superlattices.” In: *Science* 351.6273 (2016), pp. 582–586 (cit. on p. 8).
- [71] W. Liu, J. Halverson, Y. Tian, A. V. Tkachenko, and O. Gang. “Self-organized architectures from assorted DNA-framed nanoparticles.” In: *Nature Chemistry* 8.9 (2016), pp. 867–873 (cit. on p. 8).
- [72] G. Ke, M. Liu, S. Jiang, X. Qi, Y. R. Yang, S. Wootten, F. Zhang, Z. Zhu, Y. Liu, C. J. Yang, et al. “Directional Regulation of Enzyme Pathways through the Control of Substrate Channeling on a DNA Origami Scaffold.” In: *Angewandte Chemie International Edition* 55.26 (2016), pp. 7483–7486 (cit. on p. 8).
- [73] Z. Zhao, J. Fu, S. Dhakal, A. Johnson-Buck, M. Liu, T. Zhang, N. W. Woodbury, Y. Liu, N. G. Walter, and H. Yan. “Nanocaged enzymes with enhanced catalytic activity and increased stability against protease digestion.” In: *Nature Communications* 7 (2016), p. 10619 (cit. on p. 8).
- [74] E. Kopperger, T. Pirzer, and F. C. Simmel. “Diffusive transport of molecular cargo tethered to a DNA origami platform.” In: *Nano Letters* 15.4 (2015), pp. 2693–2699 (cit. on p. 8).
- [75] M. Teichmann, E. Kopperger, and F. C. Simmel. “Robustness of Localized DNA Strand Displacement Cascades.” In: *ACS nano* 8.8 (2014), pp. 8487–8496 (cit. on p. 8).
- [76] J. Fu, Y. R. Yang, A. Johnson-Buck, M. Liu, Y. Liu, N. G. Walter, N. W. Woodbury, and H. Yan. “Multi-enzyme complexes on DNA scaffolds capable of substrate channelling with an artificial swinging arm.” In: *Nature Nanotechnology* 9.7 (2014), pp. 531–536 (cit. on p. 8).
- [77] J. Fu, M. Liu, Y. Liu, N. W. Woodbury, and H. Yan. “Interenzyme Substrate Diffusion for an Enzyme Cascade Organized on Spatially Addressable DNA Nanostructures.” In: *Journal of the American Chemical Society* 134.12 (2012), pp. 5516–5519 (cit. on p. 8).

- [78] M Iwaki, S. F. Wickham, K Ikezaki, T Yanagida, and W. M. Shih. “A programmable DNA origami nanospring that reveals force-induced adjacent binding of myosin VI heads.” In: *Nature Communications* 7 (2016), p. 13715 (cit. on p. 8).
- [79] R. F. Hariadi, M Cale, and S Sivaramakrishnan. “Myosin lever arm directs collective motion on cellular actin network.” In: *Proceedings of the National Academy of Sciences* 111.11 (2014), pp. 4091–4096 (cit. on p. 8).
- [80] N. D. Derr, B. S. Goodman, R Jungmann, A. E. Leschziner, W. M. Shih, and S. L. Reck-Peterson. “Tug-of-war in motor protein ensembles revealed with a programmable DNA origami scaffold.” In: *Science* 338.6107 (2012), pp. 662–665 (cit. on p. 8).
- [81] J. J. Funke, P. Ketterer, C. Lieleg, P. Korber, and H. Dietz. “Exploring Nucleosome Unwrapping Using DNA Origami.” In: *Nano Letters* (2016), acs.nanolett.6b04169–8 (cit. on p. 8).
- [82] J. J. Funke, P Ketterer, C Lieleg, S Schunter, P Korber, and H Dietz. “Uncovering the forces between nucleosomes using DNA origami.” In: *Science Advances* 2.11 (2016), e1600974–e1600974 (cit. on p. 8).
- [83] M. Endo and H. Sugiyama. “Single-molecule imaging of dynamic motions of biomolecules in DNA origami nanostructures using high-speed atomic force microscopy.” In: *Accounts of Chemical Research* 47.6 (2014), pp. 1645–1653 (cit. on pp. 8, 19).
- [84] Y. Suzuki, M. Endo, C. Cañas, S. Ayora, J. C. Alonso, H. Sugiyama, and K. Takeyasu. “Direct analysis of Holliday junction resolving enzyme in a DNA origami nanostructure.” In: *Nucleic Acids Research* 42.11 (2014), pp. 7421–7428 (cit. on p. 8).
- [85] M. Endo, K. Tatsumi, K. Terushima, Y. Katsuda, K. Hidaka, Y. Harada, and H. Sugiyama. “Direct visualization of the movement of a single T7 RNA polymerase and transcription on a DNA nanostructure.” In: *Angewandte Chemie International Edition* 51.35 (2012), pp. 8778–8782 (cit. on p. 8).
- [86] M. Endo, Y. Katsuda, K. Hidaka, and H. Sugiyama. “Regulation of DNA methylation using different tensions of double strands constructed in a defined DNA nanostructure.” In: *Journal of the American Chemical Society* 132.5 (2010), pp. 1592–1597 (cit. on p. 8).
- [87] P. Zhan, P. K. Dutta, P. Wang, G. Song, M. Dai, S.-X. Zhao, Z.-G. Wang, P. Yin, W. Zhang, B. Ding, et al. “Reconfigurable Three-Dimensional Gold Nanorod Plasmonic Nanostructures

- Organized on DNA Origami Tripod.” In: *ACS nano* (2017), acsnano.6b06861 (cit. on p. 8).
- [88] A. Gopinath, E. Miyazono, A. Faraon, and P. W. K. Rothemund. “Engineering and mapping nanocavity emission via precision placement of DNA origami.” In: *Nature* 535.7612 (2016), pp. 401–405 (cit. on p. 8).
- [89] P. Wang, S. Gaitanaros, S. Lee, M. Bathe, W. M. Shih, and Y. Ke. “Programming Self-Assembly of DNA Origami Honeycomb Two-Dimensional Lattices and Plasmonic Metamaterials.” In: *Journal of the American Chemical Society* 138.24 (2016), pp. 7733–7740 (cit. on p. 8).
- [90] M. J. Urban, P. K. Dutta, P. Wang, X. Duan, X. Shen, B. Ding, Y. Ke, and N. Liu. “Plasmonic Toroidal Metamolecules Assembled by DNA Origami.” In: *Journal of the American Chemical Society* 138.17 (2016), pp. 5495–5498 (cit. on p. 8).
- [91] A. Kuzyk, Y. Yang, X. Duan, S. Stoll, A. O. Govorov, H. Sugiyama, M. Endo, and N. Liu. “A light-driven three-dimensional plasmonic nanosystem that translates molecular motion into reversible chiroptical function.” In: *Nature Communications* 7 (2016), p. 10591 (cit. on p. 8).
- [92] A. Puchkova, C. Vietz, E. Pibiri, B. Wünsch, M. Sanz Paz, G. P. Acuna, and P. Tinnefeld. “DNA Origami Nanoantennas with over 5000-fold Fluorescence Enhancement and Single-Molecule Detection at 25 μM .” In: *Nano Letters* 15.12 (2015), pp. 8354–8359 (cit. on p. 8).
- [93] T. Zhang, A. Neumann, J. Lindlau, Y. Wu, G. Pramanik, B. Naydenov, F. Jelezko, F. Schüder, S. Huber, M. Huber, et al. “DNA-Based Self-Assembly of Fluorescent Nanodiamonds.” In: *Journal of the American Chemical Society* 137.31 (2015), pp. 9776–9779 (cit. on p. 8).
- [94] E.-M. Roller, L. K. Khorashad, M. Fedoruk, R. Schreiber, A. O. Govorov, and T. Liedl. “DNA-assembled nanoparticle rings exhibit electric and magnetic resonances at visible frequencies.” In: *Nano Letters* 15.2 (2015), pp. 1368–1373 (cit. on p. 8).
- [95] A. Kuzyk, R. Schreiber, H. Zhang, A. O. Govorov, T. Liedl, and N. Liu. “Reconfigurable 3D plasmonic metamolecules.” In: *Nature Materials* 13.9 (2014), pp. 862–866 (cit. on pp. 8, 39).
- [96] P. Kühler, E.-M. Roller, R. Schreiber, T. Liedl, T. Lohmüller, and J. Feldmann. “Plasmonic DNA-origami nanoantennas for surface-enhanced Raman spectroscopy.” In: *Nano Letters* 14.5 (2014), pp. 2914–2919 (cit. on p. 8).

- [97] V. V. Thacker, L. O. Herrmann, D. O. Sigle, T. Zhang, T. Liedl, J. J. Baumberg, and U. F. Keyser. “DNA origami based assembly of gold nanoparticle dimers for surface-enhanced Raman scattering.” In: *Nature Communications* 5 (2014), p. 3448 (cit. on p. 8).
- [98] R. Schreiber, N. Luong, Z. Fan, A. Kuzyk, P. C. Nickels, T. Zhang, D. M. Smith, B. Yurke, W. Kuang, A. O. Govorov, et al. “Chiral plasmonic DNA nanostructures with switchable circular dichroism.” In: *Nature Communications* 4 (2013), p. 2948 (cit. on p. 8).
- [99] G. P. Acuna, F. M. Moller, P Holzmeister, S Beater, B Lalkens, and P Tinnefeld. “Fluorescence Enhancement at Docking Sites of DNA-Directed Self-Assembled Nanoantennas.” In: *Science* 338.6106 (2012), pp. 506–510 (cit. on p. 8).
- [100] G. P. Acuna, M. Bucher, I. H. Stein, C. Steinhauer, A. Kuzyk, P. Holzmeister, R. Schreiber, A. Moroz, F. D. Stefani, T. Liedl, et al. “Distance Dependence of Single-Fluorophore Quenching by Gold Nanoparticles Studied on DNA Origami.” In: *ACS nano* 6.4 (2012), pp. 3189–3195 (cit. on p. 8).
- [101] A. Kuzyk, R. Schreiber, Z. Fan, G. Pardatscher, E.-M. Roller, A. Högele, F. C. Simmel, A. O. Govorov, and T. Liedl. “DNA-based self-assembly of chiral plasmonic nanostructures with tailored optical response.” In: *Nature* 483.7389 (2012), pp. 311–314 (cit. on pp. 8, 19).
- [102] J. Hahn, S. F. J. Wickham, W. M. Shih, and S. D. Perrault. “Addressing the instability of DNA nanostructures in tissue culture.” In: *ACS nano* 8.9 (2014), pp. 8765–8775 (cit. on pp. 8, 9).
- [103] S. D. Perrault and W. M. Shih. “Virus-inspired membrane encapsulation of DNA nanostructures to achieve in vivo stability.” In: *ACS nano* 8.5 (2014), pp. 5132–5140 (cit. on pp. 8, 9).
- [104] Y.-X. Zhao, A. Shaw, X. Zeng, E. Benson, A. M. Nyström, and B. Högberg. “DNA origami delivery system for cancer therapy with tunable release properties.” In: *ACS nano* 6.10 (2012), pp. 8684–8691 (cit. on p. 8).
- [105] S. M. Douglas, I Bachelet, and G. M. Church. “A Logic-Gated Nanorobot for Targeted Transport of Molecular Payloads.” In: *Science* 335.6070 (2012), pp. 831–834 (cit. on pp. 8, 39).
- [106] V. J. Schueller, S. Heidegger, N. Sandholzer, P. C. Nickels, N. A. Suhartha, S. Endres, C. Bourquin, and T. Liedl. “Cellular immunostimulation by CpG-sequence-coated DNA origami structures.” In: *ACS nano* 5.12 (2011), pp. 9696–9702 (cit. on p. 8).

- [107] D. Smith, V. Schüller, C. Engst, J. Rädler, and T. Liedl. “Nucleic acid nanostructures for biomedical applications.” In: *Nanomedicine* 8.1 (2013), pp. 105–121 (cit. on pp. 9, 27).
- [108] E. Stahl, F. Praetorius, C. C. de Oliveira Mann, K.-P. Hopfner, and H. Dietz. “Impact of Heterogeneity and Lattice Bond Strength on DNA Triangle Crystal Growth.” In: *ACS nano* (2016), acsnano.6b04787 (cit. on p. 9).
- [109] B. Kick, F. Praetorius, H. Dietz, and D. Weuster-Botz. “Efficient Production of Single-Stranded Phage DNA as Scaffolds for DNA Origami.” In: *Nano Letters* 15.7 (2015), pp. 4672–4676 (cit. on pp. 9, 27, 28, 71).
- [110] A. Shaw, E. Benson, and B. Högberg. “Purification of functionalized DNA origami nanostructures.” In: *ACS nano* 9.5 (2015), pp. 4968–4975 (cit. on p. 9).
- [111] E. Stahl, T. G. Martin, F. Praetorius, and H. Dietz. “Facile and scalable preparation of pure and dense DNA origami solutions.” In: *Angewandte Chemie International Edition* 53.47 (2014), pp. 12735–12740 (cit. on pp. 9, 29).
- [112] K. F. Wagenbauer, C. H. Wachauf, and H. Dietz. “Quantifying quality in DNA self-assembly.” In: *Nature Communications* 5 (2014), p. 3691 (cit. on pp. 9, 19).
- [113] R. Sha, J. J. Birktoft, N. Nguyen, A. R. Chandrasekaran, J. Zheng, X. Zhao, C. Mao, and N. C. Seeman. “Self-Assembled DNA Crystals: The Impact on Resolution of 5′-Phosphates and the DNA Source.” In: *Nano Letters* 13.2 (2013), pp. 793–797 (cit. on p. 9).
- [114] C. Ducani, C. Kaul, M. Moche, W. M. Shih, and B. Högberg. “Enzymatic production of ‘monoclonal stoichiometric’ single-stranded DNA oligonucleotides.” In: *Nature Methods* 10.7 (2013), pp. 647–652 (cit. on pp. 9, 27, 28, 71).
- [115] C. Lin, S. D. Perrault, M. Kwak, F. Graf, and W. M. Shih. “Purification of DNA-origami nanostructures by rate-zonal centrifugation.” In: *Nucleic Acids Research* 41.2 (2013), e40 (cit. on pp. 9, 29).
- [116] J. P. J. Sobczak, T. G. Martin, T. Gerling, and H. Dietz. “Rapid Folding of DNA into Nanoscale Shapes at Constant Temperature.” In: *Science* 338.6113 (2012), pp. 1458–1461 (cit. on pp. 9, 16, 17, 19, 28).
- [117] T. G. Martin and H. Dietz. “Magnesium-free self-assembly of multi-layer DNA objects.” In: *Nature Communications* 3 (2012), p. 1103 (cit. on pp. 9, 18).

- [118] A. Rajendran, M. Endo, Y. Katsuda, K. Hidaka, and H. Sugiyama. “Photo-cross-linking-assisted thermal stability of DNA origami structures and its application for higher-temperature self-assembly.” In: *Journal of the American Chemical Society* 133.37 (2011), pp. 14488–14491 (cit. on p. 9).
- [119] Q. Mei, X. Wei, F. Su, Y. Liu, C. Youngbull, R. Johnson, S. Lindsay, H. Yan, and D. Meldrum. “Stability of DNA Origami Nanoarrays in Cell Lysate.” In: *Nano Letters* 11.4 (2011), pp. 1477–1482 (cit. on p. 9).
- [120] R. Dahm. “Discovering DNA: Friedrich Miescher and the early years of nucleic acid research.” In: *Human Genetics* 122.6 (2008), pp. 565–581 (cit. on p. 11).
- [121] O. T. Avery, C. M. MacLeod, and M. McCarty. “Studies on the chemical nature of the substance inducing transformation of pneumococcal types.” In: *Journal of Experimental Medicine* 79.2 (1944), pp. 137–158 (cit. on p. 11).
- [122] A. D. Hershey and M. Chase. “Independent functions of viral protein and nucleic acid in growth of bacteriophage.” In: *The Journal of general physiology* 36.1 (1952), pp. 39–56 (cit. on p. 11).
- [123] J. D. Watson and F. H. Crick. “Molecular structure of nucleic acids; a structure for deoxyribose nucleic acid.” In: *Nature* 171.4356 (1953), pp. 737–738 (cit. on p. 11).
- [124] V. A. Bloomfield, D. M. Crothers, and I. Tinoco. *Nucleic Acids: Structures, Properties, and Functions*. University Science Books, 2000 (cit. on p. 11).
- [125] J. Lipfert, S. Doniach, R. Das, and D. Herschlag. “Understanding nucleic acid-ion interactions.” In: *Annual Review of Biochemistry* 83 (2014), pp. 813–841 (cit. on p. 13).
- [126] G. R. Strobl. *The Physics of Polymers*. 3rd edition. Springer, 2007 (cit. on p. 14).
- [127] S. B. Smith, Y. Cui, and C. Bustamante. “Overstretching B-DNA: the elastic response of individual double-stranded and single-stranded DNA molecules.” In: *Science* 271.5250 (1996), pp. 795–799 (cit. on pp. 14, 19, 47).
- [128] A. Panjkovich and F. Melo. “Comparison of different melting temperature calculation methods for short DNA sequences.” In: *Bioinformatics* 21.6 (2005), pp. 711–722 (cit. on p. 15).
- [129] R. B. Wallace, J. Shaffer, R. F. Murphy, J. Bonner, T. Hirose, and K. Itakura. “Hybridization of synthetic oligodeoxyribonucleotides to phi chi 174 DNA: the effect of single base pair mismatch.” In: *Nucleic Acids Research* 6.11 (1979), pp. 3543–3557 (cit. on p. 15).

- [130] J Sambrook and D. W. Russell. *Molecular cloning: a laboratory manual 3rd edition*. ColdSpring-Harbour Laboratory Press, 2001 (cit. on pp. 15, 20, 27).
- [131] P. M. Howley, M. A. Israel, M. F. Law, and M. A. Martin. “A rapid method for detecting and mapping homology between heterologous DNAs. Evaluation of polyomavirus genomes.” In: *Journal Of Biological Chemistry* 254.11 (1979), pp. 4876–4883 (cit. on p. 15).
- [132] K Breslauer. “Predicting DNA duplex stability from the base sequence.” In: *Proceedings of the National Academy of Sciences of the United States of America* 83.11 (1986), pp. 3746–3750 (cit. on p. 15).
- [133] J. SantaLucia and D. Hicks. “The thermodynamics of DNA structural motifs.” In: *Annual review of biophysics and biomolecular structure* 33.1 (2004), pp. 415–440 (cit. on p. 15).
- [134] E. S. Andersen, M. Dong, M. M. Nielsen, K. Jahn, R. Subramani, W. Mamdouh, M. M. Golas, B. Sander, H. Stark, C. L. P. Oliveira, et al. “Self-assembly of a nanoscale DNA box with a controllable lid.” In: *Nature* 459.7243 (2009), pp. 73–76 (cit. on pp. 17, 19).
- [135] Y Ke, S. Douglas, M Liu, J Sharma, A Cheng, A Leung, Y Liu, W. Shih, and H Yan. “Multilayer dna origami packed on a square lattice.” In: *Journal of the American Chemical Society* 131.43 (2009), pp. 15903–15908 (cit. on pp. 17, 18).
- [136] D Han, S Pal, Y Yang, S Jiang, J Nangreave, Y Liu, and H Yan. “DNA Gridiron Nanostructures Based on Four-Arm Junctions.” In: *Science* 339.6126 (2013), pp. 1412–1415 (cit. on p. 18).
- [137] P. C. Nickels, Y. Ke, R. Jungmann, D. M. Smith, M. Leichenring, W. M. Shih, T. Liedl, and B. Högberg. “DNA origami structures directly assembled from intact bacteriophages.” In: *Small* 10.9 (2014), pp. 1765–1769 (cit. on pp. 19, 31, 73).
- [138] S. M. Douglas, A. H. Marblestone, S. Teerapittayanon, A. Vazquez, G. M. Church, and W. M. Shih. “Rapid prototyping of 3D DNA-origami shapes with caDNAno.” In: *Nucleic Acids Research* 37.15 (2009), pp. 5001–5006 (cit. on p. 18).
- [139] D.-N. Kim, F. Kilchherr, H. Dietz, and M. Bathe. “Quantitative prediction of 3D solution shape and flexibility of nucleic acid nanostructures.” In: *Nucleic Acids Research* 40.7 (2012), pp. 2862–2868 (cit. on p. 18).

- [140] T. E. Ouldridge, A. A. Louis, and J. P. K. Doye. “Structural, mechanical, and thermodynamic properties of a coarse-grained DNA model.” In: *The Journal of Chemical Physics* 134.8 (2011), p. 085101 (cit. on pp. 18, 72).
- [141] T. E. Ouldridge. “DNA nanotechnology: understanding and optimisation through simulation.” In: *Molecular Physics* 113.1 (2014), pp. 1–15 (cit. on pp. 18, 72).
- [142] B. E. K. Snodin, F. Randisi, M. Mosayebi, P. Šulc, J. S. Schreck, F. Romano, T. E. Ouldridge, R. Tsukanov, E. Nir, A. A. Louis, et al. “Introducing improved structural properties and salt dependence into a coarse-grained model of DNA.” In: *The Journal of Chemical Physics* 142.23 (2015), p. 234901 (cit. on pp. 18, 72).
- [143] B. E. K. Snodin, F. Romano, L. Rovigatti, T. E. Ouldridge, A. A. Louis, and J. P. K. Doye. “Direct Simulation of the Self-Assembly of a Small DNA Origami.” In: *ACS nano* 10.2 (2016), pp. 1724–1737 (cit. on pp. 18, 72).
- [144] Y. Ke, G. Bellot, N. V. Voigt, E. Fradkov, and W. M. Shih. “Two design strategies for enhancement of multilayer-DNA-origami folding: underwinding for specific intercalator rescue and staple-break positioning.” In: *Chemical science* 3.8 (2012), pp. 2587–2597 (cit. on p. 18).
- [145] X.-C. Bai, T. G. Martin, S. H. W. Scheres, and H. Dietz. “Cryo-EM structure of a 3D DNA-origami object.” In: *Proc. Natl. Acad. Sci* 109.49 (2012), pp. 20012–20017 (cit. on p. 19).
- [146] S. Fischer, C. Hartl, K. Frank, J. O. Rädler, T. Liedl, and B. Nickel. “Shape and Interhelical Spacing of DNA Origami Nanostructures Studied by Small-Angle X-ray Scattering.” In: *Nano Letters* 16.7 (2016), pp. 4282–4287 (cit. on p. 19).
- [147] L. K. Bruetzel, T. Gerling, S. M. Sedlak, P. U. Walker, W. Zheng, H. Dietz, and J. Lipfert. “Conformational Changes and Flexibility of DNA Devices Observed by Small-Angle X-ray Scattering.” In: *Nano Letters* 16.8 (2016), pp. 4871–4879 (cit. on p. 19).
- [148] M Rief, H Clausen-Schaumann, and H. Gaub. “Sequence-dependent mechanics of single DNA molecules.” In: *Nature Structural Biology* 6.4 (1999), pp. 346–349 (cit. on pp. 19, 47).
- [149] H Clausen-Schaumann, M Rief, C Tolksdorf, and H. Gaub. “Mechanical stability of single DNA molecules.” In: *Biophysical Journal* 78.4 (2000), pp. 1997–2007 (cit. on pp. 19, 47).

- [150] W. Shu, D. Liu, M. Watari, C. Riener, T. Strunz, M. Welland, S. Balasubramanian, and R. McKendry. “DNA molecular motor driven micromechanical cantilever arrays.” In: *Journal of the American Chemical Society* 127.48 (2005), pp. 17054–17060 (cit. on p. 19).
- [151] D. J. Kauert, T. Kurth, T. Liedl, and R. Seidel. “Direct mechanical measurements reveal the material properties of three-dimensional DNA origami.” In: *Nano Letters* 11.12 (2011), pp. 5558–5563 (cit. on p. 19).
- [152] E. Pfitzner, C. Wachauf, F. Kilchherr, B. Pelz, W. M. Shih, M. Rief, and H. Dietz. “Rigid DNA Beams for High-Resolution Single-Molecule Mechanics.” In: *Angewandte Chemie International Edition* 52.30 (2013), pp. 7766–7771 (cit. on pp. 19, 47).
- [153] D. Koirala, P. Shrestha, T. Emura, K. Hidaka, S. Mandal, M. Endo, H. Sugiyama, and H. Mao. “Single-molecule mechanochemical sensing using DNA origami nanostructures.” In: *Angewandte Chemie International Edition* 53.31 (2014), pp. 8137–8141 (cit. on p. 19).
- [154] P. Shrestha, T. Emura, D. Koirala, Y. Cui, K. Hidaka, W. J. Maximuck, M. Endo, H. Sugiyama, and H. Mao. “Mechanical properties of DNA origami nanoassemblies are determined by Holliday junction mechanophores.” In: *Nucleic Acids Research* 44.14 (2016), pp. 6574–6582 (cit. on p. 19).
- [155] F. Kilchherr, C. Wachauf, B. Pelz, M. Rief, M. Zacharias, and H. Dietz. “Single-molecule dissection of stacking forces in DNA.” In: *Science* 353.6304 (2016), aaf5508–aaf5508 (cit. on pp. 19, 47).
- [156] B. Yurke, A. Turberfield, A. Mills, F. Simmel, and J. Neumann. “A DNA-fuelled molecular machine made of DNA.” In: *Nature* 406.6796 (2000), pp. 605–608 (cit. on p. 19).
- [157] T. Liedl and F. C. Simmel. “Switching the Conformation of a DNA Molecule with a Chemical Oscillator.” In: *Nano Letters* 5.10 (2005), pp. 1894–1898 (cit. on p. 19).
- [158] J. Kim, K. S. White, and E. Winfree. “Construction of an in vitro bistable circuit from synthetic transcriptional switches.” In: *Molecular systems biology* 2 (2006), p. 68 (cit. on p. 19).
- [159] J. J. Schmied, C. Forthmann, E. Pibiri, B. Lalkens, P. Nickels, T. Liedl, and P. Tinnefeld. “DNA origami nanopillars as standards for three-dimensional superresolution microscopy.” In: *Nano Letters* 13.2 (2013), pp. 781–785 (cit. on p. 19).

- [160] R. Inuma, Y. Ke, R. Jungmann, T. Schlichthaerle, J. B. Woehrstein, and P. Yin. “Polyhedra Self-Assembled from DNA Tripods and Characterized with 3D DNA-PAINT.” In: *Science* 344.6179 (2014), pp. 65–69 (cit. on p. 19).
- [161] C. R. Cantor, M. M. Warshaw, and H SHAPIRO. “Oligonucleotide interactions. 3. Circular dichroism studies of the conformation of deoxyoligonucleotides.” In: *Biopolymers* 9.9 (1970), pp. 1059–1077 (cit. on p. 20).
- [162] M. J. Cavalluzzi and P. N. Borer. “Revised UV extinction coefficients for nucleoside-5'-monophosphates and unpaired DNA and RNA.” In: *Nucleic Acids Research* 32.1 (2004), e13–13 (cit. on p. 20).
- [163] H. G. Hansma, M Bezanilla, F Zenhausern, M Adrian, and R. L. Sinsheimer. “Atomic force microscopy of DNA in aqueous solutions.” In: *Nucleic Acids Research* 21.3 (1993), pp. 505–512 (cit. on p. 22).
- [164] brewbooks (flickr username). *Electron Microscope Deutsches Museum*. May 2006 (accessed January 25, 2017) (cit. on p. 23).
- [165] T. Förster. “Zwischenmolekulare Energiewanderung und Fluoreszenz.” In: *Annalen der Physik* 437.1-2 (1948), pp. 55–75 (cit. on p. 24).
- [166] J. R. Lakowicz. *Principles of Fluorescence Spectroscopy*. Springer US, 2007 (cit. on p. 24).
- [167] R. M. Clegg, A. I. Murchie, A Zechel, and D. M. Lilley. “Observing the helical geometry of double-stranded DNA in solution by fluorescence resonance energy transfer.” In: *Proceedings of the National Academy of Sciences of the United States of America* 90.7 (1993), pp. 2994–2998 (cit. on p. 25).
- [168] A. N. Kapanidis, N. K. Lee, T. A. Laurence, S. Doose, E. Margeat, and S. Weiss. “Fluorescence-aided molecule sorting: analysis of structure and interactions by alternating-laser excitation of single molecules.” In: *Proceedings of the National Academy of Sciences* 101.24 (2004), pp. 8936–8941 (cit. on p. 26).
- [169] A. N. Kapanidis, T. A. Laurence, N. K. Lee, E. Margeat, X. Kong, and S. Weiss. “Alternating-laser excitation of single molecules.” In: *Accounts of Chemical Research* 38.7 (2005), pp. 523–533 (cit. on p. 26).
- [170] J. Ross, P. Buschkamp, D. Fetting, A. Donnermeyer, C. M. Roth, and P. Tinnefeld. “Multicolor Single-Molecule Spectroscopy with Alternating Laser Excitation for the Investigation of Interactions and Dynamics.” In: *The Journal of Physical Chemistry B* 111.2 (2007), pp. 321–326 (cit. on p. 26).

- [171] U. B. Gyllensten and H. A. Erlich. “Generation of single-stranded DNA by the polymerase chain reaction and its application to direct sequencing of the HLA-DQA locus.” In: *Proceedings of the National Academy of Sciences* 85.20 (1988), pp. 7652–7656 (cit. on p. 27).
- [172] M. M. Ali, F. Li, Z. Zhang, K. Zhang, D.-K. Kang, J. A. Ankrum, X. C. Le, and W. Zhao. “Rolling circle amplification: a versatile tool for chemical biology, materials science and medicine.” In: *Chem. Soc. Rev.* 43.10 (2014), pp. 3324–3341 (cit. on p. 27).
- [173] C. Ducani, G. Bernardinelli, and B. Högberg. “Rolling circle replication requires single-stranded DNA binding protein to avoid termination and production of double-stranded DNA.” In: *Nucleic Acids Research* 42.16 (2014), pp. 10596–10604 (cit. on p. 27).
- [174] H. Gu and R. R. Breaker. “Production of single-stranded DNAs by self-cleavage of rolling-circle amplification products.” In: *BioTechniques* 54.6 (2013), pp. 337–343 (cit. on p. 27).
- [175] F. H. T. Nelissen, E. P. M. Goossens, M. Tessari, and H. A. Heus. “Enzymatic preparation of multimilligram amounts of pure single-stranded DNA samples for material and analytical sciences.” In: *Analytical Biochemistry* 475 (2015), pp. 68–73 (cit. on p. 27).
- [176] T. Hultmann, S. Stahl, E. Hornes, and M. Uhlen. “Direct Solid-Phase Sequencing of Genomic and Plasmid Dna Using Magnetic Beads as Solid Support.” In: *Nucleic Acids Research* 17.13 (1989), pp. 4937–4946 (cit. on p. 27).
- [177] G. Bellot, M. A. McClintock, J. J. Chou, and W. M. Shih. “DNA nanotubes for NMR structure determination of membrane proteins.” In: *Nature protocols* 8.4 (2013), pp. 755–770 (cit. on p. 27).
- [178] A. Rajendran, M. Endo, Y. Katsuda, K. Hidaka, and H. Sugiyama. “Programmed two-dimensional self-assembly of multiple DNA origami jigsaw pieces.” In: *ACS nano* 5.1 (2011), pp. 665–671 (cit. on p. 29).
- [179] Z. Zhao, Y. Liu, and H. Yan. “Organizing DNA Origami Tiles into Larger Structures Using Preformed Scaffold Frames.” In: *Nano Letters* 11.7 (2011), pp. 2997–3002 (cit. on p. 29).
- [180] Z. Zhao, H. Yan, and Y. Liu. “A route to scale up DNA origami using DNA tiles as folding staples.” In: *Angewandte Chemie International Edition* 49.8 (2010), pp. 1414–1417 (cit. on p. 29).

- [181] E. Pound, J. R. Ashton, H. A. Becerril, and A. T. Woolley. “Polymerase Chain Reaction Based Scaffold Preparation for the Production of Thin, Branched DNA Origami Nanostructures of Arbitrary Sizes - Nano Letters (ACS Publications).” In: *Nano Letters* 9.12 (2009), pp. 4302–4305 (cit. on p. 29).
- [182] Y. Yang, D. Han, J. Nangreave, Y. Liu, and H. Yan. “DNA Origami with Double-Stranded DNA As a Unified Scaffold.” In: *ACS nano* (2012), p. 120727170029009 (cit. on p. 29).
- [183] H. Zhang, J. Chao, D. Pan, H. Liu, Q. Huang, and C. Fan. “Folding super-sized DNA origami with scaffold strands from long-range PCR.” In: *Chemical Communications* 48.51 (2012), p. 6405 (cit. on p. 29).
- [184] B. Högberg, T. Liedl, and W. M. Shih. “Folding DNA origami from a double-stranded source of scaffold.” In: *Journal of the American Chemical Society* 131.26 (2009), pp. 9154–9155 (cit. on p. 29).
- [185] A. N. Marchi, I. Saaem, B. N. Vogen, S. Brown, and T. H. LaBean. “Toward Larger DNA Origami.” In: *Nano Letters* 14.10 (2014), pp. 5740–5747 (cit. on p. 29).
- [186] H. Gu, W. Yang, and N. C. Seeman. “DNA scissors device used to measure MutS binding to DNA mis-pairs.” In: *Journal of the American Chemical Society* 132.12 (2010), pp. 4352–4357 (cit. on pp. 39, 48).
- [187] C. Albrecht, K. Blank, M. Lalic-Mülthaler, S. Hirler, T. Mai, I. Gilbert, S. Schiffmann, T. Bayer, H. Clausen-Schaumann, and H. E. Gaub. “DNA: a programmable force sensor.” In: *Science* 301.5631 (2003), pp. 367–370 (cit. on p. 39).
- [188] P. C. Nickels, H. C. Høiberg, S. S. Simmel, P. Holzmeister, P. Tinnefeld, and T. Liedl. “DNA Origami Seesaws as Comparative Binding Assay.” In: *ChemBioChem* 17.12 (2016), pp. 1093–1096 (cit. on pp. 41, 103).
- [189] M. S. Kellermayer, S. B. Smith, H. L. Granzier, and C. Bustamante. “Folding-unfolding transitions in single titin molecules characterized with laser tweezers.” In: *Science* 276.5315 (1997), pp. 1112–1116 (cit. on p. 47).
- [190] M. Rief, M. Gautel, F. Oesterhelt, J. M. Fernandez, and H. E. Gaub. “Reversible unfolding of individual titin immunoglobulin domains by AFM.” In: *Science* 276.5315 (1997), pp. 1109–1112 (cit. on p. 47).
- [191] J. M. Fernandez and H. Li. “Force-clamp spectroscopy monitors the folding trajectory of a single protein.” In: *Science* 303.5664 (2004), pp. 1674–1678 (cit. on p. 47).

- [192] K. C. Neuman and A. Nagy. “Single-molecule force spectroscopy: optical tweezers, magnetic tweezers and atomic force microscopy.” In: *Nature Methods* 5.6 (2008), pp. 491–505 (cit. on p. 47).
- [193] N. Ribbeck and O. A. Saleh. “Multiplexed single-molecule measurements with magnetic tweezers.” In: *The Review of scientific instruments* 79.9 (2008), p. 094301 (cit. on p. 47).
- [194] D. Yang, A. Ward, K. Halvorsen, and W. P. Wong. “Multiplexed single-molecule force spectroscopy using a centrifuge.” In: *Nature Communications* 7 (2016), p. 11026 (cit. on p. 47).
- [195] G. Sitters, D. Kamsma, G. Thalhammer, M. Ritsch-Martel, E. J. G. Peterman, and G. J. L. Wuite. “Acoustic force spectroscopy.” In: *Nature Methods* 12.1 (2015), pp. 47–50 (cit. on p. 47).
- [196] W. Shen, M. F. Bruist, S. D. Goodman, and N. C. Seeman. “A Protein-Driven DNA Device That Measures the Excess Binding Energy of Proteins That Distort DNA.” In: *Angewandte Chemie International Edition* 43.36 (2004), pp. 4750–4752 (cit. on p. 48).
- [197] H. Shroff, B. M. Reinhard, M. Siu, H. Agarwal, A. Spakowitz, and J. Liphardt. “Biocompatible Force Sensor with Optical Readout and Dimensions of 6 nm³.” In: *Nano Letters* 5.7 (2005), pp. 1509–1514 (cit. on p. 48).
- [198] C. Grashoff, B. D. Hoffman, M. D. Brenner, R. Zhou, M. Parsons, M. T. Yang, M. A. McLean, S. G. Sligar, C. S. Chen, T. Ha, et al. “Measuring mechanical tension across vinculin reveals regulation of focal adhesion dynamics.” In: *Nature* 466.7303 (2010), pp. 263–266 (cit. on p. 48).
- [199] S. Hohng, S. Hohng, R. Zhou, R. Zhou, M. K. Nahas, M. K. Nahas, J. Yu, J. Yu, K. Schulten, K. Schulten, et al. “Fluorescence-force spectroscopy maps two-dimensional reaction landscape of the holliday junction.” In: *Science* 318.5848 (2007), pp. 279–283 (cit. on p. 48).
- [200] P. C. Nickels, B. Wünsch, P. Holzmeister, W. Bae, L. M. Kneer, D. Grohmann, P. Tinnefeld, and T. Liedl. “Molecular force spectroscopy with a DNA origami-based nanoscopic force clamp.” In: *Science* 354.6310 (2016), pp. 305–307 (cit. on pp. 51, 113).
- [201] H. Gu and R. R. Breaker. “Production of single-stranded DNAs by self-cleavage of rolling-circle amplification products.” In: *BioTechniques* 54.6 (2013), pp. 1–5 (cit. on p. 71).

- [202] H. Gu, K. Furukawa, Z. Weinberg, D. F. Berenson, and R. R. Breaker. “Small, Highly Active DNAs That Hydrolyze DNA.” In: *Journal of the American Chemical Society* 135.24 (2013), pp. 9121–9129 (cit. on p. 71).
- [203] L Chasteen, J Ayriss, P Pavlik, and A. R. M. Bradbury. “Eliminating helper phage from phage display.” In: *Nucleic Acids Research* 34.21 (2006), e145–e145 (cit. on p. 71).
- [204] J. N. Zadeh, C. D. Steenberg, J. S. Bois, B. R. Wolfe, M. B. Pierce, A. R. Khan, R. M. Dirks, and N. A. Pierce. “NUPACK: Analysis and design of nucleic acid systems.” In: *Journal of Computational Chemistry* 32.1 (2010), pp. 170–173 (cit. on p. 72).
- [205] B. van den Broek, M. C. Noom, and G. J. L. Wuite. “DNA-tension dependence of restriction enzyme activity reveals mechanochemical properties of the reaction pathway.” In: *Nucleic Acids Research* 33.8 (2005), pp. 2676–2684 (cit. on p. 72).